Metal Carbonyls as Carbon Monoxide Delivery Systems

Suzanne McMahon B.Sc.

Thesis Submitted for the Award of PhD

School of Chemical Sciences

Dublin City University

Under the Supervision of Dr. Mary Pryce

January 2016

Declaration

I hereby certify that this material, which I now submit for assessment on the programme of study leading to the award of Doctor of Philosophy is entirely my own work, and that I have exercised reasonable care to ensure that the work is original, and does not to the best of my knowledge breach any law of copyright, and has not been taken from the work of others save and to the extent that such work has been cited and acknowledged within the text of my work.

Signed: _____ I.D. No.: _____ Date: _____

Dedicated to my parents and to the memory of my grandparents.

Acknowledgments

Firstly I would like to thank my supervisor, Dr. Mary Pryce for giving me this great opportunity. Thank you so much for your constant encouragement, expert advice, motivation, support and patience throughout the entire research project. Thank you for always going above and beyond to make time for us no matter how big or small the problem or question at hand may have been. I have been very lucky to have you as my supervisor and am eternally grateful.

I would like to express my sincere thanks to Prof. Conor Long for all of the help and guidance especially throughout the many trips to the University of Amsterdam. Likewise, I would like to thank Prof. Wybren Jan Buma and Dr. Saeed Amirjalayer for making it possible to perform time resolved IR studies at the University of Amsterdam. I would also like to thank the Irish Research Council for funding my PhD research project.

Many thanks to all the staff in the School of Chemical Sciences, Veronica, Damien (especially for the help with my many lamps and for making lab tutoring such an enjoyable experience), John (thank you for allowing me to carry out my NMR studies), Ambrose, Catherine, Vinny, Brendan, Mary and Claire. None of this research would have been possible without your constant support.

To MPRG, thank you, Nive (it was such an honour for it to be possible to work with you from the first day of my 4th year research project until the very last day of my postgrad project, I am forever grateful for your endless support and inspiration) Jen, Yvonne, Diana, Liam, Finn, Laura, Ahmed and Aoife for being the best lab group I could have ever asked for. Thank you for your constant support and encouragement (especially during the write up – I couldn't have done any of it without you all). Thanks for making the lab so much fun to work in. You made it such a pleasure to come to work every day. Liam and Nive, we had some very good times in Amsterdam also!

I would also like to thank Aaron, Chris, Aurelien and Colm for all the hawwt cawwfees and few ginz, the rants and bants were had every day. Thanks for making it so fun to work in DCU and always reassuring me that it'll all be graaaaaand! Thanks so much for all your help especially towards the end, wouldn't have gotten through it without

you all. G’laaads. Thanks to Andrea, Claire, Mohammad and Eadaoin who made all the coffee breaks and postgrad nights out so much fun.

A huge thank you to the best roomates, Flor and David. It was such a pleasure living with you both during my research. Thank you for always looking after me and especially for all of the amazing food.

To Ash, Creina and Eimear, not too many people are given the amazing opportunity to study and work with their best friends from undergrad to postgrad, I am one of the lucky ones. Ash, I think we spent almost every day of the last three years together. I could write a whole chapter on the times we have had. Thank you so so much for every single thing, for always being there – it just can’t even be put into words.

Finally, I would like to thank my parents. I cannot describe how grateful I am for your unconditional love and support. I owe everything to you.

Table of Contents

List of Abbreviations

Abbreviation	Explanation
BBO	β-barium borate
BID	barrier discharge ionisation detector
BODIPY	boron dipyrromethene
bpy	2,2´- bipyridine
CO	carbon monoxide
CORM	carbon monoxide releasing molecule
CORM-A	carbon monoxide releasing material
CV	cyclic voltammetry
deoxy-Mb	deoxygenated myoglobin
DFG	difference frequency generation
DFT	density functional theory
DMSO	dimethylsulfoxide
E_a	activation energy
E_{pa}	anodic peak potential
ESI	electrospray ionisation
ET- CORM	enzyme triggered carbon monoxide releasing molecule
eV	electon volts
Fac-	facial
FBS	fetal bovine serum
FLIM	fluorescence lifetime imaging microscopy
fs	femtosecond
FT-IR	Fourier transform IR
FWHM	full width at half maximum
Hb	haemoglobin
HbCO	carbonmonoxy-haemoglobin

HO	heme oxygenase
HO-1	heme oxygenase-1
HO-2	heme oxygenase-2
HOMO	highest occupied molecular orbital
i.p.	intraperitoneal
i.v.	intravenous
iCORM	negative control for a CORM
iNOS	inducible nitric oxide synthase
IONP	iron oxide nanoparticles
IR	infrared
ISC	intersystem crossing
K_{obs}	observed rate constant
L	ligand
LED	light emitting diode
LF	ligand field
LUMO	lowest unoccupied molecular orbital
M	metal
MALDI	matrix assisted laser desorption / ionisation
Mb	myoglobin
Mb-CO	carbonmonoxy myoglobin
M-CO	metal carbonyl
MCT	mercury cadmium telluride
MI	matrix isolation
MLCT	metal to ligand charge transfer
MO	molecular orbital
NADPH	nicotinamide adenine dinucleotide phosphate (reduced form)
NF-κb	nuclear factor kappa-light-chain-enhancer of activated B cells
NIR	near infrared
NMR	nuclear magnetic resonance

NO	nitric oxide
ns	nanosecond
OPA	optical parametric amplifier
PBS	phosphate buffered saline
PEG	polyethyleneglycol
photoCORM	photoactivatable carbon monoxide releasing molecule
PLE	pig liver esterase
ppm	parts per million
psTRIR	picosecond time resolved infrared
RAL	Rutherford Appleton Laboratories
RPMI	Roswell Park Memorial Institute (media)
R_T	retention time
SD	sodium dithionite, $Na_2S_2O_4$
SHG	second harmonic generation
Sol	solvent
$t_{¼}$	quarter-life
$t_{1/2}$	half-life
$TBAPF_6$	tetrabutylammonium hexafluorophosphate
TDDFT	time dependent density functional theory
TRIR	time resolved infrared
TZVP	triple zeta valence basis set
UV	ultraviolet
λ_{exc}	wavelength of excitation
τ	lifetime
Φ_{CO}	quantum yield for CO loss
Φ_{fl}	quantum yield of fluorescence

Abstract

Suzanne McMahon

Metal Carbonyls as Carbon Monoxide Delivery Systems

Chapter 1 serves as an introduction to the concept of carbon monoxide releasing molecules (CORMs) and their potential therapeutic applications. Previous work based on transition metal carbonyl complexes is explored. This is followed by a brief outline of the techniques used such as matrix isolation (MI) and picosecond time resolved infrared (psTRIR) spectroscopy.

Chapter 2 describes the synthesis and characterisation of methoxy-based chromium and tungsten Fischer carbene complexes. Their potential as CO delivery systems is assessed by investigating their photochemical and photophysical properties to underpin the mechanism of CO release. A novel CO release trigger, electrochemically induced CO loss is described, monitored by gas chromatography (GC).

Chapter 3 is based on a study of amino-substituted Fischer carbene complexes. The synthesis and investigation of their CO releasing abilities using photochemical, thermal and electrochemical approaches is explored. The photochemical and thermal CO releasing potential was indicated using the myoglobin assay and quantified *via* headspace analysis by GC. PsTRIR spectroscopy was used to probe the early state dynamics leading to CO loss. Electrochemically induced CO loss, using bulk electrolysis was also determined. Finally, the effects of different solvents on CO release were investigated.

Chapter 4 involves the synthesis and characterisation of a range of novel and previously reported ferrocenyl- and styryl- based Fischer carbene complexes. The photochemistry of the complexes were investigated using psTRIR spectroscopy. Electrochemically induced CO release was also assessed.

Chapter 5 highlights the synthesis and characterisation of a range of novel boron dipyrromethene (BODIPY) metal carbonyl complexes. The photophysical properties and electrochemical properties are reported. The photochemically activated CO releasing ability of these complexes is quantified in biologically compatible media using gas chromatography.

1 Chapter 1 Introduction to Carbon Monoxide Releasing Molecules (CORMs)

Abstract

This chapter illustrates the use of metal carbonyl complexes as carbon monoxide releasing molecules, termed CORMs, for use as efficient delivery systems for carbon monoxide (CO). CO is formed in mammals from the oxidation of heme by heme oxygenase enzymes. It participates in the mediation of essential biological functions and exhibits potential therapeutic properties e.g. in anti-inflammation and vasodilation. Under physiological conditions, it is essential that CO is delivered in a safe and controlled manner to specific sites due to the dangerous attributes associated with its over-exposure. These concepts lead to the development of this novel class of compounds. CORMs are mainly formed from metal carbonyls and have the ability to generate precise amounts of CO and mimic the bioactivity of CO that is formed endogenously. Various forms of CORMs based on transition metal carbonyl complexes have been investigated and analysed for their future therapeutic potential. The emphasis of this work is to highlight the previous developments of CORMs.

1.1 Introduction to CO and Carbon Monoxide Releasing molecules (CORMs)

CO is a colourless, odourless and chemically stable diatomic gas that results from incomplete combustion reactions or oxidative reactions in nature and can be found in exhaust fumes.[1-3] It has a derogatory reputation due to the fact that over-exposure of high concentrations of this gas causes many deaths each year. CO gas contains noxious properties due to the fact that it has a high affinity for the Fe^{2+} ions contained in haemoglobin in the blood. CO has the ability to poison humans as it will bind preferentially to haemoglobin, over oxygen forming carbonmonoxy-haemoglobin (HbCO), and therefore impairs oxygen transport around the body to the vital tissues and organs.[4-6] However, the predominant issue with CO is not necessarily the interference with blood, the main danger occurs when CO concentrations are elevated in the tissues causing a disturbance in mitochondrial function.[7]

Nitric oxide (NO), another common air pollutant formed from the burning of fossil fuels was found to be a critically important messenger molecule and in 1998, the Nobel Prize was awarded for discoveries based on the topic, "nitric oxide as a signalling molecule in the cardiovascular system." It was proposed that NO, a gas produced in the body, was critical for signalling.[8a] This novel principle suggested that the signal transmission by a gas which is generated in one cell, then penetrates membranes and leads to cellular function regulation. The discovery prompted further investigations into possible biological roles for other gaseous transmitters. A well-known example of a NO therapeutic agent, sodium nitroprusside, $Na_2[Fe(CN)_5NO].H_2O$ has been investigated for over 60 years.[8b] It is a hypotensive agent, administered intravenously, which has been found to decrease blood pressure by relaxation of the vascular smooth muscle as well as dilation of arteries and veins through the release of NO.[8c] Since NO^+ is isoelectronic to CO and due to the successful therapeutic actions of NO, the use of CO as a potential therapeutic agent, became a topic of interest. The first studies based on CO's ability to function as a physiological regulator were reported in 1993 by Verma *et al.* who suggested that CO may be involved in neuronal signalling.[9] Fujita *et al.* found that in wild type mice, CO gas inhalation reduced ischemia / reperfusion-induced acute lung injury by 50 %.[10] Similarly to CO, NO gas inhalation also causes a 50 % reduction of mortality caused by severe ischemia / reperfusion of the lung.

Humans produce CO endogenously in small quantities during the breakdown of heme by the heme oxygenase enzymes.[11] The basal amount of CO produced endogenously is ~16 μmol h^{-1}.[12] HO-1 and HO-2 are isoforms of heme oxygenase and are present in tissues, with high abundance in the brain (HO-2), liver (HO-1 and HO-2), spleen (HO-1), vascular endothelial cells and smooth muscle tissues (HO-1 and HO-2).[13] HO-1 expression is inducible and may be triggered in the presence of free heme whereas, HO-2 is expressed constitutively.[14] The rate of CO production in the body is increased in various pathological states, for example in asthma, which suggests that the formation of CO increases to counteract stressful conditions.[15] Also, the expression of HO-1 is increased when the body undergoes oxidative stress and inflammation. A common example of this heme breakdown and hence CO formation can be observed in bruising (Figure 1.1).[16] During the injury that leads to the development of a bruise, haemoglobin is liberated from lysed red blood cells which results in a purple / dark red colour which is evident under the skin. The colour is associated with deoxygenated haemoglobin. CO is then enzymatically produced during the metabolism of heme, present in the vascular tissue, by heme oxygenase. Consequently, oxygen is consumed in the extravascular space forming a blue coloured oxygen-free haemoglobin. This proposed reaction also generates ferrous iron (Fe^{2+}) and biliverdin (a green pigment antioxidant) which is further reduced to bilirubin (yellow colour which gradually fades away) by biliverdin reductase (Scheme 1.1).[17] Some CO can bind to haemoglobin's Fe centre forming a bright red coloured product known as carbonmonoxyhaemoglobin (Mb-CO).[16,18]

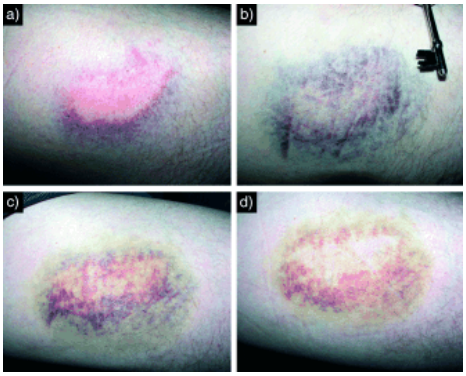

Figure 1.1 The changing visualisation of a bruise with increasing time. a) Taken 12 hours after injury occurred, red and purple in colour due to liberated oxygenated heme; b) Taken 48 hours after injury occurred, biliverdin is formed resulting in green tinges; c) Taken 48 hours after injury, following the formation of bilirubin, a yellow colour is noted; d) Taken 10 days after injury; some residual bilirubin is observed and the bright red colour is attributed to the formation of Mb-CO.[16]

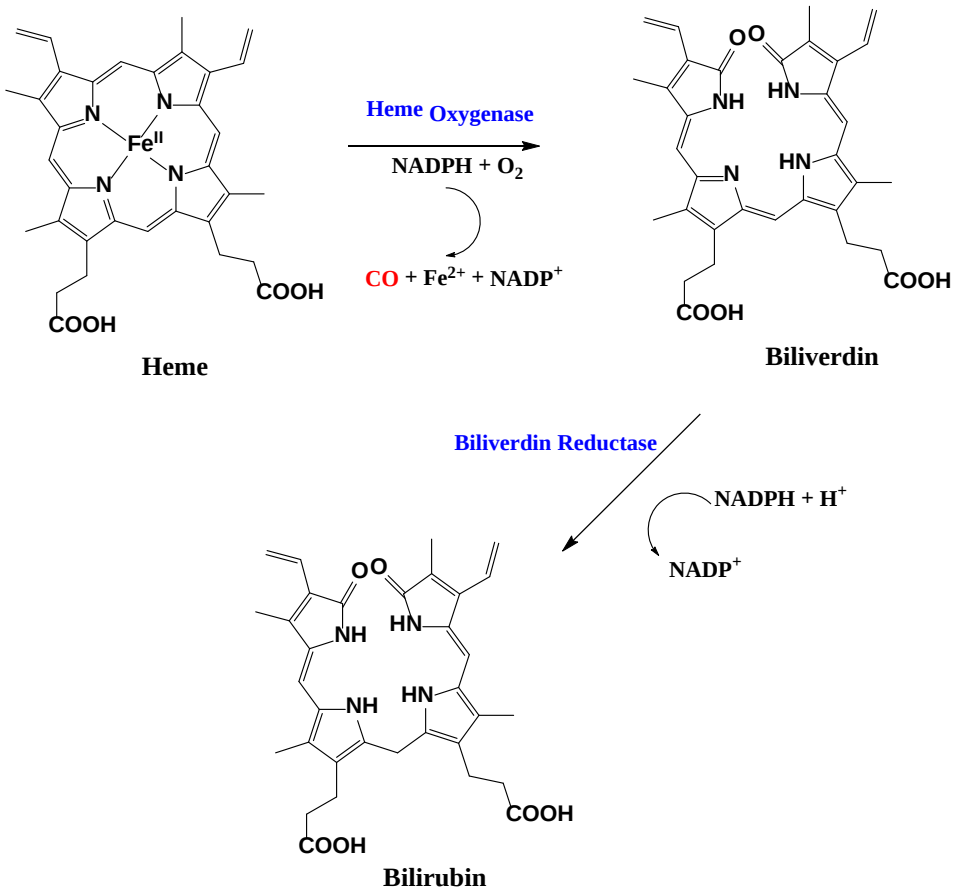

Scheme 1.1 The proposed breakdown of heme by HO to form CO, Fe^{II} and biliverdin.[17]

CO has many versatile advantages associated with it. It has anti-inflammatory, anti-apoptotic, anti-proliferative and vasorelaxant properties.[15] CO can protect against ischemia reperfusion injury and plays a dominant role in the alleviation of cardiovascular disorders and in organ transplantation.[13] Other benefits have been seen in functions of neuroendocrine and in ion channel activation. These key advantages of CO gas therapy have lead it to clinical trials.[19] However, the use of CO gas inhalation poses many problems. When inhaled, it passes through the lungs as a mixture of air and CO, usually with an administration concentration of 200 ppm. It is difficult to control and the whole body is targeted as opposed to defined areas.[20] It is highly necessary that CO gas, when used therapeutically is administered in a controlled and safe manner to target sites. Exact concentrations of CO should be delivered to precise locations under physiological conditions. A safer method of delivery was developed in the form of a novel class of compounds known as carbon monoxide-releasing molecules (CORMs).[1,21] These are compounds that have the means to transport controlled, defined amounts of CO to target areas and specific sites of interest.[22] It was found that transition metal carbonyls can function as CORMs and have a similar bioactivity to that of endogenously produced CO.[23] Figure 1.2 shows the advantages of CORMs over CO gas inhalation.

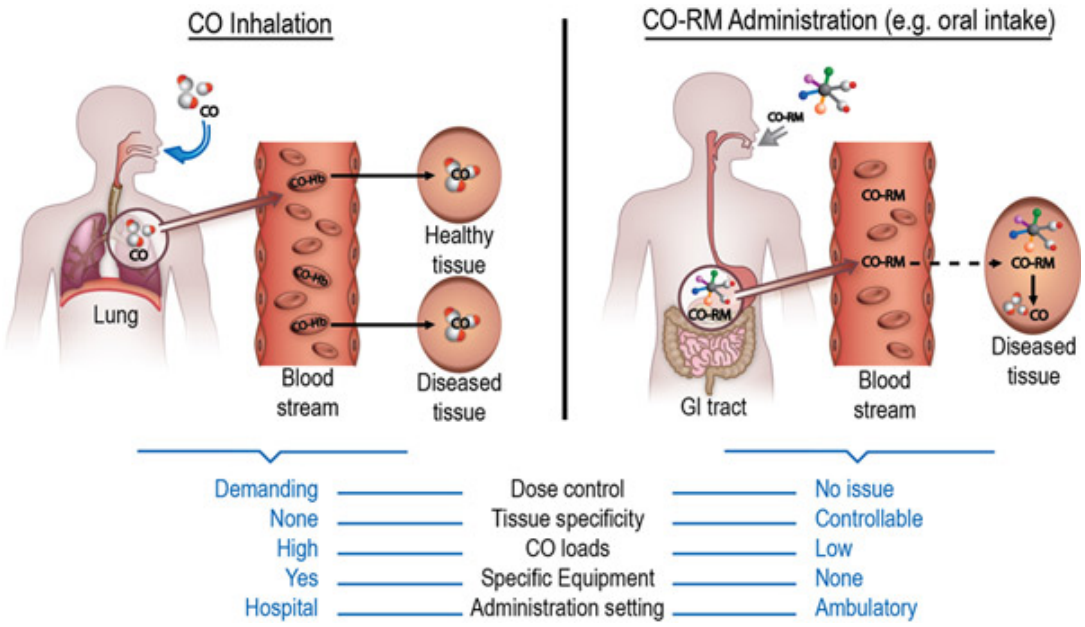

Figure 1.2 A comparison of the advantages and disadvantages of CO gas inhalation *vs.* CORMs. [17]

Iron pentacarbonyl ($Fe(CO)_5$), dimanganese decacarbonyl ($[Mn_2(CO)_{10}]$), the latter more commonly known as CORM-1 and the tricarbonyldichloro ruthenium(II) – dimer, $[Ru(CO)_3Cl_2]_2$, termed CORM-2, were the first complexes investigated for CO release, reported by Motterlini *et al.*[21] These complexes exhibited CO releasing properties in biological systems that mimicked the pharmacological effects of heme oxygenease - derived CO. However, $Fe(CO)_5$ is a highly toxic complex and was not further tested *in vivo*. CORM-1 and CORM-2 did not promote any detectable toxicity and exhibited therapeutic action against cardiovascular disorders, for example, hypertension. However, these complexes are only soluble in organic solvents. It was also necessary to use UV irradiation for $Fe(CO)_5$ and CORM-1 to release CO. The method used to detect CO release from these systems was first reported by Motterlini and co-workers and is known as the myoglobin assay.[21]

The myoglobin (Mb) assay (deoxygenated-myoglobin (deoxy-Mb) / carbonmonoxy-myoglobin (Mb-CO) UV-vis assay) is the primary method of analysis to determine the release of CO from CO releasing molecules.[21] It quantifies the release of CO, generated from CORMs in a protein-based aqueous media at physiological temperature, 37 °C and pH, 7.4.[21] The main theory behind the assay is that, if a certain complex can liberate CO into solution, deoxy-Mb will be readily converted to Mb-CO. This concept is illustrated in the Q-band region of the heme group, present in deoxy-Mb and Mb-CO. UV-vis spectroscopy is the principal tool used for this measurement.[24,25] The concentration of Mb-CO is measured by determining the change in absorbance at a fixed wavelength (usually 540 nm). The most commonly used method for comparing CORMs is by quoting their half-life ($t_{½}$) values which quantitatively compare CO release from different CORM systems that may occur by different mechanisms. Regarding CORMs, it is explained as the time taken for a solution of a CORM with a concentration of 60 µM to produce a solution of Mb-CO with a concentration of 30 µM (or 40 µM to form 20 µM and 20 µM to form 10 µM).[21] An example of a myoglobin assay CO release profile is illustrated in Figure 1.3.

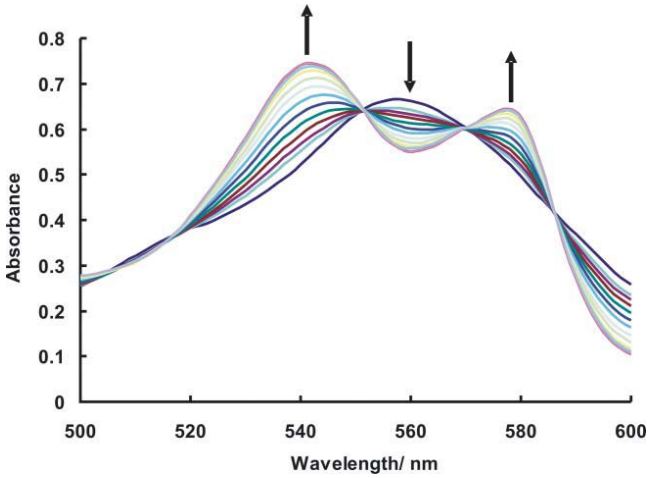

Figure 1.3 Release profile for the representative CORM, $[Et_4N][CrI(CO)_5]$, demonstrating the conversion of deoxy-Mb to Mb-CO over time using the Q band region of the heme group. The increasing lines indicated by the upward arrows highlight the formation of Mb-CO and downward arrows show the depletion of deoxy-Mb. [26]

1.2 Metal Free CORMs

Initially, a number of organic compounds (e.g. dialkylaldehydes, oxalates, silacarboxylic acids, and haloalkanes) were investigated for potential use as CORMs in biological applications. However, these systems were not suitable due to their CO release rate and toxicological profiles. Hence, development of these compounds was not pursued.[17] For example, silacarboxylic acids require harsh temperatures or harsh conditions i.e. strong bases to activate CO release and are therefore incompatible with biological systems.[27] However, a noteworthy exception to this was the development of the water soluble complex, $Na_2[H_3BCO_2]$, termed CORM-A1, a main group boranocarbonate, Figure 1.4.[28] CORM-A1 releases CO at a slow rate ($t_{½}$ = ~21 min, 60 μM) and is pH and temperature dependent.[29] More recently, the development of organic based CORMs was reported by Antony *et al.* who showed that a fluorescein xanthene-9-carboxylic acid derivative was an efficient metal-free photoactivatable CO releasing molecule (photoCORM) when irradiated at 500 nm, Figure 1.4.[30] Peng *et al.* also developed a fluorescent metal free photoCORM based on a micelle encapsulated unsaturated 1, 2 - diketone (DK) which released CO following irradiation at 470 nm.[31]

These systems can be tracked by fluorescence imaging microscopy. Most CORMs to-date have been mostly based on transition metal carbonyl complexes.

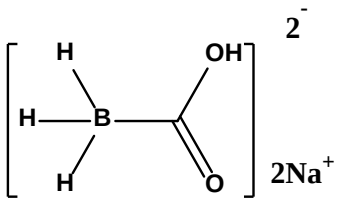

CORM-A1

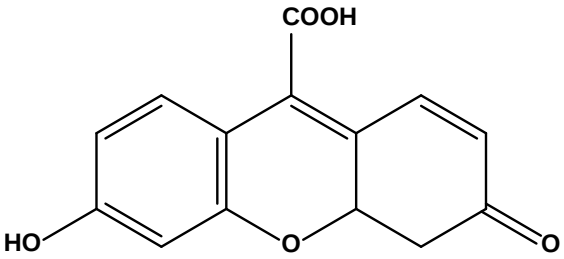

Fluorescein xanthene-9-carboxylic acid based CORM

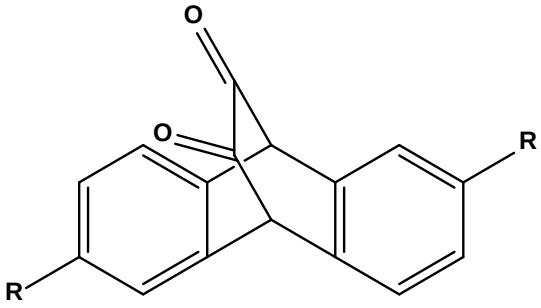

DK

Figure 1.4 The structural representations of some transition metal free CORMs, CORM-A1, the fluorescein xanthene-9-carboxylic acid derivative and an unsaturated 1, 2 - diketone (DK).[28, 30, 31]

1.3 Transition Metal Carbonyl Complexes as CORMs

Transition metal carbonyl complexes pose as excellent candidates for CO delivery systems and are the preferred complexes of choice due to their design flexibility. Metal carbonyl complexes have been available for decades, however, more recently, their ability to lose CO has been exploited in biological systems for therapeutic use. Different metals and functionalities can be incorporated into these systems to aid CO release, promote water solubility and in some cases direct the CORM to target areas in the body. Metal carbonyl complexes can have many CO ligands attached. This is beneficial as it means lower doses of the CORM could be administered as there would

be less accumulation of metal and ligand by-products in the body. The nature of the metal and co-ligands that make up the 'CORM sphere' can determine the rate of CO release. It has not been established whether CO release should be fast or slow and it will depend on the nature of the medical condition.[7] Some metal-based CORMs contain trace elements present in the body such as Fe, Mn and Co.[14] Other CORMs incorporate non-physiological metals; W and Re. Certain criteria should be met in order for a metal carbonyl complex to function as a CORM. Ideally, the complexes should not exhibit cytotoxic properties prior to and post CO release and reaction products should be identified. They should be stable for storage under ambient conditions. The CORM must be active and potent at the diseased tissues and survive circulation so that they can reach their target sites. There should be a controlled, defined release of CO and the complexes should be preferably water soluble or at least soluble in an aqueous based media.[17,32] However, recently, novel technologies have been developed to overcome the by-product toxicity and water solubility problems associated with CORMs by incorporating polymer conjugates,[33,34] nanoporous non-wovens[35] and nanoparticles into the CORM sphere.[36]

Understanding the chemistry of transition metals is critical for the development of CORMs. CO is a stable naturally occurring compound. The carbon is in a rare 2^+ oxidation state. Ten valence electrons are distributed over three bonds and one lone pair is present on each atom.[17] There are σ-donor HOMO (Highest Occupied Molecular Orbital) and π-acceptor LUMO (Lowest Unoccupied Molecular Orbital) orbitals which interact with metal ions / atoms forming a metal to carbonyl (M-CO) bond.

An electron pair from the HOMO of CO is donated to an empty metal orbital (MO) resulting in the formation of a σ bond. When the energies are degenerate, back-bonding may occur. This happens when another π-acceptor interaction occurs when the occupied metal *d* orbitals overlap with the empty low lying MOs on CO. This is a main feature of transition metal carbonyl complexes. Since CO accepts electrons in orbitals containing π symmetry, CO can be termed as a π acceptor or π acid. The M-CO bond is synergistic in nature. This means that the donation of a stronger σ bond will increase the electron density centred at the metal which will enhance π back donation. This bonding concept is favoured for low oxidation state metals with filled

high energy *d* electrons allowing back-bonding to occur (Figure 1.5). This explains why the formation of carbonyl complexes with transition metal centres is favoured. The manipulation of electron withdrawing and electron donating co-ligands on the metal carbonyl complex can alter the strength of the M-CO bond and hence, fine tune the reactivity of the complex. Backbonding will be weakened by a decrease of *d* electron density of the metal since an increase of positive charge of a metal ion compromises effective back donation. This promotes CO release due to the labilisation of the bond. This can occur in a number of ways. The low-valent metal centre can be oxidised by chemical or electrochemical means.[7,17] Photochemically, electron density is transferred from the electron rich metal centres to the π* MOs of the ligand frame *via* strong metal to ligand charge transfer (MLCT) transitions. The absorption of light can reduce the metal charge density in the excited state which would weaken the M-CO backbonding, promoting the photo release of CO.[7,17]

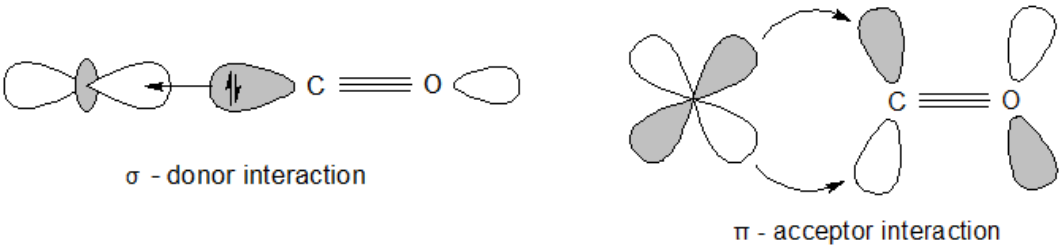

Figure 1.5 Backbonding nature of metal carbonyl complexes.

1.4 Activation of CO Release from CORMs

Essentially, CORMs are pro-drugs that upon activation, release CO. Various triggers such as thermal, photochemical, electrochemical or enzymatic stimulation can cause dissociation of CO from CORMs. A substitution reaction may also occur in co-ordinating solvents i.e. CH_3CN or H_2O. The release rate of CO can also be influenced by the biological environment, for example, the oxidation environment and pH.[6]

1.4.1 Thermally Activated CO Release

Metal carbonyl complexes undergo a general thermal dissociation reaction. Upon heating, the M-CO bond breaks and CO is released. The vacant position that remains can then be occupied by another ligand, to stabilise the complex. This ligand substitution can occur *via* thermally activated dissociative or associative mechanisms. However, the application of thermal CO release is restricted biologically as temperatures cannot exceed that of body temperature, 37 °C. For "thermal dissociation" to occur (CO release at body temperature), the starting complex would need to be rather unstable at room temperature. This poses problems regarding the synthesis and stability of the complexes. To date, most metal carbonyl complexes have been activated for CO loss in this way. CORMs must survive circulation to ensure they can localise and be activated at their target sites. This is the main disadvantage associated with thermal CORMs.

The first thermal CORM developed was $[Ru(CO)_3Cl_2]_2$ (CORM-2), followed by its water soluble analogue $[Ru(CO)_3Cl(glycinate)]$, (CORM-3). Both CORMs are illustrated in Figure 1.6. CORM-2 releases CO spontaneously in neat DMSO with a half-life of 0.5 min and CORM-3 exhibits a solvent dependent CO release profile which is further influenced by pH. CORM-3 releases one mole equivalent of CO per one mole of complex *via* ligand exchange with a half-life of 4 - 18 min. [6,37,38]

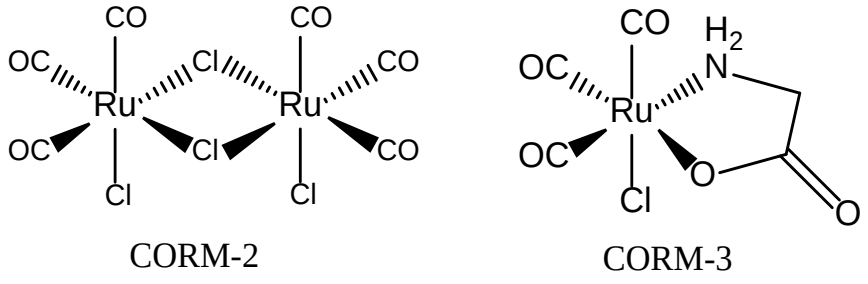

CORM-2 CORM-3

Figure 1.6 Structural representations of $[Ru(CO)_3Cl_2]_2$, CORM-2 and $[Ru(CO)_3Cl(glycinate)]$, CORM-3.[37]

Many examples of thermal CO releasing molecules have been reported since the discoveries of CORM-2 and CORM-3. 2-pyrone iron (0) carbonyl complexes have been developed and investigated for CO release.[39,40] These complexes are representative of the first developed CO-releasing molecules that consist of a η^4-co-ordinated diene ligand and an iron tricarbonyl moiety. The halogen substituent on the 2- pyrone ring affects the extent and rate of CO release. The release rate of CO was measured using the myoglobin assay and it was discovered that when the bromide substituent at position 3 of the 2-pyrone ring, CORM-F3, is replaced with a chlorine substituent; CORM-F8, the release rate decreases from 0.19 μM / min to 0.041 μM / min. When the 4- and 6-positions of CORM-F3 are exchanged with a methyl group ([η^4-4-(4-methyl-6-methyl-2-pyrone) tricarbonyl iron(0)], CORM-F11 and a hydrogen group ([η^4-4-(4-chloro-2-pyrone) tricarbonyl iron(0)], CORM-F7, the release rate further decreases. Cytotoxicity studies were performed and the results indicated that CORM-F3 and CORM-F8 were the least cytotoxic such that no detectable toxicity was observed at 10 – 100 μM concentrations. In general, CORM concentrations of 20 - 60 μM are tested for CO release. CORM-F8 exhibited weak toxic effects at 100 μM whereas CORM-F7 and CORM-F11 were very damaging to cells at 100 μM. The η^4 – pyrone iron tricarbonyl based CORMs can be observed in Figure 1.7.

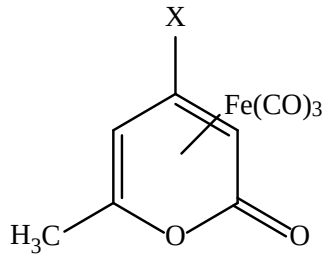

X = Br (CORM-F3),
Cl (CORM-F8),
CH_3 (CORM-F11)

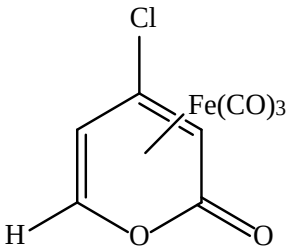

CORM-F7

Figure 1.7 η^4 – Pyrone iron (0) carbonyl complexes assessed for CO release.[39,40]

1.4.1.1 Thermal-CORMs based on Group 6 Transition Metals Cr, Mo and W

Fairlamb *et al*. also evaluated the CO releasing abilities of 2 - pyrone iron(II) and molybdenum(II) complexes.[41] The iron complexes did not release CO when monitored using the myoglobin assay. In contrast, the Mo based CORMs did release CO under the same conditions. For CORM-F10, rapid CO release (17.0 µM) was observed after 5 minutes whereas on the same timescale, CORM-F4 released 0.6 µM of CO. After 1 hour, CORM-F10 released a total of 49.0 µM of CO and CORM-F4 released 7.2 µM of CO. The structural representations of CORM-F10 and CORM-F4 are highlighted in Figure 1.8. These results reinforce how subtle modifications in the structure of CORMs can significantly alter the CO release profile.

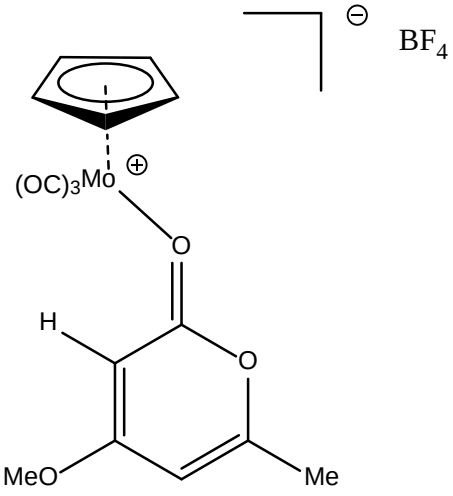

CORM-F4

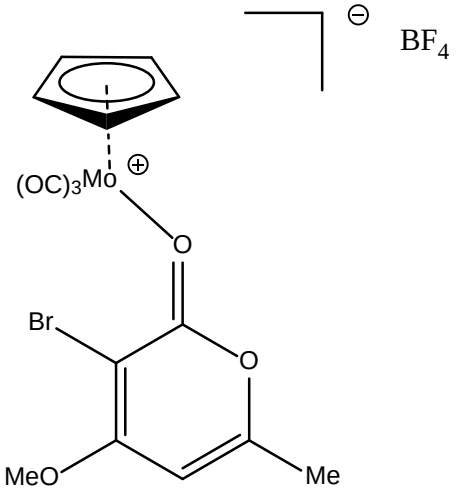

CORM-F10

Figure 1.8 Structural representations of 2-pyrone molybdenum tricarbonyl complexes.[41]

Other possible CORMs may be present in the form of cationic and anionic complexes. Cationic complexes, for example, $[Mn(CO)_4(bpy)]^+$ (bpy = 2,2′-bipyridine), exhibit slow liberation of CO ($t_{½}$ = 5,000 min) whereas anionic complexes, for example, $[Mn(CO)_4Br_2]^-$, demonstrate a rapid release of CO ($t_{½}$ = < 2 min). However, the mechanism of action for such ions is inconclusive.[1]

Lynam and co-workers studied a diverse range of metal carbonyl complexes for their CO releasing potentials.[26] For octahedral d^6 complexes, the CO release rate increased

in the following manner, $FeI_2(CO)_4$ > $[NEt_4][V(CO)_6]$ > $MnBr(CO)_5$ > $Cr(CO)_6$. This suggests that, in this case, CO release is not solely dependent on the strength of the metal – carbon bond. In contrast, d^4 metal complexes depend on the nature of the metal e.g. $[NEt_4][MX(CO)_5]$ (where M = Mo or W and X = Br or I). CO release investigations using the myoglobin assay revealed that Mo carbonyls generate CO more rapidly than W based carbonyls but at a slower rate than Cr carbonyls. A mechanistic study into the way in which CO is released from these complexes, on the water soluble $[MX(CO)_5]^-$ systems, demonstrated that hydrolysis of the M–X bond determines the CO release rate in aqueous systems. In addition, the following potential CORMs; $[NEt_4][CrCl(CO)_5]$ and $[NEt_4][CrBr(CO)_5]$ liberate approximately two molecules of CO per CORM which exhibits promising therapeutic potential.[26]

Zhang *et al*. showed that amino acids and amino esters may be incorporated into the co-ordination sphere of group 6 metal carbonyl complexes to improve biocompatibility by aiding water solubility and reducing potential toxic effects.[42] Investigations were performed on $M(CO)_5$ based CORMs (where M = Cr, Mo or W). These $M(CO)_5L$ based molecules, (where L is a biologically compatible leaving group), are interesting targets with the potential to liberate five CO molecules per metal complex. This would be beneficial in lowering the dosages of CORMs required for administration. It was found that the biocompatible organic group plays a significant role in the control of CO release and the principle mode of action is based on the loss of this group. A clear correlation between the electrophilic nature of the carbene carbon and rate of CO released, quantified by the myoglobin assay has been established which indicates that a primary step in this process may be due to nucleophilic attack by water. The nature of the metal and amino ester present in a specific complex determines the release rate of CO. For example, the half-lives of the complexes illustrated in Figure 1.9, at a concentration of 60 μM are as follows (**1**)–Cr (573 s), (**1**)-Mo (247 s), (**1**)-W (3,350 s*) and (**2**) did not release CO (* = time taken to reach a Mb-CO concentration of 10 μM). This investigation proved that the concept offers significant potential in the control of the release rate of CO which may determine the optimum conditions needed in certain circumstances.

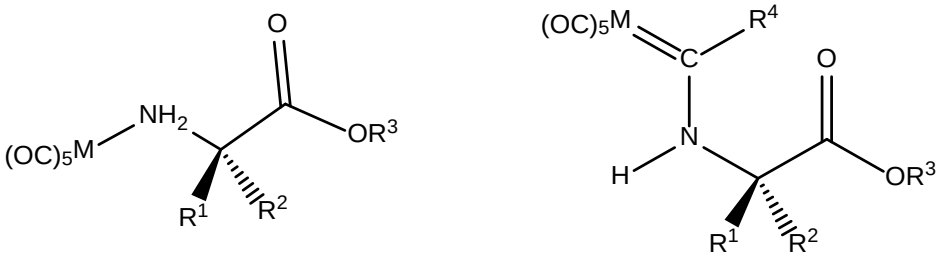

(1) **(2)**

Figure 1.9 Examples of the structural representations of the developed bio-compatible metal carbonyl complexes, (**1**) $[M(CO)_5(NH_2CH\{R^1\}\{R^2\}CO_2R^3)]$ where M = Cr, Mo, W, R^1 = H, R^2 = H and R^3 = Et. (**2**) $[(CO)_5M{=}C\{R^4\}(NHCH\{R^1\}\{R^2\}CO_2R^3)]$ where M = Cr, R^1 = H, R^2 = H, R^3 = Et and R^4 = Me.[42]

More recently Marques *et al.* studied a series of molybdenum (0) carbonyl complexes, $Mo(CO)_5(L)$ or $Mo(CO)_3(L)_3$ where L = monodentate ligands.[43] These Mo based CORMs were used to treat liver disease caused by acetaminophen poisoning. The CORMs were assessed in a murine model of acetaminophen induced acute liver injury. The complexes were designed to preferentially distribute to the liver and release CO through liver metabolism. A complex termed, ALF794 (Figure 1.10), is the first CORM to specifically target and release CO to an organ *in vivo* in a controlled and specific manner.

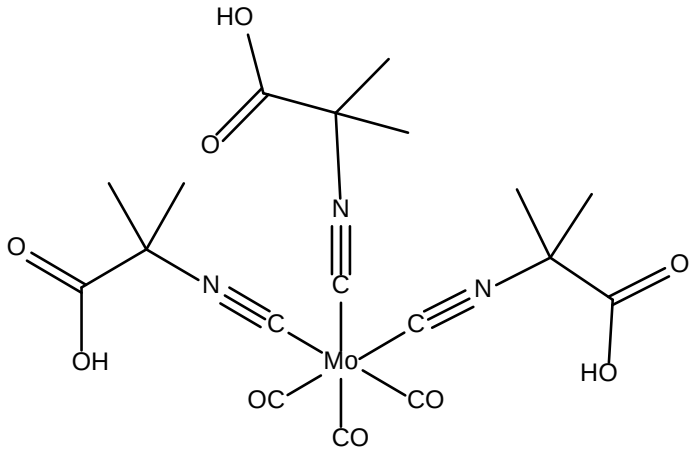

ALF794

Figure 1.10 The first CORM, ALF794, to target an organ (the liver) in a specific and controlled way.[43]

Seixas *et al.* also focused on molybdenum carbonyl complexes and investigated the complex, *fac*-[Mo(CO)$_3$(histidinate)]Na, termed ALF186 (Figure 1.11).[44] This complex is soluble and stable in degassed water. It is also stable in normal air at room temperature for up to two months. However, when in water, in the presence of oxygen, the complex readily decomposes. Therefore, CO release into the blood and other tissues begins rapidly upon administration of ALF186 by intravenous (i.v.), intraperitoneal (i.p.) or by oral means. This complex is known as an oxygen triggered CORM.

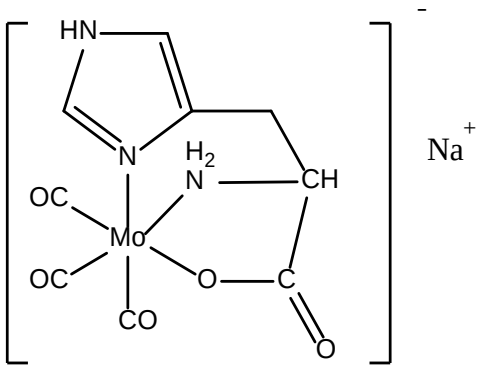

ALF186

Figure 1.11 *fac*-[Mo(CO)$_3$(histidinate)]Na, termed ALF186; an oxygen triggered CORM.[44]

1.4.2 Photochemically Activated CO Release

CORMs that release CO upon photochemical stimulation are known as photoCORMs. They are a highly useful class of compounds as they allow for specific control meaning the dosage, location and timing are easily regulated. Certain metal carbonyls undergo photo-excitation of the M-CO bond which results in CO release.[45] Of course, it is necessary to use various wavelengths of incident light to promote CO loss depending on the nature of the metal carbonyl complex and the strength of the M-CO bonds. Ideally, the CORM should absorb sufficiently to release CO upon irradiation from low energy photons, within the photodynamic therapeutic window (600 - 800 nm) to minimise damage to healthy tissues which may come in contact with the beam (Figure

1.12).[32] Also, it should be ensured that sufficient penetration occurs to target the site. The wavelength of the light source used should be selected carefully for this reason. The penetration depth of light into targeted tissues is wavelength dependent. Very little penetration is possible using UV light. Improvement in penetration depth occurs as the absorbance of the particular CORM is red shifted with optimal penetration at the near IR region of the spectrum. In addition, the CORM should be stable in air and in the absence of light in a bio-compatible solvent for a period of time long enough for accumulation of the CORM to localise at the targeted site. The main strategies employed to meet this criteria are as follows;[46]

1) Red shift the absorption maximum of the photoCORM by using suitable combinations of metals and co-ligands.
2) Attach a photosensitiser to the metal carbonyl functionality i.e. organic dyes.
3) Use two photon absorption to promote CO release.

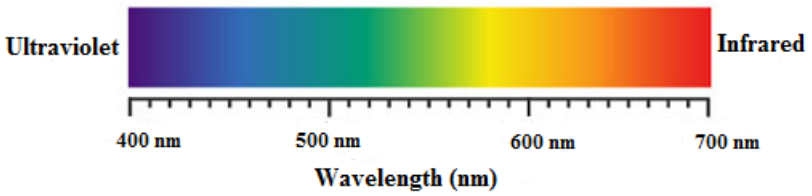

Figure 1.12 Visible light spectrum.

Figure 1.13 gives a simple schematic on the mechanism representing CO dissociation that occurs from a sample CORM upon irradiation. The CORM is stimulated and CO is released. The CORM interacts with the solvent, and the solvent binds to the vacant site at the metal centre to stabilise the complex.

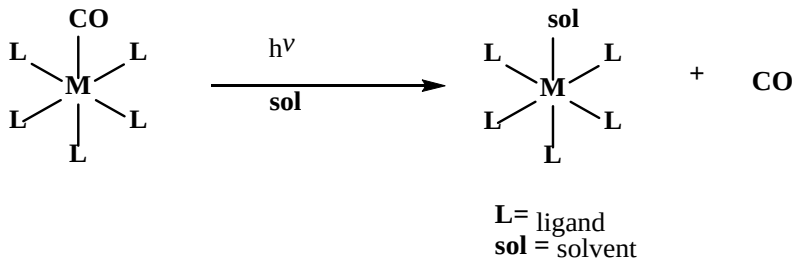

Figure 1.13 Solvent interaction upon photolysis of a CORM.

The first identified photoCORMs for use in biological applications, CORM-1, ($Mn_2(CO)_{10}$), and $Fe(CO)_5$ were reported by Motterlini *et al.*[21] The myoglobin assay confirmed CO release was promoted by UV light. Since, CORM-1 exhibited cardio-protective properties, further developments based on photoCORMs arose. Also, as previously mentioned in the introduction, $Fe(CO)_5$ is volatile and very toxic and could not be used as a CORM.[21] However, further developments on iron based photoCORMs have since been reported.

The water soluble complex, dicarbonyl - bis (cysteamine) iron (II), *cis*-$[Fe(CO)_2(H_2NCH_2CH_2S)_2]$, termed CORM-S1, is an iron based CORM containing biogenic ligands (ligands produced from a living organism; cysteamine is produced *in vivo* from the degradation of cysteine). CORM-S1 showed rapid CO release at λ_{exc} > 400 nm, quantified by the myoglobin assay. The irradiated, 50 μM sample was 31 times more efficient at releasing CO than the dark sample over the duration of the experiment (15 minutes).[47] This compound showed potential as a photoCORM since it is comprised of bio-compatible ligands and is water soluble. However, photo-induced CO released by irradiation further towards the red region of the spectrum would be more suitable. Also, the stability of the parent complex would need to be assessed over a longer time frame.

1.4.2.1 Photo-CORMs based on Group 6 Transition Metals Cr, Mo and W

Long before the concept of using CORMs for CO delivery *via* phototherapy, photochemically active group 6 metal carbonyl complexes were widely studied due to their rich photochemical and photophysical properties.[48] However, they have not been widely studied as CORMs; systems that release CO in biocompatible solvents for therapeutic applications. The use of group 6 metal carbonyls for photo-induced CO loss as potential CORMs has been reported in the literature mainly by Rimmer, Pierri and Ford.[32] Rimmer *et al.* investigated the CO releasing ability of the complex ions; $M(CO)_5(TPPTS)^{3-}$ (M = Cr, Mo and W and TPPTS = 3,3,3´ phosphane triyltris(benzene sulfonic acid)trisodium salt) shown in Figure 1.14.[49] The chromium and tungsten analogues were stable in the absence of light in aerated aqueous buffer solutions. UV irradiation (313 nm) of both species resulted in spectroscopic changes

and hence, CO release in argon deaerated solutions. However, in aerated solutions, when irradiated at 313 nm, different spectroscopic changes were observed. In addition, precipitates formed which indicated that the photoproducts formed post CO release were air sensitive. The tungsten analogue showed the best CO releasing ability (~0.9 equivalents of CO per mole of complex were released in the primary photochemical step). This was measured in different ways; using FTIR analysis, flash photolysis, quantum yields for CO loss and by gas chromatography. It was observed that the intermediate generated upon photolysis, $[W(CO)_4(H_2O)(TPPTS)]^{3-}$ may continue to lose CO under aerobic conditions. This was thought to be a significant factor for CO delivery strategies; the conversion of an air stable CO carrier to an easily oxidised species upon photoexcitation. The intermediate produced is known as a "pro-CORM". Again, although CO is released, irradiation at 313 nm would be harmful to the body and further developments were needed.

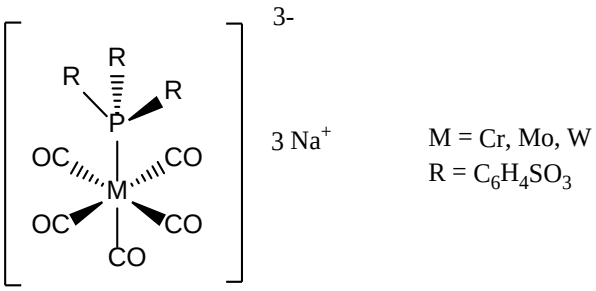

M(CO)$_5$(TPPTS)

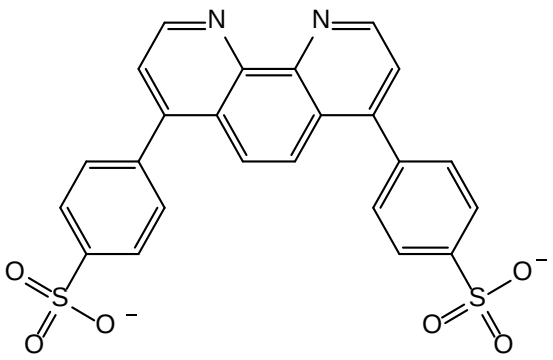

BPSA

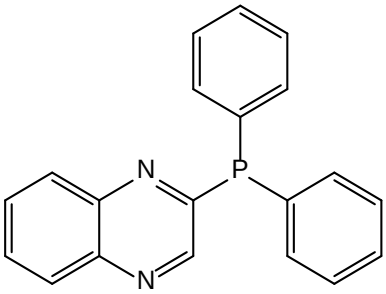

DPPQ

Figure 1.14 Group 6 metal carbonyl CORMs and ligand structures reported by Rimmer *et al.* [49]

Rimmer *et al.* continued investigations on Cr, Mo and W based CORMs. The complexes $Na_2[M(CO)_4(BPSA)]$, where M = Cr, Mo, W and BPSA = bathophenanthrolinedisulfonate (Figure 1.14) were analysed for CO release. The Cr and W based complexes were not studied as potential CORMs due to their unstable nature. The Mo analogue exhibited reversible photolabilisation in deaerated aqueous media but not in aerobic aqueous solutions. However, thermal degradation in aerobic aqueous solutions occurred and therefore hindered development. Hence, no further studies were undertaken.[32]

The complexes, $M(CO)_4(DPPQ)$ where M = Cr, Mo, W and DPPQ = diphenylphosphinoquinoxaline (Figure 1.14) were studied for CO release. These complexes were thermally stable in the absence of light and released CO when irradiated into the lowest MLCT transition at 436 nm. The chromium analogue demonstrated the most efficient CO loss profile and had the highest quantum yield value for CO loss. All four CO ligands were dissociated. However these complexes had limited solubility.[32]

Another study involving group 6 metals incorporated into photoCORMs was reported by Lynam and co-workers (Reaction 1.1).[50] The photo CO releasing abilities of molybdenum complexes containing functionalised alkynyl ligands were analysed. When $[MoCl(\eta^5\text{-}C_5H_5)(CO)_3]$ is reacted with propargyl alcohols ($HC{\equiv}CCR^1R^2OH$) using NEt_2H as a solvent, in the presence of catalytic quantities of CuI, alkynyl complexes i.e. $[Mo(C{\equiv}CCR^1R^2OH)(\eta^5\text{-}C_5H_5)(CO)_3]$ are formed. CO release was exhibited from a water soluble sugar substituted alkynyl complex which contained a β-D-fructopyranose group following irradiation at 325 nm. Incorporating biocompatible groups such as sugars into the co-ordination sphere of a bio-compatible metal, Mo, is an attractive design for photoCORMs, however, high energy UV light is required for CO release.

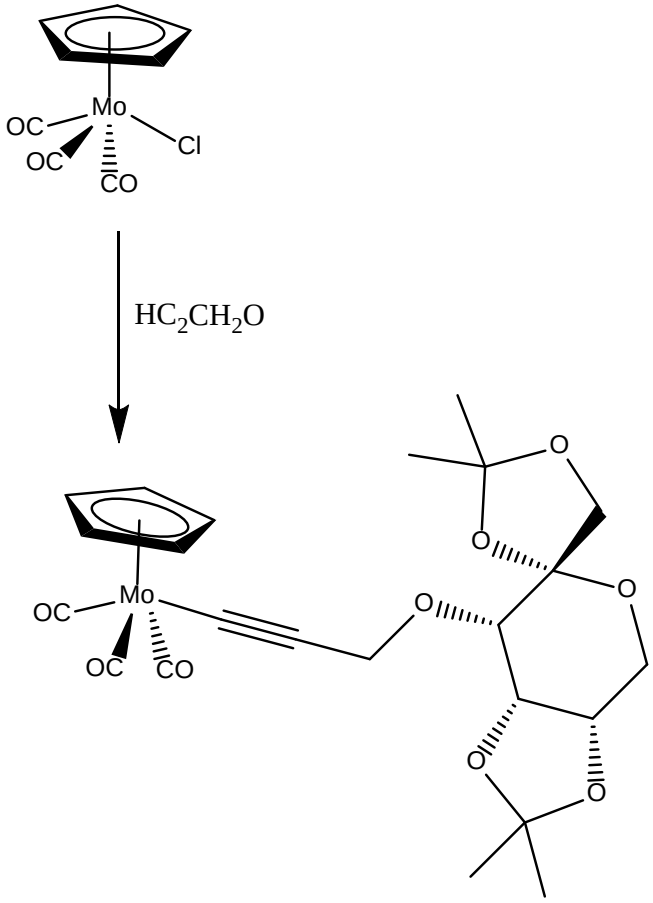

Reaction 1.1 Reaction of the novel water soluble, β-D-fructopyranose molybdenum carbonyl complex.[50]

The work presented in the forthcoming chapters will focus on CO release from chromium and tungsten based pentacarbonyl complexes. These metals were chosen due to their potential to release five CO molecules per mole of metal complex.

1.4.3 Enzyme Triggered CO Release

It is essential to have control over the CO release exerted from CORMs. Since some CORMs that undergo ligand exchange reactions start to release CO as soon as they enter biological environments, recent developments have been made to design CORM prodrugs that are stable in biological media and are triggered by a very specific stimulus. This lead to the progress of a new class of CORMs, enzyme-triggered CORMs (ET-CORMs), introduced by Schmalz and co-workers.[51-53]

Initially, a range of acyloxybutadiene-iron tricarbonyl complexes were synthesised. These compounds are stable in buffer under physiological conditions. Esterase triggered CO liberation was activated by enzymatic hydrolysis. Pig liver esterase (PLE) and lipase from *candida rugosa* (LCR) were found to be most suitable. The enzymatic cleavage of an ester bond results in a rearrangement forming intermediates that are prone to oxidative decomposition. This weakens the Fe-CO bond and hence three CO equivalents per molecule of complex are released, as observed *in vitro* using the myoglobin assay in the presence of the esterases. The biological potential was then probed and anti-inflammatory effects were assessed by cellular assays based on the inhibition of NO production by inducible NO synthase (iNOS). It was found that cytotoxicity, the rate of esterase-triggered release and iNOS inhibition of these ET-CORMs are strongly dependent on the acyloxy substituent.[51]

Further developments by this group incorporated water soluble functionality into complexes based on dienylphosphate iron tricarbonyl complexes (the first water soluble ET-CORMs), illustrated in Figure 1.15. CO release was induced by different phosphatases and was measured using headspace gas chromatography at 37 °C in 0.1 M phosphate buffer (pH = 7.4).[54]

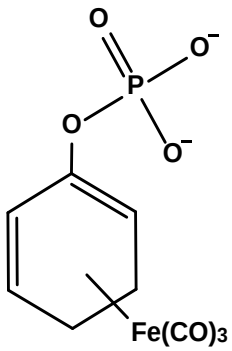

Figure 1.15 The first water soluble based enzyme triggered CORM, a dienylphosphate iron tricarbonyl complex.[54]

Examples of the ET-CO release process is illustrated in Scheme 1.2. Healthy and diseased sites express different quantities esterases and since CO release is dependent on the certain type of esterase, it may allow for locally restricted CO release in target areas.[7]

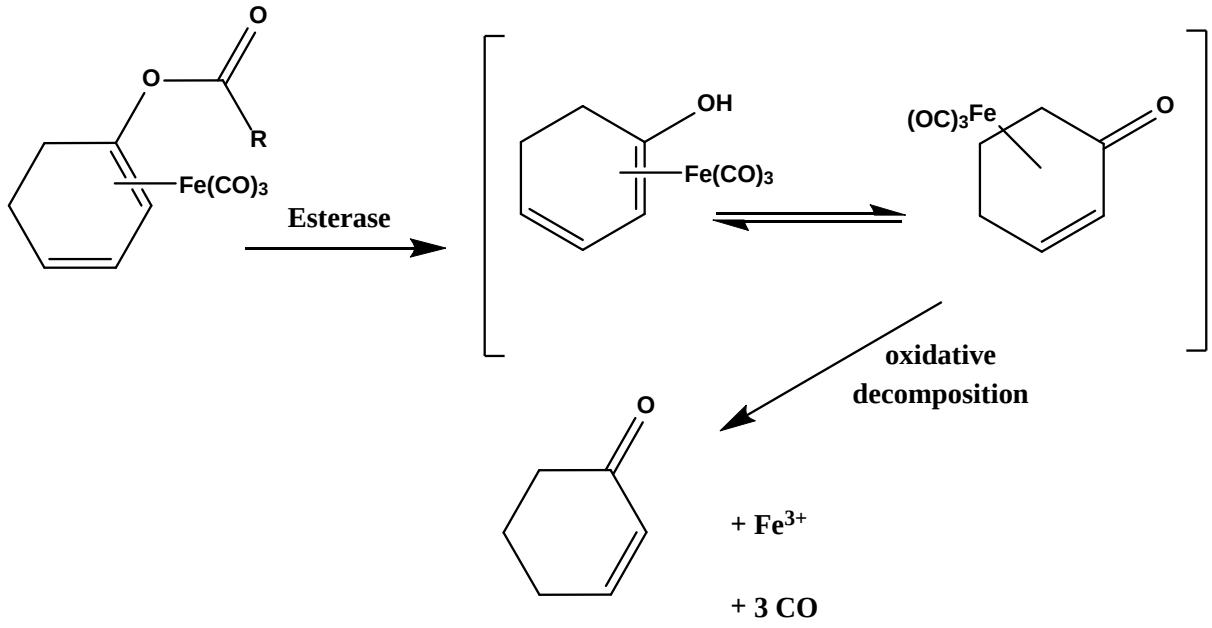

Scheme 1.2 Enzyme Triggered CO release from acyloxybutadiene-iron tricarbonyl complexes.[51-53]

1.5 CORM Carriers

1.5.1 Polymer based CORMs

The administration of CO from CORMs has been faced with problems for use in medical applications. Many technologies have been developed to overcome solubility issues or bio-instability of CORMs. For example, following the development of CORM-1 and CORM-2, drawbacks were demonstrated regarding their insolubility in aqueous media. This prompted the development of the first prototypic water soluble CORM, tricarbonylchloro (glycinato) ruthenium (II) (CORM-3). This is a modified version of CORM-2 i.e. glycine (an amino acid) is co-ordinated to the ruthenium metal centre (Figure 1.6). This compound releases one mole equivalent of CO per one mole of CORM-3 and CO release occurs *via* ligand exchange (substitution of the chloride or glycinate ligands with electron withdrawing ligands e.g. thiol compounds).[6,37,38] CORM-3 displays vasoactive and cardio protective properties. It has a half-life of 98 hours in distilled water at 37 °C. However, in the presence of human plasma, this is

reduced to just 3.6 min.[55] CORMs will instantly come in contact with high concentrations of biomolecules when administered intravenously. Therefore, there needs to be a balance between the half-life in a biological environment and the time taken for the CORM to localise at a target area in the body.[7]

To counteract this issue, CORM-3 was incorporated into a triblock copolymer, comprised of hydrophilic and hydrophobic units, Figure 1.16.[34] The polymers form a CO releasing micelle (a lipid molecule that self-arranges into a spherical form in aqueous solutions). These micelles were developed in order to delay tissue diffusion. CO release analysis revealed that the micelles exhibited stability in physiological buffer and serum and upon interference with thiol-based compounds (e.g. cysteine), CO was liberated. The CO releasing ability of the micelle-CORM was slower than that of CORM-3 alone. The incorporation of CORM-3 into micelles reduced cytotoxicity in comparison to CORM-3 exclusively, measured using an MTT cell viability assay. In addition, the micelle-CORM displayed anti-inflammatory properties i.e. attenuated the lipopolysaccharide-induced NF-κB activation of human monocytes. In contrast, CORM-3 alone showed no beneficial effects under the same conditions. This study elegantly enforces the fact that polymeric nanocarriers allow for the delivery of hydrophobic and hydrophilic drugs. Polymeric micelles in particular, possess unique attributes i.e. ease of formulation, low toxicity and they have high drug loading capacities. Therefore, these CO releasing micelles allow for a safer delivery system for CO in biological systems and should be considered when faced with stability and water solubility issues.[34]

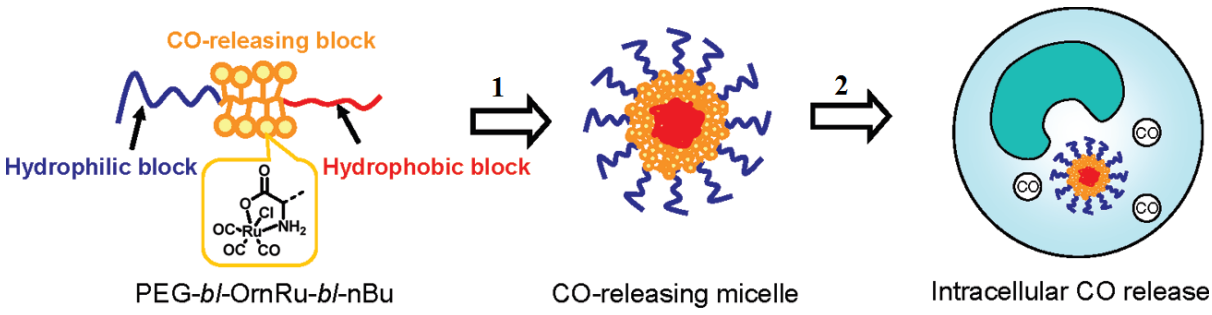

Figure 1.16 1) Micelle formation of PEG-b-OrnRu-b-nBu triblock copolymer and 2) CO release following cellular uptake.[34]

Using a similar concept, Kunz and co-workers reported a series of CORMs that were conjugated onto polymeric carrier systems to aid passive transport to areas of inflammation or tumour tissue sites.[33] *Fac*-$Mn(CO)_3$ copolymer conjugates released CO when irradiated at 365 nm. In the absence of light, the complexes do not readily decompose and do not generate CO in a spontaneous fashion.

Schiller and co-workers devised a new method to overcome water solubility issues and to reduce harmful effects that may be associated with metal based by-products. Light induced CO release was observed using nanoporous non-wovens (Figure 1.17).[35] CORM-1, the first developed CORM, is water insoluble and photoactive. It is an attractive molecule nonetheless since it has 10 molecules of CO per molecule of complex. However, it is much less used in medical investigations in comparison to the water soluble, CORM-3. In this study, CORM-1 was embedded into a polylactide based fibre. This biocompatible support matrix was chosen to permit water solubility. The system is created using electrospinning techniques. During this process, slight decomposition is observed at ambient conditions which leads to slight CO release from the CORM inside the non-woven. However, an advantage of this is that the CO released, induces nanoporous structures in the fibre generating an efficient photoactivatable delivery platform for CO. Wavelength dependent CO release was observed from the nanoporous non-woven CORM, CORM A. Higher energy UV irradiation (λ_{exc} = 365 nm) lead to CO release that was four times faster than that observed at (λ_{exc} = 480 nm). Not only do these systems enable water solubility and exhibit wavelength dependent photochemistry, they also display photochemically activated cytotoxicity i.e. in the absence of light the hybrid material is non-toxic, whereas when UV-light is applied, a photo cytotoxic effect is observed. This novel technology overcomes water solubility problems and more importantly traps CORM degradation products within the scaffold post CO release.[35]

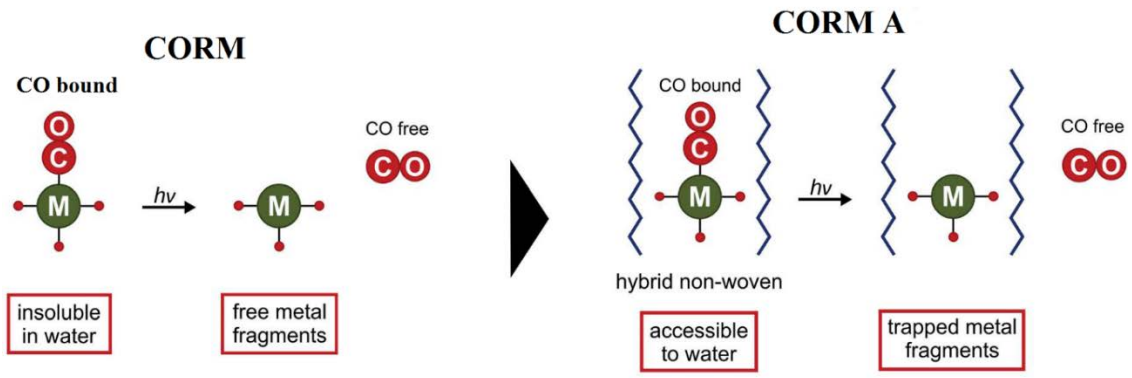

Figure 1.17 The incorporation of a CORM i.e. CORM-1 (Mn_2CO_{10}) into a polymeric non-woven, termed CORM A. The CO release product i.e. remaining metal fragment (inactive CORM, iCORM) is trapped and CO is released.[35]

1.5.2 Nanoparticle or Nanomaterial based CORMs

Doerdelmann *et al.* functionalised silicium dioxide nanoparticles onto the photoCORM, $[Mn(CO)_3(tpm)]^+$ where tpm = tris(pyrazolyl)methane with the idea of using them as delivery agents for CORMs in solid tumours, Figure 1.18.[56] The myoglobin assay illustrated that similar spectroscopic changes characteristic of CO release profiles were observed for both the CORM functionalised nanoparticles as well as the free CORM complex upon irradiation at 365 nm. A direct quantification of the CORM-nanoparticles was not possible since these experiments are required to be carried out under saturated conditions with the nanoparticle manganese carbonyl bound complex in excess over myoglobin. The free complex released 2-3 equivalents of CO per mole of complex. A control experiment demonstrated that photoreactivity was not observed in the absence of light for either complex.[56]

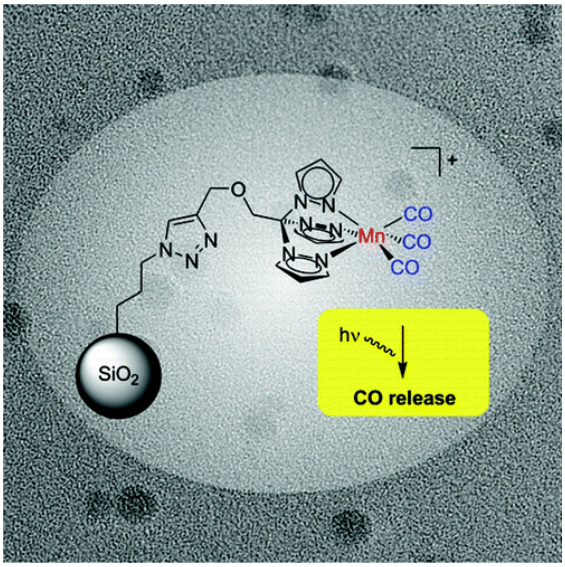

Figure 1.18 Silicium dioxide nanoparticles used as carriers for manganese carbonyl based photo-CORMs.[56]

Dordlemann *et al.* further developed this concept and used a modified nanodiamond as a biocompatible photoCORM carrier.[57] Nanondiamonds demonstrate good cellular uptake with no reported cytotoxic effects. CO release, upon irradiation at 365 nm, was indicated due to the characteristic spectroscopic changes identified by the myoglobin assay. However, yet again, the amount of CO released could not be quantified since higher dosages lead to the formation of a cloudy dispersion, formed as the nanodiamond-CORM was added to the aqueous myoglobin solution. Therefore, only very low dosages could be tested such as dispersions with a low concentration of nanodiamond and hence, a low manganese carbonyl content. A new method of CO release detection must be developed to further quantify the CO released from the nanodiamond derived CORM.[57]

Recently, Ford and co-workers, developed a water soluble nano-carrier for photochemical CO releasing using NIR light (Figure 1.19).[58] This was synthesised by incorporating a single unit NIR-to-visible upconverting nanoparticle, and an active photoCORM, $[Mn(bpy)(CO)_2(PPh_3)_2]^+$ encapsulated into a phospholipid functionalised biocompatible polymer (PEG) which afforded water solubility. The system releases CO when irradiated at 980 nm (monitored in PBS using gas chromatography). Not only is the CO releasing ability and water solubility advantageous, the hydrophobic region of the system allows for the attachment of an

organic soluble photoCORM and therefore aqueous solubility issues may be overcome. The use of the polymer surface means that modifications could be designed to target active sites. This identifies the first delivery strategy based on the photochemical uncaging of CO using NIR light.

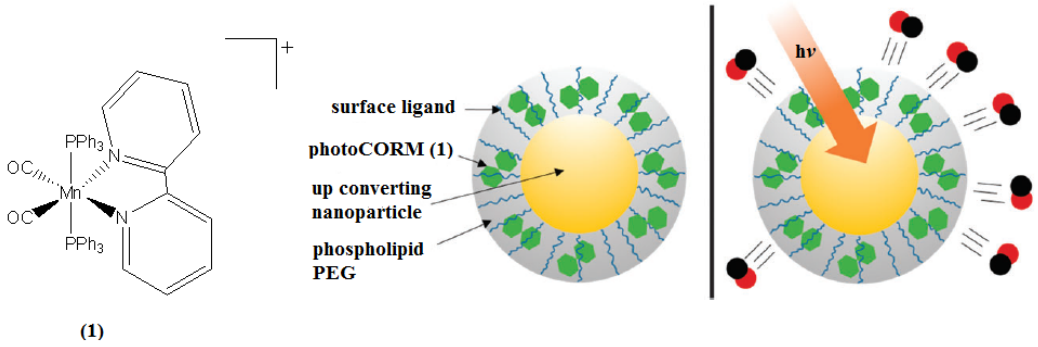

Figure 1.19 (**1**) The structure of the photoCORM. The representation in the middle shows the water-soluble nanocarrier developed for the photochemical uncaging of CO. The representation (right) shows that when irradiated at 980 nm (red arrow), up-converted visible range emission from the upconverted nanoparticle is re-absorbed by the photoCORM, resulting in CO dissociation.[58]

More recently, Kunz *et al.* reported the use of biocompatible magnetic iron oxide, maghemite (Fe_2O_3) nanoparticles (IONPs) which were covalently bound to the surface of a modified CORM-3 unit (a dioxyphenyl-alaninato group replaced the glycinato group in order for immobilisation to occur). CO release was triggered by exposure to a magnetic field which locally induces heating whereby ligand exchange can occur. CO is exchanged with the medium (Figure 1.20). This was analysed using the myoglobin assay. In the presence of an external magnetic field, a two-fold accelerated increase in the CO release rate is observed when compared to CO release in the absence of a magnetic field i.e. $t_{1/2}$ = 7 min $\pm$ 2 min compared to $t_{1/2}$ = 2.7 $\pm$ 0.2 min at 25 °C respectively. This novel method of CO delivery combines external stimulation with ligand exchange.[36]

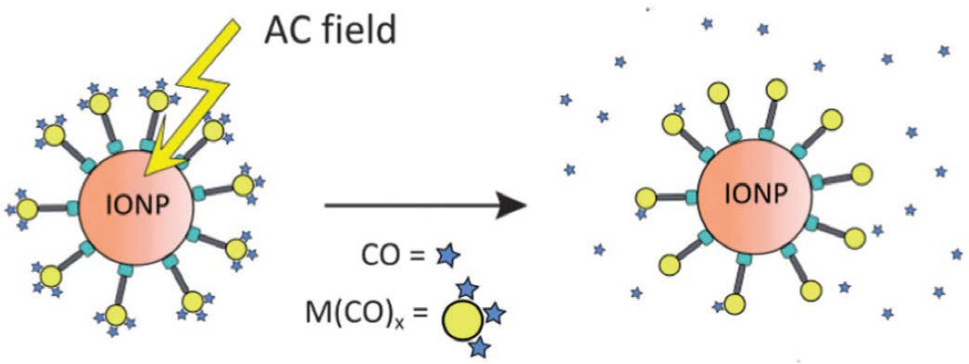

Figure 1.20 CO release induced by a magnetic (AC) field.[36]

1.6 Techniques to Elucidate Photochemical Pathways to CO release

It is very important to quantify the amount of CO released from a CORM and to characterise the products formed as a result of the CO release. For $Mn(CO)_3$ complexes, discrepancies between the myoglobin assay and IR investigations have been noted.[59] Infrared spectroscopy is a direct technique which is very sensitive and selective for detecting the release of CO.[60] Many research groups are now employing this technique to monitor the progress of photo-induced CO loss.[59-61] This method can monitor the deterioration of a CORM to its CO loss product form as the reaction proceeds as well as quantifying the total amount of CO released. Recently, Kunz and co-workers used time resolved IR spectroscopy (TRIR) in addition to the UV-vis based myoglobin assay to investigate tricarbonyl manganese complexes.[61] TRIR experiments were carried out for a maximum of 90 minutes. The various complexes of the type $[LMn(CO)_3]^+$ released different quantities of CO, approximately 1.04 – 2.28 moles of CO per mole of complex. Therefore, a transient species must have formed which invoked the idea to use TRIR spectroscopy for the elucidation of the mechanism of CO photorelease. In some cases where L was a bulky ligand, upon irradiation at 365 nm in methanol, TRIR studies showed the depletion of the parent tricarbonyl bands with no formation of new bands. TRIR data did not agree with the myoglobin assay data as loss of one CO equivalent (deduced from the myoglobin assay) should form a dicarbonyl species. In contrast, the TRIR results illustrated the

loss of 3 CO equivalents since there was full depletion of the parent tricarbonyl bands with no formation of new bands.[61] It would be very useful to carry out picosecond TRIR to probe the early state dynamics leading to CO release on a very short timescale 10^{-12} s. In conjunction with TRIR, matrix isolation would aid to trap and hence characterise photochemically generated intermediates to elucidate the pathways to CO loss. An understanding of the photo-excited states is paramount to explaining why CO release may / may not occur at incident wavelengths.

1.6.1 Matrix Isolation

The term matrix isolation (MI), first coined by Pimentel and co-workers, involves the entrapment of molecules or atoms in a solid host matrix.[62] It is achieved by co-condensing / spraying the matrix gas and the selected sample (active species) at freezing temperatures onto a host material (a crystalline or glass matrix formed from the frozen gas). Low temperatures are necessary for the preservation of the structure of the reactive or unstable species. Temperatures of 12 - 20 K are needed to form these rigid matrices. This can be achieved by using liquid helium. Since such low temperatures are required, sample diffusion kinetic information cannot be obtained. Due to the low temperatures employed, the trapped species present in the rigid host matrix is unable to diffuse and therefore bimolecular reactions are prevented, except those reactions that can occur with the host matrix. The active molecules are immobile in a non-reactive environment. It is therefore possible to irradiate the sample material on the inert matrix and observe intermediate species. This permits the formation of the active molecules followed by the trapping process. To analyse and characterise the intermediates / photoproducts formed upon irradiation, it is necessary to have a spectroscopic detector attached such as UV-vis, Raman, IR spectrophotometer or fluorimeter. MI allows for the characterisation of photo produced species which may be too-short lived or unstable to study and detect at ambient temperatures.

Initially, organic glasses were used in matrix isolation investigations. However, it has also been observed that solidified noble gases e.g. methane and nitrogen are advantageous since they are chemically inert and are transparent in appearance. It is possible for these gases to interact and form complexed species with photoproducts

derived upon irradiation of the parent complex. The solidified matrix gas forms a "cage" around the reactant species which can block some photochemical pathways due to the prevention of the escape of intermediate / reactant species. This can lead to regeneration of the parent complex. For metal carbonyls, upon irradiation of the matrix sample, CO is liberated. The fragment and ejected CO molecule are then present in the same "cage" and recombination may not occur if the vacant site on the metal centre rotates in a different direction to that of the CO molecule. In Chapter 2, MI will be used for the detection of excited state species formed upon photolysis at varying wavelengths and to elucidate the photochemical mechanism leading to CO loss.

1.6.2 Picosecond Time Resolved Infrared Spectroscopy (psTRIR)

Time resolved infrared (TRIR) spectroscopy is a well-established technique that studies the photophysical and photochemical processes that occur in chemical compounds and makes the assignment of excited state identities possible. It can be used in many diverse research areas such as organic photochemistry, chemical physics and in biological mechanistic studies.[63] TRIR spectroscopy allows for the detection of a transient species using infrared spectroscopy *vs.* time. In particular, it applies to the investigation of photochemically generated transient species formed in a liquid solution. Fast (ps) time-resolved infrared spectroscopy techniques (psTRIR) are now available which can probe early-stage dynamic processes in the photoinduced CO loss reaction by monitoring changes in the mid-infrared region of the spectrum where metal carbonyl's distinct stretching modes are observed.[64] TRIR allows for the observation of transient species with characteristic absorption frequencies that evolve over time which allows for the identification of structural information and elucidation of photo induced excited states / products that occur over the course of the experiment. It is then possible to determine the kinetic data. This technique is particularly useful for the characterisation of transient species of organometallic compounds due to their distinct functionality with strong characteristic frequencies that are susceptible to molecular structural changes. It is therefore possible to elucidate transient species by monitoring these frequencies. Complexes containing CO (or CN) ligands have high oscillation strengths due to the CO / CN stretching vibrations. CO and CN act as "reporter

ligands" to elucidate the electronic and molecular structures. The stretching frequencies and band-widths are sensitive to changes in electronic and molecular structure due to backbonding.[63] In the case of this thesis, the M-CO stretching vibrations will be investigated. Upon excitation, it is possible for changes to occur on the femtosecond to microsecond timescale. The excited state determines the magnitude of the shifts in the υCO bands that occur between ground and excited states due to the redistribution of electrons and the influence it has on $d\pi$-π^* (CO) backbonding.

TRIR includes a "pump and probe" set up. The laser pulse excites ("pumps") and IR spectroscopy "probes" the formation of transient species. TRIR can operate with varying timescales, femto- to nanosecond time resolution. Results from two types of experimental set-up will be presented in the forthcoming chapters.

1.7 Concluding Points

CORMs are a class of compounds with an exploitable wide range of properties that may be useful therapeutically. In conjunction with experimental data, CORMs have elicited consistent therapeutic applications with reference to the alleviation of cardiovascular disorders and inflammation. Also, their importance in renal dysfunction and organ graft rejection has been clearly indicated. The emerging developments from extensive studies focusing on CORMs are fortifying indications of their therapeutic use.[23] The adaptable nature of CORMs is advantageous regarding drug development. The use of metal carbonyl complexes allows for a relative ease of synthesis and design. It is possible to control and adjust the substitution of ligands to the metal centre to suit certain requirements, hence controlling the kinetics of CO generation. CORMs may be engineered to release CO with distinctive release rates and with selective delivery to specific sites. In some circumstances, it is possible to manipulate these release rates, depending on the intended application by tuning the metal and ligand functionalities. For example, CORM-A1 generates CO in a slow, prolonged and controlled way whereas CORM-F10, an iron based CORM, possesses and exceptionally rapid release rate. Mo carbonyls generate CO more rapidly than W based carbonyls but at a slower rate than Cr based CORMs.[26] It has also been

demonstrated that, in some cases, cationic complexes exhibit a slow liberation of CO whereas anionic complexes demonstrate a rapid release.[1]

This chapter has focused mainly on transition metal carbonyls as a plausible strategy for the delivery of CO. A wide range of transition metal carbonyls have been discussed ranging from the first discovered CORMs; CORM-1 and CORM-2 to more recent developments; water-soluble CORMs, photo-CORMs, and enzyme triggered-CORMs. Novel technologies to overcome solubility and toxic effects of by-products have also been explored.

The recent concepts of transition metal carbonyl complexes as photoCORMs illustrate their significance as safe and controlled delivery systems. Metal pentacarbonyl, $M(CO)_5$ based CORMs, for example, Fischer carbene complexes, described in the forthcoming chapters, have the potential to liberate five molecules of CO per mole of complex and are therefore of interest to researchers. The release of elevated quantities of CO would be extremely beneficial in lowering the dosage needed for administration. Chapters 2 and 3 will focus on the synthesis of simple Fischer carbene pentacarbonyl complexes of chromium and tungsten systems. Matrix isolation, psTRIR, the myoglobin assay and gas chromatography will be carried out in order to assess their photochemical CO releasing properties and elucidate their photochemical mechanisms leading to CO loss. Thermal and electrochemically induced CO release will also be investigated. Finally the suitability of the myoglobin assay and the introduction of different techniques to quantify CO release will be explored.

Chapter 4 will extend the focus on Fischer carbene complexes. The photochemistry of bimetallic ferrocenyl Fischer carbene complexes in addition to the corresponding styryl complexes is probed using psTRIR spectroscopy. The final chapter, focuses on BODIPY tethered metal carbonyl compounds. BODIPY dyes are dual functioning as they can function as luminescent reporters and the dye also extends absorption towards the red region of the spectrum, thus facilitating low energy photons to induce CO release.

1.8 References

1. Mann, B. E.; Motterlini, R. CO and NO in medicine. *Chem. Commun.* **2007**, *41*, 4197-4208.

2. Mann, B.; Motterlini, R. Therapy from CO a silent killer. *Chem. Ind.* **2005**, *16*, 16-18.

3. Nobre, L. S.; Seixas, J. D.; Romao, C. C.; Saraiva, L. M. Antimicrobial action of carbon monoxide-releasing compounds. *Antimicrob. Agents Chemother.* **2007**, *51*, 4303-4307.

4. Johnson, R.; Kozma, F.; Colombari, E. Carbon monoxide: from toxin to endogenous modulator of cardiovascular functions. *Braz. J. Med. Biol. Res.* **1999**, *32*, 1-14.

5. Gorman, D.; Drewry, A.; Huang, Y.; Sames, C. The clinical toxicology of carbon monoxide. *Toxicology* **2003**, *187*, 25-38.

6. Alberto, R.; Motterlini, R. Chemistry and biological activities of CO-releasing molecules (CORMs) and transition metal complexes. *Dalton Trans.* **2007**, *17*, 1651-1660.

7. Schatzschneider, U. Novel lead structures and activation mechanisms for CO-releasing molecules (CORMs). *Br. J. Pharmacol.* **2015**, *172*, 1638-1650.

8[a]. Thiemermann, C. Inhaled CO: Deadly gas or novel therapeutic? *Nat. Med.* **2001**, *7*, 534-535.

8[b]. Page, I.; Corcoran, A.; Dustan, H.; Koppanyi, T. Cardiovascular Actions of Sodium Nitroprusside in Animals and Hypertensive Patients. *Circulation* **1955**, *11*, 188-198.

8[c]. Patik, J. C.; Christmas, K. M.; Hurr, C.; Brothers, R. M. Impaired endothelium independent vasodilation in the cutaneous microvasculature of young obese adults. *Microvasc. Res.* **2016**, *104*, 63-68.

9. Verma, A.; Hirsch, D.; Glatt, C.; Ronnett, G.; Snyder, S. Carbon-Monoxide - a Putative Neural Messenger. *Science* **1993**, *259*, 381-384.

10. Fujita, T.; Toda, K.; Karimova, A.; Yan, S.; Naka, Y.; Yet, S.; Pinsky, D. Paradoxical rescue from ischemic lung injury by inhaled carbon monoxide driven by derepression of fibrinolysis. *Nat. Med.* **2001**, *7*, 598-604.

11. Atkin, A. J.; Williams, S.; Sawle, P.; Motterlini, R.; Lynam, J. M.; Fairlamb, I. J. S. μ^2-Alkyne dicobalt(0)hexacarbonyl complexes as carbon monoxide-releasing molecules (CO-RMs): probing the release mechanism. *Dalton Trans.* **2009**, *19*, 3653-3656.

12. Coburn, R. Carbon Monoxide Body Stores. *Ann. N. Y. Acad. Sci.* **1970**, *174*, 11-22.

13. Foresti, R.; Bani-Hani, M. G.; Motterlini, R. Use of carbon monoxide as a therapeutic agent: promises and challenges. *Intensive Care Med.* **2008**, *34*, 649-658.

14. Heinemann, S. H.; Hoshi, T.; Westerhausen, M.; Schiller, A. Carbon monoxide - physiology, detection and controlled release. *Chem. Commun.* **2014**, *50*, 3644-3660.

15. Horvath, I.; Donnelly, L.; Kiss, A.; Paredi, P.; Kharitonov, S.; Barnes, P. Raised levels of exhaled carbon monoxide are associated with an increased expression of heme oxygenase-1 in airway macrophages in asthma: a new marker of oxidative stress. *Thorax* **1998**, *53*, 668-672.

16. Johnson, T.; Mann, B.; Clark, J.; Foresti, R.; Green, C.; Motterlini, R. Metal carbonyls: A new class of pharmaceuticals. *Angew. Chem. -Int. Edit.* **2003**, *42*, 3722-3729.

17. Romao, C. C.; Blaettler, W. A.; Seixas, J. D.; Bernardes, G. J. L. Developing drug molecules for therapy with carbon monoxide. *Chem. Soc. Rev.* **2012**, *41*, 3571-3583.

18. Maines, M. The heme oxygenase system: A regulator of second messenger gases. *Annu. Rev. Pharmacol. Toxicol.* **1997**, *37*, 517-554.

19. Queen's University Kingston Canada Study of Inhaling Carbon Monoxide to Treat Patients With Intestinal Paralysis After Colon Surgery. *https://www.clinicaltrials.gov/ct2/show/results/NCT01050712* (accessed 07/13, 2015).

20. Mann, B. E. CO-Releasing Molecules: A Personal View. *Organometallics* **2012**, *31*, 5728-5735.

21. Motterlini, R.; Clark, J.; Foresti, R.; Sarathchandra, P.; Mann, B.; Green, C. Carbon monoxide-releasing molecules - Characterization of biochemical and vascular activities. *Circ. Res.* **2002**, *90*, E17-E24.

22. Alcaraz, M. J.; Guillen, M. I.; Ferrandiz, M. L.; Megias, J.; Motterlini, R. Carbon monoxide-releasing molecules: A pharmacological expedient to counteract inflammation. *Curr. Pharm. Des.* **2008**, *14*, 465-472.

23. Boczkowski, J.; Poderoso, J. J.; Motterlini, R. CO-metal interaction: vital signaling from a lethal gas. *Trends Biochem. Sci.* **2006**, *31*, 614-621.

24. Atkin, A. J.; Lynam, J. M.; Moulton, B. E.; Sawle, P.; Motterlini, R.; Boyle, N. M.; Pryce, M. T.; Fairlamb, I. J. S. Modification of the deoxy-myoglobin/carbonmonoxy-myoglobin UV-vis assay for reliable determination of CO-release rates from organometallic carbonyl complexes. *Dalton Trans.* **2011**, *40*, 5755-5761.

25. Obirai, J. C.; Hamadi, S.; Ithurbide, A.; Wartelle, C.; Nyokong, T.; Zagal, J.; Top, S.; Bedioui, F. UV-visible and electrochemical monitoring of carbon monoxide release by donor complexes to myoglobin solutions and to electrodes modified with films containing Hemin. *Electroanal.* **2006**, *18*, 1689-1695.

26. Zhang, W.; Atkin, A. J.; Thatcher, R. J.; Whitwood, A. C.; Fairlamb, I. J. S.; Lynam, J. M. Diversity and design of metal-based carbon monoxide-releasing molecules (CO-RMs) in aqueous systems: revealing the essential trends. *Dalton Trans.* **2009**, *22*, 4351-4358.

27. Friis, S. D.; Taaning, R. H.; Lindhardt, A. T.; Skrydstrup, T. Silacarboxylic Acids as Efficient Carbon Monoxide Releasing Molecules: Synthesis and Application in Palladium-Catalyzed Carbonylation Reactions. *J. Am. Chem. Soc.* **2011**, *133*, 18114-18117.

28. Motterlini, R.; Sawle, P.; Bains, S.; Hammad, J.; Alberto, R.; Foresti, R.; Green, C. J. CORM-A1: a new pharmacologically active carbon monoxide-releasing molecule. *Faseb Journal* **2004**, *18*, 284-286.

29. Pitchumony, T. S.; Spingler, B.; Motterlini, R.; Alberto, R. Syntheses, structural characterization and CO releasing properties of boranocarbonate $[H_3BCO_2H]^-$ derivatives. *Org. Biomol. Chem.* **2010**, *8*, 4849-4854.

30. Antony, L. A. P.; Slanina, T.; Sebej, P.; Solomek, T.; Klan, P. Fluorescein Analogue Xanthene-9-Carboxylic Acid: A Transition-Metal-Free CO Releasing Molecule Activated by Green Light. *Org. Lett.* **2013**, *15*, 4552-4555.

31. Peng, P.; Wang, C.; Shi, Z.; Johns, V. K.; Ma, L.; Oyer, J.; Copik, A.; Igarashi, R.; Liao, Y. Visible-light activatable organic CO-releasing molecules (PhotoCORMs) that simultaneously generate fluorophores. *Org. Biomol. Chem.* **2013**, *11*, 6671-6674.

32. Rimmer, R. D.; Pierri, A. E.; Ford, P. C. Photochemically activated carbon monoxide release for biological targets. Toward developing air-stable photoCORMs labilized by visible light. *Coord. Chem. Rev.* **2012**, *256*, 1509-1519.

33. Bruckmann, N. E.; Wahl, M.; Reiss, G. J.; Kohns, M.; Waetjen, W.; Kunz, P. C. Polymer Conjugates of Photoinducible CO-Releasing Molecules. *Eur. J. Inorg. Chem.* **2011**, *29*, 4571-4577.

34. Hasegawa, U.; van der Vlies, A. J.; Simeoni, E.; Wandrey, C.; Hubbell, J. A. Carbon Monoxide-Releasing Micelles for Immunotherapy. *J. Am. Chem. Soc.* **2010**, *132*, 18273-18280.

35. Bohlender, C.; Glaeser, S.; Klein, M.; Weisser, J.; Thein, S.; Neugebauer, U.; Popp, J.; Wyrwa, R.; Schiller, A. Light-triggered CO release from nanoporous non-wovens. *J. Mat. Chem. B* **2014**, *2*, 1454-1463.

36. Kunz, P. C.; Meyer, H.; Barthel, J.; Sollazzo, S.; Schmidt, A. M.; Janiak, C. Metal carbonyls supported on iron oxide nanoparticles to trigger the CO- gasotransmitter release by magnetic heating. *Chem. Commun.* **2013**, *49*, 4896-4898.

37. Clark, J.; Naughton, P.; Shurey, S.; Green, C.; Johnson, T.; Mann, B.; Foresti, R.; Motterlini, R. Cardioprotective actions by a water-soluble carbon monoxide-releasing molecule. *Circ. Res.* **2003**, *93*, E2-E8.

38. Motterlini, R.; Mann, B. E.; Johnson, T. R.; Clark, J. E.; Foresti, R.; Green, C. J. Bioactivity and pharmacological actions of carbon monoxide-releasing molecules. *Curr. Pharm. Des.* **2003**, *9*, 2525-2539.

39. Fairlamb, I. J. S.; Duhme-Klair, A.; Lynam, J. M.; Moulton, B. E.; O'Brien, C. T.; Sawle, P.; Hammad, J.; Motterlini, R. η^4-Pyrone iron(0)carbonyl complexes as effective CO-releasing molecules (CO-RMs). *Bioorg. Med. Chem. Lett.* **2006**, *16*, 995-998.

40. Sawle, P.; Hammad, J.; Fairlamb, I. J. S.; Moulton, B.; O'Brien, C. T.; Lynam, J. M.; Duhme-Klair, A. K.; Foresti, R.; Motterlini, R. Bioactive properties of iron-containing carbon monoxide-releasing molecules. *J. Pharmacol. Exp. Ther.* **2006**, *318*, 403-410.

41. Fairlamb, I. J. S.; Lynam, J. M.; Moulton, B. E.; Taylor, I. E.; Duhme-Klair, A. K.; Sawle, P.; Motterlini, R. η^1-2-pyrone metal carbonyl complexes as CO-releasing molecules (CO-RMs): A delicate balance between stability and CO liberation. *Dalton Trans.* **2007**, *33*, 3603-3605.

42. Zhang, W.; Whitwood, A. C.; Fairlamb, I. J. S.; Lynam, J. M. Group 6 Carbon Monoxide-Releasing Metal Complexes with Biologically-Compatible Leaving Groups. *Inorg. Chem.* **2010**, *49*, 8941-8952.

43. Marques, A. R.; Kromer, L.; Gallo, D. J.; Penacho, N.; Rodrigues, S. S.; Seixas, J. D.; Bernardes, G. J. L.; Reis, P. M.; Otterbein, S. L.; Ruggieri, R. A.; Goncalves, A. S. G.; Goncalves, A. M. L.; De Matos, M. N.; Bento, I.; Otterbein, L. E.; Blaettler, W. A.; Romao, C. C. Generation of Carbon Monoxide Releasing Molecules (CO-RMs)

as Drug Candidates for the Treatment of Acute Liver Injury: Targeting of CO-RMs to the Liver. *Organometallics* **2012**, *31*, 5810-5822.

44. Seixas, J. D.; Mukhopadhyay, A.; Santos-Silva, T.; Otterbein, L. E.; Gallo, D. J.; Rodrigues, S. S.; Guerreiro, B. H.; Goncalves, A. M. L.; Penacho, N.; Marques, A. R.; Coelho, A. C.; Reis, P. M.; Romao, M. J.; Romao, C. C. Characterization of a versatile organometallic pro-drug (CORM) for experimental CO based therapeutics. *Dalton Trans.* **2013**, *42*, 5985-5998.

45. Wrighton, M.; Ginley, D. Photochemistry of Metal-Metal Bonded Complexes. II. Photochemistry of Rhenium and Manganese Carbonyl-Complexes Containing a Metal-Metal Bond. *J. Am. Chem. Soc.* **1975**, *97*, 2065-2072.

46. Garcia-Gallego, S.; Bernardes, G. J. L. Carbon-Monoxide-Releasing Molecules for the Delivery of Therapeutic CO In Vivo. *Angew. Chem. -Int. Edit.* **2014**, *53*, 9712-9721.

47. Kretschmer, R.; Gessner, G.; Gorls, H.; Heinemann, S. H.; Westerhausen, M. Dicarbonyl-bis(cysteamine)iron(II) A light induced carbon monoxide releasing molecule based on iron (CORM-S1). *J. Inorg. Biochem.* **2011**, *105*, 6-9.

48. Kelly, J.; Long, C.; Bonneau, R. Laser Flash-Photolysis of $Cr(CO)_6$, $Mo(CO)_6$, $W(CO)_6$ in Perfluoromethylcyclohexane - the Generation of Highly Reactive Coordinatively Unsaturated Species. *J. Phys. Chem.* **1983**, *87*, 3344-3349.

49. Rimmer, R. D.; Richter, H.; Ford, P. C. A Photochemical Precursor for Carbon Monoxide Release in Aerated Aqueous Media. *Inorg. Chem.* **2010**, *49*, 1180-1185.

50. Zhang, W.; Atkin, A. J.; Fairlamb, I. J. S.; Whitwood, A. C.; Lynam, J. M. Synthesis and Reactivity of Molybdenum Complexes Containing Functionalized Alkynyl Ligands: A Photochemically Activated CO-Releasing Molecule (PhotoCO-RM). *Organometallics* **2011**, *30*, 4643-4654.

51. Romanski, S.; Kraus, B.; Schatzschneider, U.; Neudoerfl, J. M.; Amslinger, S.; Schmalz, H. G. Acyloxybutadiene-Iron Tricarbonyl Complexes as Enzyme-Triggered

CO-Releasing Molecules (ET-CORMs). *Angew. Chem. -Int. Edit.* **2011**, *50*, 2392-2396.

52. Romanski, S.; Kraus, B.; Guttentag, M.; Schlundt, W.; Ruecker, H.; Adler, A.; Neudoerfl, J.; Alberto, R.; Amslinger, S.; Schmalz, H. Acyloxybutadiene tricarbonyl iron complexes as enzyme-triggered CO-releasing molecules (ET-CORMs): a structure-activity relationship study. *Dalton Trans.* **2012**, *41*, 13862-13875.

53. Botov, S.; Stamellou, E.; Romanski, S.; Guttentag, M.; Alberto, R.; Neudoerfl, J.; Yard, B.; Schmalz, H. Synthesis and Performance of Acyloxy-diene-Fe(CO)$_3$ Complexes with Variable Chain Lengths as Enzyme-Triggered Carbon Monoxide-Releasing Molecules. *Organometallics* **2013**, *32*, 3587-3594.

54. Romanski, S.; Ruecker, H.; Stamellou, E.; Guttentag, M.; Neudoerfl, J.; Alberto, R.; Amslinger, S.; Yard, B.; Schmalz, H. Iron Dienylphosphate Tricarbonyl Complexes as Water-Soluble Enzyme-Triggered CO-Releasing Molecules (ET-CORMs). *Organometallics* **2012**, *31*, 5800-5809.

55. Johnson, T. R.; Mann, B. E.; Teasdale, I. P.; Adams, H.; Foresti, R.; Green, C. J.; Motterlini, R. Metal carbonyls as pharmaceuticals? [Ru(CO)$_3$Cl(glycinate)], a CO-releasing molecule with an extensive aqueous solution chemistry. *Dalton Trans.* **2007**, *15*, 1500-1508.

56. Doerdelmann, G.; Pfeiffer, H.; Birkner, A.; Schatzschneider, U. Silicium Dioxide Nanoparticles As Carriers for Photoactivatable CO-Releasing Molecules (PhotoCORMs). *Inorg. Chem.* **2011**, *50*, 4362-4367.

57. Doerdelmann, G.; Meinhardt, T.; Sowik, T.; Krueger, A.; Schatzschneider, U. CuAAC click functionalization of azide-modified nanodiamond with a photoactivatable CO-releasing molecule (PhotoCORM) based on [Mn(CO)$_3$(tpm)]$^+$. *Chem. Commun.* **2012**, *48*, 11528-11530.

58. Pierri, A. E.; Huang, P.; Garcia, J. V.; Stanfill, J. G.; Chui, M.; Wu, G.; Zheng, N.; Ford, P. C. A photoCORM nanocarrier for CO release using NIR light. *Chem. Commun.* **2015**, *51*, 2072-2075.

59. Berends, H.; Kurz, P. Investigation of light-triggered carbon monoxide release from two manganese photoCORMs by IR, UV-Vis and EPR spectroscopy. *Inorg. Chim. Acta* **2012**, *380*, 141-147.

60. Klein, M.; Neugebauer, U.; Gheisari, A.; Malassa, A.; Jazzazi, T. M. A.; Froehlich, F.; Westerhausen, M.; Schmitt, M.; Popp, J. IR Spectroscopic Methods for the Investigation of the CO Release from CORMs. *J Phys Chem A* **2014**, *118*, 5381-5390.

61. Huber, W.; Linder, R.; Niesel, J.; Schatzschneider, U.; Spingler, B.; Kunz, P. C. A Comparative Study of Tricarbonylmanganese Photoactivatable CO Releasing Molecules (PhotoCORMs) by Using the Myoglobin Assay and Time-Resolved IR Spectroscopy. *Eur. J. Inorg. Chem.* **2012**, *19*, 3140-3146.

62. Whittle, E.; Dows, D.; Pimentel, G. Matrix Isolation Method for the Experimental Study of Unstable Species. *J. Chem. Phys.* **1954**, *22*, 1943-1943.

63. Butler, J. M.; George, M. W.; Schoonover, J. R.; Dattelbaum, D. M.; Meyer, T. J. Application of transient infrared and near infrared spectroscopy to transition metal complex excited states and intermediates. *Coord. Chem. Rev.* **2007**, *251*, 492-514.

64. McFarlane, K.; Lee, B.; Bridgewater, J.; Ford, P. Time resolved infrared spectroscopy as a technique to study reactive organometallic intermediates. *J. Organomet. Chem.* **1998**, *554*, 49-61.

2 Chapter 2 An Investigation into the Photochemistry and Electrochemically Induced CO Release from $[(CO)_5M=C(OMe)Me]$ (M = Cr, W) Complexes

Abstract

The basic Fischer carbene complexes; $[(CO)_5M=C(OMe)Me]$ (M = Cr, W) are reported and their potential as CO delivery systems is assessed. Also, their photochemical and photophysical properties are investigated using a range of spectroscopic techniques i.e. UV-vis spectroscopy, matrix isolation techniques (M = Cr), picosecond time resolved IR and variable temperature ^{1}H-NMR spectroscopy (M = Cr) to underpin the mechanism of CO release and additional photochemical species observed. Electrochemically induced CO loss is assessed for both $[(CO)_5CrC(OMe)Me]$ ***(1)*** *and $[(CO)_5WC(OMe)Me]$* ***(4)****, using gas chromatography.*

Publication based on this work

An Investigation into the Photochemistry of, and the Electrochemically Induced CO-loss from, $[(CO)_5MC(OMe)Me]$(M = Cr or W) Using Low-temperature Matrix Isolation, Picosecond Infrared Spectroscopy, Cyclic Voltammetry, and Time-dependent Density Functional Theory. Suzanne Mc Mahon, Saeed Amirjalayer, Wybren J. Buma, Yvonne Halpin, Conor Long, A. Denise Rooney, Sander Woutersen, and Mary T. Pryce.

Dalton Trans. **2015**, *44*, 15424-15434.

Chosen as cover of Dalton Transactions' September edition and as one of July's Hot Articles (13th July 2015).

2.1 Introduction

The mechanisms behind the photochemical CO release of CORMs are not currently well explored, therefore it was critical to gain an insight into the nature of the excited states leading to CO loss. To do this, a series of Fischer carbenes were chosen for investigation. A set of carbenes based on $[(CO)_5M=C(OMe)Me]$ where M = Cr, W were selected as optimal candidates as they are known to release CO. However, the photochemical mechanisms preceding CO loss and their excited state processes were not clearly identified i.e. the photochemical intermediates had not been confirmed.

Fischer carbene complexes were first introduced in 1964 by E.O. Fischer *et al.* with the general formula $[(CO)_nM=C(OR')R]$.[1] They consist of a carbene which is stabilised by a low valent transition metal carbonyl (usually group VI - VIII) *via* co-ordination.[2] In general, one carbene substituent consists of a saturated or unsaturated group, the other consists of a π-donor group which stabilises the carbon atom of the carbene since it is deficient of electrons. In contrast, π-acceptors (carbon monoxide, phosphine ligands, etc.) stabilise the metal centre due to its low oxidation state. Fischer carbenes are highly coloured complexes varying from yellow to red depending on the nature of the substituents and can have distinctive UV-visible spectra consisting of a low absorbing band at ~ 500 nm (spin forbidden MLCT), a stronger band at 350 - 450 nm (spin allowed MLCT) and a weaker band in the region 300 - 350 nm (LF transition).[3] Many of the first photochemical studies of Fischer carbenes focused on the effect of irradiation into the LF absorption bands with photochemically induced CO loss being the predominant process. The MLCT bands are less photosensitive, with reactivity attributed to the LF band.[4] The *anti-syn* photoisomerisation of alkoxy Fischer carbene complexes is also a photochemical feature of interest.

An equilibrium between *anti-* and *syn-* configurations arises in methoxy stablilised Fischer carbenes. It is possible for both isomers to exist due to the π-bond nature of the $C_{carbene}$-O bond as the methoxy group can rotate (Figure 2.1). In *anti-syn* isomerisation, the metal centre acts as an intramolecular photosensitiser. This results in the absorption of light which transfers electron density onto the carbene ligand which in turn facilitates the photoisomerisation process.[5]

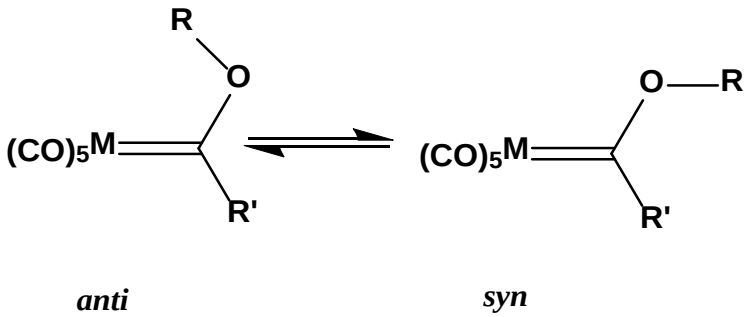

Figure 2.1 *Anti-syn* photoisomerisation of alkoxy carbenes, $[(CO)_5M=C(OR')R]$. For this particular study M = Cr (**1**) and W (**4**) (R and R´ = Me).

In the ground state, the *anti*- configuration is more favoured than the *syn*- and is therefore more stable.[6,7] Gut *et al.* studied the complex, $[(CO)_5WC(OMe)Ph]$ and found that both *anti-syn* isomerisation and photochemically induced CO loss occur as unrelated processes that arise upon photoexcitation to the LF state in solution at room temperature. The quantum yield for photoinduced CO loss; $\Phi_{CO\text{-}loss,\,(308\,nm)} = 0.017$, is ~ eighteen times less than that reported for *anti-syn* photoisomerisation, $\Phi_{anti\text{-}syn\ (308\ nm)} = 0.3$ for this complex.[8]

Fischer carbene complexes have been extensively studied due to their importance as selective reagents in organic synthetic reactions. A wide range of compounds can be formed using these carbenes upon irradiation. For example, *ß*-lactams (4-membered rings which are widely found in penicillin antibiotics) can be formed when irradiated in the presence of imines.[3,9] Initially, photoinduced CO loss was thought to be the main process involved in *ß*-lactam formation as CO release is known to occur under thermal conditions. However, under high pressures of CO, high yields of *ß*-lactam formation is observed, indicating that the mechanism does not occur *via* CO loss.[10] It was first suggested by Mc. Guire *et al*. that irradiation into the MLCT band of chromium and molybdenum (but not tungsten) Fischer carbene complexes resulted in the formation of a ketene as an intermediate in the reaction.[11] Two possible mechanisms were proposed. The first plausible path, upon irradiation into the MLCT band of chromium carbene complexes, includes the liberation of one CO molecule photolytically (Scheme 2.1 Pathway A). This allows the nitrogen (imine) to co-ordinate to the vacant site. Next, a cycloaddition reaction occurs. This is followed by an insertion of CO. Finally reductive elimination signifies the formation of the *ß*-lactam. The second plausible path involves the generation of a ketene intermediate by photolysis, succeeded by a cycloaddition of the ketene to the imine as displayed in Scheme 2.1 pathway B.[11]

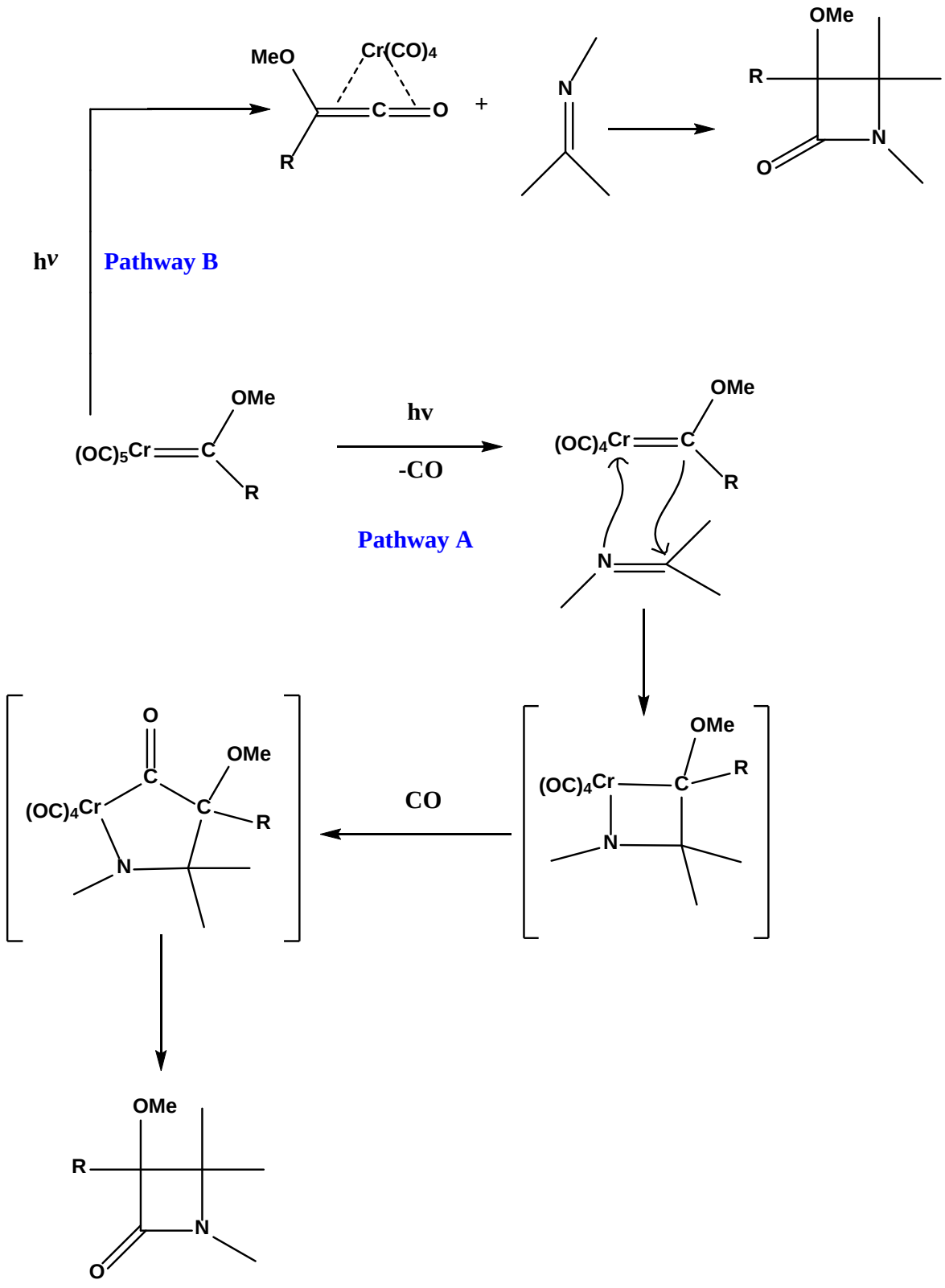

Scheme 2.1 The mechanisms proposed by Mc.Guire *et al.* for the formation of a β-lactam.[11]

Further studies by Hegedus *et al.* proposed that in the case of chromium Fischer carbene complexes, for example, $[(CO)_5Cr(OMe)Me]$ **(1)**, displayed in Figure 2.2; irradiation into the MLCT band promoted the reversible insertion of one of the *cis*-CO ligands into the double bond between the metal and carbon.[12] They proposed the formation of a short lived metallacyclopropanone (**2**) or a metallaketene (**3**) species. [12]

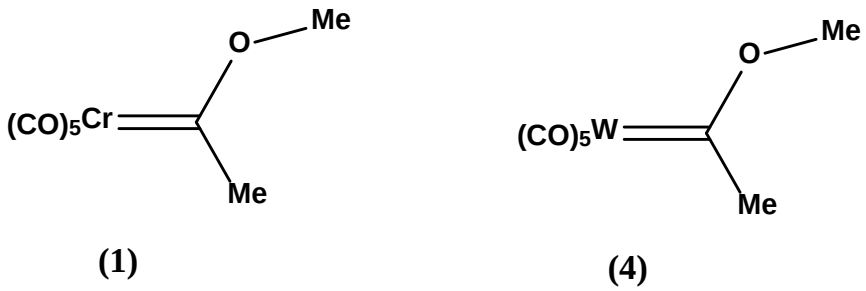

Figure 2.2 Structural representations of the parent complexes $[(CO)_5CrC(OMe)Me]$ (**1**) and $[(CO)_5WC(OMe)Me]$ (**4**) investigated in this chapter.

It is important to be able to distinguish the spectroscopic differences between the intermediates proposed by Hegedus *et al.* if they are to be identified spectroscopically. These two structures represent the extreme descriptions of the bonding in this class of complex. For example $(\eta^5\text{-}C_5H_4R)Mn(CO)_2((C_6H_5)_2C{=}C{=}O)$ (R = Me or H) has a metallacyclopropanone structure with a C=C=O angle of 145˚ and a $\nu_{CC=O}$ absorption at 1787 cm^{-1} in the so-called "bridging carbonyl" region.[13,14] However, in *trans*-$Ir(P(i\text{-}Pr)_3)_2Cl$(diphenylketene), the ketene ligand coordinates to the Ir atom as a $(\eta^2\text{-}C,O)$ ligand.[15] The C=C=O angle is 136.6(4)˚ and the $\nu_{CC=O}$ absorption occurs at 1636 cm^{-1} (to the low energy side of the bridging carbonyl region). The spectroscopic characterisation of the $(\eta^5\text{-}C_5H_5)Fe(CO)_2(CH_2CO)^+PF_6^-$ salt only exhibits ν_{CO} bands in the terminal region of the IR spectrum (1800 to 2100 cm^{-1}) and is therefore consistent with an almost linear ketene unit.[16] Thus, it is evident that the properties of these species in the infrared region are very sensitive to the coordination mode of the ketene. Consequently, it is important to distinguish between these various coordination modes. The C=C=O angle is a significant structural motif in this regard. The coordination mode, which exhibits a feature in the bridging CO region, with a C=C=O angle at almost 140°, is classified as a metallacyclopropanone. Species with near linear C=C=O units (C=C=O angles close to 170°) are classified as metallaketenes.[12] These species will exhibit a $\nu_{CC=O}$ feature in the terminal metal carbonyl region.[17]

As metal carbonyl complexes have unique "fingerprints" in the M-CO region of the IR spectrum, picosecond time resolved infrared (psTRIR) spectroscopy is an excellent technique for the characterisation of reactive intermediates and excited states. These studies are paramount to understanding the nature of the excited states leading to CO loss, a vital step in the concept of photochemical CORMs.

During the period that the experiments discussed in this chapter were carried out, Nguyen *et al.* reported the results of a psTRIR investigation into the photophysics and photochemistry of (**1**) and its tungsten analogue (**4**) in cyclohexane solution using 400 nm excitation and a pulse energy of 80 μJ.[18] This study provided fresh insights into the photophysics which underpin the photoinititated organic transformations using Fischer carbenes and showed that it was possible to identify the formation of an intermediate species by picosecond time resolved IR (psTRIR) spectroscopy. The formation of one short-lived singlet (lifetime 35 ps) and two long-lived triplet (lifetime > 2 ns) species which are referred to as "Cr-ketenes" was reported. These latter species have features in the bridging νCO region, at 1771 and 1791 cm^{-1} for the two triplet species and at 1777 cm^{-1} for the singlet species. It was proposed that the two long-lived triplet species are the synthetically important intermediates as they are the only photoproducts which were sufficiently long-lived to engage in bimolecular reactions with keteneophiles. This work supported the theoretical study postulated by Fernandez *et al.* which identified the occurrence of triplet excited states for these species.[19]

Not only are Fischer carbene complexes significant selective reagents in organic chemistry, more recently, they were found to have applications as thermal CO releasing molecules. CO releasing molecules are efficient delivery systems for carbon monoxide. As previously discussed in Chapter 1, CO is formed in mammals during the oxidation of heme by heme oxygenase enzymes. It participates in the mediation of essential biological functions and its potential therapeutic properties, for example, in anti-inflammation, vasodilation and organ graft rejection, have become an area of great interest to scientific researchers. Recently, CO release from Fischer carbene complexes have been reported *via* photochemical, thermal and electrochemical stimulation.[20,21] The concept of using Fischer carbene complexes as CORMs was first proposed by Zhang *et al.*[21] The main advantage of using metal pentacarbonyls is that they boast the potential to liberate up to five molecules of CO per complex. This means that lower quantities of the complex could be administered to achieve the ideal dose of CO. The nature of the

metal and heteroatom substituents on the carbene greatly influences the rate of CO release. Lynam and co-workers, reported results on thermally induced CO loss for a range of carbene complexes including **(1)** and **(4)** which confirmed that the order of the rate of thermal CO release is as follows; Cr > Mo > W. The most commonly used method for comparing CORMs is by quoting their half-life ($t_{½}$) values which quantitatively compare CO release from different CORM systems that may occur by different mechanisms. Regarding CORMs, it is explained as the time taken for a solution of CORM with a concentration of 60 μM to produce a solution of Mb-CO with concentration of 30 μM (or 40 μM to form 20 μM and 20 μM to form 10 μM). Thermally, tungsten Fischer carbene complexes release CO at a much slower rate than chromium based carbenes. $[(CO)_5WC(OMe)Me]$ (**4**), takes 7924 s to release 30 μM of CO from a 60 μM solution whereas $[(CO)_5CrC(OMe)Me]$ (**1**), takes 215 s under identical conditions.[21] *In vivo* studies using electrochemical methods as potential therapeutics for diseases such as various cancers have been reported in the literature and will be discussed further in later sections.[22-24]

The chapter presented herein focuses on the investigation of the photochemistry, photophysics and electrochemically activated CO loss of the complexes, $[(CO)_5CrC(OMe)Me]$ (**1**) and $[(CO)_5WC(OMe)Me]$ (**4**).

2.2 Experimental

2.2.1 Materials

All reactions were carried out under an atmosphere of nitrogen using Schlenk techniques. All solvents were supplied by the Aldrich Chemicals Company. Dichloromethane, pentane, hexane and heptane were dried over $MgSO_4$ prior to use. All solvents used for UV-vis, IR, psTRIR and cyclic voltammetry (CV) experiments were of spectrophotometric grade and were used without further purification. Nitrogen, argon and carbon monoxide were supplied by Air Products. Chromium hexacarbonyl, tungsten hexacarbonyl, anhydrous diethyl ether, methyl lithium (1.6 M in diethyl ether) and trimethyloxonium tetrafluoroborate (Aldrich Chemical Co.) were used without further purification. Column chromatography was carried out using silica gel, Merck (used as received). All mobile phases for column chromatography were dried over $MgSO_4$ before use. Cyclic voltammograms (CVs) and bulk electrolysis profiles were recorded in anhydrous acetonitrile (Aldrich Chemical Co.) with tetrabutylammonium hexafluorophosphate ($TBAPF_6$), (Aldrich Chemical Co.) as a supporting electrolyte. Argon gas was used to degas samples for cyclic voltammetry (obtained from BOC Ltd). CV experiments were carried out with the help of Dr. Yvonne Halpin.

2.3 Equipment

2.3.1 General

IR spectra were recorded on a Perkin-Elmer Spectrum One FT-IR spectrophotometer (1 cm^{-1} resolution) and acquired 16 scans per spectrum in a 0.1 mm sodium chloride liquid solution cell using spectrophotometric grade pentane. ^{1}H-NMR and ^{13}C-NMR spectra were recorded on a Bruker AC 400 spectrophotometer in $CDCl_3$ and were calibrated according to the deuterated solvent peak. UV-vis spectra were measured on an Agilent 8453 UV-vis spectrophotometer in a 1 cm quartz cell using spectroscopic grade solvents. Cyclic voltammetry experiments were carried out using a CH Instruments 750C electrochemical potentiostat (Pico-Amp booster and Faraday cage).

2.3.2 Matrix Isolation

The basis of the matrix isolation instrument used in this investigation is similar to that reported by Long *et al.*[25] The matrix isolation apparatus is made up of a closed cycle helium refrigerator, sample window shroud, deposition tube, gas mixing chamber, backing pump, diffusion pump, gas inlet and a temperature control unit. There are two windows present in the shroud which are made of CaF_2 and are positioned at opposite faces to each other. This positioning allows for IR analysis. The deposition window is made of quartz and is positioned in the middle of the chamber between the other two which allows for irradiation of the matrix. The fourth side of the shroud contains a high vacuum metal-to-glass fitting. The fitting allows the connection of afore mentioned right angled glassware containing the complex. The CaF_2 window rotates allowing for both deposition and measurement positioning. Prior to cooling the shroud, the pressure was reduced to 8×10^{-4} Torr by means of a two stage backing pump and oil diffusion pump which was fitted with a liquid nitrogen tap. When the sample window reached 20 K (cooled to 20 K by a CS202 closed cycle helium refrigerator displex unit), the pressure was 10^{-6} Torr. A lakeshore 330 autotuning temperature control unit maintained this low temperature. The pressure of the gas when entering the gas handling line is recorded by two manometers. One has a range of 0-10 Torr, while the other has a larger range of 0-1000 Torr.

Host gases (Cryo Service) were deposited from the gas mixing chamber. This was achieved *via* a needle valve which was connected to the two inlet jets situated at either side of the sample tube. The deposition rate was kept constant at ~ 0.5 Torr / min providing an adequate sample host dilution. The isolating gas was firstly deposited for 15 mins at this rate. Different mixtures of the gases (CO, CH_4) were deposited from a right-angled glass tube which was surrounded by an acetone / liquid N_2 mix depending on the conditions of the individual experiment. Next, both the sample and isolating gases were deposited simultaneously. The complex, (**1**), was sublimed from a right angled tube which was cooled to -25 °C using acetone / liquid nitrogen slurry. Deposition was completed when the absorbance of the most intense metal carbonyl υCO bands reached an absorbance value of ~ 1 A.U. The matrix was photolysed using LEDs of varying wavelengths (470, 415, 395 and 355 nm). The matrix was analysed *via* IR spectroscopy

and spectra were recorded using a Perkin-Elmer One FTIR spectrophotometer in an inert atmosphere. The spectra resulted from the average of 16 interferograms.

2.3.3 Picosecond Time Resolved Infrared Spectroscopy

The picosecond time resolved IR apparatus used was based in the University of Amsterdam. UV pump and mid-IR probe pulses generated by a Ti : sapphire laser with a repetition rate of 1 kHz were utilised. The UV pump pulse (400 or 320 nm) was generated by single harmonic generation (SHG). Typical pulse energies generated were 0.8 - 1.0 μJ. IR probe pulses were generated by difference frequency generation (DFG) of the signal and idler from a β-barium borate (BBO)-based optical parametric amplifier (OPA) in $AgGaS_2$. The delay positions were scanned by mechanically adjusting the beam-path of the UV pump using a translation stage. The temporal resolution of 200 fs has been obtained from the full width at half maximum (FWHM) of the pump-probe cross-correlate function. Solutions were continually circulated (flowed) through IR cells containing CaF_2 windows with a path length of 500 μm.

2.3.4 Variable Temperature ^{1}H NMR Studies

^{1}H-NMR spectra were recorded using a Bruker AC 400 spectrophotometer in deuterated dichloromethane (CD_2Cl_2) and were calibrated according to the deuterated solvent peak at a range of temperatures (incremental decrease in temperature of -5 °C) from 20 °C to -70 °C. Spectra were analysed and characterised based on the chemical shifts of the Me and OMe groups.

2.3.5 Quantum Chemical Calculations

Density Functional Theory (DFT) calculations were performed by Prof. Conor Long (DCU) in order to obtain a theoretical insight regarding the explanation of the photophysics and photochemistry of the complexes. All quantum chemical calculations were performed using the Gaussian 09 program suite (Revision D.01)[26] on either the

Stokes or Fionn computers at the Irish Centre for High-End Computing. Fragment contributions to valence orbitals were calculated using the AOMix software.[27,28] Molecular structures were visualised using GaussView.[29]

2.3.6 Cyclic Voltammetry and Electrochemical CO Loss

Electrochemical experiments were carried out with the help of Dr. Yvonne Halpin. Experimental cyclic voltammograms (CVs) and bulk electrolysis profiles were recorded in anhydrous acetonitrile (Sigma-Aldrich) with tetrabutylammonium hexafluorophosphate ($TBAPF_6$) (0.1 M), as a supporting electrolyte. The concentration of the sample was 0.001 M throughout. Experiments were carried out using a CH Instruments 750C electrochemical potentiostat. All electrochemical experiments were performed at room temperature (20 °C) unless stated otherwise. A three electrode cell was employed which consisted of a glassy carbon working electrode, a Pt wire auxiliary electrode and Ag/AgCl reference electrode ($E_{1/2}$ Fc/Fc^+ redox couple = + 0.43 V). The scan rate was 0.1 V s^{-1} unless otherwise stated. All experiments were performed with the cell in the absence of light. CO release was detected using a Shimadzu GC-2010 Plus unit (Lab Solutions version 5.57 software) with a dielectric barrier discharge ionisation detector (BID) and a ShinCarbon micropacked column with 0.53 mm internal diameter.

2.3.7 Synthesis

2.1.1.1 Synthesis of [(CO)$_5$CrC(OMe)Me] (1)

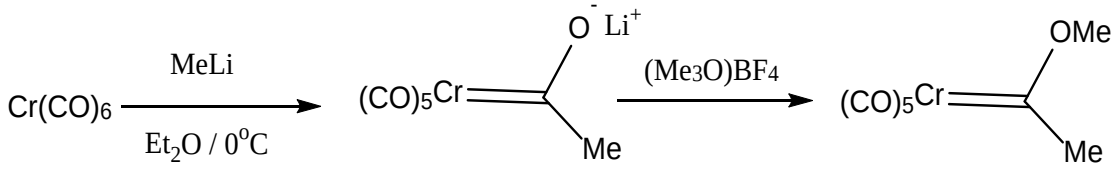

Scheme 2.2 Synthesis of [(CO)$_5$CrC(OMe)Me] (**1**).

The synthesis of (**1**) was carried out as previously reported with some modifications.[30] $Cr(CO)_6$ (2.0030 g, 9.09 mmol) was dissolved in 25 ml of dry diethyl ether. The reaction flask was cooled to 0 °C. A 10 % excess of MeLi (5.8 ml of a 1.6 M) solution in diethyl ether was added in a drop-wise manner *via* syringe. The reaction mixture reached room temperature and was left to stir for 1 hour. The solvent was removed under reduced pressure. The remaining residue was dissolved in 25 ml of deionised water and trimethyloxonium tetrafluoroborate salt was added until the aqueous phase reached pH 3 - 4. Four, 25 ml aliquots of CH_2Cl_2, extracted the product from the aqueous phase. The organic extracts were combined and dried over $MgSO_4$. The solvent was removed under reduced pressure. A light brown oil remained. This oil was washed with cold pentane and dried under high vacuum resulting in a yellow solid. Spectroscopic data agreed with reported data.[30]

% Yield: 1.86 g, 7.44 mmol, 82 % yield.

^{1}H NMR: (400 MHz, $CDCl_3$) 2.96 (3H, s), 4.74 (3H, s) ppm.

IR: (pentane) 2065, 1984, 1964 and 1948 cm^{-1}.

2.1.1.2 Synthesis of $[(CO)_5WC(OMe)Me]$ (4)

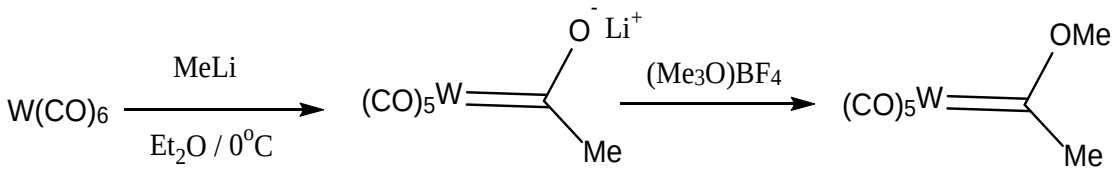

Scheme 2.3 Synthesis of $[(CO)_5WC(OMe)Me]$ (**4**).

$[(CO)_5WC(OMe)Me]$ was synthesised in the same manner as for $[(CO)_5CrC(OMe)Me]$.[30] $W(CO)_6$ (1.63 g, 4.63 mmol) was dissolved in 25 ml of dry diethyl ether. The reaction flask was cooled to 0 °C. A 10 % excess of MeLi (3.13 ml of a 1.6 M solution in diethyl ether) was added in a drop wise manner *via* syringe. The reaction mixture reached room temperature and was left to stir for 1 hour. The solvent was removed under reduced pressure. The remaining residue was dissolved in 25 ml of deionised water and trimethyloxonium tetrafluoroborate salt was added until the aqueous phase reached pH 3 - 4. Four, 25 ml aliquots of CH_2Cl_2, extracted the product from the aqueous phase. The organic extracts were combined and dried over $MgSO_4$. The solvent was removed under reduced pressure. A light brown oil remained. This oil was washed with cold pentane and dried under high vacuum resulting in a yellow solid. Spectroscopic data agreed with reported data.[30]

% Yield: 1.16 g, 3.07 mmol, 66 % yield.

^{1}H NMR: (400 MHz, $CDCl_3$) 2.88 (3H, s), 4.59 (3H, s) ppm.

IR: (pentane) 2073, 1983, 1960 and 1945 cm^{-1}.

2.4 Results and Discussion

2.4.1 UV-vis Spectroscopy

The electronic absorption properties have been previously described for compounds (**1**) and (**4**).[5,31,32] The overlaid UV-vis absorbance spectra of the Fischer carbene complexes are displayed in Figure 2.3. In general, the UV-vis spectra of Fischer carbene complexes consist of a low absorbing band at ~ 500 nm (spin forbidden MLCT), a stronger band at 350 - 450 nm (spin allowed MLCT) and a weaker band at 300 - 350 (LF transition).[3] Complex (**4**) exhibits absorption bands with λ_{max} at approximately 350 and 370 nm. The band at 350 nm has previously been assigned to a LF band and the band at 370 nm has been assigned to an MLCT band.[5] In the case of the chromium analogue (**1**), the MLCT and LF bands tend to overlap with λ_{max} at 377 nm in *n*-heptane which is in agreement with that reported in the literature.[31,32] The main difference between the spectra is that the spectrum of the tungsten complex (**4**) exhibits a weak shoulder on the low energy side of the lowest energy absorption maximum. This is assigned to the singlet to triplet transition.[33] This feature is absent in the case of the chromium complex (**1**). This observation is consistent with studies previously reported which state that optical population of the triplet state in Group 6 metal complexes is only possible for tungsten and not for chromium nor molybdenum complexes.[34,35]

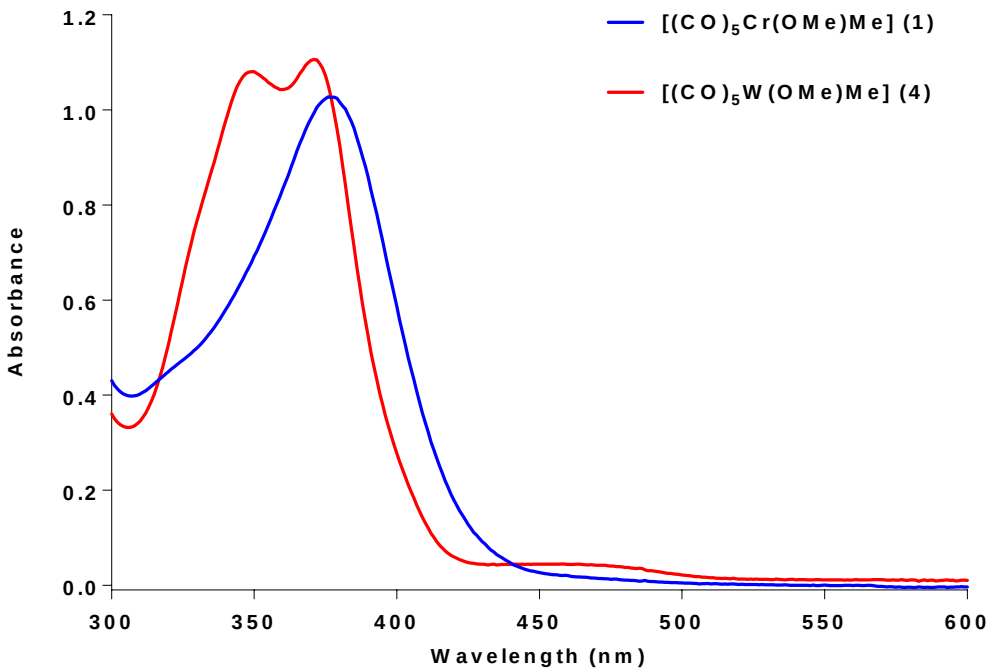

Figure 2.3 The UV-vis. spectra of **(1)** and **(4)** recorded in *n*-heptane solution. The singlet to triplet transition is evident as a shoulder in the spectrum of **(4)**, this feature is absent in the spectrum of **(1)**. Concentration in the order of 10^{-5} M.

2.4.2 Matrix Isolation

The Matrix isolation (MI) experiments were carried out at 20 K. Many different gas mixtures were utilised and repeated such as neat CH_4, CH_4 (99 %): CO (1 %), CH_4 (95 %): CO (5 %), CH_4 (90 %): CO (10 %) and neat N_2. A range of wavelengths were used i.e. 528 nm, 470 nm, 415 nm, 395 nm, 355 nm, white light and broadband irradiation in various successions. The optimum conditions for detection of the intermediates were in neat CH_4 and mixed CH_4 (95 %): CO (5 %) matrixes. Three excitation conditions were used in these experiments, broad-band irradiation using wavelengths greater than 470 nm, and two monochromatic sources using 395 or 355 nm light. These wavelengths were chosen to investigate the wavelength dependent nature of the photochemistry of **(1)**. 470 nm represents the onset wavelength for the lowest energy absorption of **(1)** and therefore should populate only the lowest accessible excited state. The matrix was subjected to irradiation with $\lambda_{exc} > 470$ nm initially followed by irradiation with 395 nm and finally using a 355 nm light source. The FT-IR spectra of (**1**) is displayed in Figure 2.4.

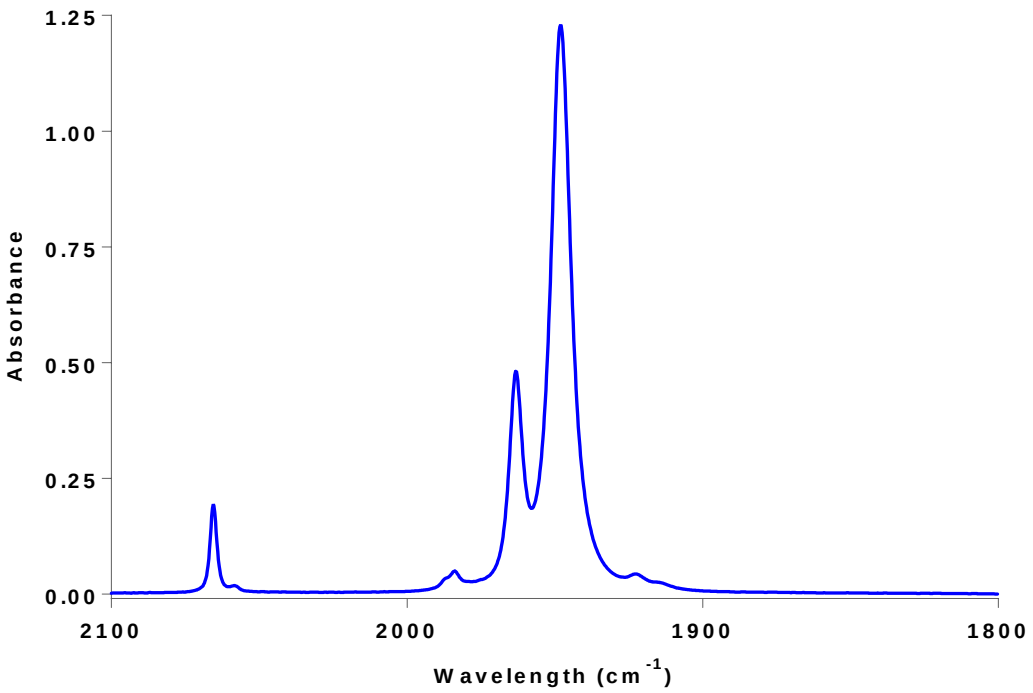

Figure 2.4 The FTIR spectrum of $[(CO)_5CrC(OMe)Me]$ (**1**) in *n*-heptane.

The infrared spectrum of a freshly deposited sample of **(1)** in either a neat CH_4 matrix or the mixed CH_4 / CO matrix at 20 K showed bands in the terminal metal carbonyl region (υCO) at 2067 (w), 1986 (w), 1961 (s), 1950 (shoulder) and 1945 (s) cm^{-1}. A weak feature at 1255 cm^{-1} was also observed which corresponds to the $C_{carbene}$-OMe stretching vibration (this band is sensitive to the isomeric changes to the carbene ligand). DFT calculations indicated that the *anti*- isomer of **(1)** is marginally more stable than then *syn*- isomer (Figure 2.5). Therefore these features have been assigned to the *anti*-isomer which should predominate at 20 K.

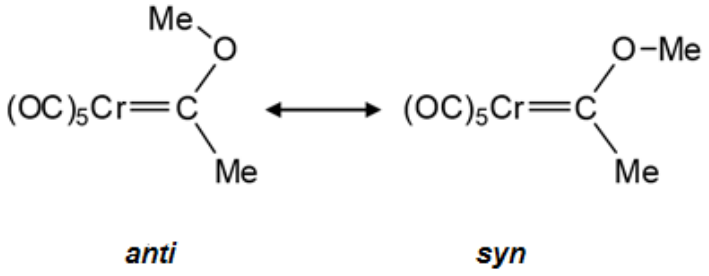

Figure 2.5 Representations of the structures of the *anti*- and *syn*-isomers of (**1**).

2.4.2.1 Pure CH_4 matrix studies

A freshly deposited matrix of **(1)** was irradiated for 18 hours with λ_{exc} > 470 nm. Following this irradiation, there were no changes observed in the υCO region of the spectrum, however the band at 1255 cm^{-1} was shifted to 1247 cm^{-1} indicating *anti* to *syn* isomerisation at the carbene ligand. *Anti-syn* isomerisation of alkoxy carbenes has also been observed using MI techniques, by Rooney *et al.*[32] Peaks for the *anti*- isomer were seen at 2071 (m), 1991 (w), 1967 (br) and 1950 (br), 1254 (m) cm^{-1}, in an argon matrix using broadband irradiation (λ > 390 nm).[32] The *syn*- isomer exhibited bands at 2072 (m), 1996 (w), 1970 (br) and 1951 (br), 1248 (m) cm^{-1} under identical conditions (note the spectra reported here were the average of 16 scans with 1 cm^{-1} resolution whereas the spectra from the Rooney group were the average of 128 scans with 1 cm^{-1} resolution). A notable shift in the $C_{carbene}$-O bond was observed which is consistent with this data. This confirms that isomerisation is achieved following excitation into the lowest accessible excited state at low energy irradiation.

Subsequent irradiation of this matrix using λ_{exc} = 355 nm, resulted in a decrease in the intensity of the υCO bands of (**1**) and the formation of new υCO bands at 2043, 1988, 1949 (obscured by parent bleach), 1911, and 1899 cm^{-1} as well as the characteristic absorption of "free" CO at 2140 cm^{-1} (Figure 2.6 (a)). These new bands are assigned to two species, firstly, the expected CO loss species [$(CO)_4CrC(OMe)(Me)$] (2043 and 1899 cm^{-1}), also observed by Rooney *et al.* (2047, and 1906 cm^{-1}) in an Ar matrix at λ > 390 nm.[32] Secondly, the bands at 2040, 1988, 1949 (obscured by the parent bleach), 1925 and 1911 cm^{-1} are assigned to the ketene species (**3**) (see Scheme 2.4 in section **2.3.3**). These assignments are based on a combination of results from these MI studies, psTRIR studies and DFT calculations which will be described later.

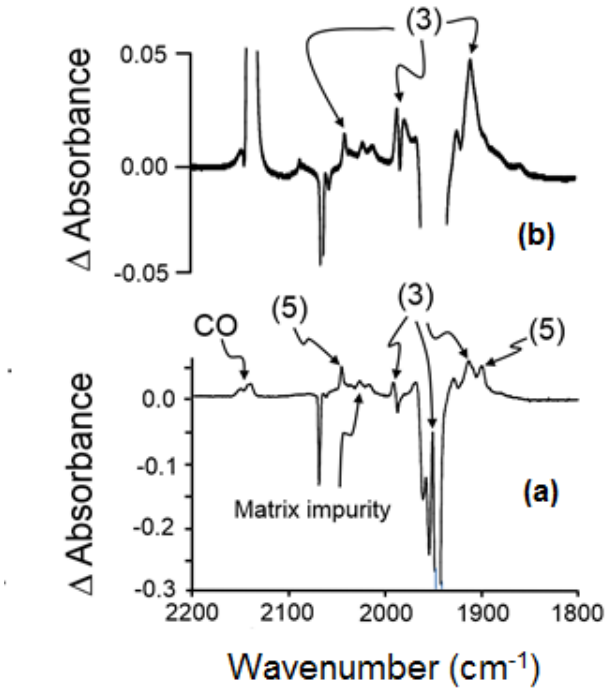

Figure 2.6 (a) A difference IR spectrum obtained following irradiation of (**1**) at 355 nm in a CH_4 matrix at 20 K showing the formation of (**3**) and (**5**) and uncoordinated CO in the matrix and (b) the difference spectrum obtained following irradiation with 395 nm light in a CH_4/CO matrix (95 : 5) showing primarily the formation of (**3**). See Scheme 2.4 in section **2.3.3**.

2.4.2.2 Mixed CH_4 / CO matrix studies

A sample of **(1)** was deposited in a mixed matrix consisting of 95 % CH_4 and 5 % CO. The presence of CO in the matrix was intended to suppress the CO loss process and allow the observation of products which are not the result of a CO loss process. Under these conditions, irradiation using 395 nm light produced product bands at 2043, 1990, 1949, 1925 and 1911 cm^{-1} (Figure 2.6 (b)). The bands are assigned to the metallaketene species (see Scheme 2.4, in section **2.3.3**, for TRIR generated transient signals).

2.4.3 Picosecond Time Resolved Infrared Spectroscopy

A psTRIR investigation of (**1**) and (**4**) in *n*-heptane solution was undertaken at 293 K. Infrared spectral changes were monitored in the 2150 – 1700 cm^{-1} region covering both the terminal and bridging ν_{CO} regions. Resolution was between 3 and 5 cm^{-1}. All rate constants obtained in these experiments were measured at 293 K using an excitation pulse of 200 fs. The pulse energy was between 0.8 - 1 µJ. Two excitation wavelengths were used in these experiments, 400 and 320 nm. These wavelengths were chosen because they are close to the excitation wavelengths used in the matrix isolation experiments described previously. The FTIR spectrum of (**1**) can be seen in Figure 2.4 and the FTIR spectrum of (**4**) is shown below in Figure 2.7.

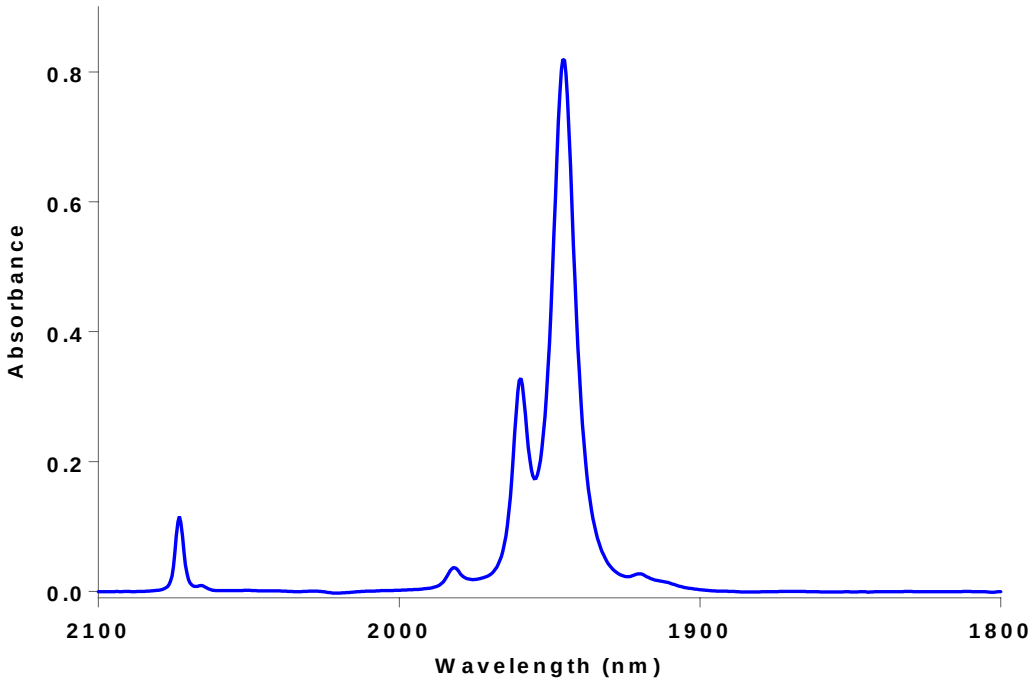

Figure 2.7 The FTIR spectrum of $[(CO)_5WC(OMe)Me]$ (**4**) in *n*-heptane.

2.4.3.1 psTRIR studies of $[(CO)_5CrC(OMe)Me]$

2.4.3.1.1 psTRIR studies of $[(CO)_5CrC(OMe)Me]$ (1) using 400 nm excitation

The psTRIR difference spectra obtained upon excitation of **(1)** at 400 nm are presented in Figure 2.8. Within the excitation pulse (200 fs), the parent bands at 2058 and 1940 cm^{-1} were bleached (represented by downward features in the difference spectrum) and a broad feature centred at 1970 cm^{-1} was produced. These bands are assigned to an electronically excited (**1**), i.e. (**1***) as depicted in Scheme 2.4. During the subsequent 10 ps the broad feature decayed and sharper features at 2060, 1986, 1945 and 1770 cm^{-1} were produced with identical rate constants (k_{obs} = 2.4 ($\pm$0.3) $\times 10^{11}$ s^{-1}). This new species is assigned to the excited metallacyclopropanone (**2***) intermediate because of the bridging carbonyl ligand absorbing at 1770 cm^{-1}. Since this band was not observed in the MI experiments at 20 K, it is believed to be an excited state species. The metallacyclopropanone excited state then decayed (k_{obs} = 2.8 ($\pm$0.1) $\times 10^{10}$ s^{-1}) giving rise to a long lived species, which absorbed at 1981, 1965, 1945, and 1919 cm^{-1} (the latter being very weak), however, no features in the bridging υCO region were observed (Figure 2.8 (b)). These bands are assigned to the metallaketene intermediate. Figure 2.8 (a) also illustrates the time dependent behaviour of selected bands. It should be noted that the parent band at 1940 cm^{-1} recovers with a bi-exponential time dependence (k_1 = 2.0 ($\pm$0.3) $\times 10^{11}$ s^{-1} and k_2 = 3.2 ($\pm$0.6) $\times 10^{10}$ s^{-1}). This means that both the initially produced excited state (**1***) and (**2***), and the metallacyclopropanone excited state regenerates the parent complex, (**1**). Based on the residual depletion of the parent absorbance at 1940 cm^{-1}, the quantum yield of the ketene formation is estimated at approximately 10 % following 400 nm excitation. Scheme 2.4 indicates the photophysical processes of (**1**) leading to the formation of the metallaketene (400 nm) and the CO loss species $[(CO)_4(S)CrC(OMe)Me]$ following 320 nm irradiation (S = *n*-heptane). The formation of a solvated CO loss species is consistent with that previously reported for other Fischer carbene complexes.[20]

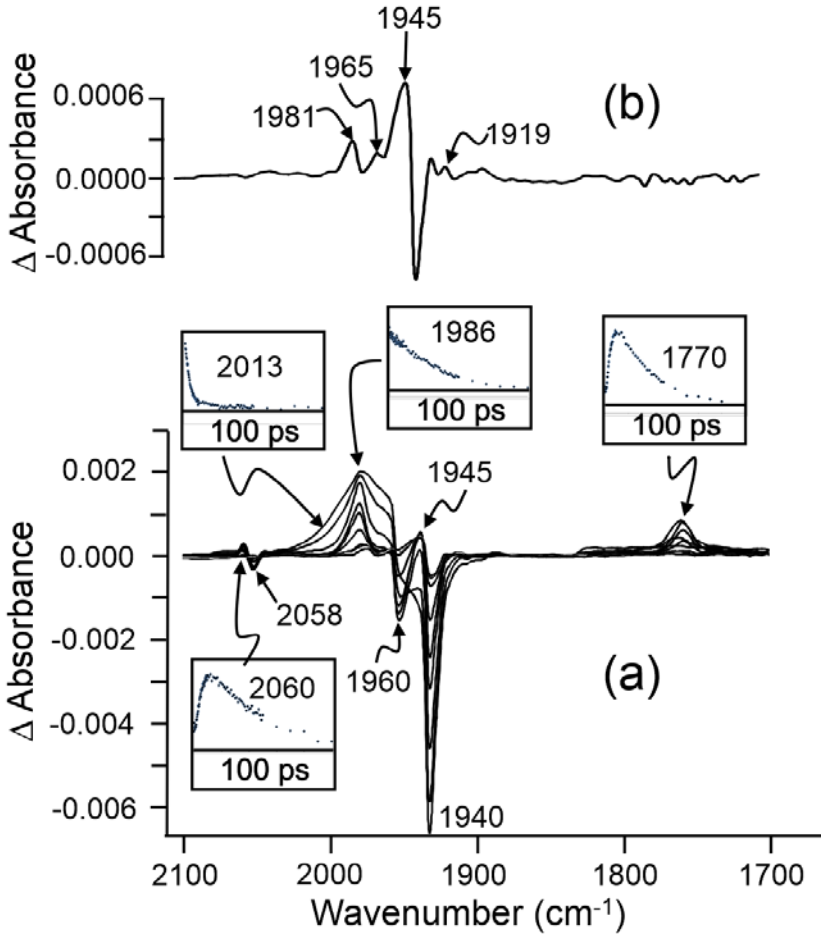

Figure 2.8 (a) The infrared spectra obtained at 0.4, 2, 6, 30, 50, 100, 120, and 180 ps after 400 nm excitation of (**1**) in *n*-heptane solution showing depletion of the parent bands at 1958, 1960, and 1940 cm^{-1}. The inserts show the time dependence at the indicated wavenumber. **(b)** The expanded final difference spectrum (wavenumber scale as per part **(a)**) obtained at 1500 ps after excitation showing the long-lived features of the metallaketene species at 1981, 1965, 1945 and 1919 cm^{-1}.

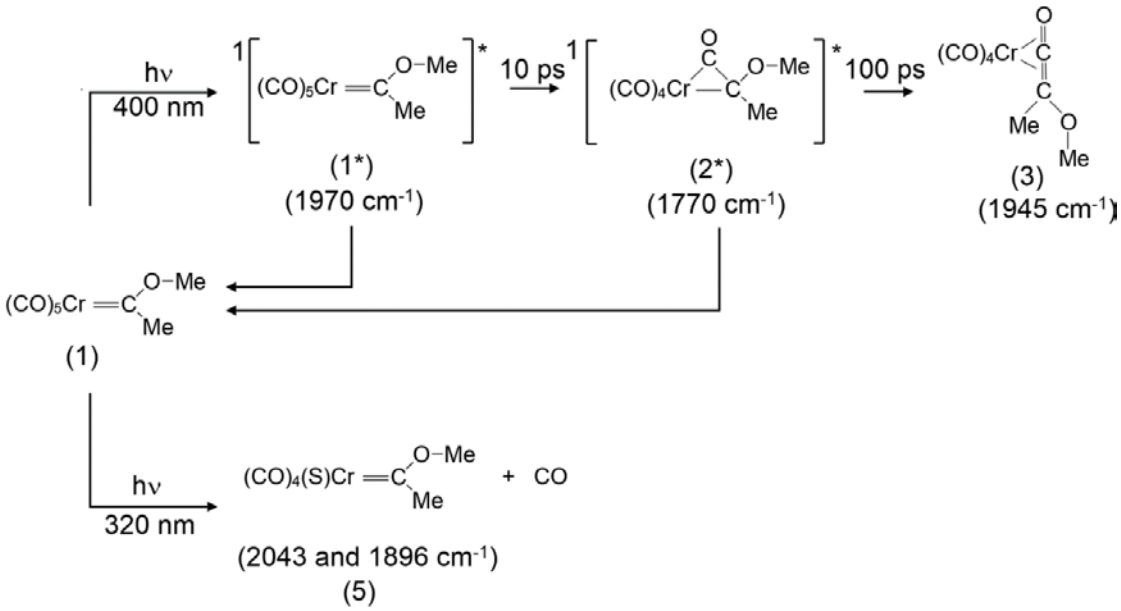

Scheme 2.4 The photophysical processes of (**1**) leading to the formation of the metallaketene (following excitation at 400 nm) (diagnostic IR bands in parentheses) and the CO loss species [$(CO)_4$(S)CrC(OMe)Me] following 320 nm irradiation (S = *n*-heptane).

2.4.3.1.2 psTRIR studies of [$(CO)_5$CrC(OMe)Me] (1) using 320 nm excitation.

The spectroscopic changes observed following 320 nm excitation (0.8 μJ) of **(1)** in *n*-heptane are presented in Figure 2.9. Within the excitation pulse (200 fs), the parent bands at 2058 and 1940 cm^{-1} were bleached and no significant peaks were observed. The CO loss product [$(CO)_4$(*n*-heptane)CrC(OMe)Me] (**5**), was formed over the subsequent 50 ps with bands at 2043 and 1896 cm^{-1}. The infrared spectra obtained 1 and 44 ps after excitation at 320 nm are displayed in Figure 2.9. These bands are in similar positions with those reported for the tetracarbonyl photoproduct, [$(CO)_4$CrC(OMe)Me], which exhibited band positions at 2047 and 1906 cm^{-1} in low temperature matrices.[32] Thus, CO loss requires excitation using wavelengths on the high-energy side of the lowest energy absorption maximum of this complex. The quantum efficiency for CO loss was estimated at 35 % for (**1**) following excitation at 320 nm.

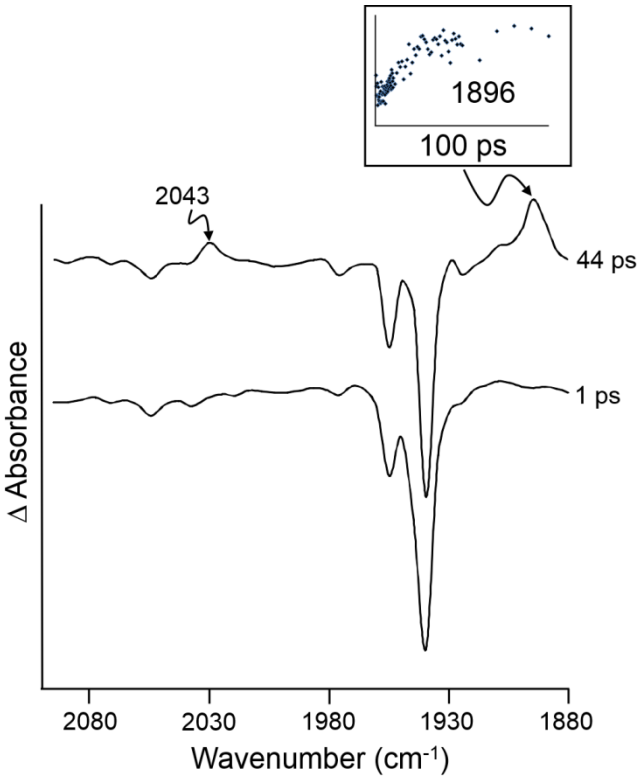

Figure 2.9 The infrared spectra obtained 1 and 44 ps after a 320 nm excitation pulse showing the formation of the CO loss product (**5**) with bands at 2043 and 1896 cm^{-1}.

2.4.3.2 psTRIR studies of $[(CO)_5W(OMe)Me]$

2.4.3.2.1 psTRIR study of $[(CO)_5WC(OMe)Me]$ (4) using 400 nm excitation.

The psTRIR difference spectrum obtained following 400 nm excitation of (**4**) in *n*-heptane is presented in Figure 2.10. Within the excitation pulse, the bands of the parent (1935, 1950 cm^{-1} and 2069 cm^{-1}) were depleted and a broad absorption centered at 1965 cm^{-1} was produced (**4*a**). Over the subsequent 20 ps this peak decayed (k = 2.6 (± 0.9) $\times 10^{11}$ s^{-1}) producing a new species with a broad peak at 1920 cm^{-1} and a weak peak at 2051 cm^{-1} (**4*b**) (k = 2.5 (±0.1) $\times 10^{11}$ s^{-1}). (**4*a**) and (**4*b**) are assigned to two triplet excited states with different structures (Scheme 2.5), the first being directly populated from the ground state in the excitation event. It should be noted that the UV-vis spectrum of (**4**) exhibits a weak shoulder on the low-energy side of the lowest energy λ_{max} (Figure 2.3) which indicates that the direct population of low lying triplet states is possible from

the ground state. This is because of the large spin orbit coupling for tungsten compared to chromium where singlet-to-triplet transitions are strictly spin forbidden. Over the subsequent 40 ps, the features at 1920 and 2051 cm^{-1} (**4*b**) decay producing absorptions at 1930, 1983 and 2059 cm^{-1} which is assigned to the ground state (singlet) metallaketene (**6**) formed by intersystem crossing of the triplet state to the ground-state singlet hypersurface. Due to the significant spectral overlap of these features with the depleted and recovering parent absorptions it is very difficult to accurately determine peak positions in these experiments. However, it is clear is that no bands are observed in the bridging carbonyl region. In contrast to the chromium system, no metallacyclopropanone excited states are produced in the tungsten system. The photophysical processes following irradiation of (**4**) leading to the metallaketene (**6**) are illustrated in Scheme 2.5.

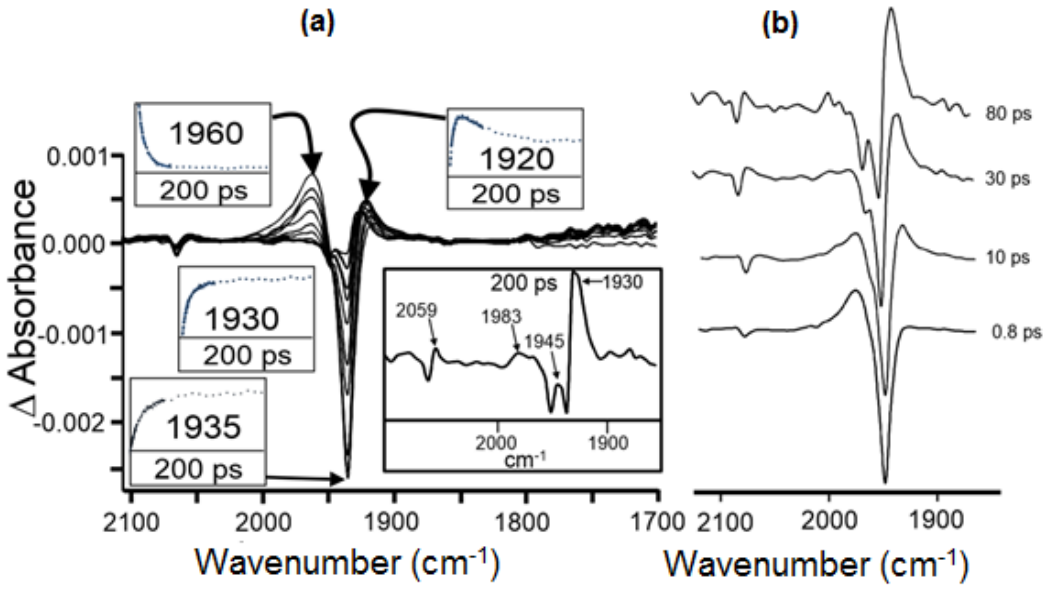

Figure 2.10 (a) The psTRIR spectra obtained following 400 nm excitation of (**4**) in *n*-heptane, spectra obtained at 2, 4, 6, 10, 16, 24, 40, 50, 80, 120 and 180 ps after the excitation with the spectrum at 200 ps presented in an inset; the time-dependence of selected bands are also presented in insets, **(b)** selected spectra at indicated delays after 400 nm excitation showing the initial excited state as a broad feature at 1960 cm^{-1} (the vertical axis is Δ Absorbance with various scales).

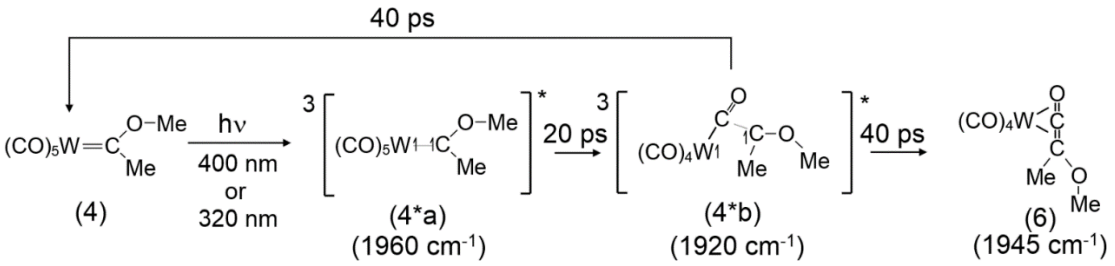

Scheme 2.5 The photophysical processes following irradiation of (**4**) leading to the metallaketene (**6**) formation *via* triplet excited states, the half arrows indicate the location of large spin density from DFT calculations.

2.4.3.2.2 psTRIR study of [(CO)$_5$WC(OMe)Me] (4) using 320 nm excitation.

The spectral changes of (**4**) observed following excitation at 320 nm were identical to those observed following excitation at 400 nm described above, with one exception, namely the production of a weak feature at 1886 cm^{-1}. This feature is assigned to the CO loss product. The CO loss product is formed within the excitation pulse (200 fs). Thus, the photochemistry of (**4**) is substantially independent of the excitation wavelength, and efficient internal conversion processes occur which predominantly populate the lowest energy triplet state. No features were observed in the bridging υCO region following excitation at 320 nm. The quantum efficiency for CO loss was estimated as 9 % for (**4**) at 320 nm.

2.4.4 Quantum Chemical Calculations

Table 2.1 depicts the calculated and observed νCO bands represented in MI and psTRIR experiments.

Table 2.1 The observed and calculated νCO bands for (**1**), (**3**), (**4**), (**5**) and (**6**).

Complex	Observed FTIR		Observed MI		Observed psTRIR		Corrected˜	
1	2065	w	2067	w	2058	w	2065	w
	1984	w	1986	w	*		1983	w
	1964	m	1961	m	*		1960	m
	1948	s	1950		*		1951	s
			1945		1940	s	1950	s
3			2040	w	#		2050	w
			1988	m	1981	m	1968	m
			1949	s	1965	w	1952	s
			1925	m	1945	s	1936	m
			1911	w	1919	w	1917	w
4	2073	w			2069	w	2072	w
	1983	w			*		1982	w
	1960	m			*		1958	m
	1945	s			1935	s	1945	s
							1946	s
5			2043	w	2043	w	2017	w
					#		1950	m
					#		1937	s
			1899	m	1896	m	1899	m
6					2059	w	2050	w
					1983	w	1961	m
							1945	vs
					1930	s	1900	m
							1856	vw

*Obscured by excited-state absorption #obscured by parent bleach

2.4.5 Variable Temperature ^{1}H-NMR Spectroscopy

Quantum calculations by Prof. Long, indicate that, in the ground state, the *anti*- isomer of (**1**) is slightly more stable (7 kJ mol^{-1}) than the *syn*- isomer.[33] This suggests that (**1**) exists as a mixture of both *anti*- and *syn*- isomers at almost matching concentrations at room temperature which is evident from Figure 2.11.

The activation energy for the *anti* to *syn* isomerisation of (**1**) was determined by variable temperature ^{1}H-NMR experiments over the temperature range 20 to – 70 °C in CD_2Cl_2. The temperature was decreased in increments of - 5 °C. The methyl protons resonate at ~ 2.8 ppm relative to TMS. At - 5 °C, a second peak becomes evident at ~ 2.91 ppm. As the temperature is decreased further, this peak grows and becomes sharper confirming that the thermal barrier between *anti*- and *syn*- isomerisation has been overcome. At - 20 °C to - 25 °C, a steady state is achieved. The Me signal was used in this determination and the peak width at half height was measured at each temperature. A new peak was evident at 2.91 ppm at temperatures lower than - 5 °C. The rate constant for the isomerisation (*anti-syn*) was estimated using the method described by Gasparro and Kolodny.[36] An Arrhenius plot (Figure 2.12) of the data yielded the activation energy (E_a) of the isomerisation process as 57 kJ mol^{-1}. Theoretical quantum chemical calculations determined the activation energy required to overcome the barrier as 60 kJ mol^{-1}. The value obtained in this study is in close agreement with that reported by Kreiter *et al.*[37]

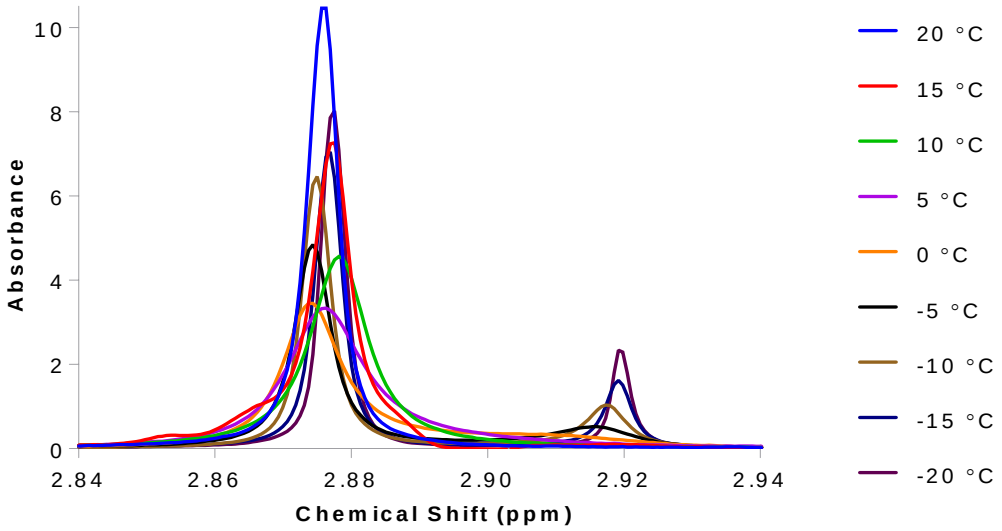

Figure 2.11 Overlaid ^{1}H-NMR Spectra of Me group of **(1)** in CD_2Cl_2 at temperatures ranging from 20 °C → -20 °C.

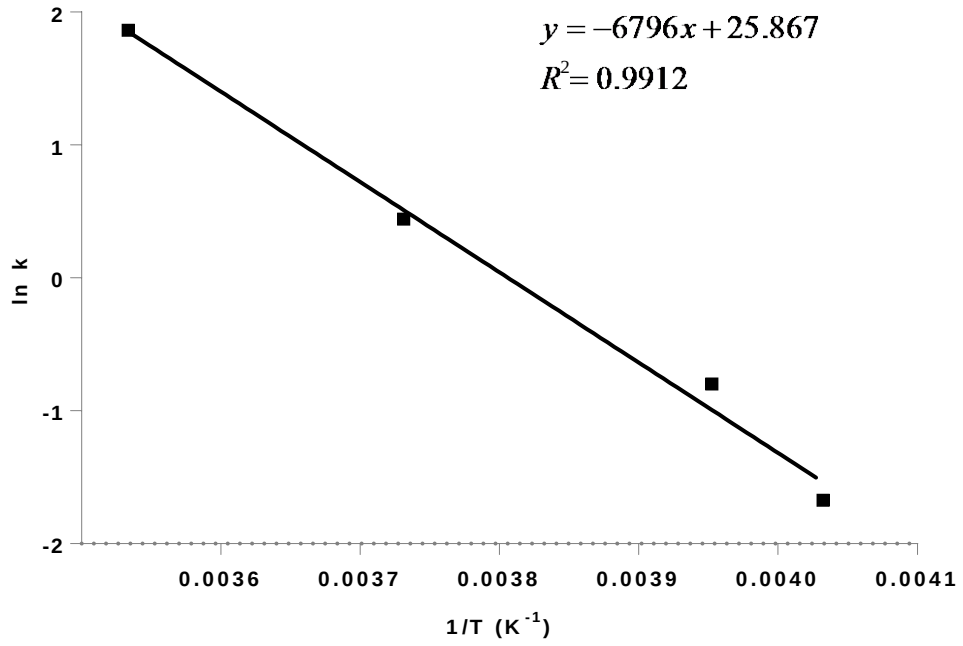

Figure 2.12 Plot of ln k. *vs.* 1/T of Me at various temperatures in order to determine the activation energy (E_a) required to overcome the barrier of *anti-syn* isomerisation of **(1)**.

In summary, matrix isolation, psTRIR and variable temperature ^{1}H-NMR in conjunction with quantum chemical calculations were performed to ascertain the photophysical and photochemical processes which underpin the use of group 6 metal carbene complexes as reagents in organic syntheses as well as to understand the photochemical pathway to CO loss. At low energy irradiation (470 nm), *anti-syn* isomerisation is observed. This is confirmed by variable temperature ^{1}H-NMR which agrees with quantum chemical calculations.

Similarly to the psTRIR study reported by Nguyen *et al.* at 400 nm, a band at 1777 cm^{-1} was observed. Nyugen *et al.* assign this species to a singlet excited state metallaketene. However, in contrast to this assignment, our studies suggest that this band is due to a metallacyclopropanone rather than a metallaketene species.[18] Furthermore, the evidence from the MI and psTRIR results presented here, strongly suggests that this species reacts to form a long-lived ground-state metallaketene. In addition, no evidence for the triplet species, reported by Nguyen *et al*., was observed. Consequently, an alternative explanation to that proposed by Nguyen *et al.* is that only singlet excited states are involved in the photophysics of (**1**). It should be noted that in the psTRIR study presented here, typical pulse energies were in the 0.8 to 1 μJ range (with one exception where 8 μJ pulses were used) with a duration of 200 fs. Nguyen *et al.* used pulse energies of 80 μJ and a pulse duration of 1 ps.[18]

Quantum chemical modelling indicates that only the *syn*-isomer can form the reactive metallaketene intermediate. It is interesting to note that Hegedus proposed the intermediate formation of this metallacyclopropanone leading to the metallaketene in his seminal work of 1988.[12] The infrared characteristics of the metallacyclopropanone excited state with a peak in the bridging υCO region (1770 cm^{-1}) is significantly different to the infrared spectrum of the metallaketene which exhibits υCO bands only in the terminal M-CO region between 1800 and 2100 cm^{-1}. In contrast to the previous study, no appreciable CO loss was found following 400 nm excitation.[18]

It is clear from the psTRIR experiments that the photophysics of the tungsten complex (**4**) is significantly different to that of the chromium complex (**1**). Nguyen *et al.* explained the spectroscopic changes by the *anti* to *syn* isomerisation of the carbene ligand, but the experimental data obtained by us is more consistent with assigning this species as a metallaketene.[18] The metallaketene (**6**) is produced without the intermediate formation of a metallacyclopropanone excited state which was observed in the case of

the chromium analogue (*vide supra*). Consequently, it is proposed that in this case the lowest energy triplet state is responsible for the observed photochemistry. The experimental data presented here which are supported by quantum chemical calculations show that both the chromium (**1**) and tungsten (**4**) systems form the appropriate metallaketene following suitable irradiation.

It is clear that at 320 nm, CO loss is more efficient for the chromium system (**1**) in comparison to the tungsten analogue, (**4**), therefore, (**1**) would be a more efficient photo CORM that (**4**). However, 320 nm is not an ideal wavelength for photo induced CO release as irradiation at such high energies is damaging to the skin. Therefore, in forthcoming chapters, photochemical CO release using lower energy irradiation from novel systems will be analysed and discussed.

2.4.6 Electrochemically Induced CO Loss

Electrochemical analyses of the carbene complexes **(1)** and **(4)** were performed in acetonitrile solution using 0.1 M tetrabutylammonium hexafluorophosphate ($TBAPF_6$) as the electrolyte, the results of which are in agreement with other Cr and W Fischer carbene complexes previously reported.[38] Cyclic voltammetry reveals a quasi-reversible first oxidation peak for **(1)** (E_{pa} = + 0.45 V *vs.* Fc/Fc^+) and an electrochemically irreversible first oxidation for **(4)** under the experimental conditions employed (scan rate = 0.1 V s^{-1}). The fact that the W analogue is oxidised at a more positive potential ($\Delta E_{p\ (W - Cr)}$ = 0.23 V) than the Cr analogue is due to the difference in the first ionisation potential of the metals[38] and supports the assignment of the first oxidation as being predominantly metal centred representing the $Cr^{0/1}/W^{0/I}$ redox couple.[39,40]

In vivo studies using electrochemical methods as potential therapeutics for diseases such as various cancers have been previously reported.[22,23,24] Compounds **(1)** and **(4)** were investigated to assess their ability to lose CO by electrochemical means focusing on their individual first oxidation positions. Electrochemical initiation of CO-release from a 1 mM solution of both complexes in CH_3CN was confirmed and was measured over five time intervals (over ~100 minutes). The amount of CO generated was quantified *via* headspace analysis using gas chromatography, Figure 2.13. Continuous bulk electrolysis was applied just after the first oxidation and before any further Faradaic processes of

each complex (the potential applied for **(1)** was + 0.57 V and for **(4)**, + 0.88 V). There is a notable difference in CO loss for these systems with the chromium analogue being much more efficient.

The amount of CO produced from **(1)** (~ 5×10^{-5} moles) is over an order of magnitude greater than that from **(4)** (~ 6×10^{-7} moles) at the end of the 1.5 hour experiment. In the case of tungsten carbene complexes, it is common for electrode coating to occur which causes passivation ("blocking") at the surface of the electrode which decreases the efficiency of the bulk electrolysis. This was observed in the case of **(4)**.[41]

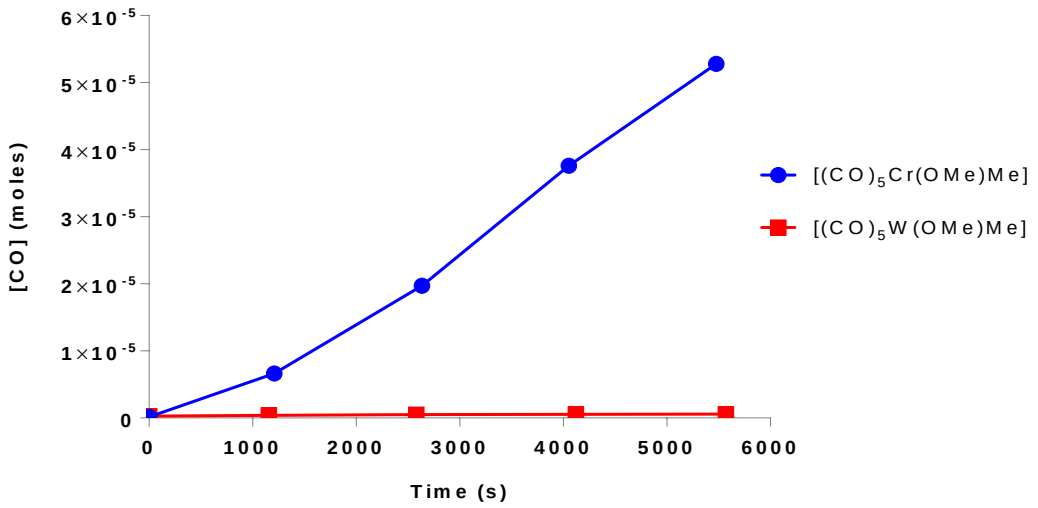

Figure 2.23 Profile for the electrochemically induced CO release over time for both **(1)** and **(4)** in acetonitrile under potentiostatic conditions (E = + 0.57 V and + 0.88 V *vs.* Fc/Fc^{+}, respectively). Concentrations of both complexes were 1 mM and the solution was continuously stirred (n = 1).

2.5 Conclusion

In this chapter, the results of a photochemical and photophysical, psTRIR investigation of (**1**) and (**4**) using 0.8 μJ pulses of 400 nm or 320 nm photons are reported and an alternative explanation for the psTRIR results to that published by Nguyen *et al.* is discussed.[34] Variable temperature ^{1}H-NMR and low-temperature matrix isolation (MI) studies are reported as well as time-dependent density functional theory calculations (TDDFT) to support the experimental results. Excited state dynamics along reaction coordinates to either CO loss or ketene formation is also presented. Evidence for the formation of the elusive ground-state and long-lived metallaketenes (**3**) and (**6**), which contain no bridging carbonyl ligands are presented. These intermediates are analogous to that first proposed by Hegedus as the reactive intermediates responsible for cyclobutanone formation.[8] Furthermore, the psTRIR studies confirm that for the chromium system, the metallaketene is formed *via* a singlet metallacyclopropanone excited state (**2***), where the asterisk indicates an excited state which has a lifetime of approximately 30 ps and a bridging ν_{CO} band at 1770 cm^{-1}. For the tungsten analogue (**4**) however, the metallaketene is produced *via* a triplet state which does not contain a bridging CO ligand.

Electrochemical and photochemical CO release occur more efficiently for the chromium complex in contrast to the tungsten complex. Therefore, (**1**) would be the superior photo- or electro- CORM for future applications. A new method of elucidating the photochemistry of CORMs has been verified and clearly explains how CO is released at certain wavelengths and why CO is not released at others. PsTRIR will be used for future CORMs designed and synthesised in the forthcoming chapters.

2.6 References

1. Fischer, E. O.; Maasbol, A. On the Existence of a Tungsten Carbonyl Carbene Complex. *Angew. Chem. -Int. Edit.* **1964**, *3*, 580-581.

2. Dotz, K.; Tomuschat, P. Annulation reactions of chromium carbene complexes: scope, selectivity and recent developments. *Chem. Soc. Rev.* **1999**, *28*, 187-198.

3. Hegedus, L. Chromium carbene complex photochemistry in organic synthesis. *Tetrahedron* **1997**, *53*, 4105-4128.

4. Foley, H.; Strubinger, L.; Targos, T.; Geoffroy, G. Photochemistry of $[W(CO)_5(C(OMe)Ph)]$ - Formation of Alkyne Carbene Complexes and Studies of their Decomposition Reactions. *J. Am. Chem. Soc.* **1983**, *105*, 3064-3073.

5. Rooney, A.; McGarvey, J.; Gordon, K. Time-Resolved Raman-Spectroscopy and Matrix-Isolation Studies of Anti-Syn Photoisomerization in Metal-Carbonyl Carbenes. *Organometallics* **1995**, *14*, 107-113.

6. Bechara, J.; Bell, S.; McGarvey, J.; Rooney, J. Ligand-Field Photolysis of the Fischer Complex, $(CO)_5W=C(OMe)Ph$ - Time-Resolved Resonance Raman-Spectroscopic Evidence for Alkyl Metal Interaction Following CO Photodissociation. *J. Chem. Soc. - Chem. Commun.* **1986**, *24*, 1785-1787.

7. Bell, S.; Gordon, K.; McGarvey, J. Time-Resolved Resonance Raman-Spectroscopy and Solution Kinetics of Photogenerated Transients in the Metal Carbene Complex $(OC)_5W=C(OMe)Ph$. *J. Am. Chem. Soc.* **1988**, *110*, 3107-3112.

8. Gut, H.; Welte, N.; Link, U.; Fischer, H.; Steiner, U. Formation and reactions of tetracarbonyl intermediates of the fischer carbene complex $(CO)_5W=C(OMe)Ph$. A laser flash photolysis study using time-resolved infrared and UV/Vis spectroscopy. *Organometallics* **2000**, *19*, 2354-2364.

9. Sierra, M.; Hegedus, L. Formation of Cyclobutanones by the Photolytic Reaction of $(CO)_5Cr=C(OMe)Me$ with Electron-Rich Olefins. *J. Am. Chem. Soc.* **1989**, *111*, 2335-2336.

10. Hegedus, L.; McGuire, M.; Schultze, L.; Yijun, C.; Anderson, O. Reaction of Chromium Carbene Complexes with Imines - Synthesis of Beta-Lactams. *J. Am. Chem. Soc.* **1984**, *106*, 2680-2687.

11. McGuire, M.; Hegedus, L. Synthesis of Beta-Lactams by the Photolytic Reaction of Chromium Carbene Complexes with Imines. *J. Am. Chem. Soc.* **1982**, *104*, 5538-5540.

12. Hegedus, L.; DeWeck, G.; Dandrea, S. Evidence for the Intermediacy of Chromium Ketene Complexes in the Synthesis of Beta-Lactams by the Photolytic Reaction of Chromium Carbene Complexes with Imines - use in Amino-Acid Synthesis. *J. Am. Chem. Soc.* **1988**, *110*, 2122-2126.

13. Herrmann, W. First Pi-Diphenylketene-Carbonyl-Transition Metal-Complexes. *Angew. Chem. -Int. Edit. Engl.* **1974**, *13*, 335-336.

14. Redhouse, A.; Herrmann, W. Molecular Structure of $C_5H_5Mn(CO)_2[(C_6H_5)_2C=C=O]$.—Out-of-Plane Deformation of the Diphenylketene Ligand. *Angew. Chem. -Int. Edit. Engl.* **1976**, *15*, 615-616.

15. Grotjahn, D.; Collins, L.; Wolpert, M.; Bikzhanova, G.; Lo, H.; Combs, D.; Hubbard, J. First direct structural comparison of complexes of the same metal fragment to ketenes in both C,C- and C,O-bonding modes. *J. Am. Chem. Soc.* **2001**, *123*, 8260-8270.

16. Bodnar, T.; Cutler, A. Formation of a Stable (η-2-C,C) Ketene Compound $(C_5H_5)Fe(CO)_2(CH_2CO)^+PF_6^-$ by Carbonylation of an Iron Methylidene Complex - a Novel Entry into CO-Derived C_2 Chemistry. *J. Am. Chem. Soc.* **1983**, *105*, 5926-5928.

17. Geoffroy, G.; Bassner, S. Interaction of Ketenes with Organometallic Compounds - Ketene, Ketenyl, and Ketenylidene Complexes. *Adv. Organomet. Chem.* **1988**, *28*, 1-83.

18. Nguyen, S. C.; Lomont, J. P.; Zoerb, M. C.; Pham, P. V.; Cahoon, J. F.; Harris, C. B. Direct Observation of Metal Ketenes Formed by Photoexcitation of a Fischer Carbene using Ultrafast Infrared Spectroscopy. *Organometallics* **2014**, *33*, 6149-6153.

19. Fernandez, I.; Sierra, M.; Gomez-Gallego, M.; Mancheno, M.; Cossio, F. Computational and experimental studies on the mechanism of the photochemical

carbonylation of Group 6 Fischer carbene complexes. *Chem. -Eur. J.* **2005**, *11*, 5988-5996.

20. McMahon, S.; Rochford, J.; Halpin, Y.; Manton, J. C.; Harvey, E. C.; Greetham, G. M.; Clark, I. P.; Rooney, A. D.; Long, C.; Pryce, M. T. Controlled CO release using photochemical, thermal and electrochemical approaches from the amino carbene complex $[(CO)_5CrC(NC_4H_8)CH_3]$. *Phys. Chem. Chem. Phys.* **2014**, *16*, 21230-21233.

21. Zhang, W.; Atkin, A. J.; Thatcher, R. J.; Whitwood, A. C.; Fairlamb, I. J. S.; Lynam, J. M. Diversity and design of metal-based carbon monoxide-releasing molecules (CO-RMs) in aqueous systems: revealing the essential trends. *Dalton Trans.* **2009**, *22*, 4351-4358.

22. Tello, M.; Oliveira, L.; Parise, O.; Buzaid, A. C.; Oliveira, R. T.; Zanella, R.; Cardona, A. Electrochemical therapy to treat cancer (in vivo treatment). *2007 Annual International Conference of the Ieee Engineering in Medicine and Biology Society, Vols 1-16* **2007**, 3524-3527.

23. Olaiz, N.; Maglietti, F.; Suarez, C.; Molina, F. V.; Miklavcic, D.; Mir, L.; Marshall, G. Electrochemical treatment of tumors using a one-probe two-electrode device. *Electrochim. Acta* **2010**, *55*, 6010-6014.

24. Breton, M.; Mir, L. M. Microsecond and nanosecond electric pulses in cancer treatments. *Bioelectromagnetics* **2012**, *33*, 106-123.

25. Long, C.; Maher, K.; Pryce, M. T. The photochemistry of $(\eta^3$-2-R-$C_3H_4)Fe(CO)(NO)(X)$(R = H or Cl; X = CO or PPh_3) in room temperature solution or frozen gas matrixes. *J. Organomet. Chem.* **2006**, *691*, 3298-3304.

26. Frisch, M.; Trucks G; Schlegel, H.; Scuseria, G.; Robb, M.; Cheeseman, J.; Zakrzewski, V.; Montgomery, J.; Stratmann, R.; Burant, J.; Dapprich, S.; Millam, J.; Kudin, D.; Strain, M.; Farkas, O.; Tomasi, J.; Barone, V.; Cossi, M.; Cammi, R.; Mennucci, B.; Pomelli, C.; Adamo, C.; Clifford, S.; Ochterski, J.; Petersson, G.; Ayala, P.; Cui, Q.; Morokuma, K.; Malick, D.; Rabuck, D.; Raghavachari, K.; Foresman, J.; Cioslowski, J.; Stefanov, R.; Liu, G.; Liashenko, A.; Piskora, P.; Komaromi, R.; Gomperts, R.; Martin, D.; Fox, K.; Ailaham, M.; Peng, C.; Nanayakkara, A.; Gonzalez,

C.; Challacombe, M.; Gill, M.; Johnson, B.; Chen, W.; Wong, M.; Andres, C.; Gonzalez, M.; Gordon, E.; Pople, A. Gaussian 03, Gaussian, Inc. **2003**.

27. Gorelsky, S. I. *AOMix program, http://www.sg-chem.net/*, version 6.4; University of Ottawa: Ottawa, 2010.

28. Gorelsky, S.; Lever, A. Electronic structure and spectral, of ruthenium diimine complexes by density functional theory and INDO/S. Comparison of the two methods. *J. Organomet. Chem.* **2001**, *635*, 187-196.

29. Gaussian Inc. Pittsburgh, PA, USA Gauss View 3.0. **2003**, *3.0*.

30. Aumann, R.; Fischer, E. Transition Metal-Carbene Complexes. Addition of Isonitriles to Methylmethoxycarbeneopentacarbonyl Chromium. *Chem. Ber. -Recl.* **1968**, *101*, 954.

31. Rooney, A.; McGarvey, J.; Gordon, K.; McNicholl, R.; Schubert, U.; Hepp, W. Laser Photochemistry and Transient Raman-Spectroscopy of Silyl-Substituted Fischer-Type Carbene Complexes. *Organometallics* **1993**, *12*, 1277-1282.

32. Gallagher, M.; Greene, J.; Rooney, A. Matrix isolation study into the mechanism of photoinduced cyclization reactions of chromium carbenes. *Organometallics* **1997**, *16*, 5260-5268.

33. McMahon, S.; Amirjalayer, S.; Buma, W. J.; Halpin, Y.; Long, C.; Rooney, A. D.; Woutersen, S.; Pryce, M. T. An investigation into the photochemistry of, and the electrochemically induced CO-loss from, $[(CO)_5MC(OMe)Me]$(M = Cr or W) using low-temperature matrix isolation, picosecond infrared spectroscopy, cyclic voltammetry, and time-dependent density functional theory. *Dalton Trans.* **2015**, *44*, 15424-15434.

34. Wrighton, M.; Hammond, G.; Gray, H. Emission from Tungsten Carbonyl Complexes. *J. Am. Chem. Soc.* **1971**, *93*, 4336-4337.

35. Lees, A. Luminescence Properties of Organometallic Complexes. *Chem. Rev.* **1987**, *87*, 711-743.

36. Gasparro, F.; Kolodny, N. NMR Determination of Rotational Barrier in N,N-Dimethylacetamide - A Physical-Chemistry Experiment. *J. Chem. Educ.* **1977**, *54*, 258-261.

37. Kreiter, C.; Fischer, E. Hindered Rotation about C-O Bond in Methoxy(methyl)carbene Ligands. *Angew. Chem. -Int. Edit.* **1969**, *8*, 761-762.

38. Baldoli, C.; Cerea, P.; Falciola, L.; Giannini, C.; Licandro, E.; Maiorana, S.; Mussini, P.; Perdicchia, D. The electrochemical activity of heteroatom-stabilized Fischer-type carbene complexes. *J. Organomet. Chem.* **2005**, *690*, 5777-5787.

39. Landman, M.; Liu, R.; Fraser, R.; van Rooyen, P. H.; Conradie, J. Fac and mer dppe-substituted Fischer carbene complexes of chromium: X-ray, DFT and electrochemical study. *J. Organomet. Chem.* **2014**, *752*, 171-182.

40. Hoskovcova, I.; Rohacova, J.; Meca, L.; Tobrman, T.; Dvorak, D.; Lukvik, J. Electrochemistry of chromium(0)-aminocarbene complexes - The use of intramolecular interaction LFER for characterization of the oxidation and reduction centre of the complex. *Electrochim. Acta* **2005**, *50*, 4911-4915.

41. Lloyd, M.; McClever, J.; Orchard, D.; Connor, J.; Hall, M.; Hillier, I.; Jones, E.; McEwen, G. Electrochemical Oxidation of Organometallic Complexes - Carbene and Lewis Base Complexes of Chromium, Molybdenum, and Tungsten Carbonyls. *J. Chem. Soc. -Dalton Trans.* **1973**, *17*, 1743-1747.

3 Chapter 3 The assessment of the Photochemical, Thermal and Electrochemical CO Releasing Potential of $[(CO)_5M=C(NC_4H_8)Me]$ (M = Cr, W)

Abstract

In this chapter, the amino Fischer carbene complexes; $[(CO)_5M=C(NC_4H_8)Me]$ (M = Cr, W) are reported and their CO releasing abilities are investigated using photochemical, thermal and electrochemical approaches. The photochemical CO releasing potential is indicated using the myoglobin assay and quantified via headspace analysis by gas chromatography. PsTRIR spectroscopy is used to probe the early state dynamics leading to CO loss. The thermal CO release study is carried out both using the myoglobin assay and via headspace analysis using gas chromatography (GC). In addition, the effects of different solvents on CO release are also investigated. Lastly, electrochemically induced CO loss, using bulk electrolysis is determined via GC.

Publications based on this work

1. Controlled CO release using photochemical, thermal and electrochemical approaches from the Amino Carbene complex $[(CO)_5CrC(NC_4H_8)CH_3]$. Suzanne Mc Mahon, Jonathan Rochford, Yvonne Halpin, Jennifer C. Manton, Emma C. Harvey, Gregory M. Greetham, Ian P. Clark, A. Denise Rooney, Conor Long and Mary T. Pryce.

Phys. Chem. Chem. Phys. **2014**, *16*, 21230-21233.

2. Efficient photochemical CO-loss from the Fischer carbene complex, $[(CO)_5WC(NC_4H_8)Me]$: A Picosecond Time-Resolved Infrared, Electrochemical and Time-dependent Density Functional Theory Study (Manuscript in preparation).

3.1 Introduction

It is well known that chromium carbene complexes can release CO both thermally and photochemically.[1] Previously, Rooney and co-workers have investigated alkoxy carbenes such as those described in Chapter 2; $[(CO)_5MC(OMe)Me]$, M = Cr, W. *Anti-syn* isomerisation occurs for such methoxy carbenes. Amino carbenes, however, do not undergo this type of isomerisation. Therefore, the photochemistry of these complexes were investigated to determine the difference caused by attaching an amino *vs.* methoxy group at the carbene carbon.

Metal pentacarbonyl complexes are an attractive class of complexes to use as CO delivery systems due to the fact that they may potentially release five molecules of CO per metal which allows for lower quantities to be administered in order to reach a certain dosage of CO. Lynam and co-workers reported the suitability of a range of metal pentacarbonyl complexes as thermal CORMs using the myoglobin assay.[2] The nature of the metal and heteroatom substituents on the metal carbonyl complex greatly influences the rate of CO release. The order of the rate of CO release for the Fischer carbene complexes is as follows; Cr > Mo > W.[2]

Thermally, tungsten pentacarbonyl complexes release CO at a much slower rate than chromium based pentacarbonyl complexes, $[NEt_4][WBr(CO)_5]$, takes 3486 s to release 15 µM from a 60 µM solution whereas the chromium derivative takes 183 s to release 30 µM from a 60 µM solution.[2]

Rapid CO release was observed for the chromium, thio- and methoxy pentacarbonyl complexes ($t_{1/2}$ = 313 s and 306 s, respectively, for a 60 µM solution of the complex to achieve a Mb-CO concentration of 30 µM), compared to slow release in the case of the amino analogue which required more than 2 hours for a 60 µM solution of the complex to form 10 µM of carboxy-myoglobin (Mb-CO). In addition, the chromium carbonyls investigated, demonstrated the fastest and most regulated CO release characteristics compared to the molybdenum or tungsten analogues studied.[2]

The myoglobin (Mb) assay (deoxygenated-myoglobin (deoxy-Mb) / carbonmonoxy-myoglobin (Mb-CO) UV-vis assay), initially, was the primary method of analysis to determine the release rate of carbon monoxide which is liberated from CO releasing

molecules.[3,4] This assay was first carried out by Motterlini *et al*.[3] It quantifies the release of CO which is generated from CORMs.

As discussed previously in Chapter 1, the main principle behind the assay is that if a certain complex can liberate CO into solution, deoxy-Mb will be readily converted to Mb-CO. UV-vis spectroscopy is the principal tool for this measurement. The concentration of Mb-CO is measured by determining the change in absorbance at a fixed wavelength (usually 540 nm). External factors such as turbidity can decrease the accuracy of Mb-CO concentration calculations and should be taken into account by the use of isosbestic points, which occur at a certain wavelength where two chemical species have the same molar absorption coefficient value. The preparation of myoglobin (derived from lyophilised horse heart) is performed by dissolving it in a solution containing phosphate buffered saline (PBS) at a physiological pH (pH 7.4). 0.1 % sodium dithionite (SD) converts the stock Mb to deoxy-Mb. A small volume (ca. 2 ml) of deoxy-Mb is utilised to produce a deoxy-Mb spectrum. CO is then bubbled through the deoxy-Mb sample for 30 minutes, to obtain an Mb-CO spectrum. In order to test the various CORMs, they are dissolved in an appropriate solvent e.g. DMSO or ethanol. Next, aliquots of the dissolved solution are added to a cuvette depending on the desired concentrations. This can be mixed and overlaid with a mineral oil to hinder the escape of CO and to prevent the oxygenation of myoglobin.[3,4]

The myoglobin assay is carried out at a physiological temperature (37 °C). To measure the amount of deoxy-Mb that has been converted to Mb-CO, the absorbance changes, at a wavelength of 540 nm, are determined. Using the standard spectra of deoxy-Mb and Mb-CO, in conjunction with the concentration of myoglobin, it is possible to measure the concentration of Mb-CO formed.[3,4] This correlates to the measurement of CO that is liberated by the CORM at various time points. An example of a CO release profile for a CORM demonstrating the conversion of deoxy Mb to Mb-CO over time using the Q band region of the heme group is displayed in Figure 3.1.[2]

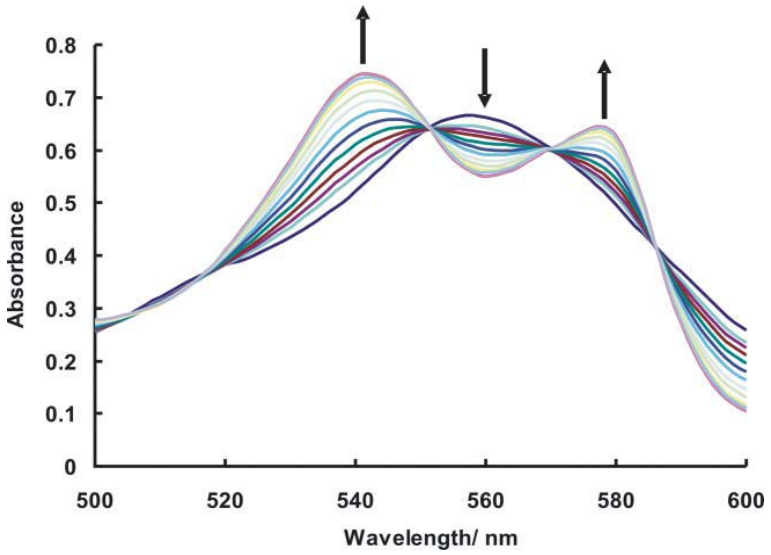

Figure 3.1 Release profile for a representative CORM, ([Et_4N][$CrI(CO)_5$]), demonstrating the conversion of deoxy Mb to Mb-CO over time using the Q band region of the heme group over a period of 0 to approximately 700 s (maximum peak). The increasing lines indicated by the upward arrows highlight the formation of Mb-CO and downward arrows show the depletion of deoxy-Mb.[2]

The myoglobin assay is an indirect method of detection. It cannot provide information such as mechanisms of release and identify end products as a result of CORM decay. In addition, it is necessary for the assay to be performed in anaerobic conditions which may cause discrepancies in the amount of CO released in comparison to physiological conditions.[5] Various drawbacks have been detected regarding the purity of the myoglobin as well as the turbidity of the solution. Atkin *et al.* overcame this problem with a revised myoglobin assay.[4] Further issues were raised when it was observed that the reducing agent involved in the assay, sodium dithionite (SD), enhanced the rate of CO release for the well-known compound, CORM-2.[6] This lead to the development of a novel protocol, the oxy-haemoglobin assay which works similarly to the myoglobin assay but excludes the need for SD.[6]

Headspace analysis *via* gas chromatography (GC) has also been used to quantify the amount of CO released from a CORM. It is a direct method of CO detection and quantification and can provide information on several gas species.[5] Head space analysis is carried out in capped vials. Following stimulation, a controlled amount of gas is drawn from the headspace using a needle and is injected onto the GC column. The carrier gas passes the headspace gas around the column.[7] In this chapter, a solvent dependent CO release investigation is carried out *via* headspace analysis using GC.

It is very important to quantify the amount of CO released and to characterise the product formed as a result of this CO loss. For $Mn(CO)_3$ complexes e.g. $[Mn(CO)_3(tpm)](PF_6)$, where tpm = tris(pyrazolyl)methane, discrepancies between the myoglobin assay and IR investigations have also been reported.[8] Infrared spectroscopy is a sensitive and selective technique for detecting the release of CO.[5] Many research groups are now employing this technique to monitor the progress of photo induced CO loss.[5,8,9] This method can monitor the degradation process of the CORM as the reaction proceeds. This technique has been exploited in Chapter 2 and will be exploited further in this chapter.

Chromium Fischer carbenes have received significant attention as photochemical synthons for a range of organic compounds as mentioned in Chapter 2. The proposed mechanism for these reactions involves a metal-to-ligand charge transfer photoexcitation resulting in the formation of a ketene intermediate which is formed by the insertion of a *cis*-CO ligand into the adjacent Cr-carbene bond (Scheme 3.1).[10]

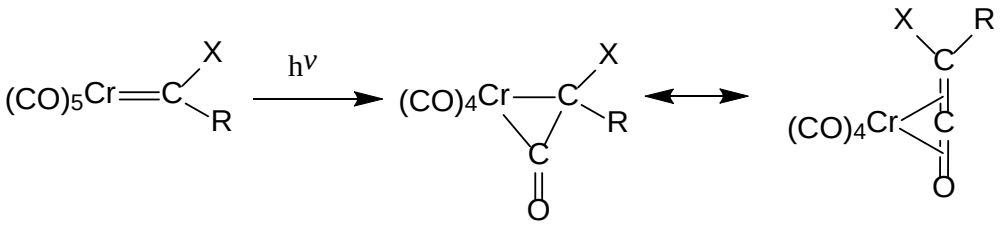

Scheme 3.1 Chromium-ketene intermediate proposed following photolysis of $[(CO)_5CrC(X)R']$. X= amino, alkoxy, and R = alkyl, aryl, H.[10]

Although spectroscopic studies have investigated photo-induced CO loss from amino Fischer carbene complexes,[11,12] up until the results were presented from this chapter, no previous data had been reported on the picosecond timescale to identify their photochemical nature. Rooney and co-workers reported a matrix isolation and laser flash photolysis study of a range of chromium amino carbenes.[11] The study investigated two classes of compounds. Class 1 represents $[(CO)_5CrC(NMe_2)Me]$, $[(CO)_5CrC(NBz_2)Me]$ and $[(CO)_5CrC(NMe_2)Ph]$. Class 2 represents $[(CO)_5CrC(NMe_2)H]$, $[(CO)_5CrC(NBz_2)H]$ and $[(CO)_5CrC(NH_2)Me]$. Class 1 exhibits low or no photoreactivity to form β-lactams in the presence of imines. Class 2 complexes, however, do undergo photochemical reactions with imines to form β-lactams. The active intermediate in this reaction is thought to be a metal-ketene complex. However, upon irradiation in matrix and solution experiments, no evidence for the

presence of this ketene intermediate was found. CO loss was the predominant photoprocess for all complexes studied.[11]

Hafner and co-workers investigated the reactivity of a range of chromium carbene complexes to form β-lactams, using ^{53}Cr-NMR spectroscopy by assessing their chemical shifts and line widths.[13] This form of analysis was chosen as the chemical shift in transition metal NMR spectroscopy is very sensitive to even minor structural alterations and can provide direct information about the metal centre and hence, reactivity. The ^{53}Cr-NMR chemical shift did not correlate with carbene reactivity associated with the formation of β-lactams and hence no clear relationship was established. However, the unreactive carbenes (those that did not generate β-lactams) exhibited a common trend; they had relatively narrow line widths (150-500 Hz) whereas reactive carbene complexes (those that formed β-lactams) had much wider line widths in excess of 1000 Hz.[13]

There are relatively few reports on the photochemistry of the equivalent tungsten carbene complexes compared to the chromium analogues. Rooney *et al.* reported a transient Raman study on $[(CO)_5WC(NC_4H_8)(SiPh_3)]$ which upon photolysis in non-coordinating solvents forms the internally stabilised 16 electron species $[(CO)_4WC(NC_4H_8)(SiPh_3)]$.[12] However, in coordinating solvents such as acetonitrile the solvated species $[(CH_3CN)(CO)_4WC(NC_4H_8)(SiPh_3)]$ was formed.

Cyclic voltammetry has also been used to characterise the complexes under investigation. It is necessary to determine the oxidation and reduction potentials to identify where the lowest potential (bulk electrolysis) may be applied to induce electrochemical CO loss. To date, electrochemical analysis of Fischer carbene complexes includes an oxidation at the central metal and a reduction process at the carbene ligand.[14] The additional electronic charge is mostly centred on the carbene atom and is partially delocalised over the attached heteroatom. The π- acidity of the ligands attached to the metal is highly influential on the oxidation potential of these complexes.[15] For the complexes, $[(CO)_5M=C(XR^1)R^2]$ where M = Cr, W; X = O, NR^3, S; R^1 = alkyl, R^2 = alkyl, aryl; R^3 = H, alkyl, as the electronegativity of X is increased, the more readily the reduction occurs.[15,16] Studies on the effect of the nature of the carbene metal have been reported by Baldoli *et al.* for chromium and tungsten Fischer carbene complexes.[14] The first oxidation step for tungsten carbenes is more difficult than for chromium carbenes.

Chromium carbenes display a chemically reversible first oxidation peak. In contrast, the second oxidation peak seems to be unaffected by the nature of the metal as oxidation potentials are at very similar potentials for both chromium and tungsten derivatives. However, tungsten carbene complexes exhibit a chemically irreversible oxidation peak. The reduction processes of carbene derivatives do not depend on the nature of the central metal, rather the substitution and nature of the ligands strongly influences the electrochemical behaviour.[14-16] The substituents on the carbene carbon i.e. alkoxy or amino groups also influence the electrochemistry. Alkoxy carbenes are harder to oxidise than amino carbenes since oxygen is more electronegative than nitrogen. [16]

In this chapter, the results of picosecond time resolved IR studies of the chromium and tungsten carbene complexes; $[(CO)_5CrC(NC_4H_8)Me]$ and $[(CO)_5WC(NC_4H_8)Me]$ will be discussed. These studies were carried out to probe the photo-induced early state dynamics preceding CO loss. These results, in conjunction with quantum chemical calculations aid in the understanding of the CO loss process that occurs *via* population of various excited states. The impact of metal variation on their thermal and electrochemical CO loss profiles is also assessed. The myoglobin assay was used for this study for consistency with previous thermal CO release studies carried out on similar Fischer carbene complexes. Due to recent reports including drawbacks of the myoglobin assay,[5] a solvent study on $[(CO)_5CrC(NC_4H_8)Me]$ was performed *via* headspace analysis by GC which included and excluded interfering reagents such as sodium dithionite (SD).

3.2 Experimental

3.2.1 Steady State Photolysis

IR spectra were measured in a liquid Omni cell containing two NaCl plates, using a Perkin Elmer spectrophotometer. The liquid cell containing the complex was irradiated at 395 nm using an LED source.

3.2.2 Picosecond Time Resolved Infrared Spectroscopy

The TRIR experiments were performed at both the Rutherford Appleton Laboratory as well as at the University of Amsterdam. The ULTRA laser system used in psTRIR studies at the Rutherford Appleton Laboratory is a cryogenically cooled Ti : Sapphire laser amplifier providing 50 fs duration pulses at 10 kHz repetition rate.[17] The 0.8 mJ, 800 nm output is divided to generate 400 nm pump and mid-IR probe beams through second harmonic generation and difference frequency generation (DFG) of signal and idler generated in an optical parametric amplifier, respectively. The pump beam was attenuated to 0.5 μJ at the sample and focused to overlap with the probe beam in the sample. The pump and probe spot sizes in the sample were 100 and 50 μm, respectively. After the sample, the IR probe beam was dispersed onto two linear 128 element mercury cadmium telluride (MCT) detector arrays acquiring spectra at 10 kHz. The signals from these two detector arrays were then averaged. By modulating the pump laser output at 5 kHz, difference spectra could be generated.[18] A portion of the IR probe taken before the sample was dispersed on to a second 64 element MCT detector array, which with interpolation was used to generate reference spectra used to remove energy and spectral instabilities of the laser. Samples were contained in flow-through cells with CaF_2 windows with a 500 μm Teflon spacer and rastered to avoid photodegradation of the sample solution.

The apparatus used in Amsterdam has been previously reported in Chapter 2.

3.2.3 Quantum Chemical Calculations

Density Functional Theory Calculations were performed by Prof. Conor Long (DCU) in order to obtain a theoretical insight underpinning the photophysics and photochemistry of the complexes.

3.2.4 Myoglobin Assay

This procedure was undertaken in the same manner as reported by Motterlini *et al.*[3] CO generated from $[(CO)_5CrC(NC_4H_8)Me]$ and $[(CO)_5WC(NC_4H_8)Me]$ was analysed spectrophotometrically by quantifying the conversion of deoxy-myoglobin (deoxy-Mb) to carboxy-myoglobin (Mb-CO). The change in absorbance of the Q-band region of the heme group at a fixed wavelength, 540 nm, was measured to detect the amount of Mb-CO released. The preparation of myoglobin (derived from lyophilised horse heart, 66 μM; final concentration) was carried out by dissolving it in phosphate buffered saline (PBS, 0.01 M) at a physiological pH (pH 7.4). 0.1 % SD was added to reduce the stock Mb to deoxy-Mb. A UV-vis spectrum of this solution (2 ml) was recorded and used as a reference standard. The deoxy-Mb solution was then purged with pure CO for 30 minutes to obtain an Mb-CO spectrum. The CORM was then dissolved in DMSO. 12 mM and 8 mM stock solutions were prepared. 10 µL aliquots of the CORM solutions were added to cuvettes containing 2 ml of deoxy-Mb. This was mixed using a pipette and overlaid with a layer of mineral oil (500 µL) to hinder the escape of CO and to prevent the oxygenation of myoglobin (final concentration of the CORM; aliquots from 12 mM solution equates to 60 µM and 8 mM solution equates to 40 µM). The CO release was measured by photochemical means (355 nm LED) and by thermal means (37 °C; body temperature). For photochemical experiments, the sample was placed with the LED standing 2 cm away (the temperature of a representative sample was monitored at this position to ensure heating of the sample was not occurring). No change in temperature of the solution was observed over the time-frame of the experiments). This was kept constant for all experiments. A sample in the absence of light was also monitored over this time frame as a control. Experiments were repeated in triplicate.

For thermal experiments, incubations of the samples were carried out in a water bath in the absence of light (samples were covered in tinfoil to ensure no external photochemical

effects could occur). The water bath temperature remained constant and was monitored using a thermometer. The spectroscopic data was analysed using the method reported by Fairlamb and co-workers.[4] Sample calculations can be found in Appendix A.

3.2.5 Cyclic Voltammetry and Electrochemical CO loss

Electrochemical experiments were carried out with the help of Dr. Yvonne Halpin. Cyclic voltammograms (CVs) and bulk electrolysis profiles were recorded in anhydrous acetonitrile (Sigma-Aldrich) with tetrabutylammonium hexafluorophosphate ($TBAPF_6$), (0.1 M) as a supporting electrolyte. The concentration of the sample was 0.001 M throughout. Experiments were carried out using both CH Instruments 600A and CH Instruments 750C electrochemical potentiostats. All electrochemical experiments were performed at room temperature (20 °C) in the absence of light. A three electrode cell was employed which consisted of a glassy carbon working electrode, a Pt wire auxiliary electrode and an Ag / AgCl reference electrode. The scan rate was 0.1 V s^{-1} unless otherwise stated. The scan rate dependency of the redox processes was analysed by varying the scan rate from 0.01 V s^{-1} to 0.05, 0.08, 0.1, 0.5, 0.8, 1.0, 10.0 15.0 and 20.0 V s^{-1}. Cited potentials are referenced relative to the ferrocene / ferrocenium (Fc / Fc^+) redox couple. The electrochemical cell was deaerated with argon prior to all experiments.

For the bulk electrolysis experiments, de-aeration of the solutions with argon prior to the experiment ensured that any CO detected in the headspace resulted from CO release from the complex. The bulk electrolysis experiments were repeated using a clean glassy carbon electrode in analyte-free electrolyte solution for comparison purposes. A control experiment was also carried out where the complex was dissolved in the electrolyte and protected from light with no potential applied. A trace amount of CO was measured from the head space, but this remained constant over the time frame of the experiment. CO-release was detected using a Shimadzu GC-2010 Plus unit (Lab Solutions version 5.57 software) with a dielectric barrier discharge ionisation detector (BID) and a ShinCarbon micropacked column with 0.53 mm internal diameter.

3.2.6 Synthesis

3.2.6.1 Synthesis of [(CO)$_5$CrC(NC$_4$H$_8$)Me]

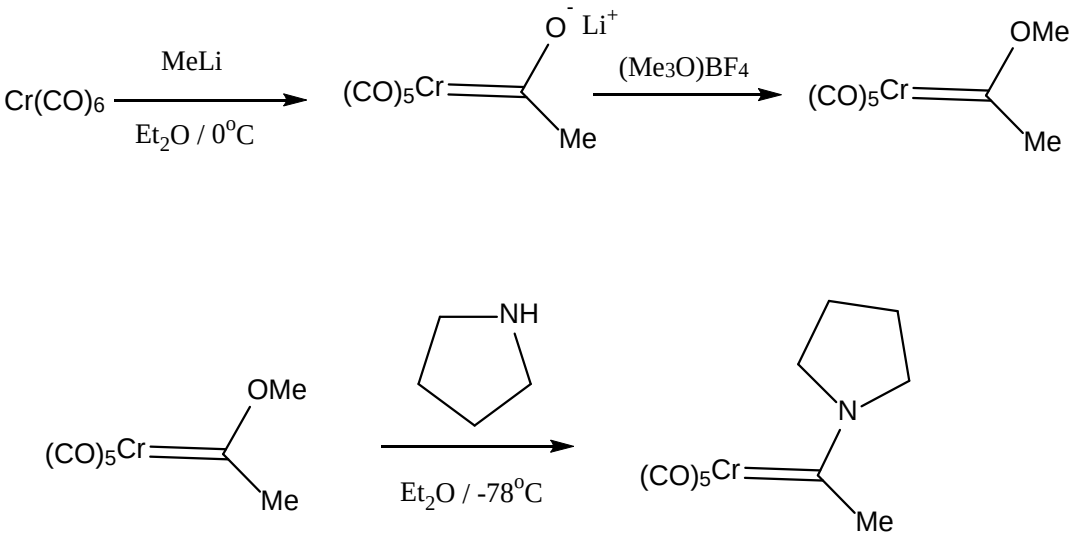

Scheme 3.2 Synthesis of [(CO)$_5$CrC(NC$_4$H$_8$)Me].

The synthesis of [(CO)$_5$CrC(NC$_4$H$_8$)Me] was carried out according to previously reported procedures.[19,20] 0.48 mmol (0.04 ml) of pyrrolidine was added *via* syringe to a solution of [(CO)$_5$CrC(OMe)Me] (synthesis previously reported in Chapter 2) (0.4 mmol, 0.100 g) in diethyl ether (15 ml) at -78 °C (this temperature was achieved by combining liquid nitrogen and acetone and monitored using an alcohol thermometer). The reaction was stirred and allowed to reach room temperature. The solution changed from a bright yellow colour to cream. The solvent and any excess pyrrolidine were removed at reduced pressure. The crude complex was purified on a silica gel column using a solvent mix of pentane : dichloromethane (9 : 1). The spectroscopic data is in agreement with reported data.[19,20]

Appearance: Cream solid.

% Yield: 0.11 g, 0.37 mmol, 93 % yield.

^{1}H NMR: (400 MHz, CDCl$_3$) 2.09 (4H, m), 2.65 (3H, s), 3.57 (2H, t), 4.13 (2H, t) ppm.

IR: (pentane) 2055, 1967 and 1928 cm^{-1}.

3.2.6.2 Synthesis of $[(CO)_5WC(NC_4H_8)Me]$

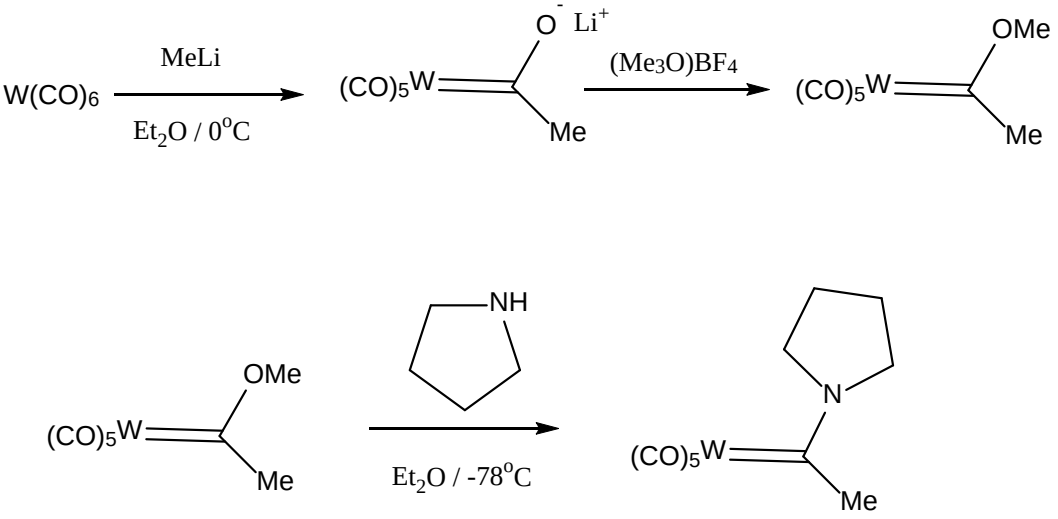

Scheme 3.3 Synthesis of $[(CO)_5WC(NC_4H_8)Me]$.

The synthesis of $[(CO)_5WC(NC_4H_8)Me]$ was carried out according to previously reported procedures.[19,20] 0.31 mmol (0.026 ml) of pyrrolidine was added *via* syringe to a solution of $[(CO)_5WC(OMe)Me]$ (synthesis previously reported in Chapter 2) (0.26 mmol, 0.100 g) in diethyl ether (15 ml) at -78 °C (this temperature was achieved by combining liquid nitrogen and acetone and monitored using an alcohol thermometer). The reaction was stirred and allowed to reach room temperature. The solution changed from a bright yellow colour to cream. The solvent and any excess pyrrolidine were removed at reduced pressure. The crude complex was purified on a silica gel column using a solvent mix of pentane: dichloromethane (9 : 1). The spectroscopic data is in agreement with reported data.[19,20]

Appearance: Cream solid.

% Yield: 0.96 g, 0.23 mmol, 88 % yield.

^{1}H NMR: (400 MHz, $CDCl_3$) 2.16 (4H, m), 2.75 (3H, s), 3.59 (2H, t), 4.02 (2H, t) ppm.

IR: (pentane) 2063, 1967, 1932 and 1925 cm^{-1}.

3.3 Results and Discussion

3.3.1 UV-vis Spectroscopy

The UV-vis absorption spectra of $[(CO)_5CrC(NC_4H_8)Me]$ and $[(CO)_5WC(NC_4H_8)Me]$ in *n*-heptane are presented in Figure 3.2 and Figure 3.3, respectively. $[(CO)_5CrC(NC_4H_8)Me]$ exhibits two bands with λ_{max} at 325 nm, attributed to a LF transition and 357 nm assigned to an MLCT transition. The tungsten analogue, $[(CO)_5WC(NC_4H_8)Me]$ exhibits two bands with λ_{max} at 337 (LF) and 364 nm (MLCT). This is in agreement with reported data on similar amino based Fischer carbene complexes.[11,12] The wavelength of excitation used in the psTRIR experiments was 400 nm as indicated by the arrows in Figure 3.2 and 3.3.

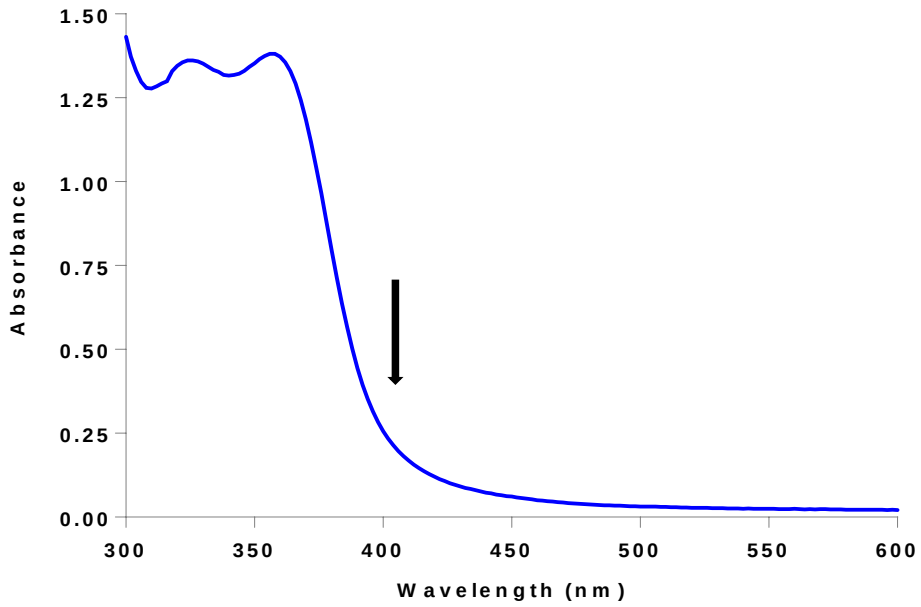

Figure 3.2 UV-vis spectrum of $[(CO)_5CrC(NC_4H_8)Me]$ in *n*-heptane. The arrow represents the wavelength of irradiation used in the psTRIR experiments.

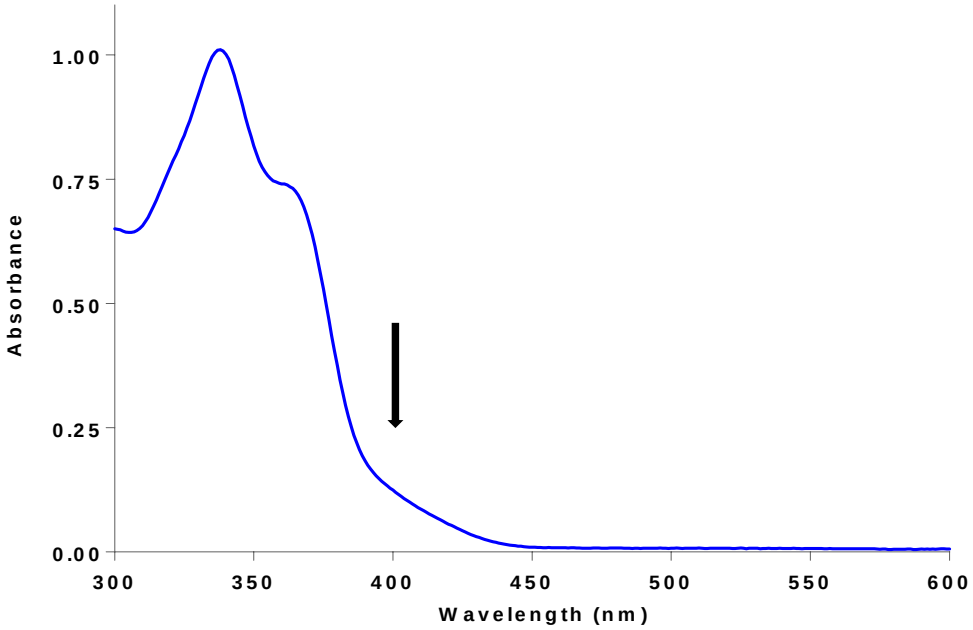

Figure 3.3 UV-vis spectrum of $[(CO)_5WC(NC_4H_8)Me]$ in *n*-heptane. The arrow represents the wavelength of irradiation used in the psTRIR experiments.

3.3.2 Steady State Photolysis

The FTIR spectrum of $[(CO)_5WC(NC_4H_8)Me]$ in *n*-heptane is displayed in Figure 3.4. The parent bands are observed at 2063, 1967, 1932 and 1925 cm^{-1}.

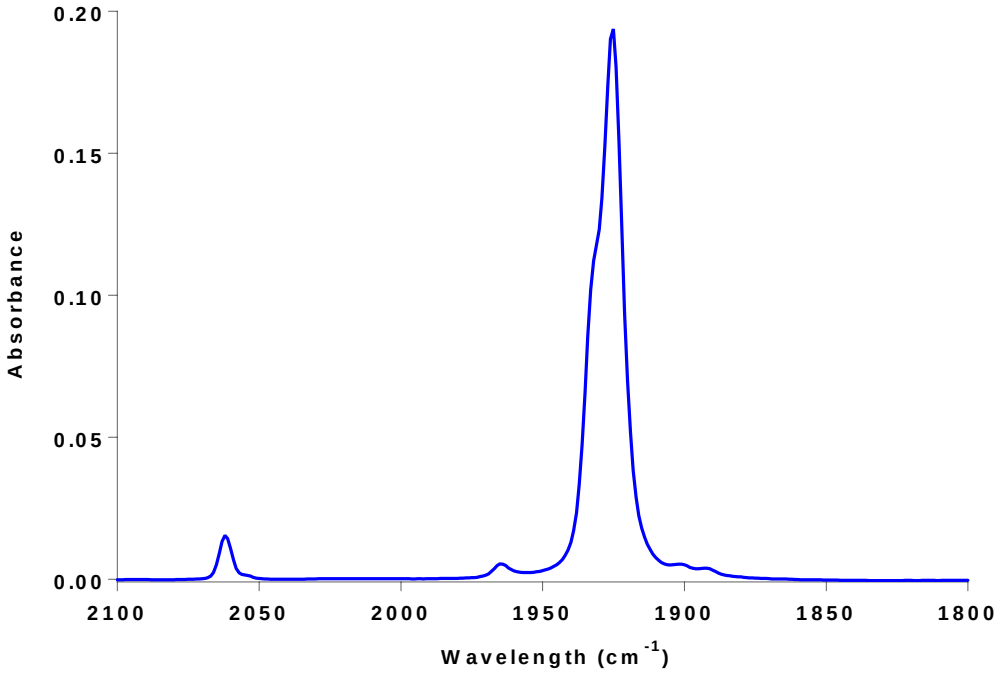

Figure 3.4 FT-IR spectrum of $[(CO)_5WC(NC_4H_8)Me]$ in *n*-heptane.

Steady state photolysis measurements were carried out at λ_{exc} = 395 nm monitored by IR spectroscopy. [$(CO)_5WC(NC_4H_8)Me$] was dissolved in pentane in the presence of a trapping ligand (PPh_3, in 1.1 molar equivalent excess). The spectral changes observed following irradiation at 395 nm are presented in Figure 3.5. Within 30 seconds, the bands of the parent complex at 2062, 1966, 1933 and 1925 cm^{-1} are depleted (shown as negative features in the difference spectum) and new bands at 2007, 1907 and 1883 cm^{-1} are formed, as indicated by the arrows. Over the subsequent 10 minutes these bands intensify and no further spectral changes become evident. These new bands are assigned to the tetracarbonyl complex, [$(PPh_3)(CO)_4WC(NC_4H_8)Me$]. These bands are consistent with those previously reported for a similar CO loss photoproduct, [$(pentane)(CO)_4WC(NC_4H_8)SiPh_3$], which exhibited IR bands at 2015, 1923, 1909 and 1856 cm^{-1}, following excitation of [$(CO)_4WC(NC_4H_8)SiPh_3$] at 355 nm in pentane.[12]

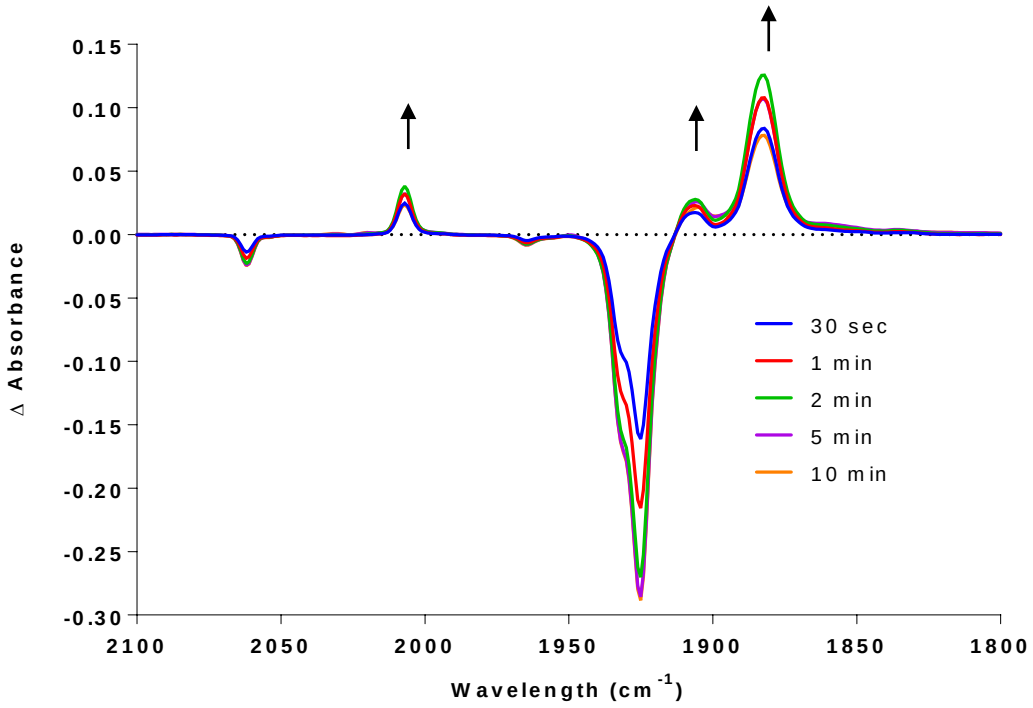

Figure 3.5 IR difference spectra following the irradiation of [$(CO)_5WC(NC_4H_8)Me$] at 395 nm in pentane using PPh_3 as a trapping ligand at selected time intervals.

3.3.3 Picosecond Time Resolved IR studies

A psTRIR investigation of $[(CO)_5CrC(NC_4H_8)Me]$ and $[(CO)_5WC(NC_4H_8)Me]$ in *n*-heptane solution was undertaken at 293 K. Infrared spectral changes were monitored in the 2150–1850 cm^{-1} region. The FT-IR spectra of $[(CO)_5CrC(NC_4H_8)Me]$ and $[(CO)_5WC(NC_4H_8)Me]$ are displayed in Figure 3.6 and Figure 3.4, respectively. All rate constants obtained in these experiments were measured at 293 K using an excitation pulse of 50 fs at 400 nm.

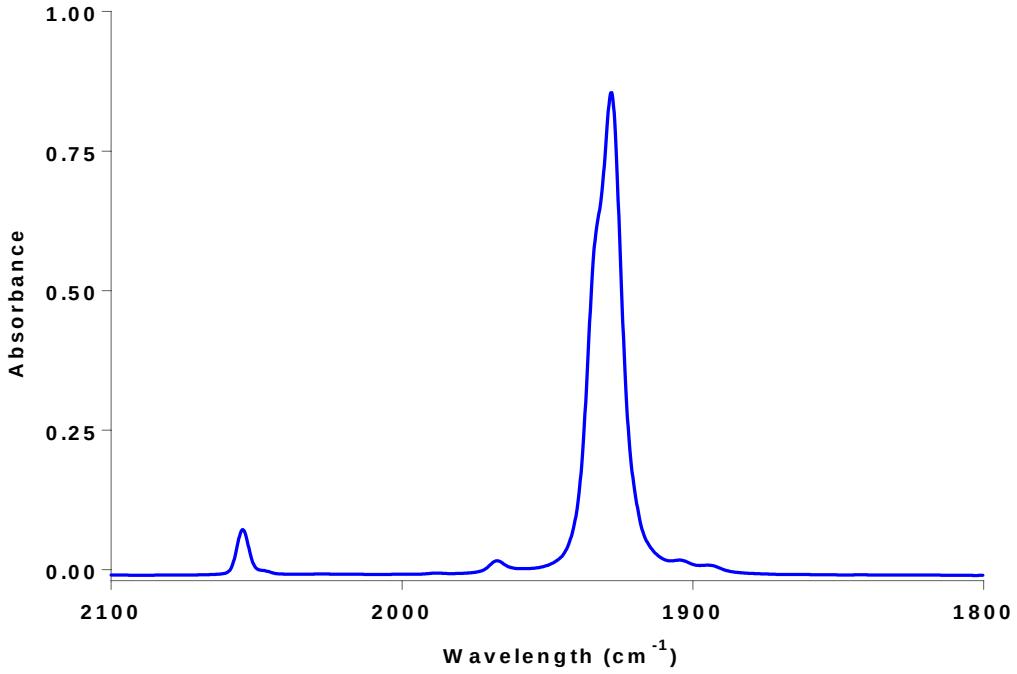

Figure 3.6 FT-IR spectrum of $[(CO)_5CrC(NC_4H_8)Me]$ in *n*-heptane.

3.3.3.1 psTRIR of $[(CO)_5CrC(NC_4H_8)Me]$ at 400 nm

The early state dynamics leading to CO loss following excitation of $[(CO)_5CrC(NC_4H_8)Me]$ at 400 nm were probed using psTRIR at the Rutherford Appleton Laboratories. The IR spectrum of the parent complex, $[(CO)_5CrC(NC_4H_8)Me]$, in *n*-heptane exhibits metal carbonyl stretching bands at 2055, 1967, and 1928 cm^{-1} (see Figure 3.6). The spectral changes observed following pulsed (50 fs) excitation of $[(CO)_5CrC(NC_4H_8)Me]$ at 400 nm are presented in Figure 3.7. The UV-vis spectrum for $[(CO)_5CrC(NC_4H_8)Me]$ can be found in Figure 3.2. The spectrum obtained 4 ps after excitation shows depletion of the parent bands as the negative features

in the difference spectrum. New bands at 2016, 1913 and 1897 cm^{-1} are formed within this timescale and these are assigned to an excited state species. Over the subsequent 50 ps these bands decay with concomitant formation of bands at 2025, 1963, 1923 and 1886 cm^{-1}. These bands are assigned to the solvated species, [(*n*-heptane)$(CO)_4CrC(NC_4H_8)Me$]. These bands are consistent with the bands previously reported for the CO loss species in low temperature matrices at 20 K by Rooney *et al.* where bands at 2028, 2025 (sh), 1938, 1923 and 1888 cm^{-1} upon irradiation of the similar amino complex, $[(CO)_4Cr(NMe_2)Me]$, at $\lambda > 320$ nm in a N_2 matrix were observed.[11] It is possible to assign the CO loss species to *cis*-$[(CO)_4CrC(NC_4H_8)Me]$ as four υCO bands of high intensity are observed whereas if the *trans*-$[(CO)_4CrC(NC_4H_8)Me]$ complex was formed, only one band of high intensity would be observed, the other three bands are weak and may not be detected.[21,22] The extent of parent band recovery provides an estimate of the overall quantum yield for the CO loss process of 65 %. The photophysical processes leading to CO loss following excitation of $[(CO)_5Cr(NC_4H_8)Me]$ at 400 nm are illustrated in Scheme 3.4.

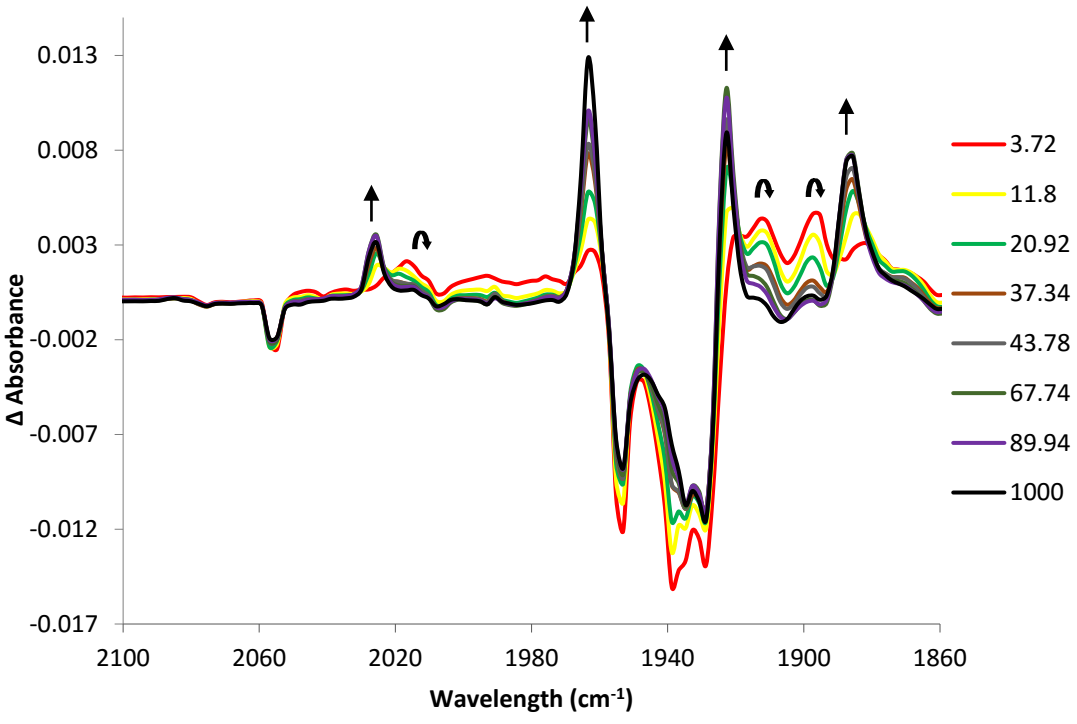

Figure 3.7 Picosecond TRIR difference spectra following 400 nm photolysis of $[(CO)_5CrC(NC_4H_8)Me]$ in *n*-heptane solution at selected time intervals; 4, 12, 21, 37, 44, 68, 90 and 1000 ps.

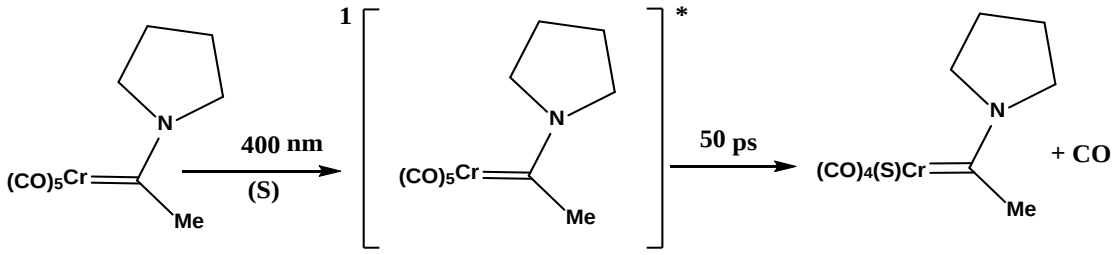

Scheme 3.4 The photophysical processes leading to the CO loss species $[(CO)_4(S)Cr(NC_4H_8)Me]$ following 400 nm irradiation, where S = *n*-heptane.

3.3.3.2 psTRIR of $[(CO)_5WC(NC_4H_8)Me]$ at 400 nm

The photochemistry of $[(CO)_5WC(NC_4H_8)Me]$ was investigated by psTRIR in *n*-heptane solution at room temperature at the University of Amsterdam. The ground state FTIR spectrum of $[(CO)_5WC(NC_4H_8)Me]$ in *n*-heptane solution exhibits metal carbonyl stretching bands at 2063, 1967, 1932 and 1925 cm^{-1} (Figure 3.4). The UV-vis spectrum for $[(CO)_5WC(NC_4H_8)Me]$ can be found in Figure 3.3. The spectral changes observed following irradiation at 400 nm are displayed in Figure 3.8. The spectrum obtained 1 ps after excitation exhibits depletion (negative features) of the bands at 2062 and 1921 cm^{-1} in the difference spectrum corresponding to the principal features of the parent (Figure 3.8). It should be noted that the psTRIR resolution is considerably less at 4 cm^{-1} than the FTIR spectrum (0.5 cm^{-1}) and the technique cannot resolve the two features at 1932 and 1925 cm^{-1}. Therefore, these bands appear as a single feature in the psTRIR difference spectrum. The very weak parent feature at 1967 cm^{-1} is not evident in the psTRIR experiment. Following excitation at 400 nm, two new intense features at 1906 and 1892 cm^{-1} and a very weak feature at approximately 2012 cm^{-1} are produced, and are assigned to an excited state species. This species quickly reacts to form a second excited state (k_{obs} = 8.8 (± 0.8) × 10^{10} s^{-1}; 293 K) with a band at 1911 cm^{-1} and a weak band at 2022 cm^{-1}. Again, the feature at 1911 cm^{-1} may be distorted by the parent bleach signal. This excited state in turn reacts (k_{obs} = 6.5 (± 0.4) × 10^{10} s^{-1}; 293 K) to form a stable (on the timescale of the psTRIR experiment) photoproduct which absorbs at 2028, 1911 and 1873 cm^{-1}, assigned to the solvated CO loss species, $[(n\text{-heptane})(CO)_4WC(NC_4H_8)Me]$. These bands are consistent with the spectral changes previously assigned to the CO loss bands for the chromium derivative $[(CO)_5CrC(NC_4H_8)Me]$ in the previous section (**3.3.3.1**). The band positions are also in

agreement with the steady state photolysis study reported in section **3.3.2**, in which the CO loss product, $[(PPh_3)(CO)_4WC(NC_4H_8)Me]$, exhibited bands at 2007, 1907 and 1883 cm^{-1}. The bleached signal at 1921 cm^{-1} recovers by 32 % after 120 ps, at a rate similar to the decay of the first observable excited (8.8 (± 0.6) × 10^{10} s^{-1}; 293 K). The bleached signal at 2062 cm^{-1} recovers more slowly (4.3 (± 0.3) × 10^{10} s^{-1}; 293 K) and to a smaller extent (21 %). This confirms that the first and second excited states and also the photoproduct absorb close to the parent bleach signal at 1921 cm^{-1}. The photophysical processes leading to CO loss following excitation of $[(CO)_5W(NC_4H_8)Me]$ at 400 nm are illustrated in Scheme 3.5.

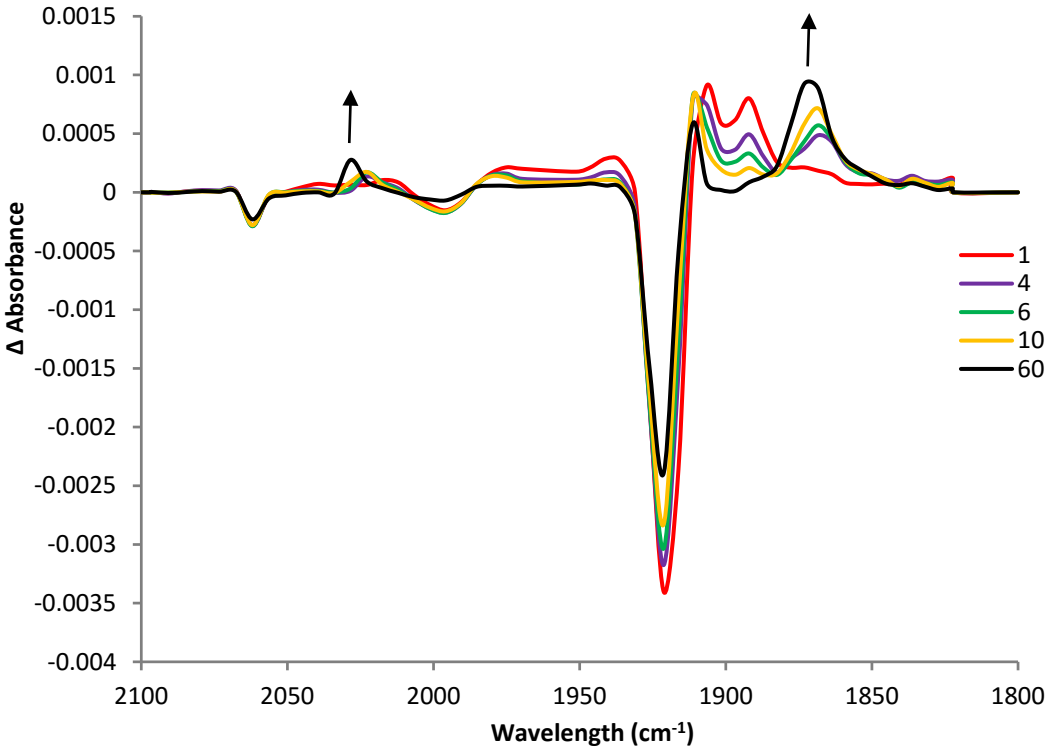

Figure 3.8 Picosecond TRIR difference spectra following 400 nm photolysis of $[(CO)_5WC(NC_4H_8)Me]$ in *n*-heptane solution at selected time intervals; 1, 4, 6, 10, and 60 ps.

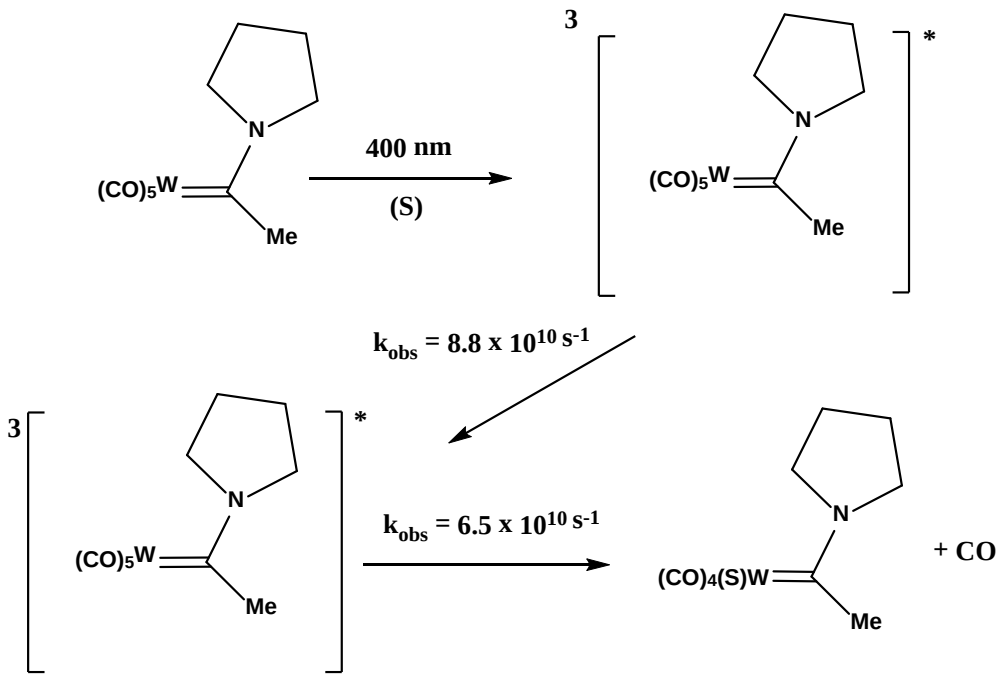

Scheme 3.5 The photophysical processes leading to the CO loss species $[(CO)_4(S)W(NC_4H_8)Me]$ following 400 nm irradiation, where S = *n*-heptane.

The psTRIR studies show that if the alkoxy group is replaced by an amino substituent i.e. from $[(CO)_5MC(OMe)(Me)]$ to $[(CO)_5MC(NC_4H_8)(Me)]$, M= Cr, W, the quantum efficiency of photoinduced CO loss can be greatly increased, and the photon energy required to achieve CO loss is reduced. For example 400 nm irradiation of $[(CO)_5CrC(NC_4H_8)(Me)]$ resulted in a rapid (< 50 ps) CO loss with a quantum yield of approximately 65 % whereas no CO loss was observed under the same conditions for $[(CO)_5CrC(OMe)(Me)]$. No evidence was obtained for the formation of metallaketene intermediates or metallacyclopropanone excited states with the amino systems unlike that observed for the methoxy systems in Chapter 2. This is not surprising as some amino Fischer carbene complexes are poor reagents in the synthesis of β-lactams.[17]

3.3.4 Quantum Chemical Calculations

Quantum chemical calculations were performed by Prof C. Long to aid with the understanding of the photophysics and photochemistry of complexes $[(CO)_5CrC(NC_4H_8)Me]$ and $[(CO)_5WC(NC_4H_8)Me]$.

3.3.4.1 Density Functional Theory Calculations of $[(CO)_5CrC(NC_4H_8)Me]$

$[(CO)_5CrC(NC_4H_8)Me]$ was modelled using a hybrid Density Functional Theory (B3LYP)[23,24]using a triple zeta quality basis set (Tzvp)[25] which has been implemented in Gaussian 09 (Revision D.01). The Cr-*cis* CO distance was chosen as a suitable reaction coordinate to model the CO loss reaction since CO loss occurs from the *cis*-CO ligand. A relaxed potential energy scan was preformed along this reaction coordinate and at each point, time-dependent DFT calculations provided the vertical excitation energies to the five lowest energy singlet excited states (TDDFT/B3LYP/Tzvp). These data were then used to construct an energy profile along this reaction coordinate for these excited states (Figure 3.9). The plots confirm that it is possible for CO to be generated from the lowest energy singlet excited state (metal-to-carbene charge-transfer in character, MLCT) by overcoming a small thermal barrier (5.6×10^{-4} kJ / mol), the latter formed by crossing with the 2nd singlet excited state which is metal centred in character. This will lead to arrested CO loss which is contrast to the ultrafast (< 100 fs) CO loss exhibited for $Cr(CO)_6$ ($\Phi_{CO} = 0.72$).[26] Along this reaction coordinate the Cr-CO distance on only one *cis*-CO is increased and consequently the symmetry and therefore the IR spectrum of the excited state will resemble that of the CO loss product. The lowest energy singlet excited state has substantial metal-to-carbene charge-transfer character while the second singlet excited state is mainly a metal-centred state. The DFT calculations showed no evidence for the population of a triplet excited state.

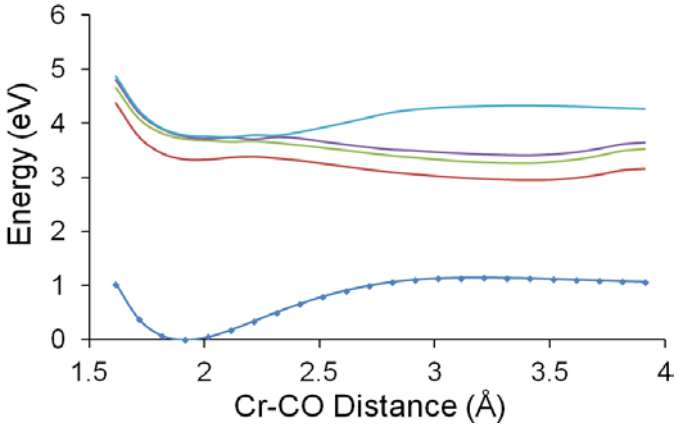

Figure 3.9 The energy of the ground state (blue) and the four lowest energy singlet excited states as the Cr-*cis* CO distance is varied, (the data interval is indicated by data point markers on the ground state curve but omitted from the excited state curves for clarity).

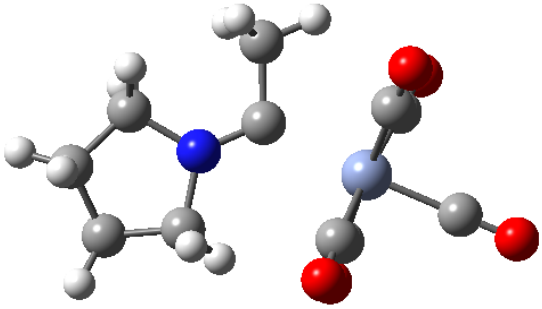

Figure 3.10 The molecular structure and orientation of [$(CO)_5CrC(NC_4H_8)Me$] as used in electron density difference maps in Figure 3.11 and Figure 3.12 shown below.

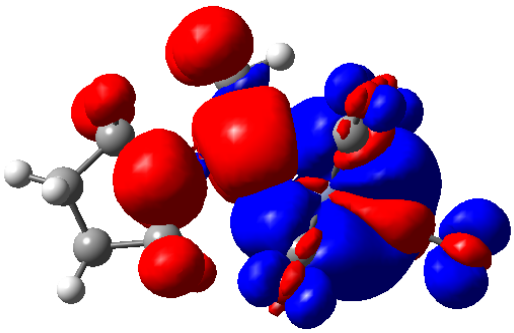

Figure 3.11 The electron density difference map for the first singlet excited state at the ground state optimised geometry, the blue volumes are the regions where the electron density is reduced in the excited state compared to the ground state and the red volumes are the regions where the electron density is greater in the excited state compared to the ground state. This excited state has substantial metal-to-carbene charge-transfer character (HOMO to LUMO).

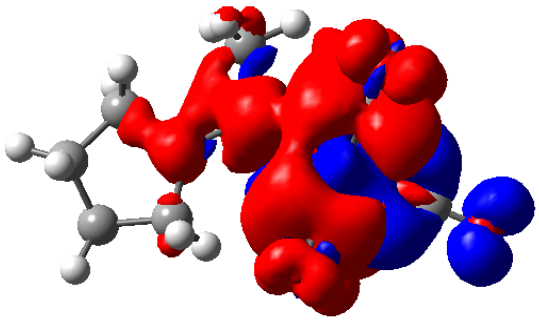

Figure 3.12 The electron density difference map for the second singlet excited state indicating a greater metal-centred character for this excited state compared to the first singlet excited state (HOMO to LUMO+1).

3.3.4.2 Density Functional Theory Calculations of $[(CO)_5WC(NC_4H_8)Me]$

The electronic structure of $[(CO)_5WC(NC_4H_8)Me]$ was modelled using a hybrid density functional method (B3LYP for singlet species and UB3LYP for triplet) and a triple zeta quality basis set (def2-TZVP).[23,24,27,28] Three reaction coordinated were investigated, CO loss of a *cis*-carbonyl ligand, CO loss of a *trans*-CO ligand and the carbonylation reaction to form the metallaketene intermediate. In each case a relaxed potential energy scan was constructed on the singlet surface, which provided a set of atomic coordinates at each step along the reaction coordinate. Each set of coordinates was then used to estimate the excited state energies, either singlet or triplet using Time-Dependent Density Functional (TDDFT) methods. The resulting plots of excited state energy against reaction coordinate provides information on the likely consequence of the population of specific excited states.

The plot of the excited state energies along the *cis*-CO and *trans*-CO loss reaction coordinate is presented in Figure 3.13. In this plot both singlet and triplet excited states are present.

(a)

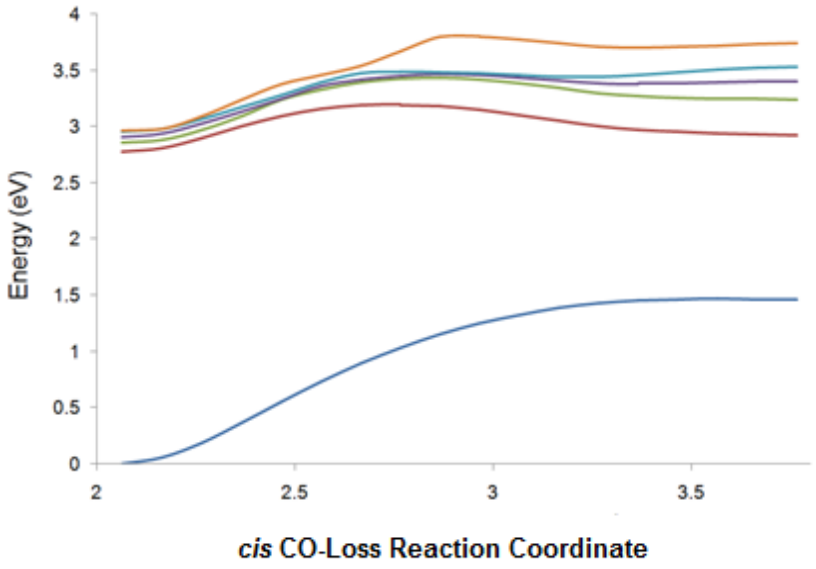

(b)

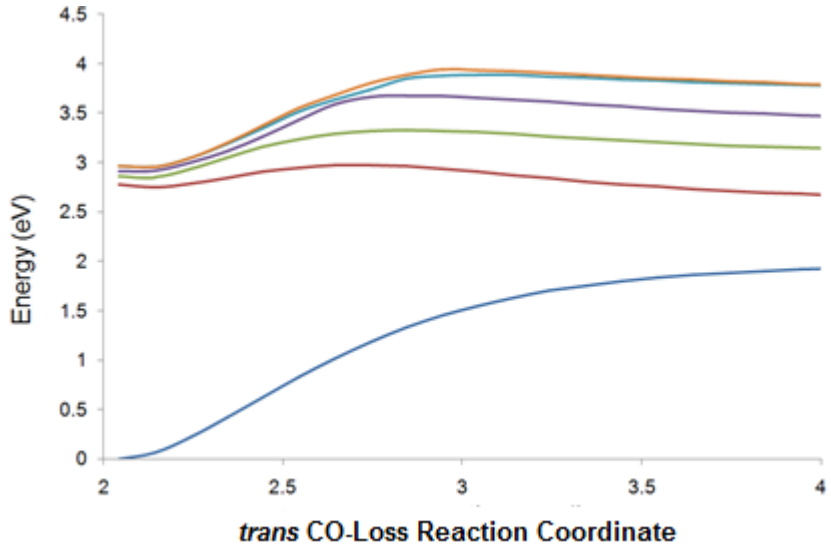

Figure 3.13 (a) The variation of excited state energies (singlet and triplet) along the *cis*-CO loss reaction coordinate showing that the five lowest energy accessible (400 nm, 3.1 eV) excited states are bound with respect to *cis*-CO loss. **(b)** A plot of the energies of the five lowest energy excited states (singlet and triplet) along the *trans*-CO loss reaction coordinate.

An excitation wavelength of 400 nm (3.1 eV) was used in the psTRIR experiments. The results presented in Figure 3.13 (a) indicate that the lowest five accessible excited states are bound with respect to *cis*-CO loss. The lowest accessible state (triplet) presents a significant (40 kJ mol^{-1}) barrier to CO loss. The energy plots for on the *trans*-CO loss reaction coordinate are presented in Figure 3.13 (b) and exhibit broadly similar behaviour. While the accessible excited states are all bound with respect to *trans*-CO loss the lowest energy triplet state presents a smaller barrier (19 kJ mol^{-1}) to *trans*-CO loss than to *cis*-CO loss. These results suggest that irradiation of $[(CO)_5WC(NC_4H_8)Me]$ at 400 nm may induce *trans*-CO loss *via* a triplet excited state.

3.3.5 Cyclic Voltammetry and Electrochemical CO loss

3.3.5.1 Cyclic Voltammetry and Electrochemical CO loss of $[(CO)_5CrC(NC_4H_8)Me]$

Electrochemical analysis of $[(CO)_5CrC(NC_4H_8)Me]$ in 0.1 M $TBAPF_6$ in acetonitrile using cyclic voltammetry reveals three redox processes within the potential window investigated (Figure 3.14). These include two oxidative processes and one reductive process (+ 0.34 V, + 1.03 V and - 2.80 V *vs.* Fc/Fc^+). The first oxidation is assigned to the $Cr^{0/I}$ redox couple as previously reported.[29,30] Oxidation of these types of metal carbene complexes is reported as being predominantly metal based[30] with reduction centred on the metal-carbene double bond.[29] Varying scan rates did not promote reversibility for the redox processes observed.

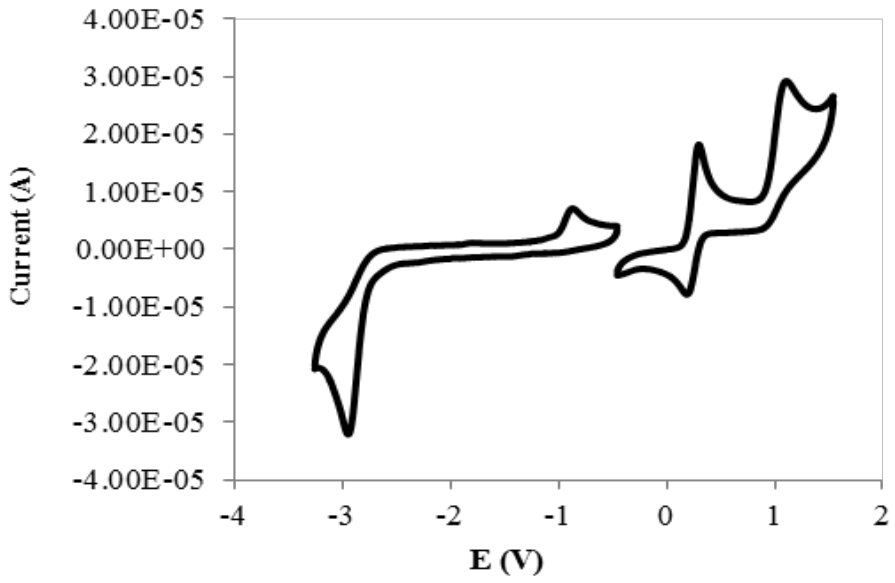

Figure 3.14 Cyclic voltammogram of oxidation and reduction of $[(CO)_5CrC(NC_4H_8)Me]$ in 0.1 M $TBAPF_6$ in CH_3CN, *vs.* Fc/Fc^+. Scan rate = 0.1 V s^{-1}.

In the present study, electrochemical initiation of CO release from the complex was confirmed and quantified *via* headspace analysis using gas chromatography (Figure 3.15).

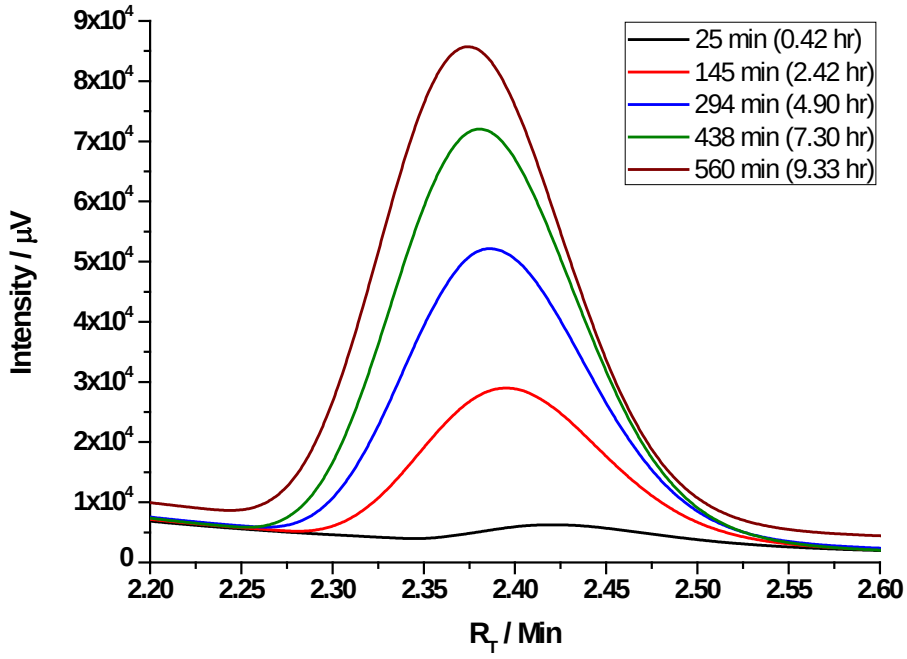

Figure 3.15 Gas chromatogram revealing the increase in CO peak area as a result of CO release with time from 1 mM of $[(CO)_5CrC(NC_4H_8)Me]$ under controlled potential electrolysis (E = + 0.36 V, *vs.* Fc/Fc^+).

Displayed in Figure 3.16 is the electrochemical CO release profile of over 10 hours of controlled potential electrolysis (*E* = + 0.36 V *vs.* Fc/Fc^+). As one-electron oxidation of $[(CO)_5CrC(NC_4H_8)Me]$ is primarily characterised by the $Cr^{(0/I)}$ couple, it is likely that the reduced capacity of Cr(I) for π back-donation results in a more labile Cr-CO bond. This was the first instance where electrochemically initiated CO loss from a CORM has been quantified.[31]

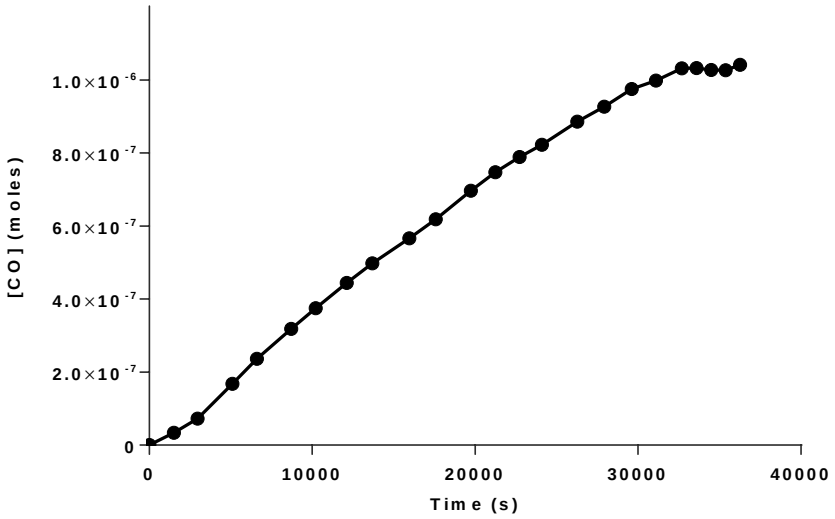

Figure 3.16 Profile for the electrochemically induced CO release over time from $[(CO)_5CrC(NC_4H_8)Me]$ in acetonitrile under potentiostatic conditions (E = + 0.36 V *vs.* Fc/Fc^+). Concentration of $[(CO)_5CrC(NC_4H_8)Me]$ was 1 mM and the solution was stirred continuously (n = 2).

Comparison of the oxidation potential of $[(CO)_5CrC(NC_4H_8)Me]$ with $[(CO)_5CrC(OMe)Me]$ (Chapter 2) reveals an increase in the oxidation potential of the latter (110 mV) and shows how the nature of the heteroatom present on the carbene carbon can affect the electrochemical activity of the compound. In this case, the increase in the first oxidation potential of the methoxy analogue can be explained by the higher electronegativity of the oxygen atom compared to the nitrogen atom of the amino analogue.[14]

3.3.5.2 Cyclic Voltammetry and Electrochemical CO loss of $[(CO)_5WC(NC_4H_8)Me]$

Electrochemical analysis of $[(CO)_5WC(NC_4H_8)Me]$ in 0.1 M $TBAPF_6$ in acetonitrile using cyclic voltammetry reveals two redox processes within a potential window of -3.0 to 1.5 V, *vs.* Fc/Fc^+, Figure 3.17. The compound is oxidised at a potential of + 0.52 V, *vs.* Fc/Fc^+, a process of which is irreversible at slow scan rates up to 1.0 V/s. This process becomes quasi-reversible at higher scan rates (up to 70 V/s, Figure 3.18) with an anodic to cathodic peak current ratio of approximately 1 : 0.5 and is assigned to the metal centred $W^{0/I}$ redox couple as previously reported.[29,30] The oxidation is metal based

with reduction centred on the metal-carbene double bond.[29,30] Comparison of the oxidation potential of $[(CO)_5WC(NC_4H_8)Me]$ with the Cr analogue, $[(CO)_5CrC(NC_4H_8)Me]$ reveals an increase in the oxidation potential of the former W complex of 180 mV. This has been shown for other Cr and W complexes and further supports the assignment of the oxidation process as metal centred.[29] The complex is reduced at a potential of - 2.75 V, *vs.* Fc/Fc^+ and is irreversible at the range of scan rates investigated (0.1 - 50 V/s). However, it is noted that three anodic processes are observed in the range of - 1.0 to - 0.4 V following the reduction of the complex, Figure 3.17.

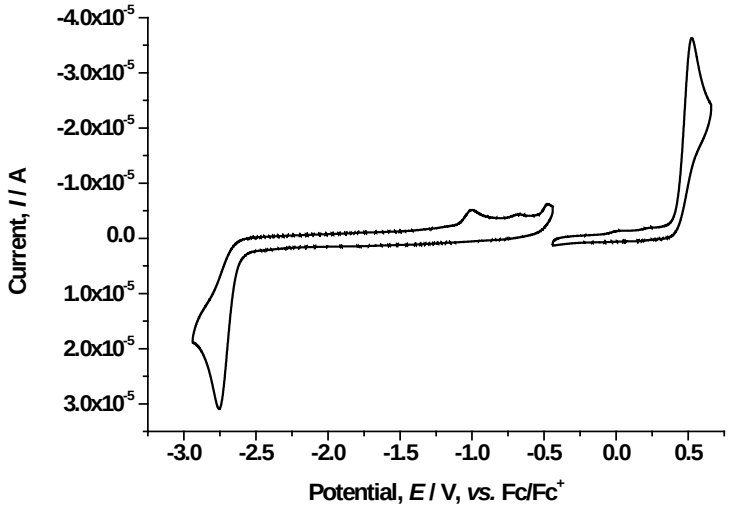

Figure 3.17 Cyclic voltammogram of the oxidation and reduction of $[(CO)_5WC(NC_4H_8)Me]$ in 0.1 M $TBAPF_6$ in CH_3CN, *vs.* Fc/Fc^+. Scan rate = 0.1 V s^{-1}.

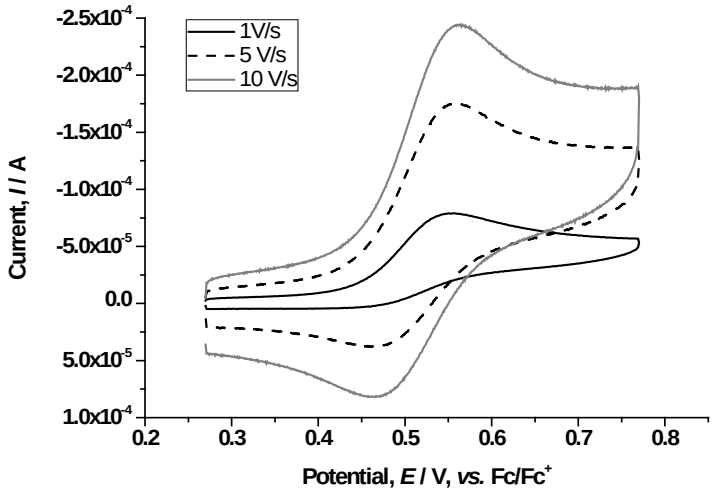

Figure 3.18 Scan rate dependence of the first oxidation process of $[(CO)_5WC(NC_4H_8)Me]$ in 0.1M $TBAPF_6$ in CH_3CN, *vs.* Fc/Fc^+. CVs for scan rate of 1.0, 5.0 and 10.0 V/s shown here.

In the present study, electrochemical initiation of CO release from a 1 mM solution of the complex in CH_3CN was confirmed, over five intervals approximately 20 minutes apart and quantified *via* headspace analysis using gas chromatography. The electrochemical CO loss profile over 1.5 hours of controlled potential electrolysis (*E* = + 0.87, *vs.* Fc/Fc^+) is displayed in Figure 3.19.

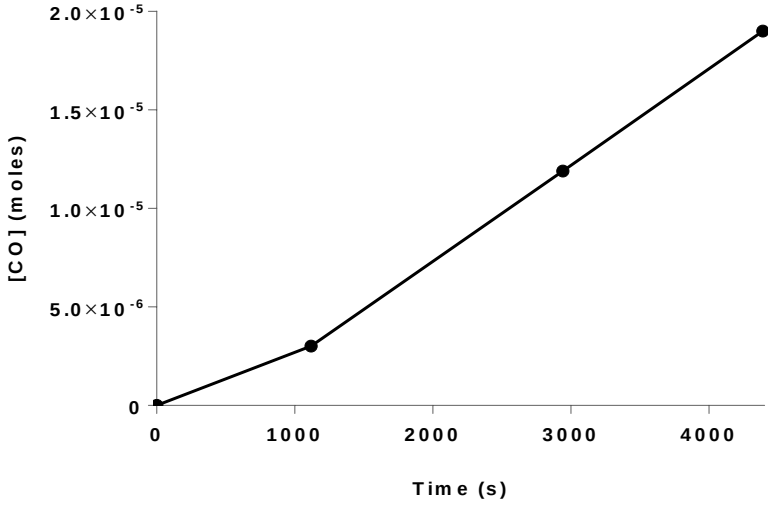

Figure 3.19 Profile for the electrochemically induced CO release over time from $[(CO)_5WC(NC_4H_8)Me]$ in acetonitrile under potentiostatic conditions (E = + 0.87 V *vs.* Fc/Fc^+). Concentration of $[(CO)_5WC(NC_4H_8)Me]$ was 1 mM and the solution was stirred continuously (n = 1).

3.3.6 Myoglobin Assay

3.3.6.1 Myoglobin Assay of $[(CO)_5CrC(NC_4H_8)Me]$

The CO releasing ability of $[(CO)_5CrC(NC_4H_8)Me]$ was determined thermally at body temperature, (37 °C) and photochemically (355 nm) using the myoglobin (Mb) assay.[3] Figure 3.20 represents the typical spectra of deoxy-Mb *vs.* Mb-CO. Mb-CO is formed by bubbling CO through deoxy-Mb for 20 minutes. This is carried out prior to each experiment to account for any minor variations in myoglobin concentrations. Figure 3.21 depicts the photochemical CO release profile at 355 nm and Figure 3.22 depicts the thermal CO release profile.

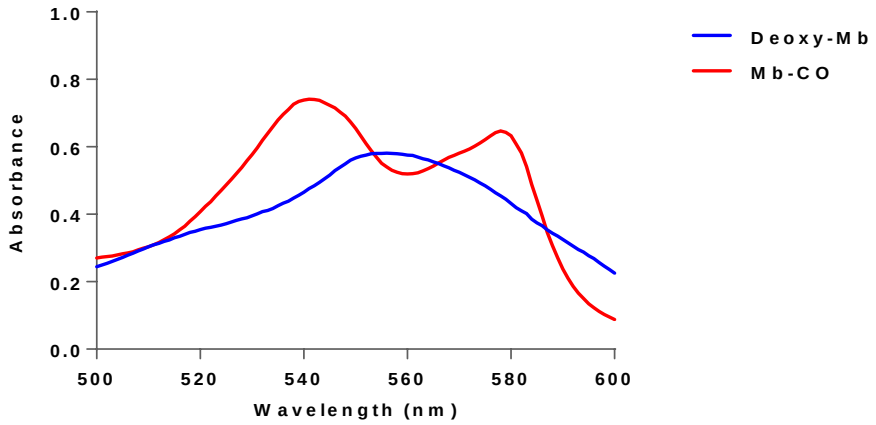

Figure 3.20 UV-vis spectra of the deoxy-Mb and Mb-CO Q-bands.

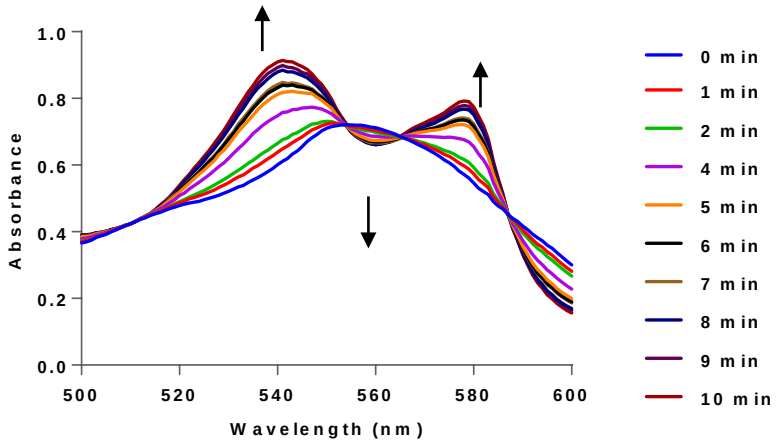

Figure 3.21 CO release profile for $[(CO)_5CrC(NC_4H_8)Me]$ (60 µM) measuring the conversion of deoxy-Mb to Mb-CO against time, photochemically at 355 nm (n = 3).

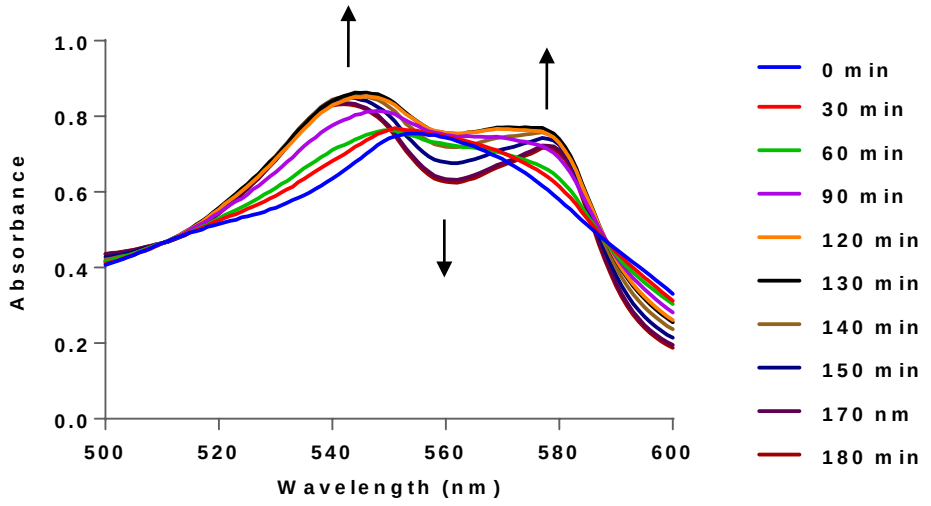

Figure 3.22 CO release profile for $[(CO)_5CrC(NC_4H_8)Me]$ (60 µM) measuring the conversion of deoxy-Mb to Mb-CO against time, thermally at 37 °C (n = 3).

During the experiments the intensity of the Mb Q-band at ~ 554 nm decreases while the characteristic peaks of Mb-CO appears at 540 nm and 578 nm upon release of CO (indicated by the arrows in Figure 3.21 and Figure 3.22).

The most commonly used method of comparison of various types of CORMs is by stating the $t_{½}$ values which quantitatively compare CO release from different CORM systems that may occur by different mechanisms. It may be defined as the time taken for a solution of CORM with a concentration of 60 µM to produce a solution of Mb-CO with a concentration of 30 µM (or 40 µM to form 20 µM and 20 µM to form 10 µM). For very slow CORMs, $t_{1/4}$ may be expressed because the lifetime of myoglobin is limited (conversion of deoxy-Mb to oxy-Mb occurs).[4]

The major notable difference between the two methods (photo *vs.* thermal) employed here for CO release is the difference in $t_{½}$ values. Complete saturation of deoxy-Mb by $[(CO)_5CrC(NC_4H_8)Me]$ was observed, but required ~3 h (Figure 3.22) at 37 °C (60 µM), ($t_{½}$ = 4544 s). This is significantly slower than that observed photochemically in Figure 3.21, where $t_{½}$ = 266 s (60 µM).

3.3.6.2 Solvent effects on the Myoglobin Assay

Due to the recent reports of the limitations of the myoglobin assay afore mentioned in the introduction section, the effects of different solvents on photochemically, thermally and electrochemically induced CO loss from the amino carbene complex $[(CO)_5CrC(NC_4H_8)Me]$ were monitored in the absence and in the presence of the reducing agent sodium dithionite (SD), which has been proven to alter the release rate of CO[5,6] using gas chromatography. $[(CO)_5CrC(NC_4H_8)Me]$ was a suitable candidate for this experiment as it released CO upon all forms of stimulation.

A range of solvents were used as shown in Table 3.1. To mimic the myoglobin assay, the sample was prepared in a similar manner (excluding myoglobin) and dissolved in DMSO (12 mM solution). Next, a 10 µL aliquot of this CORM / DMSO solution was further dissolved in 2 ml PBS (overall concentration was 60 µM). Samples were prepared with and without SD. The sample was also dissolved in the following solvent mixes; DMSO / CH_3CN to see if PBS may be playing a role and also using neat CH_3CN to see if DMSO may be having additional effects. Electrochemically, the same concentration was effectively used, however, 5 ml was the minimum amount needed for the experiment to be carried out in the V- cell (25 µL / 5 ml) and PBS was used as the electrolyte.

Table 3.1 Solvent mixes and concentrations used during photochemically, thermally and electrochemically induced CO loss experiments from $[(CO)_5CrC(NC_4H_8)Me]$ (concentration 60 µM - to mimic concentrations used in the myoglobin assay).

Photochemical (355 nm)	**Thermal (37 º C)**	**Electrochemical (+ 0.36 V *vs.* Fc/Fc^+)**
DMSO / PBS	DMSO / PBS	DMSO / PBS
DMSO / CH_3CN	DMSO / CH_3CN	DMSO / CH_3CN
Neat CH_3CN	Neat CH_3CN	Neat CH_3CN
DMSO / PBS + SD	DMSO / PBS + SD	-

Trend: Neat CH_3CN > DMSO / CH_3CN > DMSO / PBS + SD > DMSO / PBS

These experiments showed that varying the solvent and the form of stimuli to elicit CO loss alters the amount of CO released as seen in Figures 3.23 - 3.25.

Photochemically, as seen in Figure 3.23, a similar time frame (approx. 8,000 s) has been used to compare the various solvent mixes. When $[(CO)_5CrC(NC_4H_8)Me]$ is dissolved in DMSO / CH_3CN, 0.171 µM of CO is released. This corresponds to the largest amount of CO generated photochemically over the timeframe of the experiments. When dissolved in neat CH_3CN, 0.122 µM of CO is generated. However, in the biologically favoured solvent mix of DMSO / PBS, the lowest yield of CO is released; (0.058 µM CO) over this time frame. In the presence of the reducing agent, SD, in DMSO / PBS, the CO release profile is altered and 0.073 µM of CO is released. This clearly illustrates that photochemically, SD is influencing the rate of CO release for the complex, $[(CO)_5CrC(NC_4H_8)Me]$ under the conditions employed here.

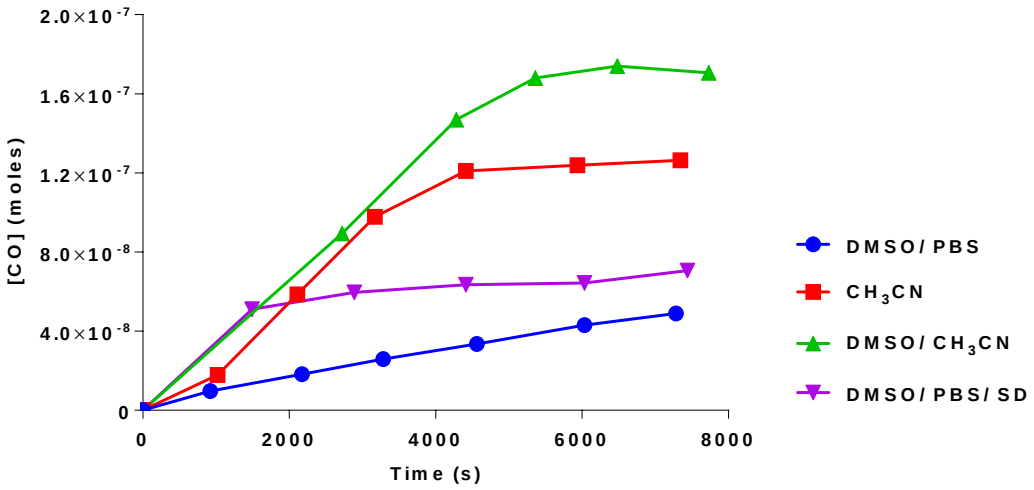

Figure 3.23 Photochemical CO release profile of $[(CO)_5CrC(NC_4H_8)Me]$ (60 µM) in various solvent mixes (n = 2).

Thermally (Figure 3.24), over approx. 22,000 s, when $[(CO)_5CrC(NC_4H_8)Me]$ is dissolved in neat CH_3CN, 0.054 µM of CO is released. This corresponds to the largest amount of CO generated over the timeframe of the experiments. When dissolved in DMSO / CH_3CN, 0.048 µM of CO is generated. However, when dissolved in DMSO / PBS, again, the lowest yield of CO is released; (0.034 µM CO). In the presence of the reducing agent, SD, 0.040 µM of CO is released. This confirms that thermally as well as photochemically, SD alters the CO release profile for the complex, $[(CO)_5CrC(NC_4H_8)Me]$.

Photochemical CO release occurs at a faster rate than thermally induced CO loss for the systems studied here. This is consistent with reported data.[31] Photochemically and

thermally CO loss is more efficient in acetonitrile. DMSO plays a very minor role in the alteration of photochemical CO release and has no effect thermally. SD alters the CO release profile for this complex. Both photochemically and thermally, SD increases the rate at which CO is released. CO release monitored by gas chromatography is a more direct method than the myoglobin assay and disregards the need for additional reagents such as SD.

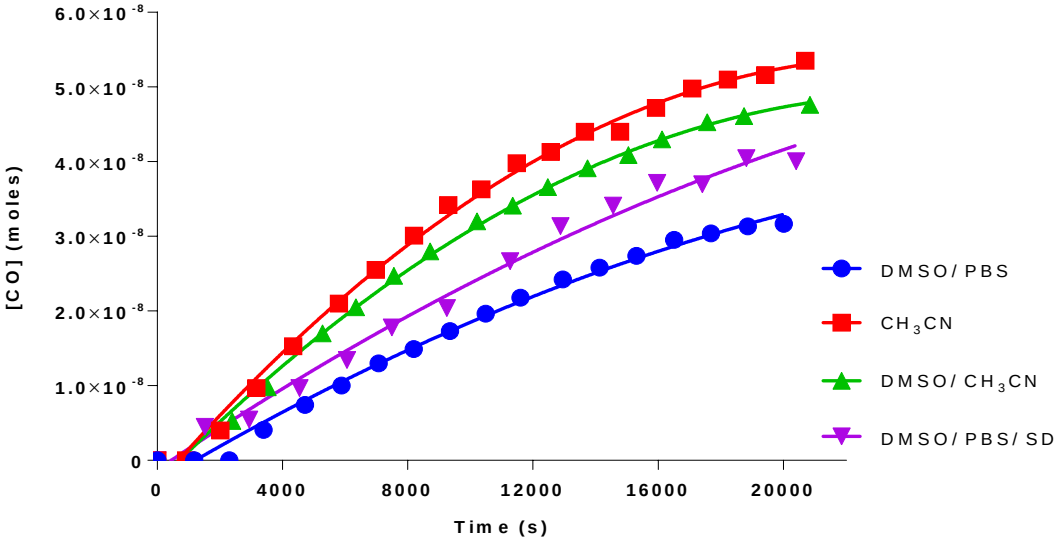

Figure 3.24 Thermal CO release profile of $[(CO)_5CrC(NC_4H_8)Me]$ (60 µM) in various solvent mixes (n = 2).

Electrochemically, over approx. 30,000 s, when the complex is dissolved in neat CH_3CN more CO (0.621 µM) is released in comparison to that released from the DMSO / CH_3CN mix (0.465 µM). DMSO / PBS did not release any CO when monitored over the same time points (Figure 3.25). In general, acetonitrile is most commonly used in electrochemical experiments so in this instance it would be the solvent of choice to monitor CO loss. It would be ideal to observe CO release from DMSO / PBS for *in vivo* applications of CO release. However, in this particular case it is not possible.

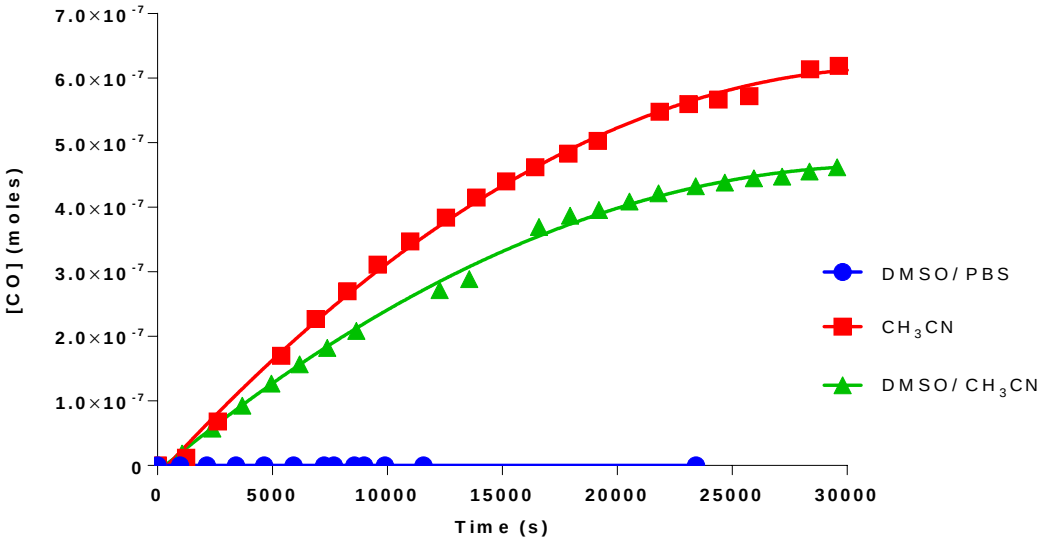

Figure 3.25 Electrochemical CO release profile of $[(CO)_5CrC(NC_4H_8)Me]$ (60 µM) in various solvent mixes (n = 2).

3.3.6.3 Myoglobin Assay of $[(CO)_5WC(NC_4H_8)Me]$

Thermal CO release did not occur from $[(CO)_5WC(NC_4H_8)Me]$ (monitored for 5 hours at 60 µM, 40 µM and 20 µM) and therefore no headspace analysis experiments were performed by GC. It may be deduced that $[(CO)_5WC(NC_4H_8)Me]$ is not a thermal CO releasing molecule. This is not too surprising as the nature of the metal and heteroatom substituents on the carbene greatly influences the rate of CO release. Lynam *et al.* reported results on the thermally induced CO loss for a range of pentacarbonyl complexes.[2] It was confirmed that the rate of CO release for Fischer carbene complexes is as follows; Cr > Mo > W. Thermally, tungsten Fischer carbene complexes release CO at a much slower rate than chromium based carbenes. For example, $[(CO)_5WC(OMe)Me]$ takes 7924 s to release 30 µM from a 60 µM solution whereas $[(CO)_5CrC(OMe)Me]$ takes 215 s at the same concentration.[2] Also, the replacement of the methoxy group with a pyrrolidino group for $[(CO)_5CrC(NC_4H_8)Me]$ significantly slows down the rate of CO release i.e. $t_{½}$ = 4544 s.[31]

3.4 Conclusion

In conclusion, three stimuli: photo, thermal and electrochemical approaches toward CO release from the amino carbene complexes, $[(CO)_5CrC(NC_4H_8)Me]$ and $[(CO)_5WC(NC_4H_8)Me]$ were assessed. $[(CO)_5CrC(NC_4H_8)Me]$ proved that, a single type of CORM can be used for either fast or slow CO release simply by altering the means of stimulation. The psTRIR studies highlight that a singlet excited state yields CO loss within 50 ps with a quantum efficiency for CO loss of 65 %, which translates to a 17-fold increase in the rate of CO-uptake by deoxy-Mb at 37 °C in PBS when $t_{1/2}$ for both thermal and photochemical CO release are compared. Picosecond time resolved infrared spectroscopy was used to probe the photo-induced early state dynamics leading to CO release, and DFT calculations confirmed that for $[(CO)_5CrC(NC_4H_8)Me]$, CO release occurs from a singlet excited state and that a *cis*-CO ligand is expelled from the lowest energy excited state which has substantial metal-to-carbene charge-transfer character. Electrochemically, CO loss was detected and quantified at a low potential in acetonitrile which is important for physiological applications.[32-34]

$[(CO)_5WC(NC_4H_8)Me]$ showed similar photochemical CO release behaviour to $[(CO)_5CrC(NC_4H_8)Me]$, also boasting a high quantum efficiency for CO loss. For $[(CO)_5WC(NC_4H_8)Me]$, based on the results of quantum chemical calculations, this species is tentatively assigned to the singlet CO loss species $^1[(CO)_4WC(NC_4H_8)Me]$ which may be formed *via* a triplet excited state. Thermally, $[(CO)_5WC(NC_4H_8)Me]$ did not lose CO over a time period of up to 5 hours. The influence of solvent effects were investigated for $[(CO)_5CrC(NC_4H_8)Me]$. The commonly used reducing agent, SD, which is used routinely in the myoglobin assay, influenced the CO release profile both photochemically and thermally. CO release (either photochemically, thermally or electrochemically) was solvent dependent. The DMSO / PBS mixture is most suitable for the analysis of CO loss as it is most commonly used in cellular studies and should be used for future experiments.

Cyclic voltammetry revealed different redox process for the Cr and W derivatives. The Cr analogue exhibits three redox processes (two oxidative (one reversible, one irreversible) and one irreversible reductive process) whereas the W analogue reveals two redox processes (one oxidative (which becomes quasi reversible at higher scan rates) and one irreversible reductive process). For $[(CO)_5CrC(NC_4H_8)Me]$, no CO loss was

observed in DMSO / PBS. Neat CH_3CN was the most efficient solvent for electro CO release and is therefore the solvent of choice for electro release of this complex. Limitations exist however, as DMSO / PBS would be much more suitable for *in vivo* applications.

For future experiments measuring CO release from CORMs, headspace analysis *via* GC should be used in a biologically compatible solvent mixture instead of the myoglobin assay as it excludes the need for additional reagents such as sodium dithionite.

3.5 References

1. Schwindt, M.; Miller, J.; Hegedus, L. Chromium Aminocarbene Complexes in Organic-Synthesis. *J. Organomet. Chem.* **1991**, *413*, 143-153.

2. Zhang, W.; Atkin, A. J.; Thatcher, R. J.; Whitwood, A. C.; Fairlamb, I. J. S.; Lynam, J. M. Diversity and design of metal-based carbon monoxide-releasing molecules (CO-RMs) in aqueous systems: revealing the essential trends. *Dalton Trans.* **2009**, *22*, 4351-4358.

3. Motterlini, R.; Clark, J.; Foresti, R.; Sarathchandra, P.; Mann, B.; Green, C. Carbon monoxide-releasing molecules - Characterization of biochemical and vascular activities. *Circ. Res.* **2002**, *90*, E17-E24.

4. Atkin, A. J.; Lynam, J. M.; Moulton, B. E.; Sawle, P.; Motterlini, R.; Boyle, N. M.; Pryce, M. T.; Fairlamb, I. J. S. Modification of the deoxy-myoglobin/carbonmonoxy-myoglobin UV-vis assay for reliable determination of CO-release rates from organometallic carbonyl complexes. *Dalton Trans.* **2011**, *40*, 5755-5761.

5. Klein, M.; Neugebauer, U.; Gheisari, A.; Malassa, A.; Jazzazi, T. M. A.; Froehlich, F.; Westerhausen, M.; Schmitt, M.; Popp, J. IR Spectroscopic Methods for the Investigation of the CO Release from CORMs. *J Phys Chem A* **2014**, *118*, 5381-5390.

6. McLean, S.; Mann, B. E.; Poole, R. K. Sulfite species enhance carbon monoxide release from CO-releasing molecules: Implications for the deoxymyoglobin assay of activity. *Anal. Biochem.* **2012**, *427*, 36-40.

7. Rimmer, R. D.; Richter, H.; Ford, P. C. A Photochemical Precursor for Carbon Monoxide Release in Aerated Aqueous Media. *Inorg. Chem.* **2010**, *49*, 1180-1185.

8. Berends, H.; Kurz, P. Investigation of light-triggered carbon monoxide release from two manganese photoCORMs by IR, UV-Vis and EPR spectroscopy. *Inorg. Chim. Acta* **2012**, *380*, 141-147.

9. Huber, W.; Linder, R.; Niesel, J.; Schatzschneider, U.; Spingler, B.; Kunz, P. C. A Comparative Study of Tricarbonylmanganese Photoactivatable CO Releasing Molecules (PhotoCORMs) by Using the Myoglobin Assay and Time-Resolved IR Spectroscopy. *Eur. J. Inorg. Chem.* **2012**, *19*, 3140-3146.

10. McGuire, M.; Hegedus, L. Synthesis of Beta-Lactams by the Photolytic Reaction of Chromium Carbene Complexes with Imines. *J. Am. Chem. Soc.* **1982**, *104*, 5538-5540.

11. Doyle, K.; Gallagher, M.; Pryce, M.; Rooney, A. A matrix isolation and flash photolysis study of the cyclization reactions of chromium amino carbenes. *J. Organomet. Chem.* **2001**, *617*, 269-279.

12. Rooney, A.; McGarvey, J.; Gordon, K.; McNicholl, R.; Schubert, U.; Hepp, W. Laser Photochemistry and Transient Raman-Spectroscopy of Silyl-Substituted Fischer-Type Carbene Complexes. *Organometallics* **1993**, *12*, 1277-1282.

13. Hafner, A.; Hegedus, L.; DeWeck, G.; Hawkins, B.; Dotz, K. Chromium-53 Nuclear Magnetic-Resonance Studies of Pentacarbonylchromium Carbene Complexes. *J. Am. Chem. Soc.* **1988**, *110*, 8413-8421.

14. Baldoli, C.; Cerea, P.; Falciola, L.; Giannini, C.; Licandro, E.; Maiorana, S.; Mussini, P.; Perdicchia, D. The electrochemical activity of heteroatom-stabilized Fischer-type carbene complexes. *J. Organomet. Chem.* **2005**, *690*, 5777-5787.

15. Hoskovcova, I.; Rohacova, J.; Dvorak, D.; Tobrman, T.; Zalis, S.; Zverinova, R.; Ludvik, J. Synthesis and electrochemical study of iron, chromium and tungsten aminocarbenes Role of ligand structure and central metal nature. *Electrochim. Acta* **2010**, *55*, 8341-8351.

16. Landman, M.; Pretorius, R.; Buitendach, B. E.; van Rooyen, P. H.; Conradie, J. Synthesis, Structure, and Electrochemistry of Fischer Alkoxy- and Aminocarbene Complexes of Tungsten: The Use of DFT To Predict and Understand Oxidation and Reduction Potentials. *Organometallics* **2013**, *32*, 5491-5503.

17. Greetham, G. M.; Burgos, P.; Cao, Q.; Clark, I. P.; Codd, P. S.; Farrow, R. C.; George, M. W.; Kogimtzis, M.; Matousek, P.; Parker, A. W.; Pollard, M. R.; Robinson, D. A.; Xin, Z.; Towrie, M. ULTRA: A Unique Instrument for Time-Resolved Spectroscopy. *Appl. Spectrosc.* **2010**, *64*, 1311-1319.

18. Towrie, M.; Grills, D.; Dyer, J.; Weinstein, J.; Matousek, P.; Barton, R.; Bailey, P.; Subramaniam, N.; Kwok, W.; Ma, C.; Phillips, D.; Parker, A.; George, M. Development of a broadband picosecond infrared spectrometer and its incorporation into an existing

ultrafast time-resolved resonance Raman, UV/visible, and fluorescence spectroscopic apparatus. *Appl. Spectrosc.* **2003**, *57*, 367-380.

19. Connor, J.; Fischer, E. Transition-metal carbene complexes. Part XII. Substituent and steric effects in aminocarbene complexes of chromium. *J. Chem. Soc. A.* **1969**, *4*, 578-584.

20. Cedillo-Cruz, A.; Carmen Ortega-Alfaro, M.; Lopez-Cortes, J. G.; Alfredo Toscano, R.; Guillermo Penieres-Carrillo, J.; Alvarez-Toledano, C. Synthesis of Fischer type-carbene complexes containing a coordinated thioimidate structural motif. *Dalton Trans.* **2012**, *41*, 10568-10575.

21. Foley, H.; Strubinger, L.; Targos, T.; Geoffroy, G. Photochemistry of $[W(CO)_5(C(OMe)Ph)]$ - Formation of Alkyne Carbene Complexes and Studies of their Decomposition Reactions. *J. Am. Chem. Soc.* **1983**, *105*, 3064-3073.

22. Servaas, P.; Stufkens, D.; Oskam, A. Matrix Photochemistry of the Complexes $(CC)_5Cr=C(OMe)Ph$, $(CO)_5W=C(OMe)Ph$ having Close-Lying Reactive MLCT and LF States. *J. Organomet. Chem.* **1990**, *390*, 61-71.

23. Becke, A. Density-Functional Exchange-Energy Approximation with Correct Asymptotic-Behavior. *Phys. Rev. A* **1988**, *38*, 3098-3100.

24. Lee, C.; Yang, W.; Parr, R. Development of the Colle-Salvetti Correlation-Energy Formula into a Functional of the Electron-Density. *Phys. Rev. B* **1988**, *37*, 785-789.

25. Schafer, A.; Huber, C.; Ahlrichs, R. Fully Optimized Contracted Gaussian-Basis Sets of Triple Zeta Valence Quality for Atoms Li to Kr. *J. Chem. Phys.* **1994**, *100*, 5829-5835.

26. Baerends, E.; Rosa, A. Metal-CO photodissociation in transition metal complexes: The role of ligand-field and charge-transfer excited states in the photochemical dissociation of metal-ligand bonds. *Coord. Chem. Rev.* **1998**, *177*, 97-125.

27. Weigend, F.; Ahlrichs, R. Balanced basis sets of split valence, triple zeta valence and quadruple zeta valence quality for H to Rn: Design and assessment of accuracy. *Phys. Chem. Chem. Phys.* **2005**, *7*, 3297-3305.

28. Weigend, F. Accurate Coulomb-fitting basis sets for H to Rn. *Phys. Chem. Chem. Phys.* **2006**, *8*, 1057-1065.

29. Hoskovcova, I.; Rohacova, J.; Meca, L.; Tobrman, T.; Dvorak, D.; Lukvik, J. Electrochemistry of chromium(0)-aminocarbene complexes - The use of intramolecular interaction LFER for characterization of the oxidation and reduction centre of the complex. *Electrochim. Acta* **2005**, *50*, 4911-4915.

30. Landman, M.; Liu, R.; Fraser, R.; van Rooyen, P. H.; Conradie, J. Fac and mer dppe-substituted Fischer carbene complexes of chromium: X-ray, DFT and electrochemical study. *J. Organomet. Chem.* **2014**, *752*, 171-182.

31. McMahon, S.; Rochford, J.; Halpin, Y.; Manton, J. C.; Harvey, E. C.; Greetham, G. M.; Clark, I. P.; Rooney, A. D.; Long, C.; Pryce, M. T. Controlled CO release using photochemical, thermal and electrochemical approaches from the amino carbene complex $[(CO)_5CrC(NC_4H_8)CH_3]$. *Phys. Chem. Chem. Phys.* **2014**, *16*, 21230-21233.

32. Tello, M.; Oliveira, L.; Parise, O.; Buzaid, A. C.; Oliveira, R. T.; Zanella, R.; Cardona, A. Electrochemical therapy to treat cancer (in vivo treatment). *2007 Annual International Conference of the Ieee Engineering in Medicine and Biology Society, Vols 1-16* **2007**, 3524-3527.

33. Olaiz, N.; Maglietti, F.; Suarez, C.; Molina, F. V.; Miklavcic, D.; Mir, L.; Marshall, G. Electrochemical treatment of tumors using a one-probe two-electrode device. *Electrochim. Acta* **2010**, *55*, 6010-6014.

34. Breton, M.; Mir, L. M. Microsecond and nanosecond electric pulses in cancer treatments. *Bioelectromagnetics* **2012**, *33*, 106-123.

4 Chapter 4 An Investigation into the Photochemistry of the Fischer carbene complexes, $[(CO)_5M=C(X)C_2H_2Fc]$ and $[(CO)_5M=C(X)C_2H_2Ph]$, M = Cr, W; X= OMe, NC_4H_8

Abstract

This chapter focuses on the synthesis of a range of novel amino styryl, and previously reported methoxy styryl and ferrocenyl based Fischer carbene complexes, $[(CO)_5M=C(X)C_2H_2Ph]$ and $[(CO)_5M=C(X)C_2H_2Fc]$ where M = Cr, W; X = OMe, NC_4H_8; Ph = phenyl and Fc = ferrocene. The photochemistry of these compounds was investigated using psTRIR spectroscopy. In the case of the styryl carbene complexes, cyclic voltammetry and electrochemically induced CO release was also carried out.

Manuscripts in Preparation

1. A Pico-second Time Resolved IR and UV-vis Laser Flash photolysis study, on Ferrocenyl Fischer carbenes together with X-ray Crystallography and Quantum Chemical calculations.

2. An Investigation into the Photochemistry and Electrochemically Induced CO loss of a range of styryl based Fischer carbene complexes.

4.1 Introduction

The diverse chemistry of group 6 Fischer carbene complexes of the type [$(CO)_5MC(XR)R'$] (where M = Cr, W; X = heteratom and R and R′ = alkyl, aryl) and their applications in organic and organometallic synthesis have been widely recognised. These structurally diverse complexes have a fascinating range of versatile thermal, photochemical and electrochemical properties as discussed in Chapter 2 and Chapter 3.[1,2] Fischer type carbene complexes involve an electron rich metal atom in a low oxidation state. The metal is co-ordinated to a substituted carbon atom by a formal double bond. This carbon is known as the carbene carbon ($C_{carbene}$). In general, π-accepting groups are attached to the metal centre and π-donating ligands are attached to the $C_{carbene}$ which results in an electrophilic carbene moiety and a nucleophilic metal centre.[3,4] Fischer carbene complexes have been extensively studied due to their importance as selective reagents in organic synthetic reactions.[5] A wide range of compounds can be formed using Fischer carbenes following photolysis. For example, β-lactams (4-membered rings which are widely found in penicillin antibiotics) can be formed when irradiated in the presence of imines.[5,6] Fischer carbenes are a unique class of compounds ranging in colour from pale yellow to deep red / purple depending on the substituents attached. Minor changes in their electronic structure, [$(CO)_5MC(XR)R'$], for example where M = Cr, W; X = heteratom and R and R′ = alkyl, aryl, may render major changes in their photoreactivity by varying the substituents XR and R'.[7]

Recently, bi and poly–metallic carbenes incorporating mono and bis-ferrocene units have have been reported.[8-10] The first reported ferrocenyl based Fischer carbene complexes, [$(CO)_5MCX(Fc)$] where M= Cr, W; X = $ONMe_4^+$, OMe, OEt, NH_2, NMe_2, NC_4H_8 and Fc = ferrocene was detailed by Connor *et al.* in 1972.[11] The next reported example surfaced in 1997.[12] The synthesis of a novel ferrocene based Fischer carbene complex, [$(CO)_5Cr=C(OMe)C_2H_2Fc$] was described by Barluenga *et al.*[12] Since then, bimetallic Fischer carbene complexes containing a ferrocenyl unit bound directly to the carbene carbon or to the carbene carbon through an unsaturated linker have been the subject of numerous investigations.[8,10,13] Studies on ferrocenyl substituted Group 6 pentacarbonyl complexes concluded that the two metal centres can communicate. The ferrocenyl group acts as an electron donor and the metal carbonyl moiety acts as the electron acceptor.[13,14] These studies made use of a range of techniques including

electrochemical methods coupled with UV-vis spectroscopy and were supported by the results of computational investigations[10] or ESI mass spectrometry.[15]

Interestingly, the attachment of a ferrocenyl moiety to the carbene carbon can significantly alter the photochemical reactivity of the Fischer carbene complex. Fischer carbene complexes readily undergo organic transformations, for example, cycloaddition reaction. Hegedus *et al.* proposed that the the cycloaddition reaction requires the intermediate formation of a ketene or metallacyclopropanone species produced by the photo-insertion of a *cis*-carbonyl ligand into the metal-carbene bond (photocarbonylation).[16] Sierra and co-workers confirmed that irradiation of the ferrocenyl Fischer carbene complex, such as that of (**1**) shown in Figure 4.1, in the presence of imines failed to produce the expected cycloaddition product (Reaction 4.1).[9] The starting materials were unconsumed following irradiation. This suggests that a strong interaction between the iron based donor and chromium acceptor exists which deactivates the excited state prior to CO insertion, consequently, rendering the complex photo-inactive.[14]

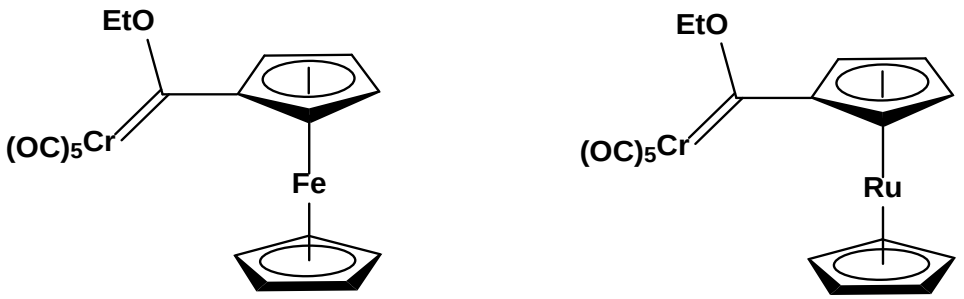

(1) **(2)**

Figure 4.1. Structural representations of chromium alkoxy Fischer carbene complexes incorporating ferrocene (**1**) and ruthenium (**2**) moieties reported by Sierra and co-workers.[9]

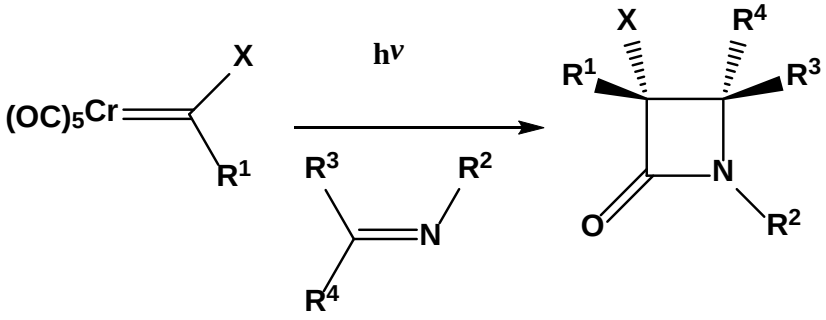

Reaction 4.1. Cycloaddition reaction of a chromium Fischer carbene in the presence of an imine, activated by photochemical means, R = Me, Ph, H and X = OMe, NR_2.[16]

However, substituting Ru for Fe in the metallocene-substituted Fischer carbene complex "switched on" photocarbonylation under the same conditions as for (**1**) with the formation of the corresponding β-lactam, Figure 4.1.[9] The difference in photochemical behaviour between the Fe (**1**) and Ru (**2**) based complexes was then investigated by computational means. Density functional theory calculations suggest that the ferrocene derivative possesses a very low energy non-carbonylated triplet and a very high energy metallacyclopropanone triplet species. Photolysis of this ferrocene compound in the presence of an imine does not form a β-lactam even following exhaustive photolysis (for up to four days).[14] Therefore, it was deduced by Sierra and co-workers that irradiation of the ferrocene carbene complex leads to the population of a low-lying centred triplet excited state which results in the inhibition of the photo-insertion of a CO ligand into the chromium carbene bond. Hence, (**1**) is deemed photoinert. In contrast, the Ru-carbene complex, contains the same two triplet states as for (**1**) which are almost degenerate. The co-existence of these two states at similar energy, allows for photochemical reactivity to occur.[7,9]

The UV-vis spectra of Fischer carbene complexes display three defined absorbance bands. These include a ligand field (LF) transition at 300 - 350 nm, another LF transition at 350 - 450 nm and a metal to ligand charge transfer (MLCT) band at ~500 nm.[5,8] There is a strong relationship between the substituent on the carbene carbon and the position of the absorbance band. This is evident on comparing the colours of the previously synthesised compounds, $[(CO)_5M{=}C(OMe)Me]$, M = Cr, W from Chapter 2 and $[(CO)_5M{=}C(NC_4H_8)Me]$, M = Cr, W from Chapter 3. On changing the functionality from a methoxy group to a pyrrolidine group, there is a colour change from bright yellow

to cream. This is reflected in the UV-vis absorbance spectra. The amino carbene complexes exhibited blue shifted λ_{max} values in comparison to the methoxy analogues.[1,2]

A time dependent density functional theory (TDDFT) study in conjunction with an experimental study was carried out by Sierra and co-workers on the electronic absorption properties of phenyl, styryl and phenylethynyl alkoxy chromium Fischer carbenes, displayed in Figure 4.2.[8]

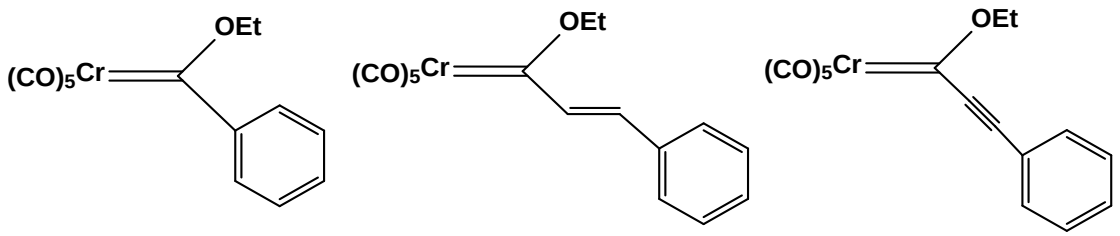

(3) **(4)** **(5)**

Figure 4.2. Phenyl based alkoxy chromium Fischer carbene complexes reported by Sierra and co-workers.[8]

Substitution of the methyl group in the case of $[(CO)_5M=C(OMe)Me]$ with a styryl group, -CH=CH-Ph, results in a colour change of the Fischer carbene complex from yellow to red / brown. Hence, there is a significant bathochromic shift in the UV-vis absorbance spectra.[8,17]

The π-linker between the metal and phenyl moiety induces a strong red shift of the MLCT absorbance band at ~400 - 500 nm. For example, the λ_{max} absorbance of the MLCT band is displayed at 406 nm for (**3**), 471 nm for (**4**) and 500 nm for (**5**) in hexane. For example, complex (**4**) exhibits a small solvatochromic effect for this band confirming its MLCT nature i.e. the λ_{max} occurs at 471 nm (hexane), 464 nm (dichloromethane) and 458 nm (acetonitrile). The LF transition involves π orbitals and is not dependent on solvent polarity.[8] The effect of substituting the phenyl group present in (**4**) with a ferrocene moiety was investigated. The ferrocenyl group is reported to act as a π-donor substituent in chromium carbene complexes.[8] The LF band is significantly affected and experiences a bathochromic shift. This is in agreement with previous research carried out.[17]

Time-resolved infrared and matrix isolation studies have been reported for a number of monometallic Fischer carbenes.[18-24] Many of the first photochemical studies of Fischer carbenes focused on the effect of irradiation into the LF absorption bands with photochemically induced CO release being the predominant pathway. The MLCT bands are less photosensitive, with reactivity attributed to the LF band.[25] In the case of the alkoxy carbenes, *anti-syn* isomerisation and CO loss processes were observed in these studies (Figure 4.3.). It is possible for both *anti*- and *syn*- isomers to exist due to the π-bond nature of the $C_{carbene}$-O bond as the methoxy group can rotate.[21]

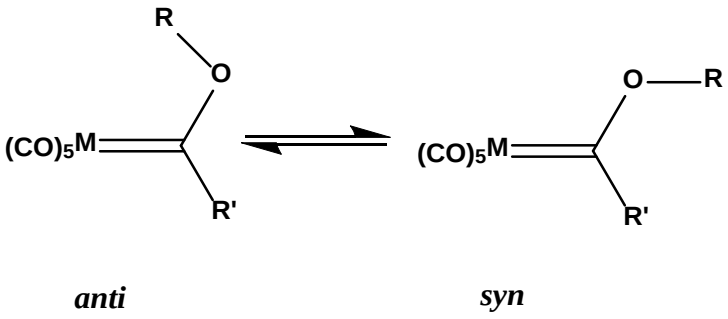

Figure 4.3. *Anti-syn* isomerisation of alkoxy Fischer carbene complexes.

In Chapter 3, a psTRIR study on the amino Fischer carbene complex $[(CO)_5Cr=C(NC_4H_8)(Me)]$ demonstrated that CO loss occurred following irradiation at λ_{exc} = 400 nm *via* a singlet excited state, with a high quantum efficiency ($\Phi_{CO\ loss}$ = 0.65), during the first 50 ps.[2] No evidence was obtained for the formation of the metallaketene or metallacyclopropanone intermediates. This is in agreement with previous reports on amino carbene complexes which are poor reagents in the synthesis of β-lactams.[27] A range of amino based carbene complexes, $[(CO)_5CrC(NMe_2)Me]$, $[(CO)_5CrC(NBz_2)Me]$, $[(CO)_5CrC(NMe_2)Ph]$, $[(CO)_5CrC(NMe_2)H]$, $[(CO)_5CrC(NBz_2)H]$ and $[(CO)_5CrC(NH_2)Me]$ were investigated using matrix isolation and UV monitored time resolved laser flash photolysis. Photoinduced CO loss is reported as the main photochemical process that occurred. [23]

The initial focus of this study was to extend the UV-vis absorbance spectra of the simple Fischer carbene complexes detailed in Chapter 2 and Chapter 3 towards the visible region of the spectrum by introducing substituents with increased conjugation to investigate if CO loss could be induced at longer wavelengths. Therefore, this chapter is an extension of the psTRIR studies reported in Chapter 2 and Chapter 3 and focuses on the photochemistry of alkoxy and amino based ferrocene-tethered Fischer carbene

complexes, $[(CO)_5M=C(X)C_2H_2Fc]$ as well as the styryl-tethered Fischer carbene complexes $[(CO)_5M=C(X)C_2H_2Ph]$ where M = Cr, W; X = OMe, NC_4H_8 and Fc = ferrocene, Ph = phenyl, as displayed in Figure 4.4, using picosecond time-resolved infrared spectroscopy.

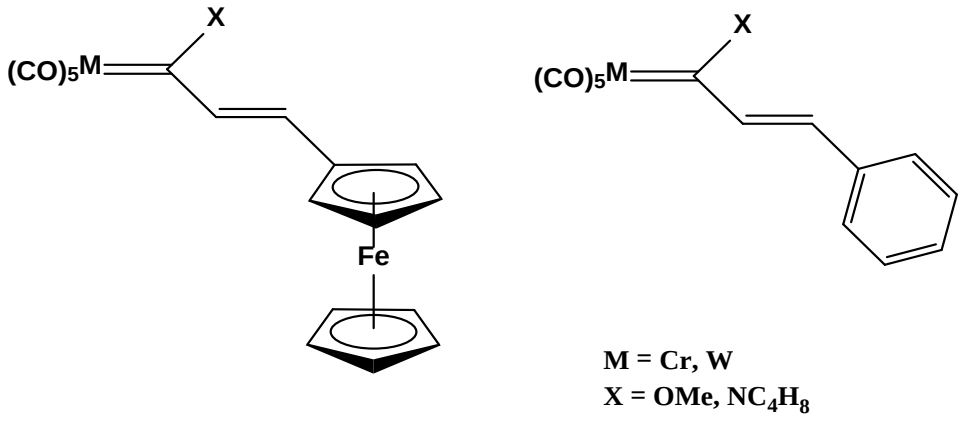

Figure 4.4. Structures of the compounds under investigation in this chapter, $[(CO)_5M=C(X)C_2H_2Fc]$ and $[(CO)_5M=C(X)C_2H_2Ph]$ where M = Cr, W; Fc = ferrocene, Ph = phenyl and X = OMe, NC_4H_8.

4.2 Experimental

4.2.1 Materials and Equipment

All reactions were carried out under an atmosphere of nitrogen using Schlenk techniques. All solvents were supplied by the Aldrich Chemicals Company. Dichloromethane, diethyl ether, pentane, hexane and heptane were dried over $MgSO_4$ prior to use. All solvents used for UV-vis, IR, psTRIR and cyclic voltammetry (CV) experiments were of spectrophotometric grade and were used without further purification. Ferrocene carboxaldehyde, benzaldehyde, triethylamine, chlorotrimethylsilane and pyrrolidine (Aldrich Chemical Co.) were used without further purification. Column chromatography was carried out using silica gel, Merck (used as received). All mobile phases for column chromatography were dried over $MgSO_4$ before use. Cyclic voltammograms (CVs) and bulk electrolysis profiles were recorded in anhydrous acetonitrile (Aldrich Chemical Co.) with tetrabutylammonium hexafluorophosphate ($TBAPF_6$), (Aldrich Chemical Co.) as a supporting electrolyte. Argon gas was used to degas samples for cyclic voltammetry (obtained from BOC Ltd). Infrared and psTRIR spectra were recorded as described in Chapter 2 and Chapter 3. CVs and electrochemically induced CO loss was carried out as reported in Chapter 2 with the help of Dr. Yvonne Halpin.

4.2.2 Synthesis

4.2.2.1 Synthesis of $[(CO)_5Cr=C(OMe)C_2H_2Fc]$

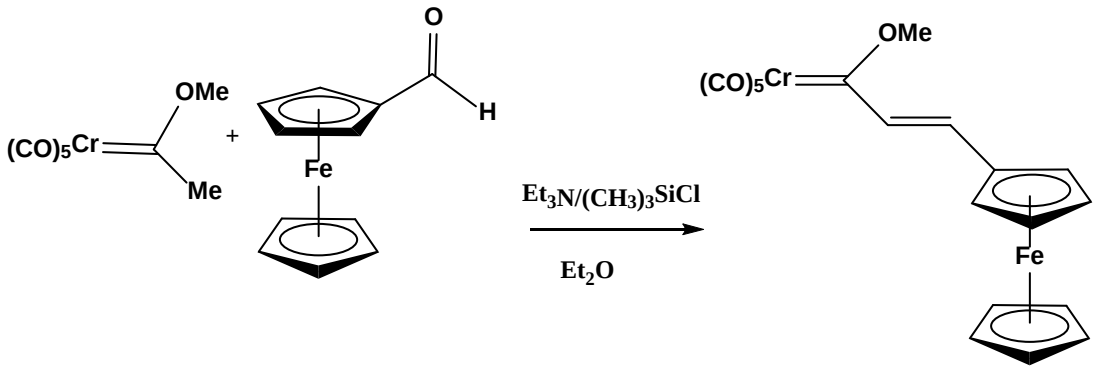

Reaction 4.2. Synthesis of $[(CO)_5Cr=C(OMe)C_2H_2Fc]$.

The synthesis of $[(CO)_5Cr=C(OMe)C_2H_2Fc]$ was carried out according to a previously reported method with some minor modifications.[12] 20 ml of dry ethyl ether was added to a clean, dry round bottomed flask and was purged with N_2 for 15 minutes. 8.0 mmol (1.12 ml) of triethylamine, 6.0 mmol (0.78 ml) of chlorotrimethylsilane, 2.0 mmol (0.428 g) of ferrocenecarboxaldehyde and 2.0 mmol (0.500 g) of $[(CO)_5Cr(OMe)Me]$ (synthesised in Chapter 2), were added to the reaction vessel under inert conditions. The reaction mixture was allowed to stir at room temperature in the absence of light for 24 hours. The colour of the reaction mixture changed from a red / brown to dark purple. The solvent was removed under reduced pressure. The crude mixture was purified using column chromatography, using silica as the stationary phase and pentane: dichloromethane (9.5 : 0.5) as the mobile phase.

Spectroscopic data agreed with reported data.[12]

Appearance: dark purple solid.

% Yield: 0.66 g, 1.48 mmol, 74 % yield.

^{1}H NMR: (400 MHz, $CDCl_3$) δ 4.20 (s, 5H), 4.59-4.61 (m, 4H), 4.68 (s, 3H), 7.18 (d, 1H), 7.52 (d, 1H) ppm.

IR: (pentane) 2056, 1980, 1955 and 1944 cm^{-1}.

4.2.2.2 Synthesis of $[(CO)_5Cr=C(NC_4H_8)C_2H_2Fc]$

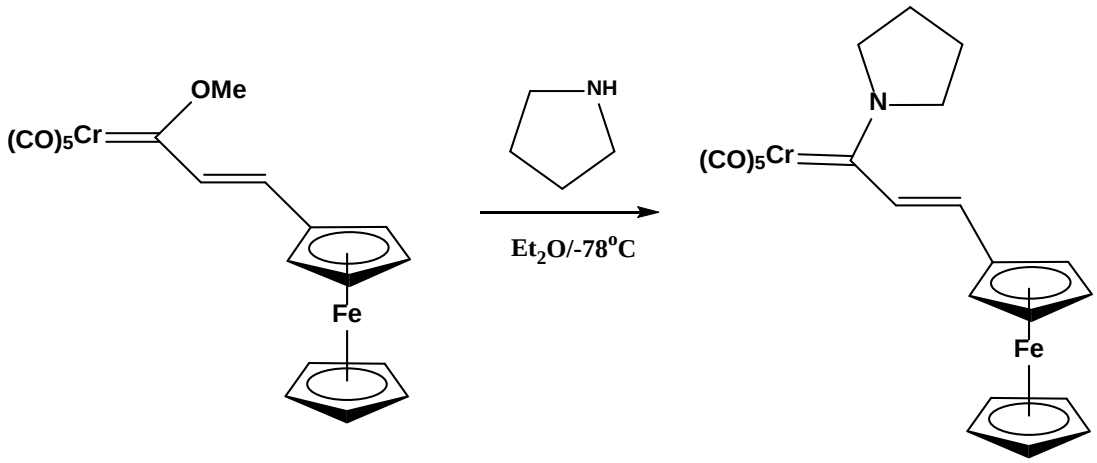

Reaction 4.3. Synthesis of $[(CO)_5Cr=C(NC_4H_8)C_2H_2Fc]$.

The synthesis of $[(CO)_5Cr=C(NC_4H_8)C_2H_2Fc]$ was carried out according to a previously reported method with some minor modifications.[17] 1.35 mmol (0.11 ml) of pyrrolidine was added *via* syringe to a solution of $[(CO)_5Cr=C(OMe)C_2H_2Fc]$ (1.12 mmol, 0.500 g) in dry diethyl ether (20 ml) at -78 °C (this temperature was achieved by combining liquid nitrogen and acetone and monitored using an alcohol thermometer). The reaction was stirred and allowed to reach room temperature. The solution changed from a dark red / purple colour to bright red. The solvent and any excess pyrrolidine were removed under reduced pressure. The crude product was purified on a silica gel column using a solvent mix of pentane : dichloromethane (9 : 1).

Spectroscopic data agreed with reported data.[17]

Appearance: orange / red solid.

% Yield: 0.51 g, 1.04 mmol, 93 % yield.

^{1}H NMR: (400 MHz, $CDCl_3$) δ 2.06-2.13 (m, 4H), 3.67 (dd, 2H), 4.16 (dd, 2H), 4.19 (s, 2H), 4.31 (2H, m), 4.39 (2H, m), 6.19 (d, 1H), 6.79 (d, 1H) ppm.

IR: (pentane) 2053, 1971, 1937 and 1930 cm^{-1}.

4.2.2.3 Synthesis of $[(CO)_5W=C(OMe)C_2H_2Fc]$

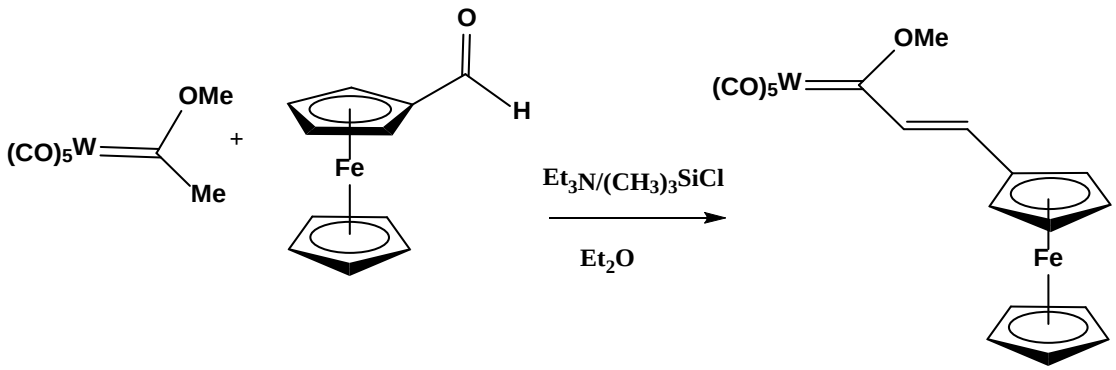

Reaction 4.4. Synthesis of $[(CO)_5W=C(OMe)C_2H_2Fc]$.

$[(CO)_5W=C(OMe)C_2H_2Fc]$ was synthesised in the same manner as reported for $[(CO)_5Cr=C(OMe)C_2H_2Fc]$, where $[(CO)_5W(OMe)Me]$, synthesised in Chapter 2, was used instead of $[(CO)_5Cr(OMe)Me]$.

Spectroscopic data agreed with reported data.[13]

Appearance: dark purple solid.

% Yield: 0.54 g, 0.09 mmol, 71 % yield.

^{1}H NMR: (400 MHz, $CDCl_3$) δ 4.20 (s, 5H), 4.54 (s, 3H), 4.61-4.63 (s, 4H), 7.39 (s, 2H) ppm.

IR: (pentane) 2064, 1978, 1951 and 1941 cm^{-1}.

4.2.2.4 Synthesis of $[(CO)_5W=C(NC_4H_8)C_2H_2Fc]$

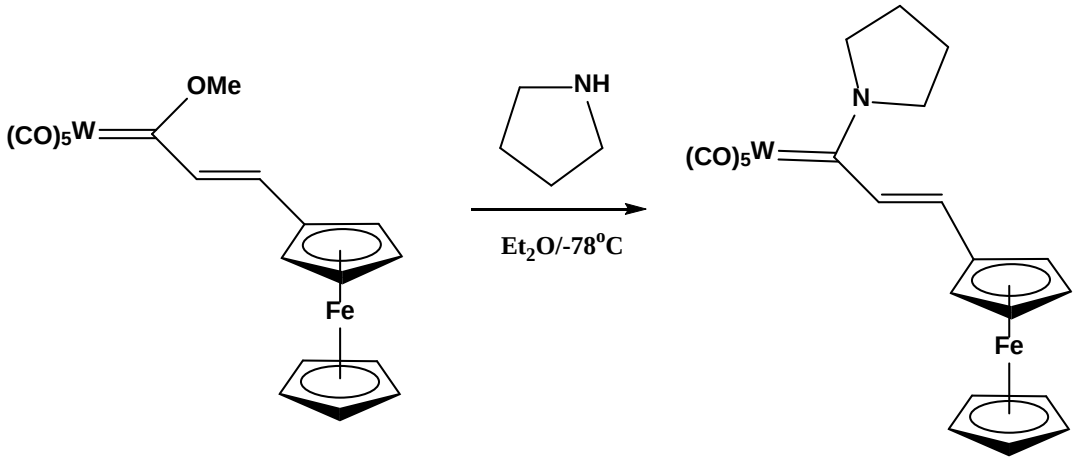

Reaction 4.5. Synthesis of $[(CO)_5W=C(NC_4H_8)C_2H_2Fc]$

$[(CO)_5W=C(NC_4H_8)C_2H_2Fc]$ was synthesised in the same manner as reported for $[(CO)_5Cr=C(NC_4H_8)C_2H_2Fc]$.[17] Spectroscopic data agreed with reported data.[17]

Appearance: orange / red solid.

% Yield: 0.63 g, 1.02 mmol, 91 % yield.

^1H NMR: (400 MHz, $CDCl_3$) δ 2.08-2.14 (m, 4H), 3.64 (t, 2H), 4.06 (t, 2H), 4.19 (s, 5H), 4.36 (t, 2H), 4.42 (t, 2H), 6.70 (s, 2H) ppm.

IR: (pentane) 2059, 1963 and 1925 cm^{-1}.

4.2.2.5 Synthesis of $[(CO)_5Cr=C(OMe)C_2H_2Ph]$

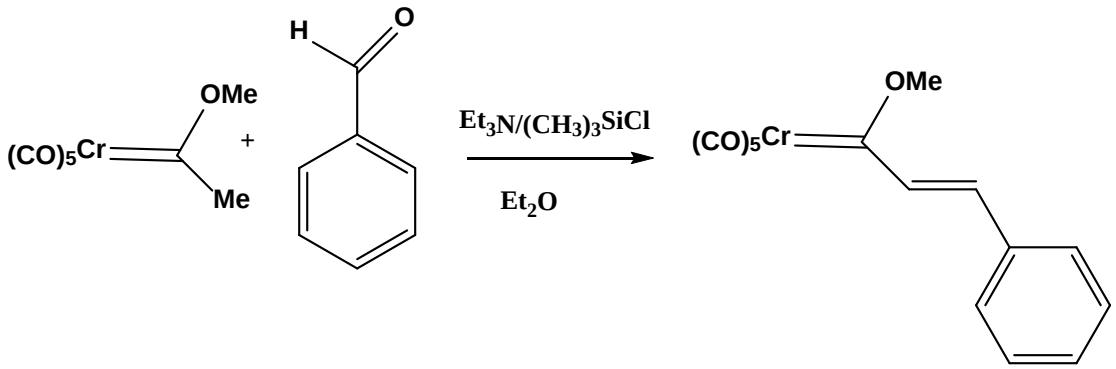

Reaction 4.6. Synthesis of $[(CO)_5Cr=C(OMe)C_2H_2Ph]$.

The synthesis of $[(CO)_5Cr=C(OMe)C_2H_2Ph]$ was carried out according to a previously reported method with some minor modifications.[12] 20 ml of dry ethyl ether was added to a clean, dry round bottomed flask and was purged with N_2. 8.0 mmol (1.12 ml) of triethylamine, 6.0 mmol (0.78 ml) of chlorotrimethylsilane, 2.0 mmol (0.20 ml) of benzaldehyde and 2.0 mmol (0.500 g) of $[(CO)_5Cr(OMe)Me]$ (synthesised in Chapter 2), were added to the reaction vessel under inert conditions. The reaction mixture was allowed to stir at room temperature in the absence of light for 24 hours. The colour of the reaction mixture changed from a red / brown to dark purple. The solvent was removed under reduced pressure. The crude mixture was purified by column chromatography, using silica as the stationary phase and neat pentane as the mobile phase.

Spectroscopic data agreed with reported data.[12]

Appearance: dark red / brown solid.

% Yield: 0.41 g, 1.22 mmol, 61 % yield.

^1H NMR: (400 MHz, $CDCl_3$) δ 4.83 (s, 3H), 6.95 (d, 1H), 7.40-7.42 (m, 3H), 7.58-7.60 (m, 2H), 7.95 (d, 1H) ppm.

IR: (pentane) 2060, 1987, 1963 and 1951 cm^{-1}.

4.2.2.6 Synthesis of $[(CO)_5Cr=C(NC_4H_8)C_2H_2Ph]$

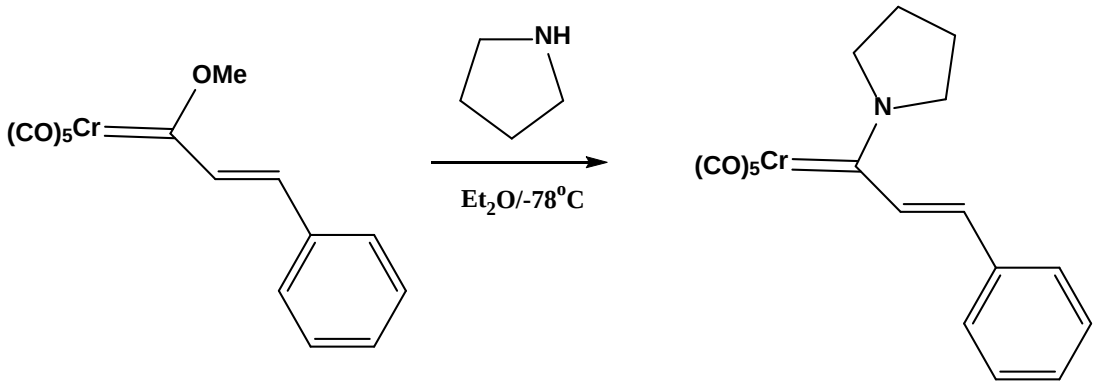

Reaction 4.7. Synthesis of $[(CO)_5Cr=C(NC_4H_8)C_2H_2Ph]$.

Compound $[(CO)_5Cr=C(NC_4H_8)C_2H_2Ph]$ was synthesised in a similar manner to $[(CO)_5Cr=C(NC_4H_8)C_2H_2Fc]$ with some modifications. 1.35 mmol (0.11 ml) of pyrrolodine was added *via* syringe to 1.12 mmol (0.41 g) of $[(CO)_5Cr=C(OMe)C_2H_2Ph]$ in dry diethyl ether (20 ml) at – 78 °C. The reaction was stirred and allowed to reach room temperature. The solution changed from a dark red / brown colour to an orange colour. The solvent was removed under reduced pressure. The crude complex was purified using column chromatography on silica gel using pentane : dichloromethane (9 : 1). NMR spectroscopic data can be found in Appendix B.

Appearance: yellow / orange solid.

% Yield: 0.38 mg, 1.01 mmol, 90 % yield.

^{1}H NMR: (400 MHz, $CDCl_3$) δ 2.03-2.10 (m, 2H), 2.14-2.21 (m, 2H), 3.72 (t, *J* = 7.0 Hz, 2H), 4.20 (t, *J* = 7.1 Hz, 2H), 6.06 (d, *J* = 16.5 Hz, 1H), 7.11 (d, *J* = 16.5 Hz, 1H), 7.27-7.29 (m, 1H), 7.35-7.42 (m, 4H) ppm.

^{13}C NMR: (400 MHz, $CDCl_3$) 25.18, 25.47, 55.55, 59.19, 122.91, 126.57, 128.02, 128.83, 136.26, 138.65, 217.83, 223.50, 264.97 ppm.

IR: (pentane) 2055, 1973, 1938, 1932 cm^{-1}.

CHN Anal. Calculated C 57.30, H 4.01, N 3.71. Found C 56.70, H 3.92, N 3.46.

4.2.2.7 Synthesis of $[(CO)_5W=C(OMe)C_2H_2Ph]$

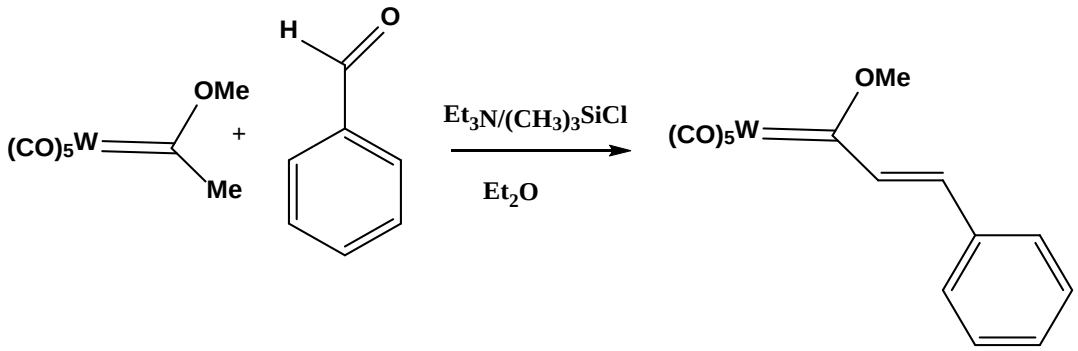

Reaction 4.8. Synthesis of $[(CO)_5W=C(OMe)C_2H_2Ph]$.

$[(CO)_5W=C(OMe)C_2H_2Ph]$ was synthesised in the same manner as reported for $[(CO)_5Cr=C(OMe)C_2H_2Ph]$, where, $[(CO)_5W(OMe)Me]$, synthesised in Chapter 2, was used instead of $[(CO)_5Cr(OMe)Me]$.

Spectroscopic data agreed with reported data.[12]

Appearance: dark brown solid.

% Yield: 0.59 g, 1.26 mmol, 63 % yield.

^{1}H NMR: (400 MHz, $CDCl_3$) δ 4.65 (s, 3H), 7.19 (d, 1H), 7.39-7.45 (m, 3H), 7.60-7.62 (m, 2H), 7.88 (d, 1H) ppm.

IR: (pentane) 2068, 1985, 1958 and 1947 cm^{-1}.

4.2.2.8 Synthesis of $[(CO)_5W=C(NC_4H_8)C_2H_2Ph]$

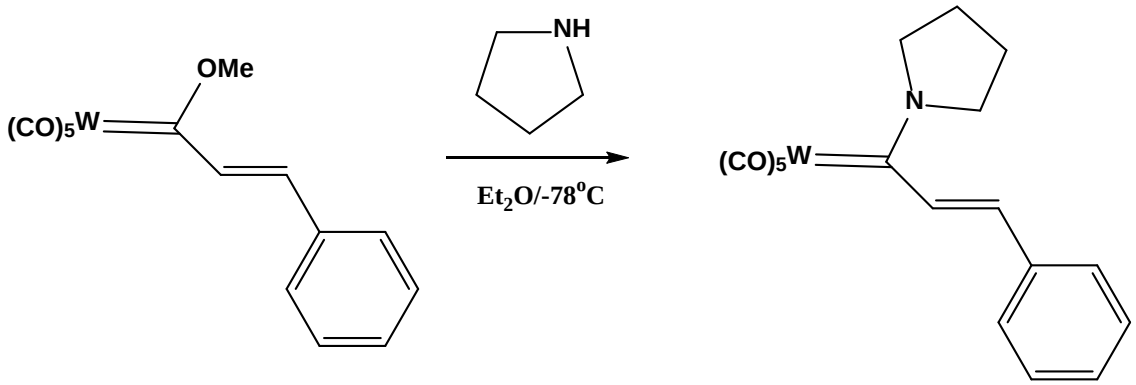

Reaction 4.9. Synthesis of $[(CO)_5W=C(NC_4H_8)C_2H_2Ph]$.

$[(CO)_5W=C(NC_4H_8)C_2H_2Ph]$ was synthesised in the same manner as reported for $[(CO)_5Cr=C(NC_4H_8)C_2H_2Ph]$. NMR spectroscopic data can be found in Appendix B.

Appearance: orange / yellow solid.

% Yield: 0.50 g, 0.99 mmol, 88 % yield.

^{1}H NMR: (400 MHz, $CDCl_3$) δ 2.10-2.17 (m, 4H), 3.69 (t, *J* = 6.5 Hz, 2H), 4.08 (t, *J* = 6.3 Hz, 2H), 6.34 (d, *J* = 16.5 Hz, 1H), 7.03 (d, *J* = 16.5 Hz, 1H), 7.28-7.30 (m, 1H), 7.35-7.39 (m, 2H), 7.41-7.44 (m, 2H) ppm.

^{13}C NMR: (400 MHz, $CDCl_3$) 24.96, 25.68, 54.03, 61.81, 126.78, 128.15, 128.38, 128.84, 135.94, 139.22, 198.90, 203.48, 246.21 ppm.

IR (*v*CO) cm^{-1} (pentane) 2063, 1971, 1935, 1928 cm^{-1}.

Anal. Calculated C 42.46, H 2.97, N 2.75. Found C 42.52, H 2.76, N 2.56.

4.3 Results and Discussion

4.3.1 UV-vis Spectroscopy

The electronic absorption properties have been previously described for the ferrocenyl complexes reported in this chapter.[8,12,17] The overlaid UV-vis absorbance spectra of the four ferrocenyl Fischer carbene complexes are displayed in Figure 4.5.

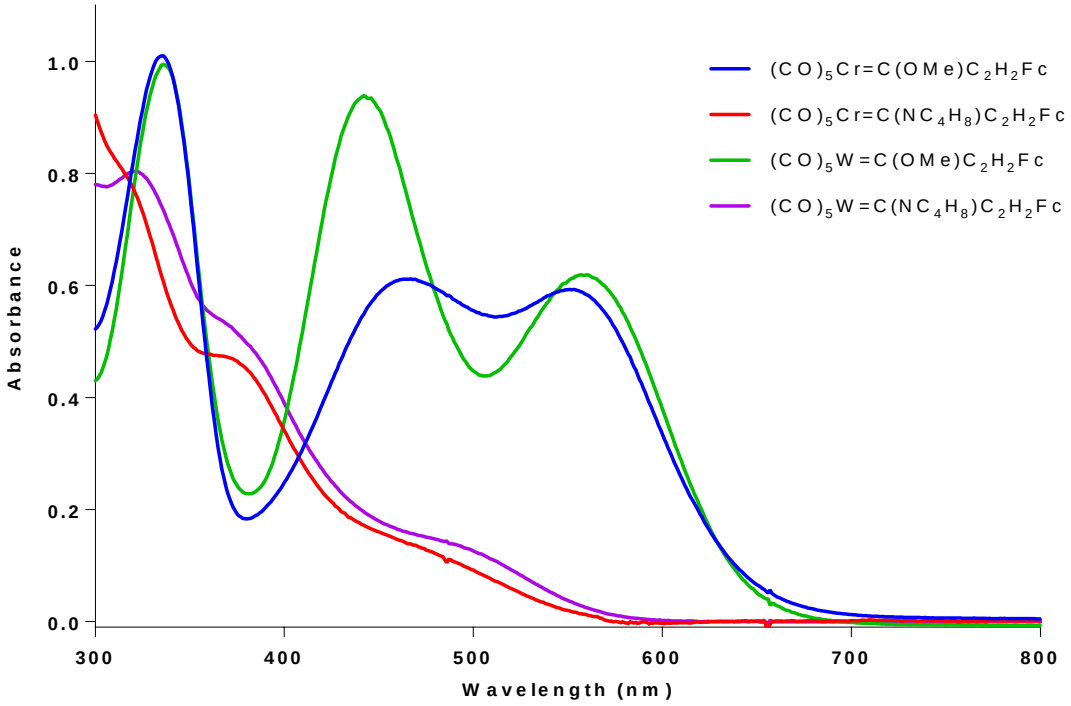

Figure 4.5 Overlaid UV-vis absorbance spectra of $[(CO)_5M{=}C(X)C_2H_2Fc]$ where M= Cr, W and X = OMe, NC_4H_8 in *n*-heptane, concentration = ~1×10^{-5} M.

The UV-vis spectrum of $[(CO)_5Cr{=}C(OMe)C_2H_2Fc]$ exhibits two low energy bands in the visible region of the spectrum at 548 nm ($\varepsilon = 6.45 \times 10^4$ $M^{-1}cm^{-1}$) and 466 nm ($\varepsilon = 6.81 \times 10^4$ $M^{-1}cm^{-1}$) and a higher lying band at 334 nm ($\varepsilon = 1.15 \times 10^5$ $M^{-1}cm^{-1}$).[17] Sarker *et al*. have previously assigned the transition at 548 nm to a metal to ligand charge transfer (MLCT) band, mainly centred on ferrocene.[13] The absorption band at 466 nm is assigned to a π–π * transition, while the remaining transition at 334 nm is thought to originate from the chromium pentacarbonyl moiety. The UV-vis spectrum of the amino carbene differs substantially to the methoxy analogue. $[(CO)_5Cr{=}C(NC_4H_8)C_2H_2Fc]$

exhibits absorption bands with λ_{max} at 315 nm ($\varepsilon = 1.10 \times 10^4$ $M^{-1}cm^{-1}$), 360 nm ($\varepsilon = 6.54 \times 10^3$ $M^{-1}cm^{-1}$) and a λ_{max} at 444 nm ($\varepsilon = 2.33 \times 10^3$ $M^{-1}cm^{-1}$), which tail to approximately 560 nm.[17]

The tungsten analogue, $[(CO)_5W{=}C(OMe)C_2H_2Fc]$, similarly exhibits two low energy bands in the visible region of the spectrum at 560 nm ($\varepsilon = 2.65 \times 10^3$ $M^{-1}cm^{-1}$) and 444 nm ($\varepsilon = 3.97 \times 10^3$ $M^{-1}cm^{-1}$), together with a higher lying band at 338 nm ($\varepsilon = 4.72 \times 10^3$ $M^{-1}cm^{-1}$) and a shoulder at *ca*. 280 nm ($\varepsilon = 3.76 \times 10^3$ $M^{-1}cm^{-1}$) in *n*-heptane solution.[13,17] $[(CO)_5W{=}C(NC_4H_8)C_2H_2Fc]$ exhibits absorption bands with λ_{max} at 298 nm ($\varepsilon = 6.68 \times 10^3$ $M^{-1}cm^{-1}$), 332 nm ($\varepsilon = 7.03 \times 10^3$ $M^{-1}cm^{-1}$), 380 nm ($\varepsilon = 4.52 \times 10^3$ $M^{-1}cm^{-1}$) and 470 nm ($\varepsilon = 1.39 \times 10^3$ $M^{-1}cm^{-1}$) which tail to approximately 570 nm.

The overlaid UV-vis absorbance spectra of the four styryl Fischer carbene complexes are displayed in Figure 4.6. Sierra and co-workers recently detailed an electronic structural study on a range of alkoxy chromium carbene complexes including the compounds, $[(CO)_5Cr{=}C(OMe)C_2H_2Fc]$ and $[(CO)_5Cr{=}C(OMe)C_2H_2Ph]$, reported in this study.[8]

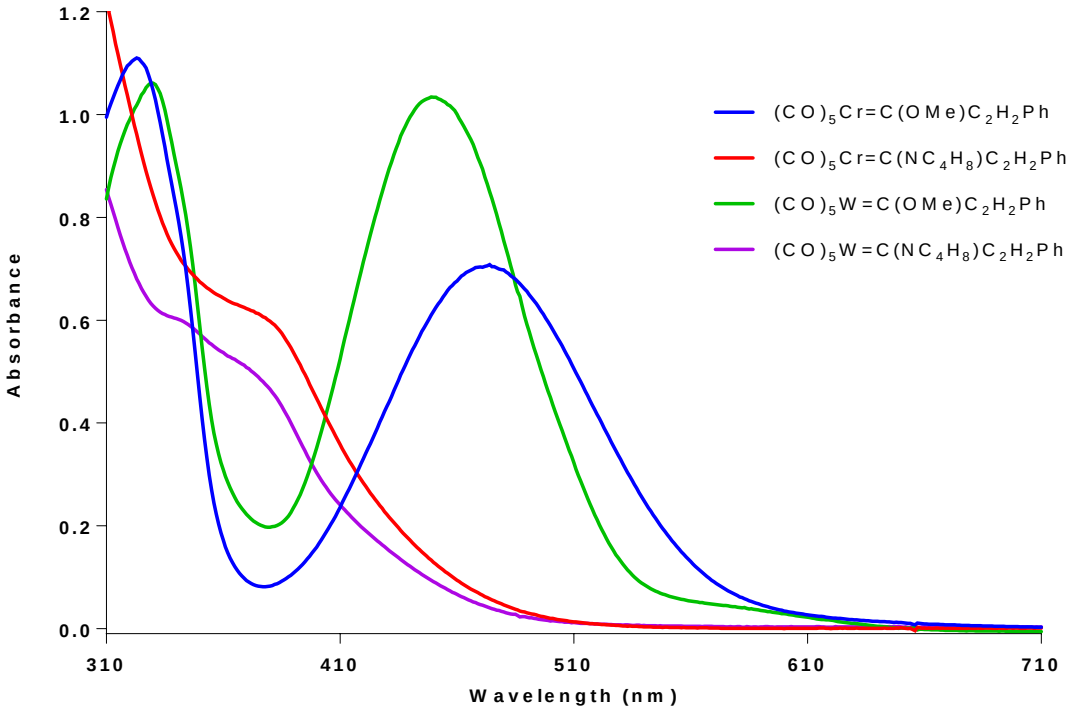

Figure 4.6 Overlaid UV-vis absorbance spectra of $[(CO)_5M{=}C(X)C_2H_2Ph]$ where M= Cr, W and X = OMe, NC_4H_8 in *n*-heptane, concentration = ~1×10^{-5} M.

The UV-vis spectrum of $[(CO)_5Cr=C(OMe)C_2H_2Ph]$ exhibits a low energy band at 472 nm ($\varepsilon = 6.86 \times 10^3$ $M^{-1}cm^{-1}$) and a higher lying band at 324 nm ($\varepsilon = 1.05 \times 10^4$ $M^{-1}cm^{-1}$).[17] The band at 472 nm has been assigned by Sierra and co-workers to a π–π * transition.[13] The absorption band at 324 nm is ascribed to a ligand field transition. In a similar fashion to the ferrocenyl carbene complexes, the UV-vis spectrum of the amino carbene differs substantially to the methoxy analogue. $[(CO)_5Cr=C(NC_4H_8)C_2H_2Ph]$ displays an absorption band with λ_{max} at 384 nm ($\varepsilon = 3.64 \times 10^3$ $M^{-1}cm^{-1}$) which tails to approximately 500 nm.

The tungsten analogue, $[(CO)_5W=C(OMe)C_2H_2Ph]$, exhibits a low energy band at 448 nm ($\varepsilon = 2.06 \times 10^4$ $M^{-1}cm^{-1}$), together with a higher lying band at 330 nm ($\lambda = 2.30 \times 10^4$ $M^{-1}cm^{-1}$) in *n*-heptane solution. $[(CO)_5W=C(NC_4H_8)C_2H_2Ph]$ displays an absorption band with λ_{max} at 370 nm ($\varepsilon = 1.42 \times 10^3$ $M^{-1}cm^{-1}$) which tails to approximately 500 nm.

4.3.2 Picosecond Time Resolved IR Spectroscopy of the Ferrocenyl Fischer Carbene Complexes

A psTRIR investigation of each of the eight Fischer carbene complexes presented in this chapter was undertaken at 293 K in *n*-heptane solution. Infrared spectral changes were monitored in the region, 2150 – 1850 and in certain cases were extended to 1700 cm^{-1} covering both the terminal and bridging ν_{CO} regions. Resolution was between 1 and 5 cm^{-1}. The pulse energy was between 0.8 - 1 μJ at the University of Amsterdam (UA) and 0.5 - 1.2 μJ at the Rutherford Appleton Laboratory (RAL). An excitation pulse of 200 fs (UA) and 50 fs (RAL) were used in these experiments. The UV-vis absorption spectra in *n*-heptane are presented in section 4.3.1. The FTIR spectra are displayed in Appendix C for each of the carbene complexes. Three excitation wavelengths were used in these experiments, 470 (UA), 400 (RAL) and 320 nm (UA).

4.3.2.1 psTRIR studies of $[(CO)_5Cr=C(OMe)C_2H_2Fc]$ at 400 nm

Picosecond time resolved IR studies were carried out on the ferrocenyl Fischer carbene complexes, using 400 nm excitation at the Rutherford Appleton Laboratories. The

psTRIR difference spectra obtained upon excitation of [$(CO)_5Cr=C(OMe)C_2H_2Fc$] at 400 nm are presented in Figure 4.7. Within the excitation pulse the υCO bands of the parent complex at 2057 1959, and 1949 cm^{-1} were depleted (represented by downward features in the difference spectrum) and broad features were formed at 2046 and 1937 and 1913 cm^{-1}. These features are at lower energy compared to the υCO bands of the parent complex and are assigned to an excited state species which decays over ~100 ps. On analysing the spectra closely, weak bands at 2037, 1988, 1933 and 1919 cm^{-1} are evident after 50 ps and are assigned to the CO loss species, [$(CO)_4$(heptane)$Cr=C(OMe)C_2H_2Fc$]. Due to the broadness of the bands for the excited state species it is difficult to determine over what timeframe the CO loss photo-product is formed. However, upon further inspection of the spectral data, the excited state species observed does not appear to be a precursor to CO loss. The recovery signal gives an indication of the efficiency of CO loss for this compound, which is loss at ~10 %. Furthermore, as all three parent bands do not recover to the same extent, this suggests that there is a further band underneath the parent band at 1949 cm^{-1}.

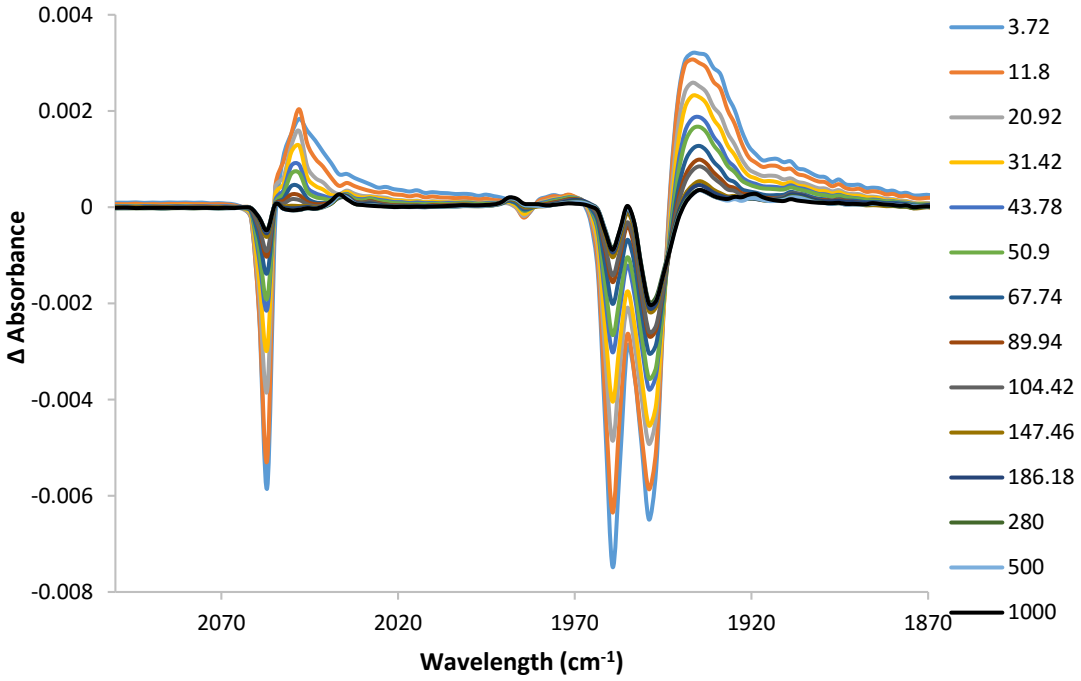

Figure 4.7. The psTRIR spectra obtained following 400 nm excitation of [$(CO)_5Cr=C(OMe)C_2H_2Fc$] in *n*-heptane. The time points included in the legend are in ps.

4.3.2.2 psTRIR studies of $[(CO)_5Cr=C(OMe)C_2H_2Fc]$ at 320 nm

The psTRIR experiments presented for $[(CO)_5Cr=C(OMe)C_2H_2Fc]$ at 320 nm were carried out at the UA. The spectroscopic changes observed following 320 nm excitation (0.8 μJ) of $[(CO)_5Cr=C(OMe)C_2H_2Fc]$ in *n*-heptane were the same as those displayed at λ_{exc} = 400 nm. The quantum efficiency for CO loss was also ~10 %.

The photochemistry of these complexes were previously investigated by photolysing a solution of the carbene complex in the presence of a ten-fold excess of triphenylphosphine with λ_{exc} > 550 > 400 and > 320 nm.[17] Following irradiation of $[(CO)_5Cr=C(OMe)C_2H_2Fc]$ with λ_{exc} > 400 nm, four new υCO absorptions grew in at 2006, 1931, 1913, and 1900 cm^{-1}. These absorptions correspond to those of the tetracarbonyl species, thereby indicating the formation of $[(PPh_3)(CO)_4Cr=C(OMe)C_2H_2Fc]$. On changing the excitation wavelength to λ_{exc} > 320 nm, the only notable difference was the increased efficiency with which $[(PPh_3)(CO)_4Cr=C(OMe)C_2H_2Fc]$ formed.[17] The psTRIR studies are therefore in agreement with previous photochemical experiments.

The TRIR data suggests that there is no evidence for bands characteristic of ketene formation. This is in agreement with a similar ferrocene based alkoxy chromium Fischer carbene complex, $[(CO)_5Cr(OEt)Fc]$ which does not appear to undergo photocarbonylation following irradiation.[14]

4.3.2.3 psTRIR studies of $[(CO)_5Cr=C(NC_4H_8)C_2H_2Fc]$ at 400 nm

The spectroscopic changes within the metal carbonyl region following excitation (λ_{exc} = 400 nm) of the pyrrolidine analogue, $[(CO)_5Cr=C(NC_4H_8)C_2H_2Fc]$ are presented in Figure 4.8. Within the excitation pulse the υCO bands of the parent complex at 2051, 1969 and 1933 cm^{-1} were depleted (negative bands in the difference spectra) and broad features were formed at 2046, 1986, 1935, and 1895 cm^{-1}. The new features were assigned to an excited state species which decays over the subsequent 90 ps, with recovery of the parent bands by > 95 %. Weak bands were observed at 2014 and 1899 cm^{-1} which persist onto the nanosecond timescale. Based on the similarity in band

positions to those for, $[(CO)_4(heptane)Cr=C(NC_4H_8)Me]$ at 2025, 1963, 1923 and 1886 cm^{-1}, these bands are assigned to the solvated CO loss species, $[(CO)_4(heptane)Cr=C(NC_4H_8)C_2H_2Fc]$.

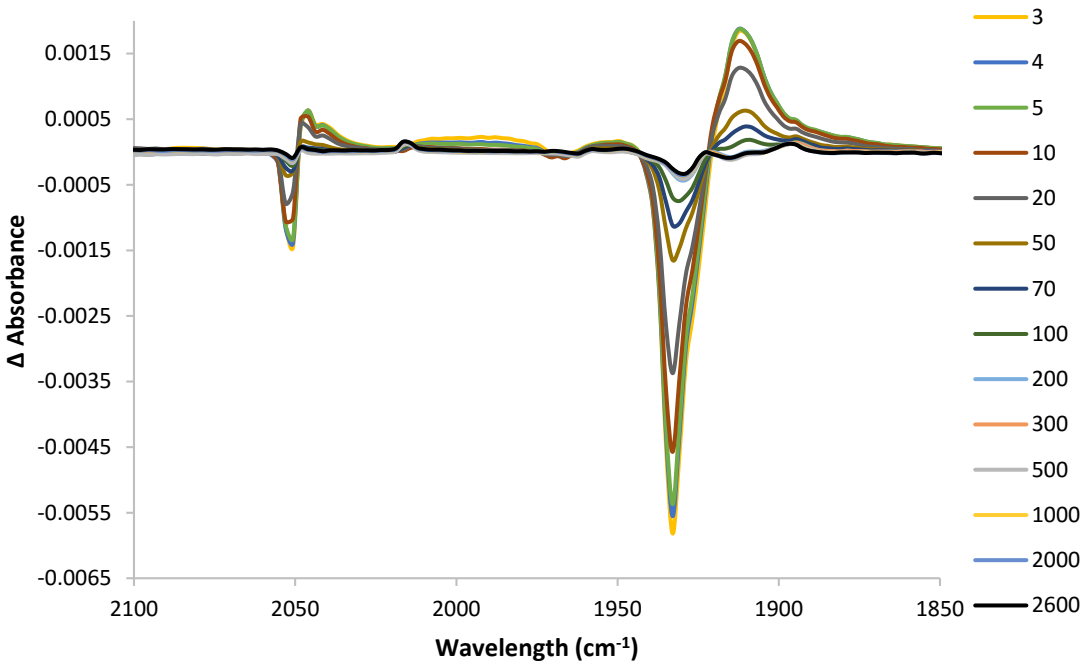

Figure 4.8. The psTRIR spectra obtained following 400 nm excitation of $[(CO)_5Cr=C(NC_4H_8)C_2H_2Fc]$ in *n*-heptane. The time points included in the legend are in ps.

4.3.2.4 psTRIR studies of $[(CO)_5Cr=C(NC_4H_8)C_2H_2Fc]$ at 320 nm

Similar spectroscopic changes were observed for this compound at λ_{exc} = 320 nm. Notably, CO loss was more efficient at this wavelength with an estimated quantum yield for CO loss of 30 %.

Previously, no changes were evident in the IR spectrum when steady state photolysis studies were carried out on $[(CO)_5Cr=C(NC_4H_8)C_2H_2Fc]$, upon irradiation at > 400 nm, in cyclohexane, in the presence of a tenfold excess of PPh_3. However, following

excitation with λ_{exc} > 320 nm, four new υCO absorptions formed at 1999, 1948, 1910 and 1884 cm^{-1} which were assigned to $[(PPh_3)(CO)_4Cr{=}C(NC_4H_8)C_2H_2Fc]$.[17]

4.3.2.5 psTRIR studies of $[(CO)_5W{=}C(OMe)C_2H_2Fc]$ at 400 nm

The spectroscopic changes within the metal carbonyl region following excitation of $[(CO)_5W{=}C(OMe)C_2H_2Fc]$ are presented in Figure 4.9. Within the excitation pulse the υCO bands of the parent complex at 2059, 1982, 1955 and 1943 cm^{-1} were depleted (negative bands in the difference spectra) and broad features formed at 2050, 1931, and 1905 cm^{-1}. The new features were assigned to an excited state species which decays over the subsequent 100 ps. As these bands decay, the parent bands recover (by ~ 95%). New bands become evident at 2028, and 1886 cm^{-1} over 100 ps. The latter bands are assigned to the solvated CO loss species $[(CO)_4(heptane)W{=}C(OMe)C_2H_2Fc]$. The same spectral changes are observed at λ_{exc} = 320 nm.

Steady state photolysis studies, in the presence of excess PPh_3, were also performed on $[(CO)_5W{=}C(OMe)C_2H_2Fc]$ in cyclohexane.[17] Irradiation of $[(CO)_5W{=}C(OMe)C_2H_2Fc]$ at λ_{exc} > 400 nm lead to minor changes but very weak bands were observed. Following irradiation at > 320 nm, the bands, assigned to the tetracarbonyl product, $[(cis\text{-}(PPh_3)(CO)_4W{=}C(OMe)C_2H_2Fc]$, increased in intensity with υCO IR absorptions at 2016, 1964, 1927 and 1900 cm^{-1}.

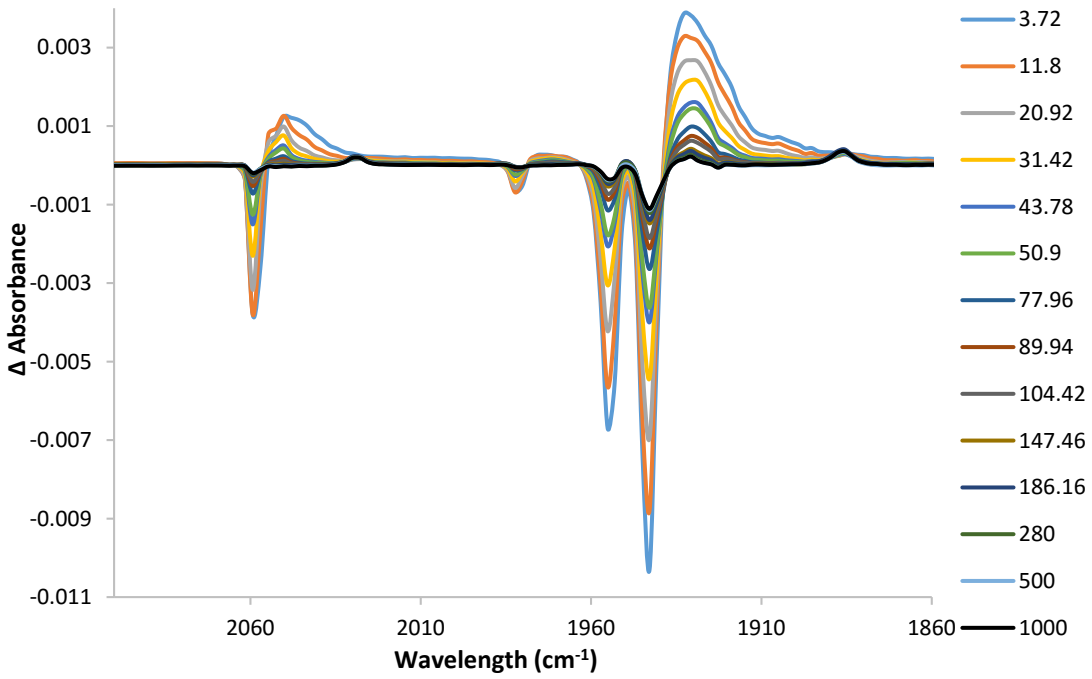

Figure 4.9. The psTRIR spectra obtained following 400 nm excitation of $[(CO)_5W{=}C(OMe)C_2H_2Fc]$ in *n*-heptane. The time points included in the legend are in ps.

4.3.2.6 psTRIR studies of $[(CO)_5W{=}C(NC_4H_8)C_2H_2Fc]$ at 320 nm

The spectroscopic changes following excitation of the pyrrolidine analogue, $[(CO)_5W{=}C(NC_4H_8)C_2H_2Fc]$, are presented in Figure 4.10. Within the excitation pulse the υCO bands of the parent complex at 2060, 1962 and 1926 cm^{-1} were depleted (negative bands in the difference spectra) and broad features were formed at 2049 and 1911 cm^{-1}. The new features were assigned to an excited state species which decays over 150 ps. As these bands decay, the parent bands fully recover. Unlike, the other three ferrocenyl Fischer carbene complexes, no evidence is observed for CO loss for $[(CO)_5W{=}C(NC_4H_8)C_2H_2Fc]$ following excitation at 320 nm in these experiments.

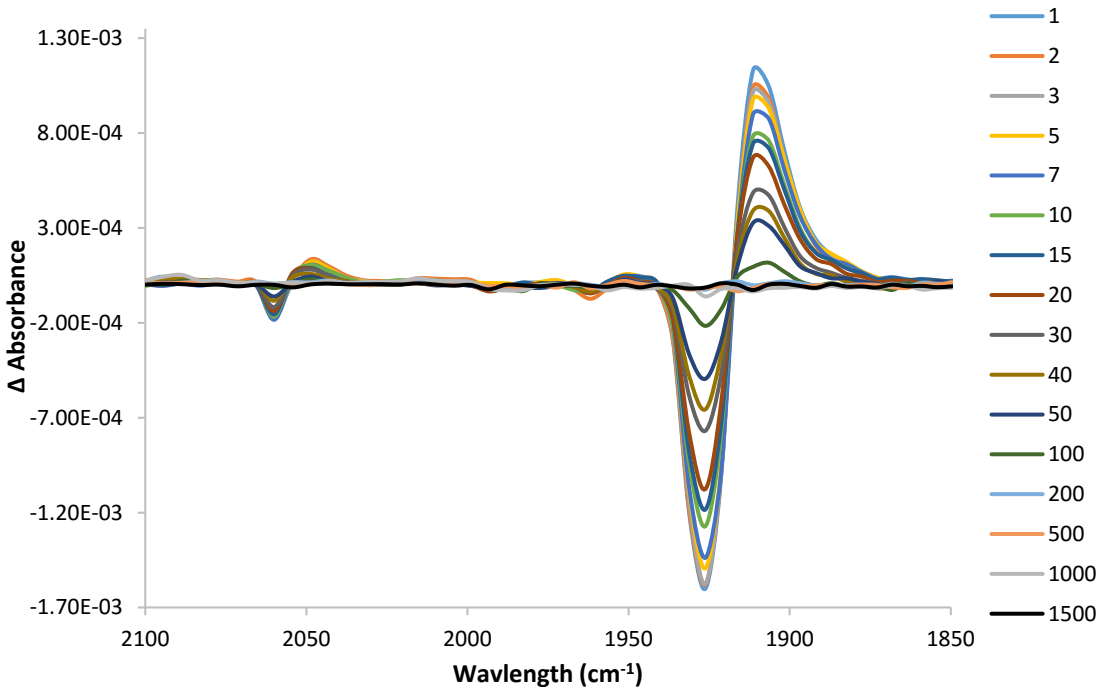

Figure 4.10. The psTRIR spectra obtained following 320 nm excitation of $[(CO)_5W{=}C(NC_4H_8)C_2H_2Fc]$ in *n*-heptane. The time points included in the legend are in ps.

In summary, for the ferrocenyl Fischer carbenes reported here, no evidence was obtained in any of the psTRIR studies to support evidence for the formation of a ketene type intermediate. This is in agreement with UV-vis laser flash photolysis studies reported by Rochford[17] and is also in agreement with that reported by Sierra and co-workers on similar ferrocene based compounds.[9,10]

4.3.3 Picosecond Time Resolved IR Spectroscopy of the Styryl Fischer Carbene Complexes

Each of the psTRIR measurements of the styryl complexes were recorded at the University of Amsterdam. Infrared spectral changes were monitored for the methoxy complexes in the range 2150 – 1700 cm^{-1}, covering both the terminal and bridging ν_{CO} regions with a resolution of 4 cm^{-1} at λ_{exc} = 482, 470, 400 and 320 nm.

4.3.3.1 psTRIR studies of $[(CO)_5Cr=C(OMe)C_2H_2Ph]$ at 470 nm

The psTRIR difference spectra obtained upon excitation of $[(CO)_5Cr=C(OMe)C_2H_2Ph]$ at 470 nm are presented in Figure 4.11. Within the excitation pulse (200 fs), the parent bands at 2060, 1962 and 1947 cm^{-1} were bleached (represented by downward features in the difference spectrum) and broad features centred at 1989 cm^{-1} and 2089 (weak) were produced. During the subsequent 20 ps, the broad features decayed, to give rise to sharper features at 2049, 1994 and 1932 cm^{-1}.

The spectral features are in similar positions and occur over a comparable timeframe to those observed in Chapter 2 following irradiation of $[(CO)_5Cr=C(OMe)Me]$ at 400 nm. However, since there was no band present in the bridging region (1700 – 1800 cm^{-1}) of the spectrum, this excited state is not assigned to a metallacyclopropanone species. This is in contrast to the findings for $[(CO)_5Cr=C(OMe)Me]$ at 400 nm which exhibited a band at 1770 cm^{-1} which decayed over 100 ps, leading to the metallaketene species.

For this Fischer carbene, however, the features at 2049, 1994 and 1932 cm^{-1} decay over 150 ps, leading to a long lived species which persists on the ns timescale. This species absorbs at 1989, 1957, 1942, and 1927 cm^{-1}. These bands are tentatively assigned to the metallaketene intermediate as the band positions are similar to those observed for the metallaketene formed following irradiation of $[(CO)_5Cr=C(OMe)Me]$ at 400 nm which exhibited bands at 1981, 1965, 1945 and 1919 cm^{-1}.[1] No evidence for CO loss is observed following excitation at 470 nm. The same spectral features were observed when the experiment was repeated at λ_{exc} = 482 nm and λ_{exc} = 400 nm.

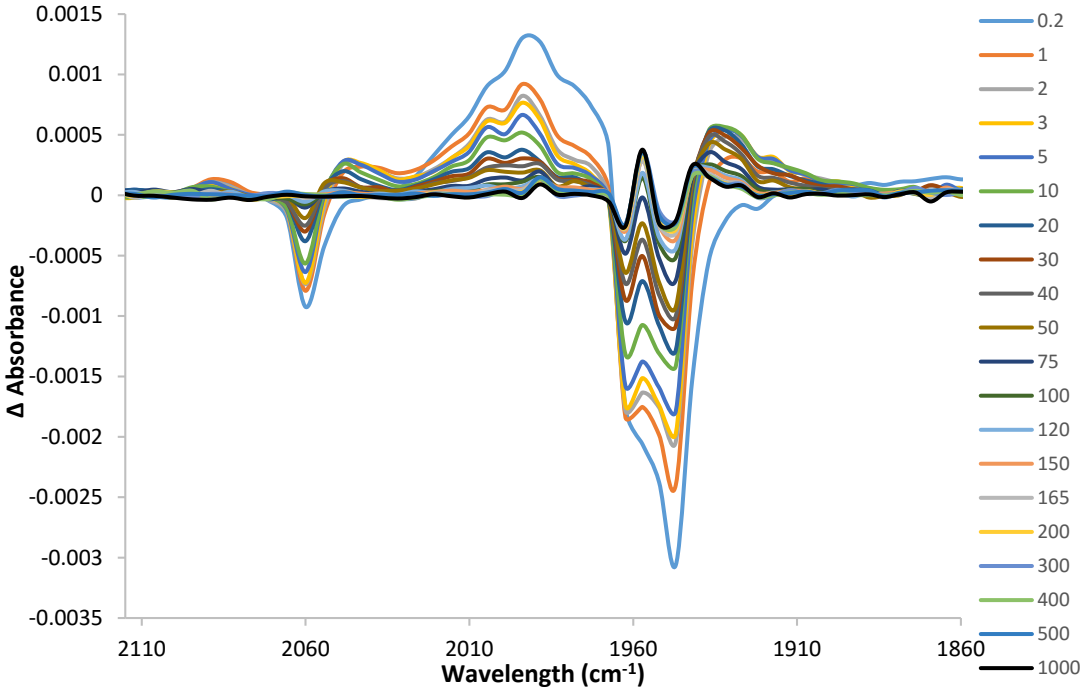

Figure 4.11 The psTRIR spectra obtained following 470 nm excitation of $[(CO)_5Cr{=}C(OMe)C_2H_2Ph]$ in *n*-heptane. The time points included in the legend are in ps.

4.3.3.2 psTRIR studies of $[(CO)_5Cr{=}C(OMe)C_2H_2Ph]$ at 320 nm

The spectroscopic changes observed following 320 nm excitation of $[(CO)_5Cr{=}C(OMe)C_2H_2Ph]$ in *n*-heptane are presented in Figure 4.12. Within the excitation pulse (200 fs), the parent bands at 2060, 1961 and 1951 cm^{-1} were bleached and new absorptions are formed at 1998, 1972, 1931 and 1911 cm^{-1}. These features are assigned to an excited state species and decay over approximately 100 ps at which point further bands became evident at 2043, 1961, 1941 and 1911 cm^{-1}. These bands persisted over the timescale of the experiment (1500 ps) and are assigned to the CO loss species, $[(CO)_4(heptane)Cr{=}C(OMe)C_2H_2Ph]$. The results suggest that CO loss requires high energy excitation. The quantum efficiency for CO loss was estimated at ~5 % at 320 nm from the recovery of the parent bands. However, since there is spectral overlap of the CO loss bands with the depleted and recovering parent absorptions an accurate reflection of the quantum efficiency for CO loss is difficult.

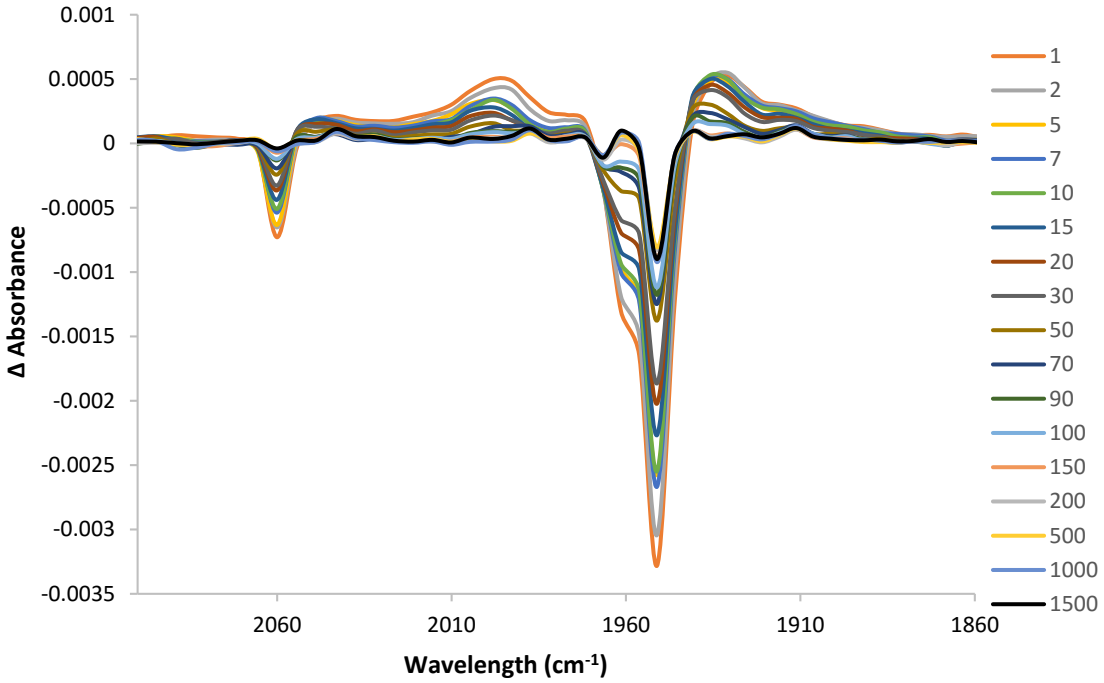

Figure 4.12 The psTRIR spectra obtained following 320 nm excitation of $[(CO)_5Cr=C(OMe)C_2H_2Ph]$ in *n*-heptane. The time points included in the legend are in ps.

4.3.3.3 psTRIR studies of $[(CO)_5Cr=C(NC_4H_8)C_2H_2Ph]$ at 320 nm

As the amino carbene complex, $[(CO)_5Cr=C(NC_4H_8)C_2H_2Ph]$ does not absorb at 470 nm, psTRIR experiments were performed at λ_{exc} = 320 nm only. The IR spectrum of the parent $[(CO)_5Cr=C(NC_4H_8)C_2H_2Ph]$ complex in *n*-heptane exhibits metal carbonyl stretching bands at 2055, 1973, 1938 and 1932 cm^{-1}. The spectral changes observed following pulsed (200 fs) excitation of $[(CO)_5Cr=C(NC_4H_8)C_2H_2Ph]$ at 320 nm are presented in Figure 4.13. The spectrum obtained 1.2 ps after excitation shows depletion of the parent bands, 2055 1973 and 1937 cm^{-1} (as the negative features in the difference spectrum). Within 1.2 ps, a broad band is initially formed at 1994 cm^{-1}. This feature decays over the subsequent 10 ps and over this time frame, new bands are formed at 1888, 1903, 1952 and 2050 cm^{-1}. These bands are assigned to an excited state species and decay over the subsequent 200 ps. Within 50 ps, bands at 2022, 1957 and 1907 cm^{-1} are formed and are assigned to the solvated species,

[(heptane)$(CO)_4Cr=C(NC_4H_8)C_2H_2Ph$]. These bands are consistent with the bands previously reported for the CO loss photoproduct [(heptane)$(CO)_4Cr=C(NC_4H_8)Me$], 2025, 1963, 1923 and 1886 cm^{-1}.[2] The fourth band from the tetracarbonyl species is obscured by the overlap with the parent bands. This has also been observed for a similar amino carbene complex also containing a phenyl group, $[(CO)_4Cr=C(NMe_2)Ph]$ which displayed three bands at 2021, 1921 and 1883 cm^{-1} in an argon matrix.[23] The extent of parent band recovery provides an estimate of the overall quantum yield for the CO loss process of 30 %. In this instance CO loss occurs *via* an independent route which is unlike the CO loss process of $[(CO)_5Cr=C(NC_4H_8)Me]$ at λ_{exc} = 400 nm which occurs *via* a singlet excited state over 50 ps.

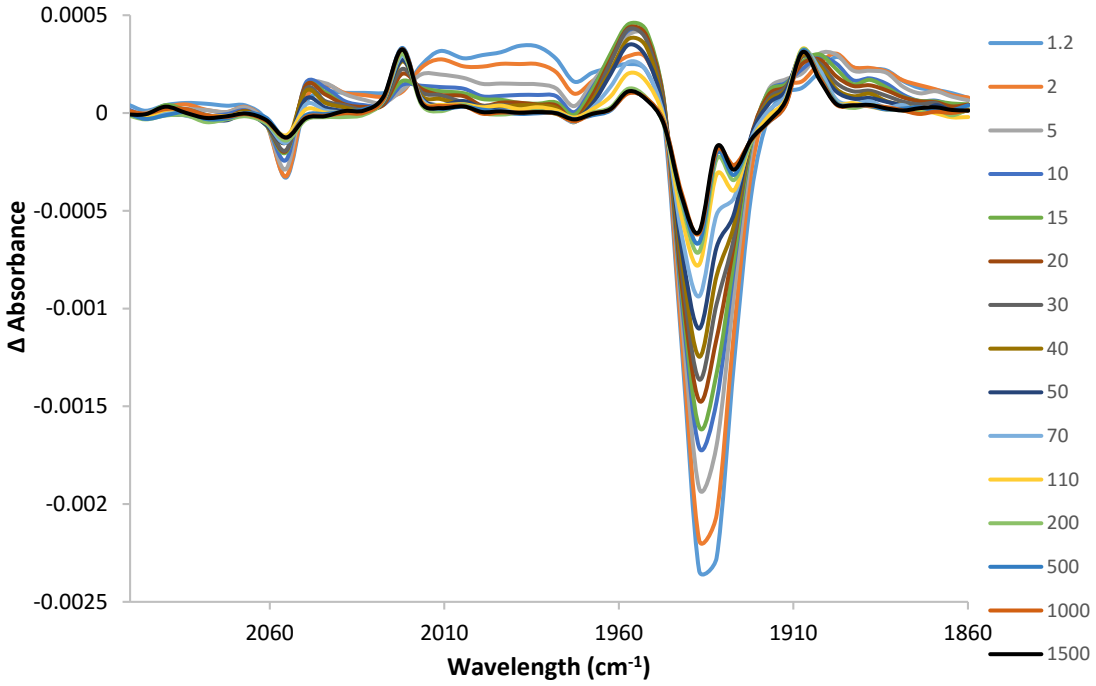

Figure 4.13 The psTRIR spectra obtained following 320 nm excitation of $[(CO)_5Cr=C(NC_4H_8)C_2H_2Ph]$ in *n*-heptane. The time points included in the legend are in ps.

4.3.3.4 psTRIR studies of $[(CO)_5W=C(OMe)C_2H_2Ph]$ at 470 nm

The psTRIR difference spectrum obtained following 470 nm excitation of $[(CO)_5W=C(OMe)C_2H_2Ph]$ in *n*-heptane is presented in Figure 4.14. Within the excitation pulse, the bands of the parent (2067, 1943 and 1953 cm^{-1}) were depleted and broad absorptions centered at 2079 and 1979 cm^{-1} were produced. Over the subsequent

20 ps, these broad peaks decayed, with the formation of new peaks at 2050 and 1923 cm^{-1}. Similar spectral features have also been observed for the Fischer carbene complex, $[(CO)_5W=C(OMe)Me]$, over the same timeframe and were assigned to two triplet excited states (Chapter 2). Over the subsequent 100 ps, the features at 2050 and 1923 cm^{-1} decay. At this point, further bands became evident at 2062, 1979, 1948 and 1933 cm^{-1} and persisted for the duration of the experiment (1000 ps). Similarly to $[(CO)_5WC(OMe)Me]$, no bands are observed in the bridging carbonyl region which suggests that a metallacyclopropanone does not form. The bands at 2062, 1979, 1948 and 1933 cm^{-1} are tentatively assigned to a metallaketene intermediate species. This is in agreement with the metallaketene bands formed (2059, 1983 and 1930 cm^{-1}) upon excitation of $[(CO)_5W=C(OMe)Me]$ at 400 nm.

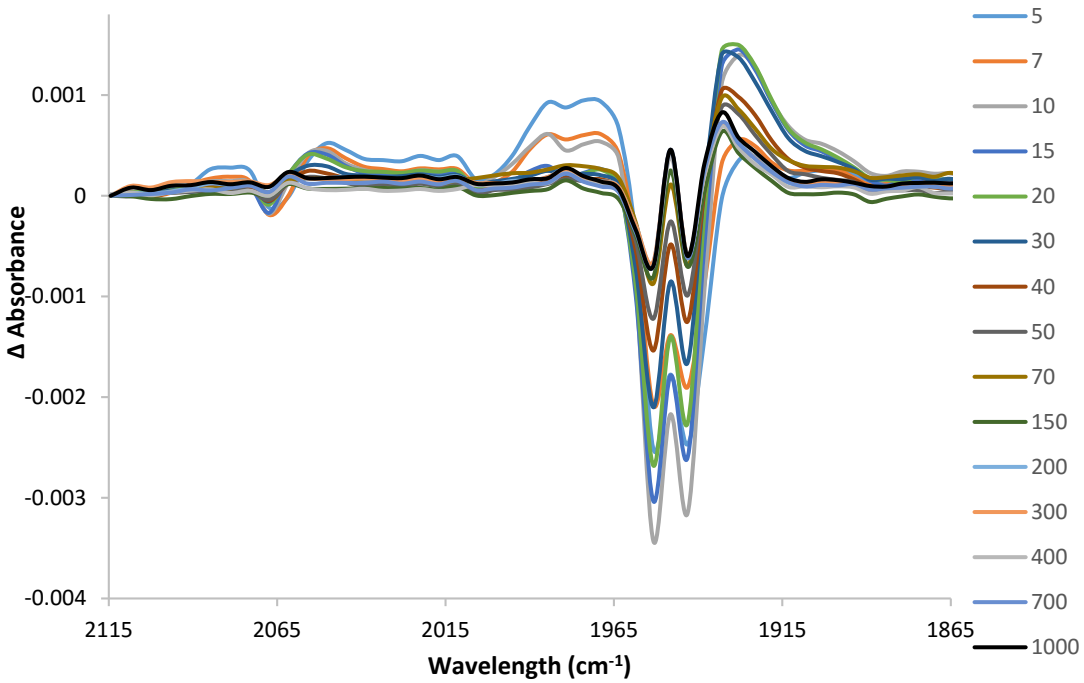

Figure 4.14 The psTRIR spectra obtained following 470 nm excitation of $[(CO)_5W=C(OMe)C_2H_2Ph]$ in *n*-heptane. The time points included in the legend are in ps.

4.3.3.5 psTRIR studies of $[(CO)_5W=C(OMe)C_2H_2Ph]$ at 320 nm

The spectral changes observed following excitation of the tungsten analogue, $[(CO)_5W=C(OMe)C_2H_2Ph]$ using 320 nm irradiation, displayed in Figure 4.15, were almost identical to those observed following excitation at 470 nm described above. Therefore, it can be deduced that the photochemistry of $[(CO)_5W=C(OMe)C_2H_2Ph]$ is substantially independent of the excitation wavelength. In addition, no features were

observed in the bridging υCO region following excitation at 470 or 320 nm This is similar to the psTRIR data reported for $[(CO)_5W=C(OMe)Me]$ at 400 nm in Chapter 2. There is no spectral features indicative of CO loss following irradiation of $[(CO)_5W=C(OMe)C_2H_2Ph]$ at this wavelength.

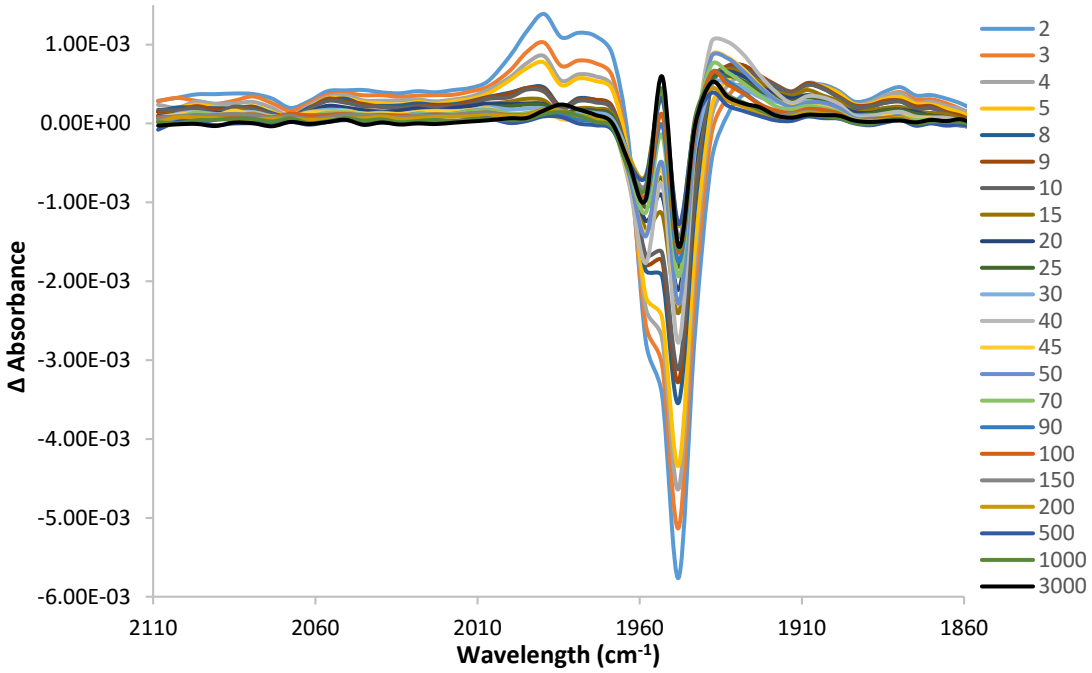

Figure 4.15 The psTRIR spectra obtained following 320 nm excitation of $[(CO)_5W=C(OMe)C_2H_2Ph]$ in *n*-heptane. The time points included in the legend are in ps.

4.3.3.6 psTRIR studies of $[(CO)_5W=C(NC_4H_8)C_2H_2Ph]$ at 320 nm

The IR spectrum of the parent complex, $[(CO)_5W=C(NC_4H_8)C_2H_2Ph]$ in *n*-heptane exhibits metal carbonyl stretching bands at 2062, 1969, 1934 and 1928 cm^{-1}. Figure 4.16, indicates the spectral changes observed following pulsed (200 fs) excitation of $[(CO)_5W=C(NC_4H_8)C_2H_2Ph]$ at 320 nm. The spectrum obtained 3 ps after excitation shows depletion of the parent bands at 2062 and 1928 cm^{-1} as the negative features in the difference spectrum. New bands at 1908, 1948, 1953 and 2012 cm^{-1} are formed within this timescale and are ascribed to an excited state species. Over the subsequent 200 ps these bands decay. Over this timescale, weak bands become evident at 1899, 1943 and 2028 cm^{-1}, which are assigned to the solvated species,

[(heptane)$(CO)_4W{=}C(NC_4H_8)C_2H_2Ph$]. The fourth band from the tetracarbonyl species is obscured by overlap with the parent bands. The bands attributed to the tetracarbonyl product are similar to those reported for the chromium analogue in section **4.3.3.3**, which displays peaks at 1907, 2022 and 1957 cm^{-1}. In addition, the peaks reported are similar to those described for the CO loss product of the tungsten amino carbene complex, [(heptane)$W{=}C(NC_4H_8)Me$] (2028, 1911 and 1873 cm^{-1}) as described in Chapter 3. The extent of parent band recovery provides an estimate of the overall quantum yield for the CO loss process and is low at < 5 %.

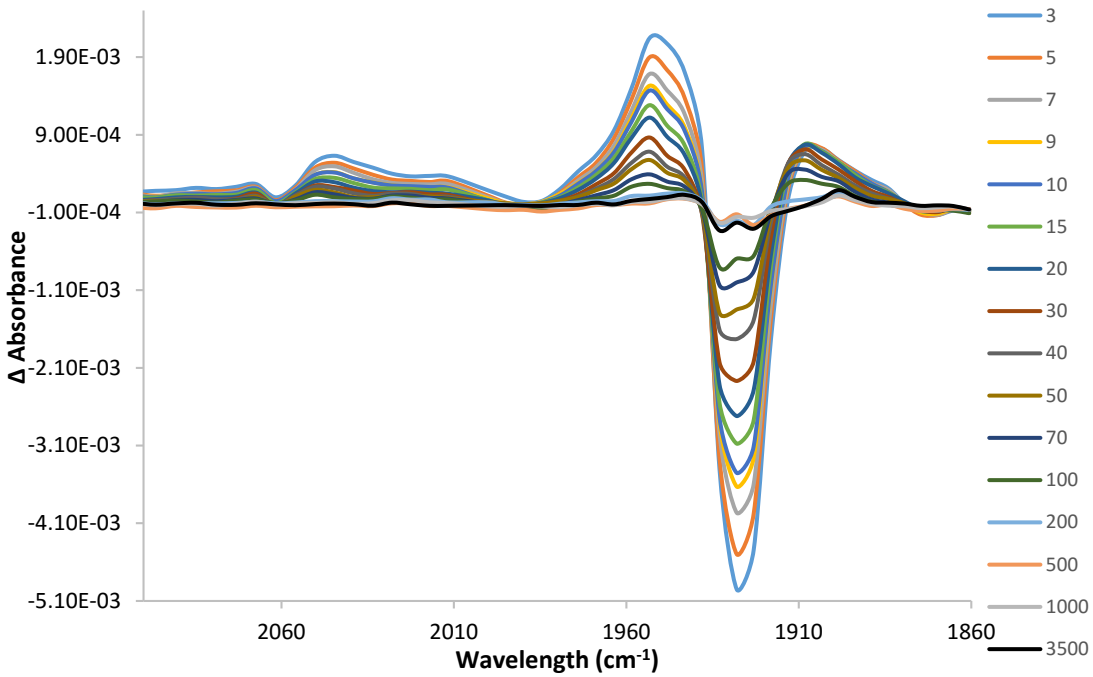

Figure 4.16 The psTRIR spectra obtained following 320 nm excitation of [$(CO)_5W{=}C(NC_4H_8)C_2H_2Ph$] in *n*-heptane. The time points included in the legend are in ps.

4.3.4 Quantum Chemical Calculations

Quantum chemical calculations were carried out for [$(CO)_5Cr=C(NC_4H_8)C_2H_2Fc$] by Prof. Conor Long. The structure of [$(CO)_5Cr=C(NC_4H_8)C_2H_2Fc$] was optimised in the gas phase using the B3LYP hybrid density functional,[27-29] and the triple zeta valence quality basis set Tzvp.[30] In this structure the vinyl spacer was almost coplanar with the substituted ferrocenyl cyclopentadenyl ring (dihedral angle 14 °), however the dihedral angle between N_{14}-C_1-C_2-C_3 is 153 ° which means that the π-system conjugation is somewhat restricted across the vinyl group. The twenty lowest energy singlet excited states were then modelled using the Time-Dependent Density Functional method (TDDFT/B3LYP/Tzvp).[31,32] The lowest energy singlet excited state is degenerate and is the result of an iron to cyclopentadienyl charge-transfer transition. The calculated excitation wavelength for this transition (λ_{calc}) is 590 nm. These excited states populate the vinyl π*-orbital and thus a potential *trans* to *cis* isomerisation will provide an effective deactivation route to the ground state species. These excited states also involve an increased electron density on the carbene carbon and the nitrogen atom of the pyrrolyl group. The next two nearly degenerate excited states are also formed by iron to cyclopentadienyl charge-transfer transitions (λ_{calc} = 490 nm). The fifth and sixth singlet excited states (with λ_{calc} of 464 and 417 nm respectively), are the result of chromium to carbene charge-transfers while the seventh and eight are produced by both chromium and iron to carbene charge transfer transitions (λ_{calc} = 406 and 401 nm respectively). The TRIR experiments provided evidence of photoinduced CO loss. To determine which of these excited states are responsible for inducing CO loss, and also the likely rate of the CO loss process from these excited states, the behaviour of the excited states were determined along the Cr-*cis*CO reaction coordinate. The ground-state structure was optimised at each 0.1 Å step along this reaction coordinate, from a Cr-*cis*CO distance of 1.61 to 2.91 Å. The equilibrium distance is 1.91 Å. At each point along this coordinate TDDFT calculations provided the excited state energies of the twenty lowest singlet excited states. The results of these calculations are presented in Figure 4.17.

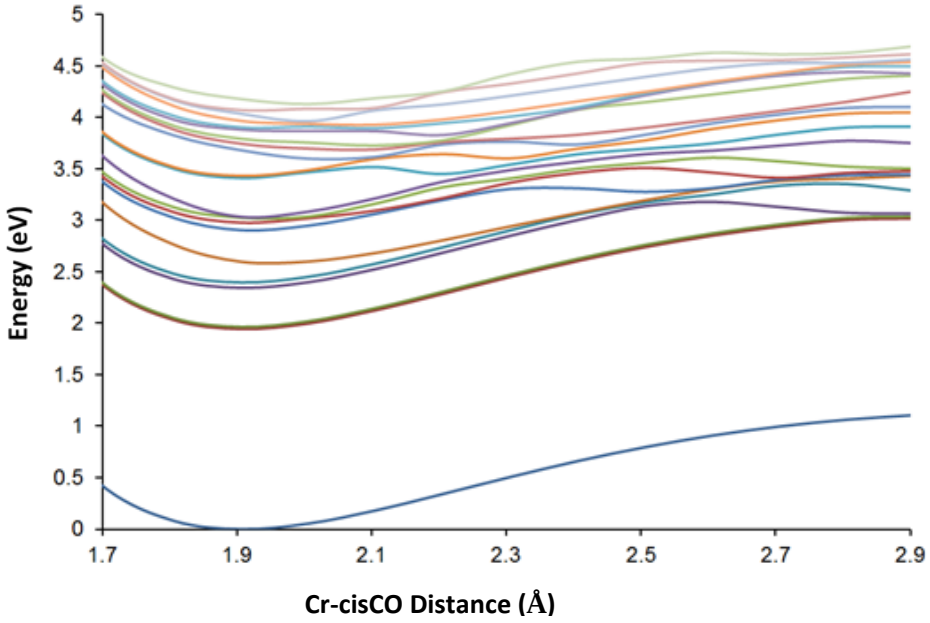

Figure 4.17 The energy (eV) of the twenty lowest energy singlet excited states of $[(CO)_5Cr{=}C(NC_4H_8)C_2H_2Fc]$ along the Cr-*cis*CO reaction coordinate.

The lowest eleven singlet excited states (S_1 to S_{11}) are all bound while the S_{12} state is unbound with respect to *cis*CO loss. Direct population of the S_{12} state would require the absorption of a photon with a wavelength of approximately 330 nm and would result in the ultrafast expulsion of CO. The S_6 to S_9 states are capable of being populated with a 400 nm excitation pulse; however these excited states are bound with respect to *cis*CO loss, and CO loss can only be achieved by overcoming a thermal barrier of approximately 40 kJ mol^{-1} in these states. The thermal barrier is formed by the crossing of the bound states with the unbound S_{12} state along the CO loss reaction coordinate. Thus excitation with 400 nm radiation should result in an arrested CO loss and excitation with 320 nm radiation should result in ultrafast CO loss.

The calculations indicate that the most intense transition is due to a Cr → carbene charge transfer excited state following 400 nm excitation whereas the lowest energy excited state is a Fe →Cp charge transfer, Figure 4.18.

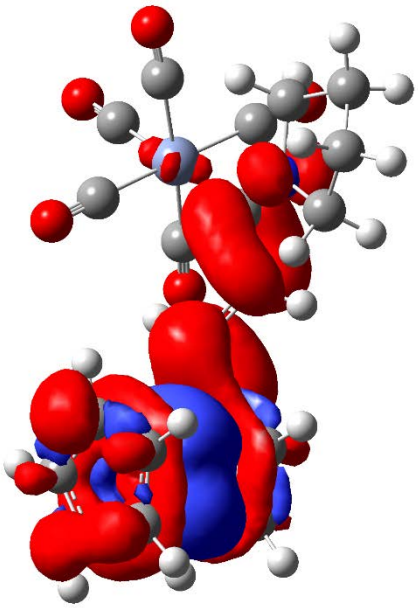

Figure 4.18 The electron density difference map for the first singlet excited state at the ground state optimised geometry, the blue volumes are the regions where the electron density is reduced in the excited state compared to the ground state and the red volumes are the regions where the electron density is greater in the excited state compared to the ground state.

The 6th excited state will undergo CO loss over a thermal barrier and will therefore be slow and compete with relaxation to the lowest excited state, which has Fe → Cp charge character. Based on the position of the new υCO bands, the excited state is tentatively assigned to a Fe → Cp charge transfer, Figure 4.19.

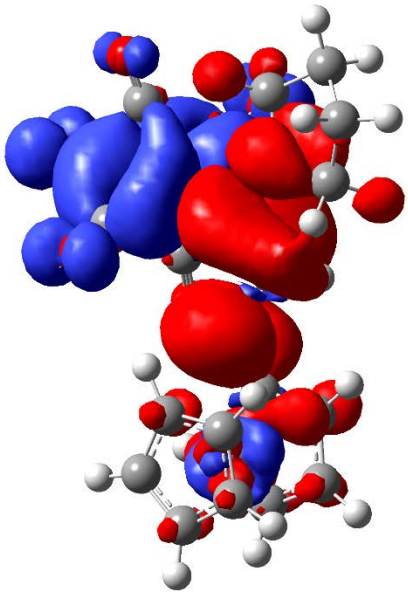

Figure 4.19 The electron density difference map for the sixth singlet excited state at the ground state optimised geometry, the blue volumes are the regions where the electron density is reduced in the excited state compared to the ground state and the red volumes are the regions where the electron density is greater in the excited state compared to the ground state.

4.3.5 Cyclic Voltammetry and Electrochemically Induced CO Loss

The electrochemical properties of the styryl Fischer carbene complexes have not been previously reported unlike the ferrocenyl carbene complexes which has been detailed in the literature.[13,17]

Electrochemical analysis was carried out with the help of Dr. Yvonne Halpin for each of the styryl Fischer carbene complexes in acetonitrile using 0.1 M $TBAPF_6$ as the electrolyte, Ag/AgCl reference electrode, glassy carbon as working electrode and Pt wire as counter electrode. The concentration of each sample was 1 mM throughout.

Cyclic voltammetry reveals at least two oxidative processes for each of the chromium based complexes. This is in agreement with reported data for a structurally similar

alkoxy carbene, $[(CO)_5Cr=C(OEt)C_2H_2Ph]$.[33] A single oxidation wave was observed for each of the tungsten based complexes within a potential window of 0 to 1.9 V, *vs.* Ag/AgCl (-0.43 to 1.47 *vs.* Fc/Fc^+, Figure 4.20 and Table 4.1).

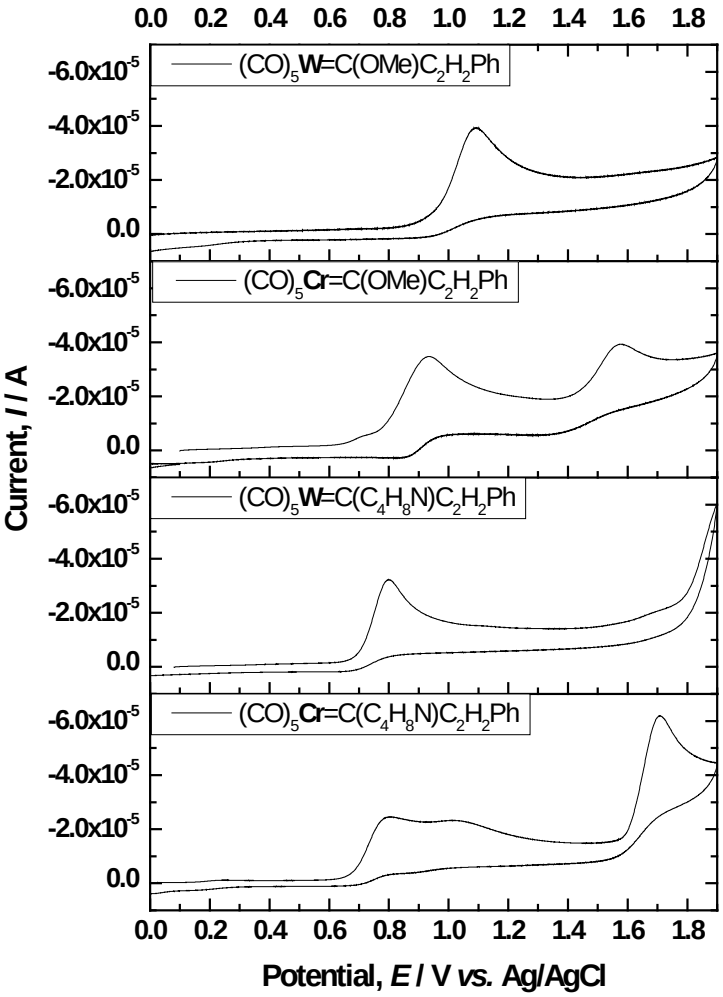

Figure 4.20 Cyclic voltammograms of the oxidative processes of the styryl Fischer carbene complexes in 0.1M $TBAPF_6$ in CH_3CN, *vs.* Ag/AgCl. Scan rate = 0.1 V s^{-1}.

Substitution of the pyrrolidino group at the carbene carbon with that of a methoxy group results in a positive shift in the first oxidation potential as a result of the stronger electron withdrawing effect of the methoxy group. Substitution of the pyrrolidine group for the methoxy moiety causes the carbene carbon to become slightly less electron deficient due to the efficient electron donating ability of pyrrolidine. The first, least positive, oxidation of each complex is electrochemically irreversible at a scan rate of 0.1 V/s and is assigned to the metal centred $Cr^{I/0}/W^{I/0}$ redox couple as previously reported.[34,35] Oxidation of these types of metal carbene complexes is reported as being predominantly metal based

with reduction centred on the metal-carbene double bond.[34,35] Comparison of the oxidation potential of [$(CO)_5Cr{=}C(NC_4H_8)C_2H_2Ph$] with the previously reported chromium analogue, [$(CO)_5Cr{=}C(NC_4H_8)Me$] (Chapter 3)[2] reveals only a small increase in the oxidation potential of the former styryl complex of 30 mV which suggests that the nature of this substituent has little influence on this metal based electrochemical process.

In each of the four complexes, it was observed that the first least positive oxidation is electrochemically irreversible at a scan rate of 0.1 V/s. For the tungsten complexes, increasing the scan rate did not lead to reversibility of this process. However, this oxidation for each of the chromium complexes becomes *quasi*-reversible beyond scan rates of 0.5 V/s, Figure 4.21.

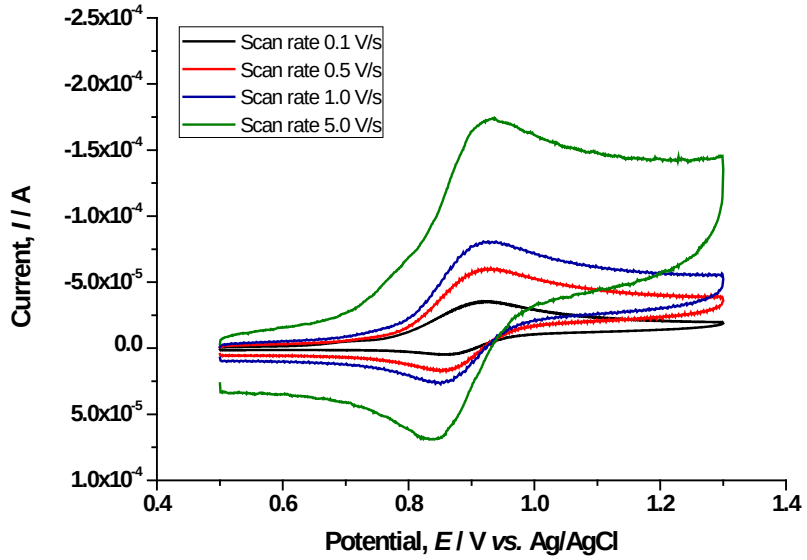

Figure 4.21 Scan rate dependence of first oxidative processes of [$(CO)_5Cr{=}C(OMe)C_2H_2Ph$] in 0.1M $TBAPF_6$ in CH_3CN, *vs.* Ag/AgCl.

The electrochemical properties of the styryl complexes are very different to their ferrocenyl counterparts. The ferrocene complexes were previously investigated by cyclic voltammetry in dry acetonitrile under argon with 0.1 M [*n*-BuN_4][BF_4], as supporting electrolyte, using a glassy carbon working electrode, a platinum wire auxiliary electrode and a saturated calomel reference electrode.[17] The methoxy and pyrrolidino ferrocene complexes exhibited reversible first oxidation steps in the

potential range of $E_{1/2}$ = 0.028 to 0.146 V. This feature was ascribed to the ferrocene / ferrocenium redox couple.[13] This couple is identical for both the Cr and W methoxy carbene complexes with $E_{1/2}$ = 0.146 V. This value is close to previously reported values of 0.135 and 0.134 V for [$(CO)_5Cr=C(OMe)C_2H_2Fc$] and [$(CO)_5W=C(OMe)C_2H_2Fc$], respectively, reported by Jayaprakash *et al.*[13] For [$(CO)_5Cr=C(NC_4H_8)C_2H_2Fc$] and [$(CO)_5W=C(NC_4H_8)C_2H_2Fc$], the ferrocene/ferrocenium couple is observed at less positive potentials at $E_{1/2}$ = 0.028 V and $E_{1/2}$ = 0.110 V, respectively.[17] The ferrocene-based HOMO orbital in these systems is therefore more strongly stabilised in the case of the methoxy carbene systems compared to the amino carbene complexes.[17] A second oxidation step is observed for the amino carbenes and is ascribed to the metal carbene moiety. For [$(CO)_5Cr=C(OMe)C_2H_2Fc$] and [$(CO)_5Cr=C(NC_4H_8)C_2H_2Fc$], the second oxidation is reversible, displayed at $E_{1/2}$ = 0.458 and 0.251 V respectively.[13] The tungsten derivatives, [$(CO)_5W=C(OMe)C_2H_2Fc$] [$(CO)_5W=C(NC_4H_8)C_2H_2Fc$] undergo irreversible oxidation processes unlike their chromium counterparts (E_{pa} = 0.552 and 0.415 V respectively).

The reductive electrochemical properties of each of the styryl carbene complexes were also assessed. Each of the styryl complexes exhibit several reductions within a potential window to -2.7 - 0 V, *vs.* Ag/AgCl in CH_3CN, Figure 4.22. The first reduction of these types of Fischer carbene complexes is reported as being localised on the metal carbene double bond.[2,35] The methoxy complexes are reduced at potentials less negative that their pyrrolidino analogues. This is in agreement with the trend in reductive electrochemistry reported for [$(CO)_5Cr=C(OMe)Me$] *vs.* [$(CO)_5Cr=C(NC_4H_8)Me$] as observed in Chapter 2 and Chapter 3.

In the case of the ferrocene compounds, the reduction profiles previously reported, are also very different.[17] Likewise, the reduction is ascribed to the carbene moiety. However, it is found to be reversible for each of the complexes except for [$(CO)_5Cr=C(NC_4H_8)C_2H_2Fc$]. In general, the reduction potentials are more negative for the chromium carbenes in comparison to the tungsten carbenes. This is due to the more efficient electron accepting ability of tungsten over chromium which is in agreement with the higher hyperpolarizability of the tungsten complexes.[13] The Fischer carbene and ferrocene groups undergo significant electrochemical communication as reported by Sarkar and co-workers.[13]

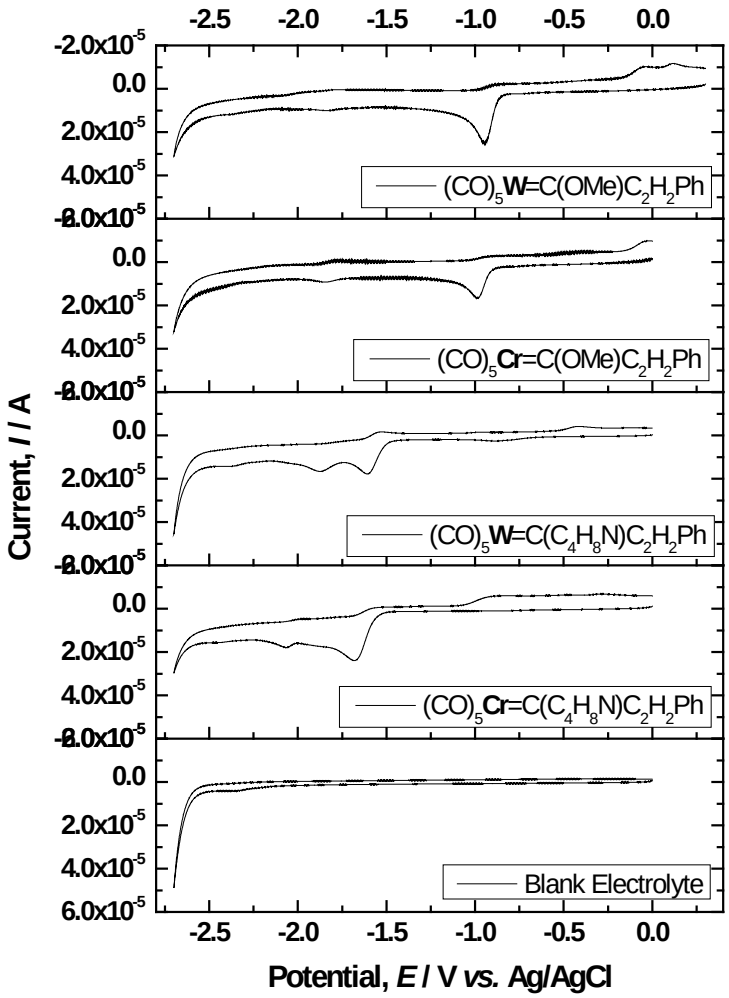

Figure 4.22 Cyclic voltammograms of the reductive processes of the styryl Fischer carbene complexes in 0.1M $TBAPF_6$ in CH_3CN, *vs.* Ag/AgCl. Scan rate = 0.1 V s^{-1}

Table 4.1 Cyclic voltammetry results and bulk electrolysis potential (*vs.* Ag/AgCl) used in the electrochemically induced CO loss experiments for the styryl Fischer carbene complexes.

Complex	E_{pa} (V)*	E_{pc} (V)*	Bulk Electrolysis Potential (V)*
$[(CO)_5Cr=C(OMe)C_2H_2Ph]$	+0.93, +1.58 [a]	-0.99 [a], -1.85	+1.00
$[(CO)_5W=C(OMe)C_2H_2Ph]$	+1.06 [a]	-0.95, -1.84, -2.07	+1.10
$[(CO)_5Cr=C(NC_4H_8)C_2H_2Ph]$	+0.80 [a], +1.01, +1.71	-1.67, -2.07	+0.88
$[(CO)_5W=C(NC_4H_8)C_2H_2Ph]$	+0.80 [a]	-1.61, -1.89	+1.00

* (*vs.* Ag/AgCl); $E_{½}$ Fc/Fc^+ = + 0.43 V, *vs.* Ag/AgCl reference electrode. 0.1 M $TBAPF_6$ / CH_3CN as electrolyte. Glassy carbon as working electrode and Pt wire as counter electrode. Concentration of each sample was 1 mM throughout. CO loss was monitored by gas chromatography. [a] Electrochemically irreversible process at 0.1 V/s scan rate.

In the present study, electrochemical initiation of CO release from a 1 mM solution of each complex in CH_3CN was confirmed, over five intervals approximately 20 minutes apart and quantified *via* headspace analysis using gas chromatography. Displayed in Table 4.1 are the electrochemical data. Electrochemically induced CO release was monitored over 1.5 hours of controlled potential electrolysis focusing on the first oxidation of each complex, Figure 4.23.

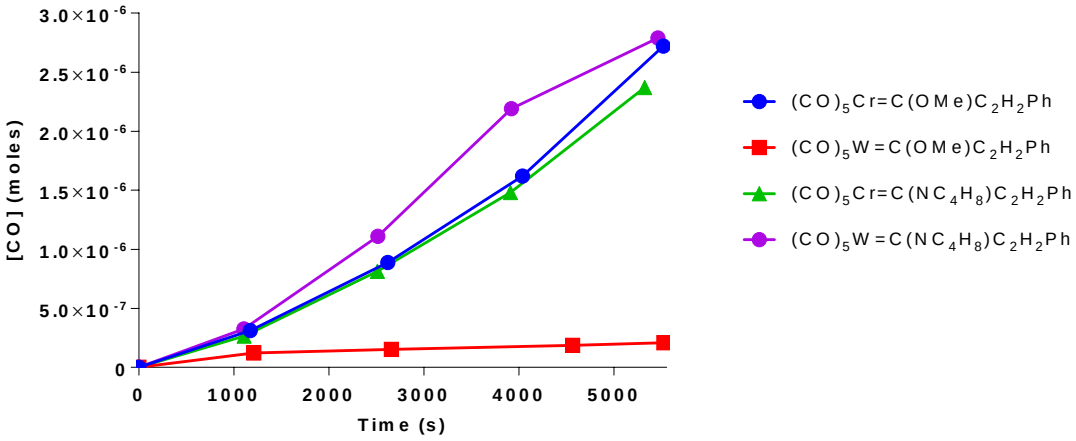

Figure 4.23 Profile for the electrochemically induced CO release over time from the carbenes, $[(CO)_5M(X)C_2H_2Ph]$ (M = Cr, W; X= OMe, NC_4H_8). Concentration of each carbene was 1 mM and the solution was stirred continuously (n = 1).

The rate and amount of CO generated from the pyrrolidino chromium and tungsten complexes and the methoxy chromium complexes are similar. However, the CO loss measured from $[(CO)_5W=C(OMe)C_2H_2Ph]$ is an order of magnitude less than that from the other three complexes at the end of the 1.5 hour experiment. This is in agreement with the trend observed from Chapters 2 and 3, where, $[(CO)_5W=C(OMe)Me]$ released less CO when compared to the corresponding, $[(CO)_5Cr=C(OMe)Me]$, $[(CO)_5Cr=C(NC_4H_8)Me]$ and $[(CO)_5W=C(NC_4H_8)Me]$ compounds under the same conditions (the point of bulk electrolysis varies with the position of the first oxidation peak).[1,2] The reason for the inefficiency of electrochemical CO loss from $[(CO)_5W=C(OMe)C_2H_2Ph]$ and $[(CO)_5W=C(OMe)Me]$ is possibly due to the fact that these tungsten based Fischer carbene compounds can coat the electrode during the experiments. This was also previously reported by Connor and co-workers.[36]

4.4 Conclusion

In this chapter, the synthesis and characterisation of the novel Fischer carbene complexes, $[(CO)_5Cr=C(NC_4H_8)C_2H_2Ph]$ and $[(CO)_5W=C(NC_4H_8)C_2H_2Ph]$ and a range of previously synthesised Fischer carbenes are reported. The results of a psTRIR investigation of the Fischer carbene complexes, $[(CO)_5M=C(X)C_2H_2Ph]$ and $[(CO)_5M=C(X)C_2H_2Fc]$ where M = Cr, W; X = OMe, NC_4H_8; Ph = phenyl and Fc = ferrocene is detailed. In the case of the Ferrocenyl Fischer carbene complexes, no evidence was observed to indicate the formation of a ketene intermediate species. In contrast, the styryl compounds, $[(CO)_5Cr=C(OMe)C_2H_2Ph]$ and $[(CO)_5W=C(OMe)C_2H_2Ph]$, upon excitation at 482, 470 and 400 nm, exhibited spectral features which are tentatively assigned to the ketene intermediate species as they are consistent with those reported for the carbene complexes, $[(CO)_5Cr=C(OMe)Me]$ and $[(CO)_5W=C(OMe)Me]$, detailed in Chapter 2. At 320 nm, for $[(CO)_5Cr=C(OMe)C_2H_2Ph]$, CO loss is observed, indicating the wavelength dependent photochemistry exerted from this complex. In contrast, the tungsten analogue, $[(CO)_5W=C(OMe)C_2H_2Ph]$, did not undergo wavelength dependent chemistry, which is also in agreement with that reported in Chapter 2.

The electrochemical CO loss profiles are similar for $[(CO)_5Cr=C(OMe)C_2H_2Ph]$, $[(CO)_5Cr=C(NC_4H_8)C_2H_2Ph]$ and $[(CO)_5W=C(NC_4H_8)C_2H_2Ph]$. In contrast, $[(CO)_5W=C(OMe)C_2H_2Ph]$ does not undergo electro- CO loss to the same extent.

The psTRIR studies on the ferrocenyl and styryl complexes presented here, are the first reported to date of these type of compounds.

4.5 References

1. McMahon, S.; Amirjalayer, S.; Buma, W. J.; Halpin, Y.; Long, C.; Rooney, A. D.; Woutersen, S.; Pryce, M. T. An investigation into the photochemistry of, and the electrochemically induced CO-loss from, $[(CO)_5MC(OMe)Me]$(M = Cr or W) using low-temperature matrix isolation, picosecond infrared spectroscopy, cyclic voltammetry, and time-dependent density functional theory. *Dalton Trans.* **2015**, *44*, 15424-15434.

2. McMahon, S.; Rochford, J.; Halpin, Y.; Manton, J. C.; Harvey, E. C.; Greetham, G. M.; Clark, I. P.; Rooney, A. D.; Long, C.; Pryce, M. T. Controlled CO release using photochemical, thermal and electrochemical approaches from the amino carbene complex $[(CO)_5CrC(NC_4H_8)CH_3]$. *Phys. Chem. Chem. Phys.* **2014**, *16*, 21230-21233.

3. Kvapilova, H.; Hoskovcova, I.; Kayanuma, M.; Daniel, C.; Zalis, S. Electronic Excitations in Fischer-Type Cr and W Aminocarbene Complexes: A Combined ab Initio and Experimental Study. *J. Phys. Chem. A* **2013**, *117*, 11456-11463.

4. Montgomery, C. Fischer and Schrock Carbene Complexes: A Molecular Modeling Exercise. *J. Chem. Educ.* **2015**, *92*, 1653-1660.

5. Hegedus, L. Chromium carbene complex photochemistry in organic synthesis. *Tetrahedron* **1997**, *53*, 4105-4128.

6. Sierra, M.; Hegedus, L. Formation of Cyclobutanones by the Photolytic Reaction of $(CO)_5Cr=C(OMe)Me$ with Electron-Rich Olefins. *J. Am. Chem. Soc.* **1989**, *111*, 2335-2336.

7. Fernandez, I.; Cossio, F. P.; Sierra, M. A. Photochemistry of Group 6 Fischer Carbene Complexes: Beyond the Photocarbonylation Reaction. *Acc. Chem. Res.* **2011**, *44*, 479-490.

8. Lage, M. L.; Fernandez, I.; Mancheno, M. J.; Sierra, M. A. Electronic structure of alkoxychromium(0) carbene complexes: A joint TD-DFT/experimental study. *Inorg. Chem.* **2008**, *47*, 5253-5258.

9. Lage, M. L.; Fernandez, I.; Mancheno, M. J.; Gomez-Gallego, M.; Sierra, M. A. Metal-Tuned Photochemistry of Metallocene-Substituted Chromium(0)-Carbene Complexes. *Chem. -Eur. J.* **2009**, *15*, 593-596.

10. Lage, M. L.; Fernandez, I.; Mancheno, M. J.; Gomez-Gallego, M.; Sierra, M. A. The Electronic Structure and Photochemistry of Group 6 Bimetallic (Fischer) Carbene Complexes: Beyond the Photocarbonylation Reaction. *Chem. -Eur. J.* **2010**, *16*, 6616-6624.

11. Connor, J.; Lloyd, J. Ferrocenyl Carbene Complexes of Chromium, Tungsten, and Manganese, Models for Alpha-Ferrocenyl Carbonium-Ion. *J. Chem. Soc. -Dalton Trans.* **1972**, *14*, 1470-1476.

12. Barluenga, J.; FernandezAcebes, A.; Trabanco, A.; Florez, J. Diastereoselective cyclopropanation of simple alkenes by 2-phenyl- and 2-ferrocenylalkenyl Fischer carbene complexes of chromium. *J. Am. Chem. Soc.* **1997**, *119*, 7591-7592.

13. Jayaprakash, K.; Ray, P.; Matsuoka, I.; Bhadbhade, M.; Puranik, V.; Das, P.; Nishihara, H.; Sarkar, A. Ferrocene in conjugation with a Fischer carbene: Synthesis, NLO, and electrochemical behavior of a novel organometallic push-pull system. *Organometallics* **1999**, *18*, 3851-3858.

14. Sierra, M.; Mancheno, M.; Vicente, R.; Gomez-Gallego, M. Synthesis of ferrocene-substituted 2-azetidinones. *J. Org. Chem.* **2001**, *66*, 8920-8925.

15. Martinez-Alvarez, R.; Gomez-Gallego, M.; Fernandez, I.; Mancheno, M.; Sierra, M. ESI mass spectrometry as a tool for the study of electron transfer in nonconventional media: The case of bi- and polymetallic carbene complexes. *Organometallics* **2004**, *23*, 4647-4654.

16. Hegedus, L.; DeWeck, G.; Dandrea, S. Evidence for the Intermediacy of Chromium Ketene Complexes in the Synthesis of Beta-Lactams by the Photolytic Reaction of Chromium Carbene Complexes with Imines - use in Amino-Acid Synthesis. *J. Am. Chem. Soc.* **1988**, *110*, 2122-2126.

17. Rochford, J. PhD Thesis, Dublin City University, 2004.

18. Bell, S.; Gordon, K.; McGarvey, J. Time-Resolved Resonance Raman-Spectroscopy and Solution Kinetics of Photogenerated Transients in the Metal Carbene Complex $(OC)_5W=C(OMe)Ph$. *J. Am. Chem. Soc.* **1988**, *110*, 3107-3112.

19. Servaas, P.; Stufkens, D.; Oskam, A. Matrix Photochemistry of the Complexes $(CC)_5Cr=C(OMe)Ph$, $(CO)_5W=C(OMe)Ph$ having Close-Lying Reactive MLCT and LF States. *J. Organomet. Chem.* **1990**, *390*, 61-71.

20. Rooney, A.; McGarvey, J.; Gordon, K.; McNicholl, R.; Schubert, U.; Hepp, W. Laser Photochemistry and Transient Raman-Spectroscopy of Silyl-Substituted Fischer-Type Carbene Complexes. *Organometallics* **1993**, *12*, 1277-1282.

21. Rooney, A.; McGarvey, J.; Gordon, K. Time-Resolved Raman-Spectroscopy and Matrix-Isolation Studies of Anti-Syn Photoisomerization in Metal-Carbonyl Carbenes. *Organometallics* **1995**, *14*, 107-113.

22. Gallagher, M.; Greene, J.; Rooney, A. Matrix isolation study into the mechanism of photoinduced cyclization reactions of chromium carbenes. *Organometallics* **1997**, *16*, 5260-5268.

23. Doyle, K.; Gallagher, M.; Pryce, M.; Rooney, A. A matrix isolation and flash photolysis study of the cyclization reactions of chromium amino carbenes. *J. Organomet. Chem.* **2001**, *617*, 269-279.

24. Gut, H.; Welte, N.; Link, U.; Fischer, H.; Steiner, U. Formation and reactions of tetracarbonyl intermediates of the fischer carbene complex $(CO)_5W=C(OMe)Ph$. A laser flash photolysis study using time-resolved infrared and UV/Vis spectroscopy. *Organometallics* **2000**, *19*, 2354-2364.

25. Foley, H.; Strubinger, L.; Targos, T.; Geoffroy, G. Photochemistry of $[W(CO)_5(C(OMe)Ph)]$ - Formation of Alkyne Carbene Complexes and Studies of their Decomposition Reactions. *J. Am. Chem. Soc.* **1983**, *105*, 3064-3073.

26. Hafner, A.; Hegedus, L.; DeWeck, G.; Hawkins, B.; Dotz, K. Chromium-53 Nuclear Magnetic-Resonance Studies of Pentacarbonylchromium Carbene Complexes. *J. Am. Chem. Soc.* **1988**, *110*, 8413-8421.

27. Kohn, W.; Becke, A.; Parr, R. Density functional theory of electronic structure. *J. Phys. Chem.* **1996**, *100*, 12974-12980.

28. Becke, A. Density-Functional Thermochemistry. III. The Role of Exact Exchange. *J. Chem. Phys.* **1993**, *98*, 5648-5652.

29. Fan, L.; Ziegler, T. The Influence of Self-Consistency on Nonlocal Density Functional Calculations. *J. Chem. Phys.* **1991**, *94*, 6057-6063.

30. Schafer, A.; Huber, C.; Ahlrichs, R. Fully Optimized Contracted Gaussian-Basis Sets of Triple Zeta Valence Quality for Atoms Li to Kr. *J. Chem. Phys.* **1994**, *100*, 5829-5835.

31. Bauernschmitt, R.; Ahlrichs, R. Treatment of electronic excitations within the adiabatic approximation of time dependent density functional theory. *Chem. Phys. Lett.* **1996**, *256*, 454-464.

32. Casida, M. E.; Jamorski, C.; Casida, K. C.; Salahub, D. R. Molecular excitation energies to high-lying bound states from time-dependent density-functional response theory: Characterization and correction of the time-dependent local density approximation ionization threshold. *J. Chem. Phys.* **1998**, *108*, 4439-4449.

33. Chu, G. M.; Fernandez, I.; Sierra, M. A. Synthesis, Structure, and Electronic Properties of Extended pi-Conjugated Group 6 Fischer Alkoxy-Bis(carbene) Complexes. *Chem. -Eur. J.* **2013**, *19*, 5899-5908.

34. Landman, M.; Liu, R.; Fraser, R.; van Rooyen, P. H.; Conradie, J. Fac and mer dppe-substituted Fischer carbene complexes of chromium: X-ray, DFT and electrochemical study. *J. Organomet. Chem.* **2014**, *752*, 171-182.

35. Hoskovcova, I.; Rohacova, J.; Meca, L.; Tobrman, T.; Dvorak, D.; Lukvik, J. Electrochemistry of chromium(0)-aminocarbene complexes - The use of intramolecular interaction LFER for characterization of the oxidation and reduction centre of the complex. *Electrochim. Acta* **2005**, *50*, 4911-4915.

36. Lloyd, M.; McClever, J.; Orchard, D.; Connor, J.; Hall, M.; Hillier, I.; Jones, E.; McEwen, G. Electrochemical Oxidation of Organometallic Complexes - Carbene and

Lewis Base Complexes of Chromium, Molybdenum, and Tungsten Carbonyls. *J. Chem. Soc. -Dalton Trans.* **1973**, *17*, 1743-1747.

5 Chapter 5 The Synthesis and Characterisation of a Series of Novel Boron Dipyrromethene (BODIPY) Metal Carbonyl Complexes

Abstract

This chapter highlights the synthesis and characterisation of a range of novel boron dipyrromethene (BODIPY) metal carbonyl complexes. The photophysical properties; UV-vis absorbance, emission, fluorescent quantum yield, lifetime, extinction coefficient and electrochemical properties (cyclic voltammetry) are reported. The photochemically activated CO releasing ability of these complexes is quantified in biologically compatible media using gas chromatography.

5.1 Introduction

The term photoCORM was first introduced in 2010 by Rimmer and co-workers.[1] PhotoCORMs are defined as compounds that release CO upon photochemical stimulation. These are a highly useful class of compounds allowing for specific control of CO release with regards to dosage regulation, timing and site of release. Of course, it is necessary to use various wavelengths of incident light to promote CO release depending on the nature of the CORM under investigation. Ideally, the CORM should absorb sufficiently to release CO upon irradiation from low energy photons, within the photodynamic therapeutic window (600 - 800 nm), thus minimising damage to healthy tissues and allowing for sufficient penetration at the target site. The CORM should be soluble in a solvent suitable for drug delivery. In addition, the CORM should be stable in the absence of light in a bio-compatible solvent, for a period of time long enough for accumulation of the CORM at the target site.[2]

Typically, metal carbonyl complexes will only release CO in the presence of UV light; hence, the majority of photoCORMs reported to date have required UV light to promote CO release.[3-5] This is not ideal due to the damage it causes to surrounding biological tissue. For example, Schatzschneider and co-workers developed the CORM, $[Mn(CO)_3(tpm)]PF_6$ where tpm = tris(pyrazolyl)methane (**1**), Figure 5.1. This complex exhibited stability in the absence of light (up to 100 µM) and two equivalents of CO were released upon irradiation at 365 nm. Anti-cancer properties were comparable to those of the well-established anti-cancer agent 5-fluoracil when tested against HT29 human colon cancer cells (when compared to non-treated cells).[6,7] Since this discovery, $[Mn(CO)_3(tpm)]^+$ has been incorporated into many delivery vehicles such as nanoparticles and nanodiamonds.[8,9] Doerdelmann *et al.* functionalised silicon dioxide (SiO_2) nanoparticles and later nanodiamonds onto the photoCORM, $[Mn(CO)_3(tpm)]^+$, to aid the delivery of CORMs to tumours from a biocompatible photoCORM carrier. Nanodiamonds demonstrate good cellular uptake with no reported cytotoxic effects. CO release was observed in each case, upon irradiation at 365 nm.[8,9]

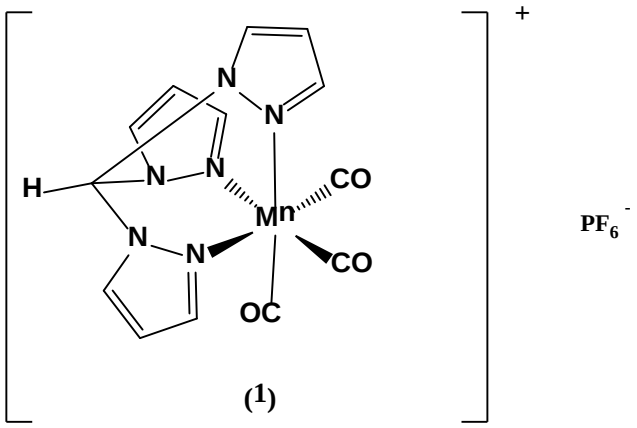

(**1**)

Figure 5.1 Structural representation of $[Mn(CO)_3(tpm)]PF_6$ (**1**) where tpm = tris(pyrazolyl)methane.[6]

Rimmer *et al.* investigated the CO releasing ability of the complex ion, $[W(CO)_5(TPPTS)]^{3-}$ (TPPTS = 3,3,3′ phosphanetriyltris(benzene sulfonic acid)trisodium salt) (**2**), Figure 5.2. This complex was stable in the absence of light in aerated aqueous buffer solutions. UV irradiation (λ_{exc} = 313 nm) was required to induce CO release (~0.9 equivalents of CO per mole of complex were released in the primary photochemical step), monitored by FTIR analysis, flash photolysis and by gas chromatography.[1] At λ_{exc} = 405 nm, the quantum yield value for CO loss was 0.6 ± 0.1. Quantum yield values for CO loss were determined by monitoring the UV-vis absorbance changes over the first 10 % of the reaction.[1]

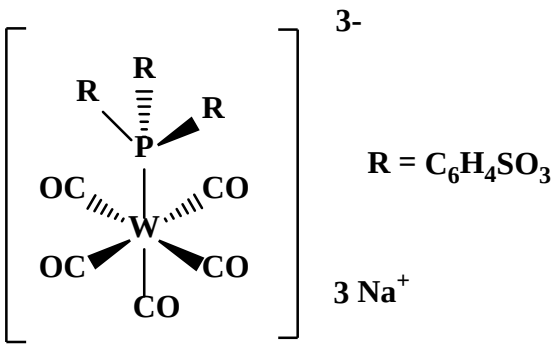

(**2**)

Figure 5.2 Structural representation of $[W(CO)_5(TPPTS)]^{3-}$ (TPPTS = 3,3,3′ phosphane triyltris(benzene sulfonic acid)trisodium salt) (**2**).[1]

Kianfar *et al.* have very recently reported quantum yields for CO release for a range of *fac*-[Re(1,2-diimine)$(CO)_3Cl$] systems, displayed in Figure 5.3, using FTIR difference absorption spectroscopy.[10] UV illumination was used (λ_{exc} = 280 nm) and CO release experiments were carried out in an organic solvent (CH_3CN), as well as in aqueous (H_2O) media (Φ_{CO} = 0.01 - 0.04). However, as irradiation at this high energy would lead to inefficient tissue penetration as well as causing photo-damage to local tissues, it is necessary to move towards the visible region of the spectrum.[10]

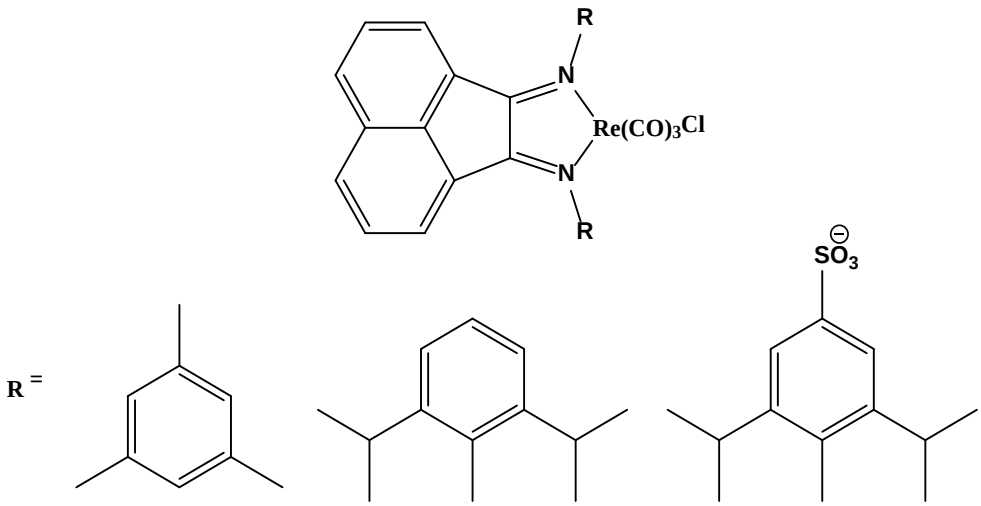

Figure 5.3. Structural representation of *fac*-[Re(1,2-diimine)$(CO)_3Cl$] systems reported by Kianfar *et al.*[10]

A critical issue that needs to be addressed with regards to CORMs is the establishment of the localisation of the CORM *in vivo* as well as the identification of the extent to which CO is released. Ford and co-workers designed a biologically compatible (air stable, non-toxic, water soluble) complex, $[(CO)_3Re(bpy)(thp)]^+$ where thp = tris(hydroxymethyl)-phosphine and bpy = 2, 2′-bipyridine (**3**), Figure 5.4. This CORM specifically liberates one of the three carbonyl ligands (the carbonyl *trans* to the phosphine unit) upon irradiation at 405 nm (Φ_{CO} = 0.11). The complex itself and the by-product, $[(CO)_2Re(sol)(bpy)(thp)]^+$ where sol = H_2O or CH_3CN, formed as a result of CO release are fluorescent (exhibiting emission at a different wavelength to the starting complex). This feature allows for the detection and cellular tracking of the complex *in vitro* using fluorescence microscopy upon excitation at 405 nm and detection at 465 - 495 nm for the starting CORM and 660 nm for the resulting solvated complex. The by-product also exhibits a different UV-vis absorption profile with λ_{max} = 290 and 405 nm. The IR bands of the parent complex *vs.* the CO loss product also exhibit different υCO

bands at 2037, 1949 and 1923 cm^{-1} for the parent *vs.* bands at 1937 and 1862 cm^{-1}, for the CO loss product. [11]

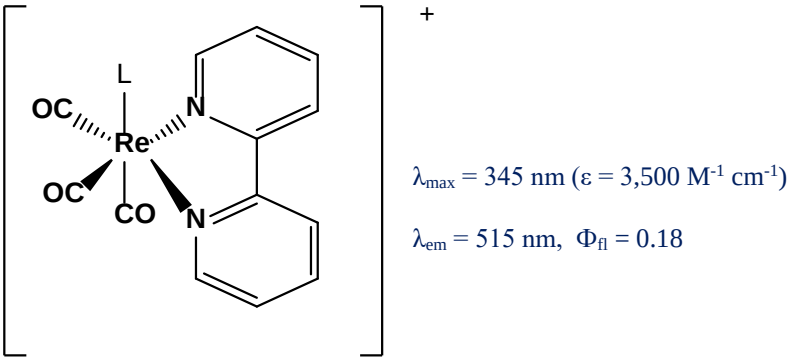

(3)

Figure 5.4 Structural representation of *fac*-[$(CO)_3Re(bpy)(L)^+$] where L = tris(hydroxymethyl)-phosphine, ($P(CH_2OH)_3$) (**3**).[11]

Arrowsmith *et al.* reported a CORM based on a modified Fischer carbene complex incorporating an emissive pyrene tag (**4**), Figure 5.5, which allowed the localisation of the CORM to be determined within cells.[12] CO release was monitored using the myoglobin assay ($t_{½}$ = 2773 s, 60 µM) at 345 nm. The CORM was incubated with HeLa cells and imaging was carried out using confocal microscopy and fluorescence lifetime imaging microscopy (FLIM). The CORM localised in the mitochondria and lipid-rich areas of the cell. However, blebbing was observed upon illumination for 10 minutes.[12]

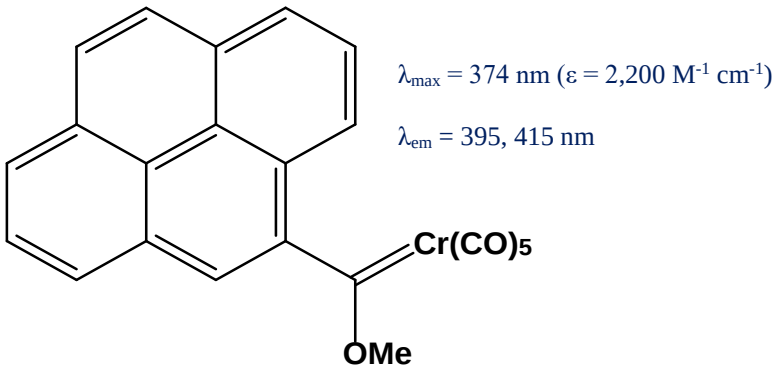

(4)

Figure 5.5 Pyrene - substituted carbene complex (**4**) reported by Arrowsmith *et al.*[12]

The fluorescent metal carbonyl complex, *fac*-[MnBr(CO)$_3$(pbt)], (pbt = 2,2-pyridyl-benzothiazole), was reported by Carrington *et al.*[13] Pbt is a highly fluorescent ligand with emission at 390 nm. Upon excitation at 330 nm, CO is released resulting in a fluorescence enhancement. This complex exhibits excellent anti-cancer properties (CO-induced apoptosis) against human breast cancer cells (MDA-MB-231 cell line). However, UV light is required for photo-activation.

Recent studies have focused on trying to design photoCORMs that may be stimulated with low power visible light. Even though many manganese tricarbonyl complexes are efficient CORMs, they require irradiation at 365 nm or greater to induce CO loss. Therefore, it was necessary to integrate ligands that could extend the CORM absorbance to lower energy.[6,7] Fairlamb and co-workers incorporated a tryptophan (amino acid) component into a Mn(CO)$_3$ system, termed TryptoCORM (**5**), illustrated in Figure 5.6.[14] This CORM released CO at 400 nm (2.0 moles / complex) and less efficiently at 465 nm (1.4 moles / complex). TryptoCORM was tested against *E.coli* W3110 to assess its antibacterial effects. Complete inhibition of bacterial cell growth was observed following irradiation. This is the first time a photoCORM has displayed bactericidal properties.

λ_{max} = 272 nm (ε = 7,505 M^{-1} cm^{-1}),

360 nm (ε = 1,443 M^{-1} cm^{-1}),

λ_{em} = 360 nm (λ_{exc} = 272 nm)

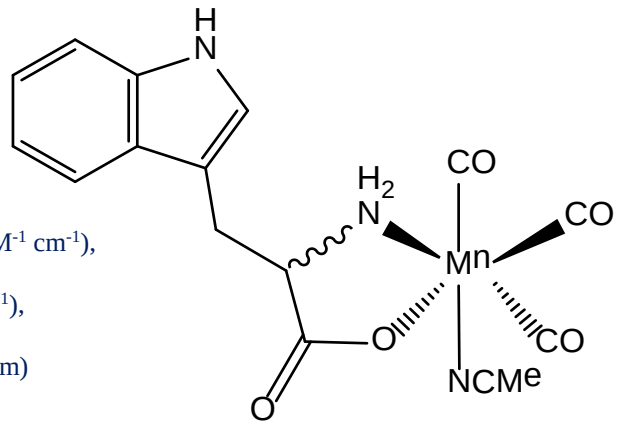

(**5**)

Figure 5.6 Structural representation of TryptoCORM (**5**).[14]

The development of organic based CORMs was reported by Antony *et al.* who showed that a fluorescein xanthene-9-carboxylic acid derivative (**6**), Figure 5.7, was an efficient metal free photoCORM when irradiated at 500 nm.[15] Peng *et al.* also designed a fluorescent metal free photoCORM based on a micelle encapsulated unsaturated 1, 2-

diketone (**7**) which released CO at 470 nm.[16] The cellular location of these systems can be tracked by fluorescence imaging microscopy.

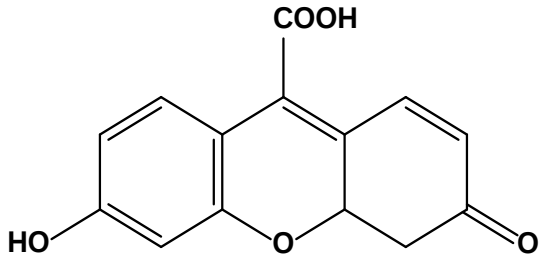

(6)

λ_{max} = 488 nm

λ_{em} = 532 nm, Φ_{fl} = 0.39

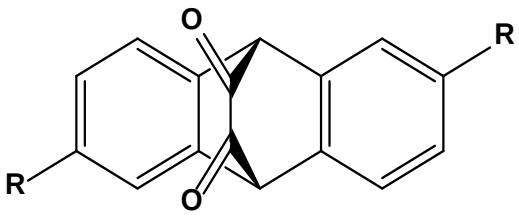

(7)

λ_{max} = 465 nm

Figure 5.7 Structure of the metal free CORMs, a fluorescein xanthene-9-carboxylic acid (**6**) and an unsaturated 1, 2-diketone (**7**).[15,16]

Very recently, photo-induced CO release was investigated from three half-sandwich iron (II) complexes, Fe (η^5-Cp)(*cis*-CO)$_2$X where Cp = cyclopentadiene and X = Cl (**8**), Br (**9**), I, (**10**) displayed in Figure 5.8.[17] The CO releasing behaviour was investigated using three types of light source, blue (λ = 470 - 475 nm), green (λ = 492 - 577 nm) and red (λ = 622 - 770 nm) in neat DMSO. Blue light was the most efficient source of photoinduced CO release, with red light being the least efficient. This was due to the very low absorption properties of the complexes in the red region of the spectrum. The results determined that the halide attached to the complex directly affected its CO releasing ability. Using blue and green light respectively, the efficiency of CO release increased upon substitution of the halide group as follows Cl > Br > I. For use in clinical applications, it is necessary to investigate the CO releasing ability in biocompatible solvents. Consequently, CO release was assessed by Liu and co-workers, in a mix of DMSO / PBS. Only complex (**9**) was examined under these conditions using one source of irradiation, blue light. CO release was monitored by IR spectroscopy.[17]

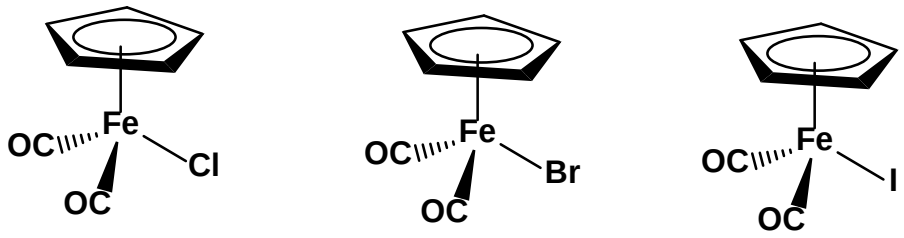

(8) **(9)** **(10)**

Figure 5.8 Structural representations of the three half-sandwich iron (II) carbonyl complexes.[17]

Many significant contributions to the area of photoCORMs have been developed by Mascharak and co-workers. This group has focused on photoinduced CO release initiated by low power visible light. Investigations into the characteristics of various ligand frameworks that could introduce a bathochromic shift of the λ_{max} of the CORM towards the visible region were conducted by introducing unsaturation and conjugation into the CORM sphere.[18,19,20] Two manganese complexes, $[MnBr(azpy)(CO)_3]$ and $[Mn(azpy)(CO)_3(PPh_3)]ClO_4$ where, azpy = 2-phenylazopyridine (**11**) (Figure 5.9) released CO upon irradiation at 520 nm in an acetonitrile : water (20 : 80) mix.[21] Although the absorbance of some new potential photoCORMs e.g. (**11**), has been red shifted, it is imperative that excitation at longer wavelengths leads to CO release in biocompatible solvents. Efficient CO release and photo-toxicity was displayed towards the malignant cell lines, HeLa (cervical) and MDA-MB-231 (breast), by the manganese complexes, $[MnBr(azpy)(CO)_3]$ and $[Mn(azpy)(CO)_3(PPh_3)]ClO_4$. For this reason the rhenium analogues, $[ReBr(azpy)(CO)_3]$ and $[Re(azpy)(CO)_3(PPh_3)]ClO_4$ were prepared (Figure 5.9).[21] Despite the presence of an absorbance band at 530 nm ($\varepsilon = 4{,}600$ $M^{-1}cm^{-1}$) for $[ReBr(azpy)(CO)_3]$, no photo-activated CO release was observed using visible light.[18] More recently, the same group reported another range of manganese carbonyls, $[MnBr\text{-}(CO)_3(BIAN)]$ and $[MnBr\text{-}(CO)_3(MIAN)]$ where BIAN = bis(4-chlorophenylimino)acenaphthene (**12**) and MIAN = 2-[(4-chlorophenyl)imino]acenaphthylen-1-one (**13**), Figure 5.9, with maximum absorbance bands at λ_{max} = 570 and 630 nm respectively. Again, CO release is reported at $\lambda \geq$ 520 nm in organic solvents, CH_2Cl_2 and CH_3CN. Even though $[MnBr\text{-}(CO)_3(MIAN)]$ has a more red shifted photo-band in comparison to $[MnBr\text{-}(CO)_3(BIAN)]$, solubility issues occur in CH_3CN and DMSO which restricts biological studies. $[MnBr\text{-}(CO)_3(BIAN]$ has

a very high quantum yield value for CO loss of 0.70 ± 2 in acetonitrile (λ_{exc} = 545 nm) and "good stability" in a water / DMSO mixture (90 : 10 v/v), although experiments were not conducted in this media. Interestingly, these complexes release CO in the solid state upon photo-illumination which was confirmed by microscopy which monitored a single crystal of the complex in Paratone oil. Upon irradiation, CO release was observed in the form of bubbles which appeared from the crystal under the oil. This was the first report of CO release from the solid state of a complex using visible light.[19]

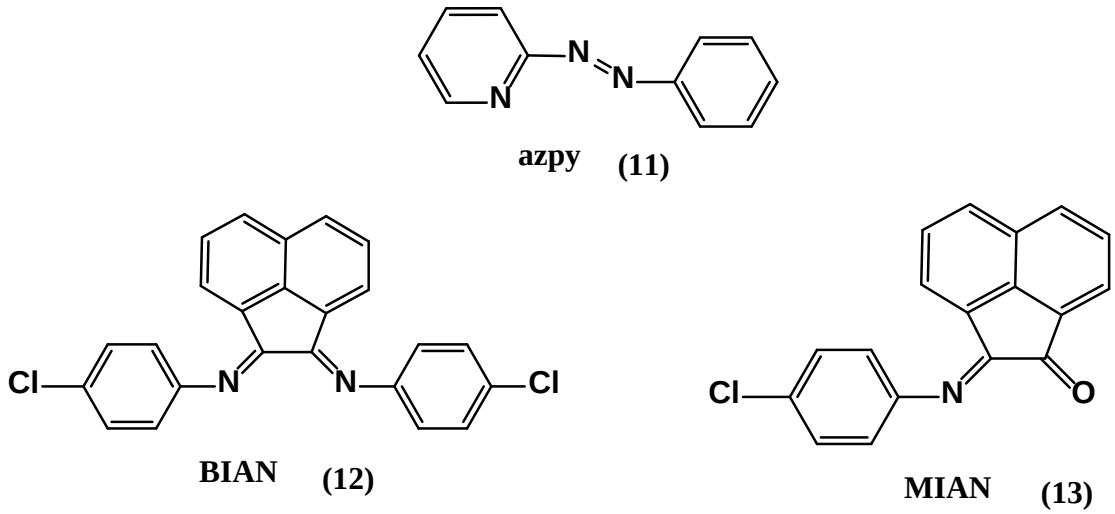

Figure 5.9 Structures of 2-phenylazopyridine (azpy (**11**)), bis (4-chlorophenylimino) acenaphthene (BIAN (**12**)) and 2-[(4-chlorophenyl)imino]acenaphthylen-1-one (MIAN (**13**)), ligands attached to $Mn(CO)_3$ and $Re(CO)_3$ reported by the Mascharak group.[19,21]

Recently, Ford and co-workers identified the first delivery strategy based on the photochemical uncaging of CO using NIR illumination. A water soluble nano-carrier was developed for photoCO release by incorporating a single unit NIR-to-visible upconverting nanoparticle. An active photoCORM, $[Mn(bpy)(CO)_2(PPh_3)_2]^+$ was then encapsulated into a phospholipid functionalised biocompatible polymer (PEG), Figure 5.10. The system releases CO when irradiated at 980 nm (monitored in PBS using gas chromatography).[22]

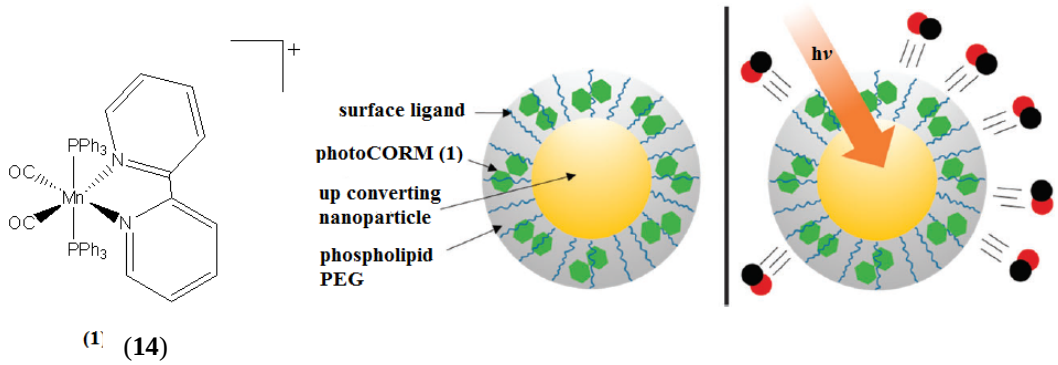

(1) **(14)**

λ_{max} = 400 nm (ε = 5,400 $M^{-1}cm^{-1}$)

Figure 5.10 (**14**) corresponds to the structure of the photoCORM ($[Mn(bpy)(CO)_2(PPh_3)_2]^+$). The representation in the middle shows the water-soluble nanocarrier developed for the photochemical uncaging of CO. The representation (right) shows that when irradiated at 980 nm (red arrow), up-converted visible range emission from the nanoparticle is re-absorbed by the photoCORM, resulting in CO dissociation.[22]

The choice of the ancillary ligands of a CORM is of utmost importance. In order to design an "ideal" photoCORM, certain criteria need to be fulfilled for potential use in future applications. As previously stated, CO release should occur using low energy photons and the location of the CORM should be easily identified *in vivo*. To combat these challenges, the focus of this chapter was to design and synthesise a range of novel photoCORMs. The CORMs are comprised of a well-known biocompatible dye, 4,4-difluoro-4-bora-3a,4a-diaza-s-indacene (BODIPY) derivative and a metal carbonyl moiety.

BODIPY derivatives were first reported by Treibs and Kreuzer in 1968 and are a very interesting class of fluorophore.[23] They are chemically and photochemically robust, relatively stable to physiological conditions, absorb strongly in the UV-vis region due to π- conjugation, with a high extinction coefficient and are particularly emissive with high quantum yields. The structure of BODIPY molecules can be readily modified which allows their photophysical properties to be exploited. Consequently, they have a wide range of applications, for example, as photosensitisers, sensors, and in photodynamic therapy and imaging.[24-26] The use of such dyes have distinct advantages in labelling and bio-imaging of living systems.[25,27] Longer wavelength irradiation would generate minimal biological photo-damage and deeper tissue penetration would be possible in comparison to shorter wavelengths.[28]

The BODIPY core and numbering system is displayed in Figure 5.11. The structure is known to be rigid across the methine bridge which restricts flexibility resulting in high fluorescent quantum yields which originate from the dipyrromethene-boron difluoride unit. Delocalisation of π electrons along the organic backbone can be tuned by modifying the core structure.[28]

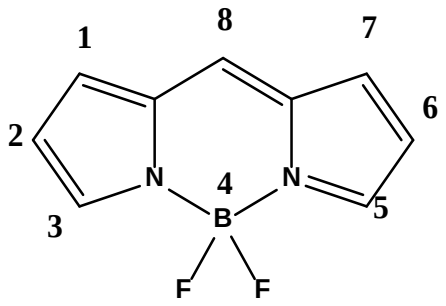

Figure 5.11 Representation of the BODIPY "core" unit and numbering system.[28]

The optical properties of BODIPYs are very interesting. They exhibit a strong absorbance at approximately 500 nm with a high molar absorptivity (ε = 40,000 - 200,000 $M^{-1}cm^{-1}$).[29] This peak is due to a $S_0 \rightarrow S_1$ (π-π*) electronic transition.[30] A shoulder is generally observed at the high energy side of the λ_{max} absorbance band at ~ 480 nm ($S_0 \rightarrow S_1$ (π-π*) vibrational transition). A weaker, broad transition is also present at ~ 370 nm and is assigned to a $S_0 \rightarrow S_2$ (π-π*) transition occurring within the dipyrromethene ligand. BODIPY derivatives have a sharp, intense emission in the yellow / green region of the spectrum and exhibit a reasonably small Stokes shift,~600 cm^{-1} which means that there is only a small difference in the excitation and emission energies.[29] Interestingly, minor structural changes in the BODIPY framework, notably influences their unique photophysical properties. It is therefore possible to tune the optical properties by introducing various substituents on the BODIPY core.

In terms of the synthesis of BODIPY compounds, a wide range have been reported by Ziessel and co-workers (Figure 5.12).[29] Compounds (**15**) and (**16**) were synthesised with very low yields (9 - 13 %) due to the likelihood that the starting materials or intermediates are unstable under the reaction conditions. An alkynyl connector was incorporated to the BODIPY unit to promote electronic communication. As well as the ethynyl-bridge, a phenyl spacer was introduced into the framework to increase conjugation and extend the absorbance spectra (**17-19**). The optical properties of each of the compounds were explored. Typically, a strong peak was observed at ~ 528 nm which is assigned to a $S_0 \rightarrow S_1$ (π-π*) transition. A weaker, broad transition is also present

at ~375 nm ($S_0 \rightarrow S_2$ (π-π^*) transition) within the dipyrromethene ligand. There is very little difference (≤ 4 cm^{-1}) in the λ_{max} absorbance band between the five compounds. However, the extinction coefficient largely depends on the number of BODIPY appendages and the orientation in which they are attached to the BODIPY core. When two BODIPY units are present, for example in compound (**19**), a very large extinction coefficient $\varepsilon = 195{,}000$ $M^{-1}cm^{-1}$ is exhibited. The lowest observed was for (**15**) where $\varepsilon = 59{,}000$ $M^{-1}cm^{-1}$. A band appears at ~320 nm which is attributed to the *n*-π^* transitions based on the polypyridine functionality (in this case bipyridine). An absorption band at ~380 nm arises due to the π-π^* transitions from the alkyne subunit. The complexes presented in Figure 5.12 display strong photoluminescence. The highest quantum yield value was observed for (**18**), $\Phi_{fl} = 0.89$ at room temperature. Small Stokes shift values (600 cm^{-1}) and lifetimes of ≤ 4 ns are in agreement with a singlet emitting state.[29] A modified version of (**18**) will be discussed further in this chapter.

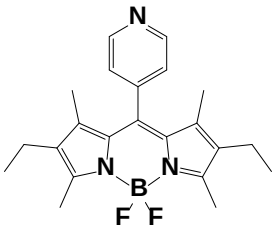

(15)

λ_{max} = 525 nm

(ε = 59,000 M^{-1} cm^{-1})

λ_{em} = 547 nm, Φ_{fl} = 0.50

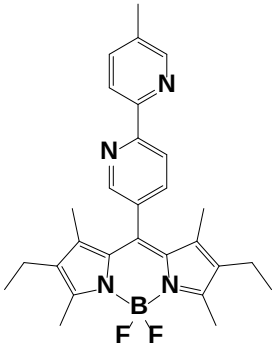

(16)

λ_{max} = 529 nm

(ε = 83,000 M^{-1} cm^{-1})

λ_{em} = 546 nm, Φ_{fl} = 0.69

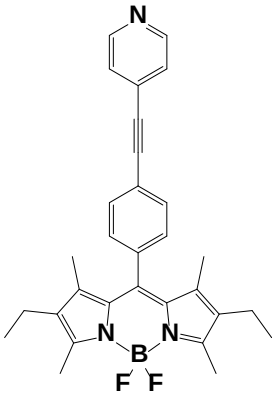

(17)

λ_{max} = 527 nm

(ε = 102,000 M^{-1} cm^{-1})

λ_{em} = 544 nm, Φ_{fl} = 0.83

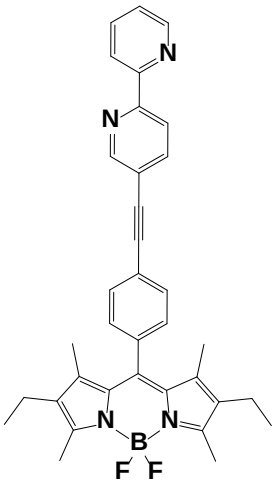

(18)

λ_{max} = 527 nm (ε = 67,000 M^{-1} cm^{-1})

λ_{em} = 545 nm, Φ_{fl} = 0.89

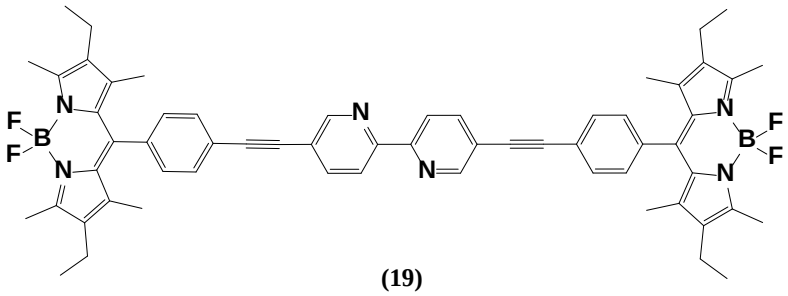

(19)

λ_{max} = 527 nm (ε = 195,000 M^{-1} cm^{-1})

λ_{em} = 544 nm, Φ_{fl} = 0.70

Figure 5.12 Structures of a range of BODIPY compounds reported by Ziessel and co-workers, spectroscopic data is reported in CH_2Cl_2.[29]

It is well known that thiophene is an efficient π-conjugation linker. Therefore, the incorporation of a thiophene subunit into the BODIPY framework renders a

bathochromic shift.[30-32] The UV-vis absorbance becomes red shifted due to a lower HOMO-LUMO gap which has been supported by density functional theory calculations.[30] Thiophene is incorporated into one of the target BODIPY compounds in this chapter due to its ability to extend the absorbance spectra of BODIPY compounds towards the visible region.

Some previously reported examples of BODIPY compounds containing thiophene, substituted at the *meso* position, namely (**20**), (**21**) and the phenyl spaced compound corresponding to (**21**), compound (**22**) are displayed in Figure 5.13.

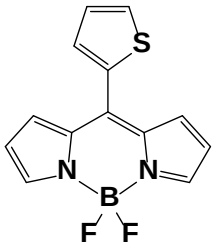

(20)

λ_{max} = 510 nm (ε = 54,000 M^{-1} cm^{-1})

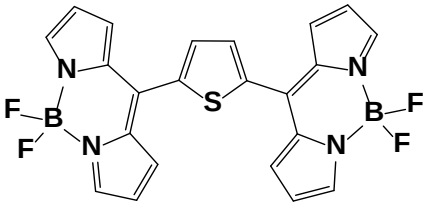

(21)

λ_{max} = 520 nm

λ_{em} = 521 nm, Φ_{fl} = 0.01

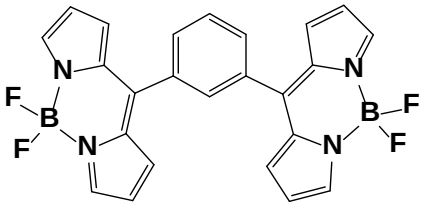

(22)

λ_{max} = 502 nm

λ_{em} = 525 nm, Φ_{fl} = 0.04

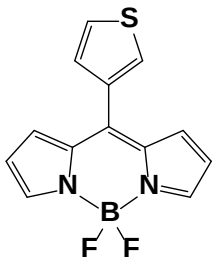

(23)

λ_{max} = 502 nm (ε = 60,000 M^{-1} cm^{-1})

λ_{em} = 522 nm, Φ_{fl} = 0.06

Figure 5.13 BODIPY compounds consisting of a thiophene substituent at the *meso* position (**20**) and (**23**) reported by Churchill and co-workers and (**21**) and (**22**) were detailed by Gupta and co-workers.[30,31]

Although the introduction of thienyl functionality causes a red shift in the spectrum, fluorescent quantum yields of thiophene BODIPY compounds are lower than their

corresponding phenyl counterparts which may be linked to the electron donating ability of the sulphur atom found in the thiophene bridge. For example, compound (**21**), Φ_{fl} = 0.01, has a lower fluorescent quantum yield value than compound (**22**), Φ_{fl} = 0.04 (in CH_2Cl_2).[30,31] Interestingly, the photophysical properties were significantly altered when the attachment of thiophene at the *meso* position was changed from the *2*- (**20**) to the *3*- (**23**) position. The absorption and emission spectra experienced a hypsochromic shift (λ_{max} shifted from from 510 nm to 502 nm in CH_2Cl_2) which suggests that there is a stronger interaction between the substituent at the *meso* position and the BODIPY unit when the heteratom (sulphur) is at the *2*- position.[31] When the absorbance spectra of (**22**) *vs.* (**21**) are compared, there is a shift in the λ_{max} from 502 nm to 520 nm (in CH_2Cl_2) from the phenyl containing compound (**22**) to the thiophene based BODIPY (**21**), indicating the bathochromic effect exerted by thiophene. Therefore, since the main aim of this study is to extend the UV-vis absorbance towards the visible region, it would be most beneficial to incorporate a thiophene unit substituted at the *2*- position.

Recently, fluorescent probes have been developed for the detection of CO. Fluorescence imaging and sensing is commonly used to probe small signalling biomolecules such as H_2O_2, NO and H_2S. Two types of fluorescent probes were identified, a small molecule probe and a biosensor.[27,33] Although distinct in nature, these fluorescent sensors operate in a similar manner by exploiting the unique binding affinity of CO to transition metals.

Chang and co-workers reported a non-toxic, biocompatible, cyclometallated BODIPY based species (COP-1) (**24**) Figure 5.14.[27] Fluorescent properties and CO reactivity were analysed in an aqueous solution buffered to physiological pH (DMSO / PBS solution). The BODIPY probe is weakly emissive as it contains palladium which diminishes the fluorescence of the BODIPY unit due to the heavy-atom effect (λ_{em} = 503 nm, Φ_{fl} = 0.01 in DMSO / PBS). Upon interaction with CO (on addition of CORM-3 at 37 °C), a ten-fold enhancement of fluorescence was observed (detection limit 1 µM), see Figure 5.14. COP-1 selectively promoted the greatest turn-on response for CO in comparison to other biomolecules including H_2O_2, hypochlorite (OCl^-), superoxide ($O_2^{\bullet-}$), H_2S, peroxynitrite ($ONOO^-$), tert-butyl hydroperoxide (tBuOOH) and NO. Confocal microscopy confirmed that COP-1 is capable of the selective tracking and imaging of CO in living cells. However, the fate of the by-products remains elusive in addition to biological effects such as membrane permeability and cell distribution.[34]

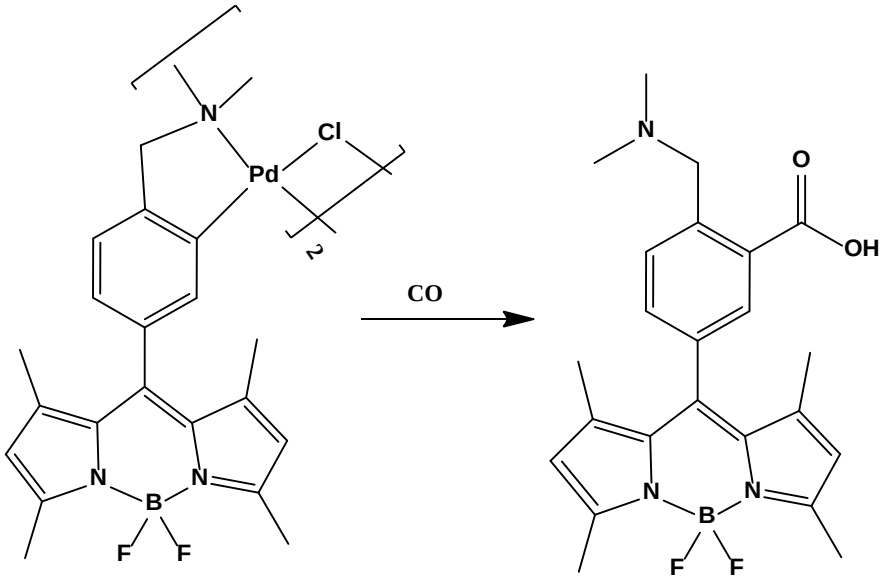

(**24**) (**25**)

λ_{em} = 503 nm, Φ_{fl} = 0.01

λ_{max} = 499 nm (ε = 23,000 M^{-1} cm^{-1})

λ_{em} = 507 nm, Φ_{fl} = 0.44

Figure 5.14 Structural representation of COP-1 (**24**) and the resulting species formed upon interaction with CO (**25**).[27]

Very recently, this probe has been employed by Bernardes and co-workers to assess CO release from $[Ru(CO)_3Cl_2(NAC)]$ (where NAC = *N*-acetyl cysteine), (**26**) at 37 °C using confocal microscopy, Figure 5.15.[35] The Bernardes group went on to study *cis*-$[Ru(CO)_2(H_2O)_4]^{2+}$ using the COP-1 probe, which released CO in live cells upon incubation at 37 °C.

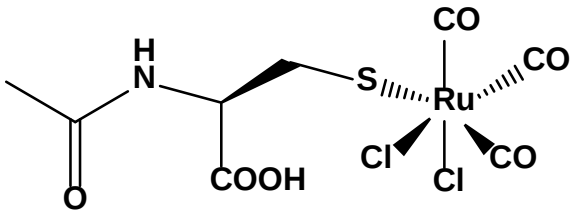

(26)

Figure 5.15 Structural representation of $[Ru(CO)_3Cl_2(NAC)]$ where NAC = *N*-acetyl cysteine (**26**).[35]

Schatzschneider and co-workers also used this probe for the *in vitro* detection of CO release from a modified manganese tricarbonyl complex, [Mn [Mn(bpea(N=CHC$_6$H$_4$R))(CO)$_3$]PF$_6$ (**27**) and [Mn(bpea(NHCH$_2$C$_6$H$_4$R))(CO)$_3$]PF$_6$ (**28**) based on the tridentate bis(pyrazolyl)ethylamine (bpea) ligand following irradiation at 365 nm in human vein endothelial cells (HUVECs), Figure 5.16.[36]

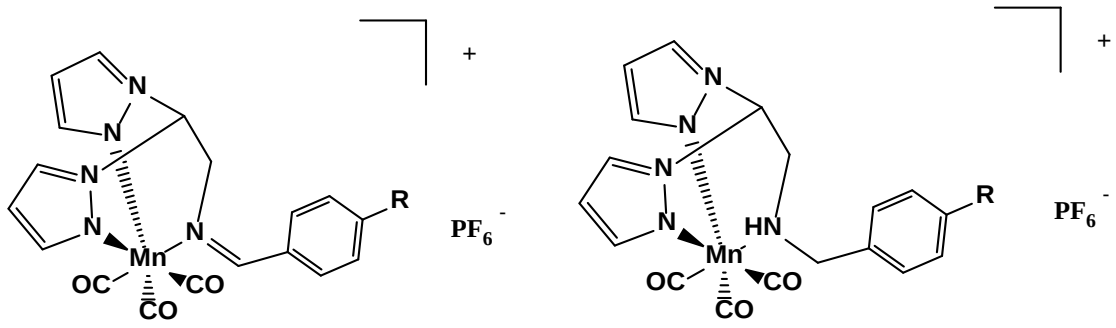

(27) **(28)**

λ_{max} = 341 - 348 nm (ε =~4,000 M^{-1} cm^{-1}) λ_{max} = 355 - 356 nm (ε =~2,000 M^{-1} cm^{1})

Figure 5.16 Structural representation of [Mn(bpea(N=CHC$_6$H$_4$R))(CO)$_3$]PF$_6$ (**27**) and [Mn(bpea(NHCH$_2$C$_6$H$_4$R))(CO)$_3$]PF$_6$ (**28**) where R = H, I.[36]

The studies carried out on COP-1 confirm that the Pd-BODIPY complex is not only biocompatible in cells but also serves as an excellent probe for CO release. The recent interest by the Bernardes and Schatzschneider groups further exemplifies its significance in the field.

Ideally, there are three main strategies to improve the design of photoCORMs; 1) Shift the UV-vis absorbance maximum to lower energy to minimise tissue damage, 2) attach an organic dye or photosensitiser to the metal carbonyl moiety to allow for tracking of the cellular localisation of the CORM and 3) where necessary, use two-photon absorption to induce CO release to avoid using high energy excitation.[2,5] This chapter focuses on using the BODIPY functionality to extend the absorbance spectra of metal carbonyl complexes to lower energy by integrating different substituents onto the BODIPY core. Firstly, a novel class of BODIPY metal carbonyl complexes were synthesised with ligands depicted in Figure 5.17. A range of substituents (H, C$_2$H$_5$ and I) were functionalised at the pyrrole rings of the dipyrromethene moiety to assess their impact on the UV-vis absorbance spectra of the compounds and subsequent

photochemical CO loss. The free BODIPY ligands have previously been synthesised and their photophysical properties have been reported by Banfi *et al*.[37] The 3-pyridyl BODIPY derivatives were chosen so that a metal carbonyl unit, in this case $M(CO)_5$ where M = Cr or W could be attached directly to the BODIPY molecule *via* the nitrogen atom of the pyridyl ring.

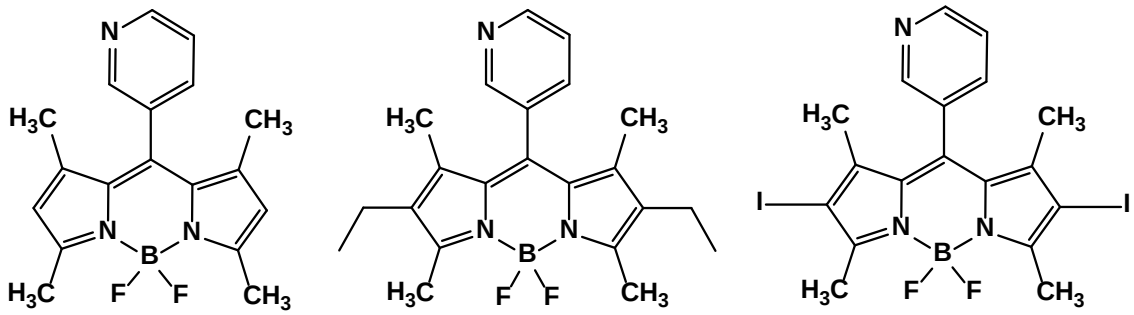

H-BODIPY **Ethyl-BODIPY** **Iodo-BODIPY**

Figure 5.17 2,6 - di-substituted BODIPY compounds, abbreviated to H-BODIPY, Ethyl-BODIPY and Iodo-BODIPY (from left to right respectively).[37]

Ideally, the UV-vis absorbance spectra of a CORM should be extended as close as possible to therapeutic window i.e. the low energy, red region of the spectrum for potential use as a phototherapeutic agent, in this case a CO delivery system. Therefore, to further increase π-conjugation, a BODIPY metal carbonyl complex incorporating a thiophene bridge, alkynyl spacer and bipyridine unit was designed and synthesised (Figure 5.18).

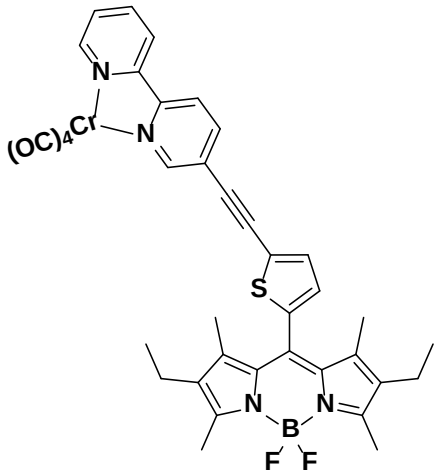

Figure 5.18 Structural representation of 1,3,5,7-tetramethyl-2,6-diethyl-8-(5-thiophene-2-ethynyl-2,2´-bipyridine)-4,4-difluoro-4-bora-3a,4a-diaza-indacene $Cr(CO)_4$, abbreviated to ThioBipyBODIPY $Cr(CO)_4$.

The photoinduced CO release of these novel BODIPY metal carbonyl complexes is reported in a biocompatible solvent commonly used in cellular assays which is paramount to future biological applications. Instead of using the BODIPY derivatives as probes for CO detection as has been previously described, the BODIPY moiety is incorporated to the CORM sphere and serves as a reporter group. The unique emission profiles of the BODIPY metal carbonyl complexes are exploited and allow for the indication of CO release. The photochemical and photophysical properties are explored prior to and post CO release. This work was carried out with the future aim of carrying out bio-imaging studies in cells using fluorescence microscopy.

5.2 Experimental

5.2.1 Materials

All reactions were carried out under an atmosphere of nitrogen using Schlenk techniques. All solvents were supplied by the Aldrich Chemicals Company. Dichloromethane, ethyl acetate, hexane and pentane were dried over $MgSO_4$ prior to use. Anhydrous solvents were used in metal carbonyl reactions (dichloromethane, tetrahydrofuran, ethanol, diisopropylamine, methanol, triethylamine and toluene). All solvents used for UV-vis, IR, emission, lifetimes and cyclic voltammetry (CV) experiments were of spectrophotometric grade and were used without further purification. Column chromatography was carried out using neutral aluminium oxide and silica gel, Merck (used as received). All mobile phases for column chromatography were dried over $MgSO_4$ before use. Cyclic voltammograms (CVs) were recorded in anhydrous acetonitrile (Aldrich Chemical Co.) with tetrabutylammonium hexafluorophosphate ($TBAPF_6$), (Aldrich Chemical Co.) as a supporting electrolyte. Argon gas was used to degas samples for cyclic voltammetry (obtained from BOC Ltd).

5.2.2 Equipment

Microwave synthesis was carried out using an Anton Paar Monowave 300 Microwave Reactor with IR temperature sensor. NMR, IR, UV, CV and GC measurements were carried out as previously described in Chapter 2. Cyclic voltammetry experiments were carried out in a sealed two-necked v-shaped cell. The concentration of the samples was 1 mM in anhydrous acetonitrile (CH_3CN) using 0.1 M tetrabutylammonium hexafluorophosphate ($TBAPF_6$) as the supporting electrolyte. Electrochemical experiments were carried out by a fellow group member, Dr. Diana Hidalgo. They were conducted using a CH Instruments 750C potentiostat in a three electrode configuration. Glassy carbon was used as the working electrode (0.07 cm^2), a Pt wire was used as the counter electrode and Ag/AgCl filled with (1 M $TBAPF_6$ and 0.1 M $AgNO_3$ in CH_2Cl_2) was used as the reference electrode. The cyclic voltammograms were recorded at a scan rate of 0.1 V s^{-1} in the potential window of CH_3CN (0 to -2) V for reduction processes. Samples were purged with argon for 20 min and experiments were performed at room

temperature (20 °C) in the absence of light. Emission spectra (accuracy ± 5 nm) were recorded using a LS50B luminescence spectrophotometer equipped with a red sensitive Hammatsu R928 PMT detector, interfaced with Elonex PC466 employing Perkin Elmer FL WinLab custom built software. Fluorescent quantum yield measurements were carried out in spectrophotometric grade acetonitrile, as previously described, using Ethyl-BODIPY as a reference which has a known fluorescent quantum yield value of 0.42 in acetonitrile (λ_{exc} = 490 nm).[37] Lifetimes were determined using an Edinburgh Analytical Instruments cooler controller with an EPLED-360 picosecond pulsed light emitting diode (λ = 360 ± 10 nm) interfaced to a CD900 TAC photon counter. Mass spectrometry measurements were performed at Trinity College by Dr. Gary Hessman under the following conditions. MALDI-TOF spectra were acquired using a Waters MALDI Q-TOF Premier. The instrument was operated in positive or negative mode as required using a nitrogen laser at 337 nm. Samples were run using DCTB (trans-2-[3-4-tert-butylphenyl)-2-methyl-2-propenylidene] malononitrile) as a matrix. 1 ml of a 5 : 1 matrix / sample mixture was loaded onto a MALDI plate and allowed to air dry. The instrument was calibrated using PEG. The internal lock mass used was $[Glu]^+$ Fibrinopetide B. MassLynx 4.1 software was used to carry out the analysis. ESI mass spectra were acquired using a Micromass TOF mass spectrometer, interfaced to a Waters 2690 HPLC. The instrument was operated in positive or negative mode as required. Leucine Enkephalin was used as an internal lock mass. Masses were recorded over the range 100 - 1000 *m/z*. Operating conditions were as follows: ESI capillary voltage 2500 V, cone voltage 25 V, desolvation temperature 300 °C, source temperature 100 °C. MassLynx 4.0 software was used to carry out the analysis.

5.2.3 Steady State Photolysis

IR spectra were measured in a liquid Omni cell containing two NaCl plates, using a Perkin Elmer spectrophotometer. The liquid cell containing the complex was irradiated at different wavelengths using 528, 470 and 355 nm LED sources. The path length remained constant eliminating any possible variables.

5.2.4 Photochemical CO Release

Photochemical CO release was monitored in 2 ml headspace vials and the amount of CO released was quantified using gas chromatography. A solvent mixture of 5 % fetal bovine serum (FBS) in phenol red free Roswell Park Memorial Institute (RPMI) media-1640 (supplied by Aldrich Chemicals Company) was used for CO release experiments. The CORM was dissolved in DMSO to give a 10 mM stock solution. For the experiments carried out at 525 nm irradiation, 5 µL of the stock solution was added (*via* auto-pipette) to the 5 % FBS / RPMI media (final volume 2 ml). The final concentration of the CORM under analysis was 25 µM (0.25 % DMSO / RPMI media). For photochemical CO releasing experiments performed using 355 nm excitation, it was necessary to increase the concentration two fold as the UV-vis absorbance of the CORMs was weaker at this wavelength. In this case, a CORM concentration of 50 µM (0.50 % DMSO / (RPMI/FBS) media) was used. For experiments performed using 620 nm excitation, the stock solution concentration was doubled (20 mM). An overall concentration of 100 µM was used since the absorbance at 620 nm is weaker than at 525 and 355 nm. The percentage of DMSO per media was 0.5 %. Experiments were performed in degassed and non-degassed samples with similar results obtained in both cases. Sample vials were sealed prior to irradiation. The headspace vials were placed in front of either 525, 355 or 620 nm LED arrays and at an equal distance away from the LED. The temperature was monitored to ensure no thermal effects arose. Control experiments were performed in the absence of light. CO release was detected using a Shimadzu GC-2010 Plus unit (Lab Solutions version 5.57 software) with a dielectric barrier discharge ionisation detector (BID) and a ShinCarbon micropacked column with 0.53 mm internal diameter. 1000 µL was extracted from a headspace vial using a gas-tight syringe over five time intervals of 0, 30, 60, 120 and 180 minutes. The extracted gas was injected onto the column and the vial was discarded after each time point. Experiments were repeated in duplicate. Data was fitted using GraphPad Prism software.

5.2.5 Synthesis

5.2.5.1 Synthesis of 1,3,5,7-tetramethyl-8-(3-pyridyl)-4,4'-difluoro-4-bora-3a,4a-diaza-indacene (H-BODIPY)

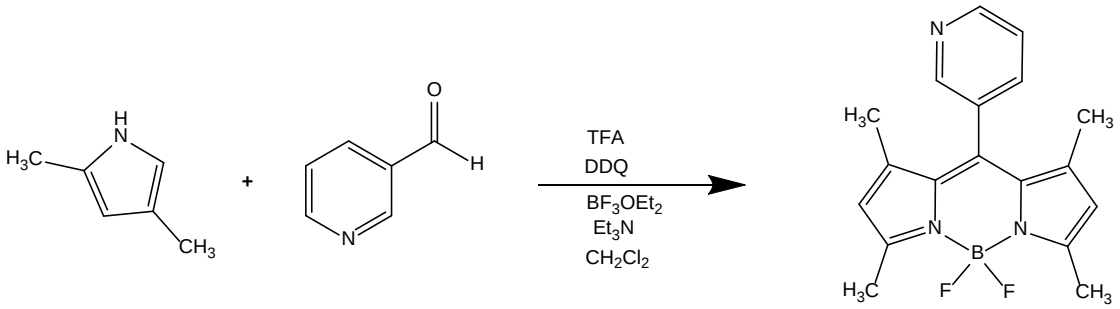

Reaction 5.1 The synthesis of 1,3,5,7-tetramethyl-8-(3-pyridyl)-4,4'-difluoro-4-bora-3a,4a-diaza-indacene (H-BODIPY).

The synthesis of H-BODIPY was carried out as previously reported with some modifications.[37] 25 ml of anhydrous CH_2Cl_2 was added to a clean dry round bottomed flask. This was purged with N_2 for 15 minutes. 0.12 ml (1.3 mmol) of 3-pyridine carboxaldehyde and 0.27 ml (2.6 mmol) of 2, 4 dimethylpyrrole were added to the reaction vessel followed by 20 µL (0.26 mmol) of trifluoroacetic acid (TFA). The reaction vessel was sealed and allowed to stir overnight under inert conditions in the absence of light. 0.40 g (1.76 mmol) of 2,3-dichloro-5,6-dicyano-1,4-benzoquinone (DDQ) was added and the reaction proceeded for a further 4 hours. Next, 1.68 ml (13.6 mmol) of boron difluoride diethyl etherate was added, followed in quick succession by 1.11 ml (7.96 mmol) of triethylamine (TEA) and the reaction proceeded overnight. The resulting solution was washed with a saturated solution of sodium bicarbonate. The organic layer was collected and dried over $MgSO_4$. This was removed using gravity filtration. Purification was carried out by column chromatography using silica and hexane : ethyl acetate (50 : 50) as the mobile phase. The spectroscopic data are in agreement with reported data.[37]

Appearance: orange / yellow solid.

% Yield: 77 mg, 0.25 mmol, 19 % yield.

^{1}H NMR: (400 MHz, $CDCl_3$) 1.39 (s, 6H, 2 × CH_3), 2.49 (s, 6H, 2 × CH_3), 6.02 (s, 2H), 7.48 (dd, 1H), 7.67 (dt, 1H), 8.58 (d, 1H), 8.76 (dd, 1H) ppm.

5.2.5.2 Synthesis of 2,6-diethyl-1,3,5,7-tetramethyl-8-(3-pyridyl)-4,4'-difluoro-4-bora-3a,4a-diaza-indacene (Ethyl-BODIPY)

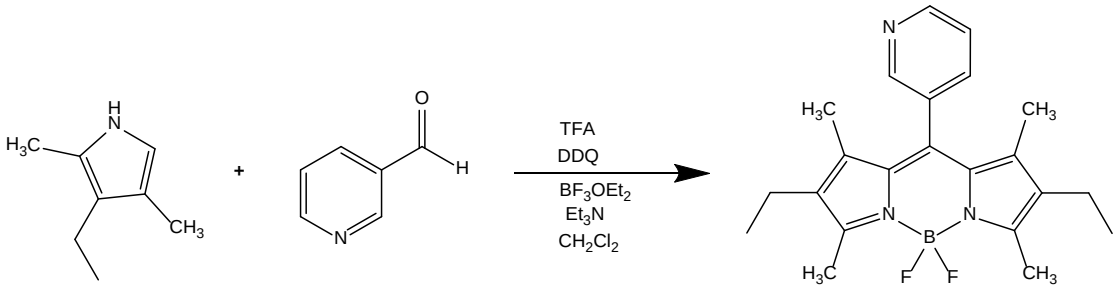

Reaction 5.2 The synthesis of 2,6-diethyl-1,3,5,7-tetramethyl-8-(3-pyridyl)-4,4'-difluoro-4-bora-3a,4a-diaza-indacene (Ethyl-BODIPY).

The synthesis and purification of this compound were carried out as described in section **5.2.5.1**.[37] The spectroscopic data are in agreement with reported data.[37]

Appearance: red flaky solid.

% Yield: 81 mg, 0.22 mmol, 17 % yield.

^{1}H NMR: (400 MHz, $CDCl_3$) 0.99 (t, 6H, 2 × CH_3), 1.29 (s, 6H, 2 × CH_3), 2.30 (q, 4H, 2 × CH_2), 2.55 (s, 6H, 2 × CH_3), 7.46 (dd, 1H), 7.65 (dt, 1H), 8.57 (d, 1H), 8.76 (dd, 1H) ppm.

5.2.5.3 Synthesis of 2,6-diiodo-1,3,5,7-tetramethyl-8-(3-pyridyl)-4,4'-difluoro-4-bora-3a,4a-diaza-indacene (Iodo-BODIPY)

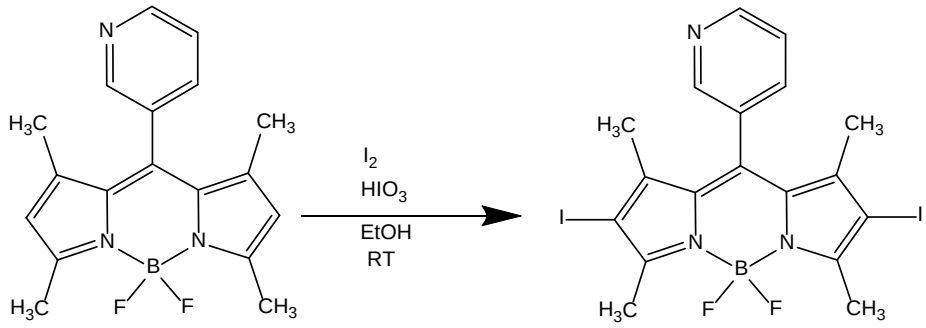

Reaction 5.3 The synthesis of 2,6-diiodo-1,3,5,7-tetramethyl-8-(3-pyridyl)-4,4'-difluoro-4-bora-3a,4a-diaza-indacene (Iodo-BODIPY).

The synthesis of Iodo-BODIPY was carried out as previously reported with some modifications.[37] 15 ml of anhydrous EtOH was added to a clean dry round bottomed flask. This was purged with N_2 for 15 minutes. 100 mg (0.32 mmol) of H-BODIPY and 162 mg (0.64 mmol) of iodine (I_2) were added to the reaction vessel followed by 112 mg (0.64 mmol) of iodic acid (HIO_3). The solvent was removed *in vacuo*. Purification was carried out using silica and 80 : 20 chloroform : ethyl acetate. The spectroscopic data are in agreement with reported data.[37]

Appearance: dark red / purple solid.

% Yield: 102 mg, 0.18 mmol, 56 % yield.

^{1}H NMR: (400 MHz, $CDCl_3$) 1.40 (s, 6H, 2 × CH_3), 2.67 (s, 6H, 2 × CH_3), 7.51 (dd, 1H), 7.63 (dt, 1H), 8.56 (dd, 1H), 8.82 (dd, 1H) ppm.

5.2.5.4 Synthesis of $Cr(CO)_5(THF)$

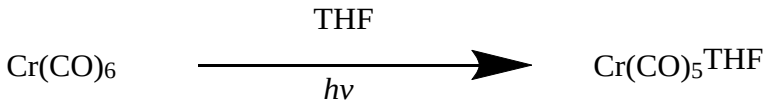

Reaction 5.4 The synthesis of $Cr(CO)_5THF$.

The synthesis $Cr(CO)_5(THF)$ was carried out as previously reported with some modifications.[38] 200 mg (0.9 mmol) of $Cr(CO)_6$ was added to a photochemical reactor containing 200 ml of anhydrous THF under inert conditions. The reaction sample was irradiated for 2 hours using an 80 W Elliptical mercury lamp. The solution changed from a colourless solution to bright yellow. The sample was characterised by IR spectroscopy for the presence of pentacarbonyl bands which agree with reported data.[39]

IR υCO: (THF) 2072, 1937 and 1894 cm^{-1}.

5.2.5.5 Synthesis of $W(CO)_5(THF)$

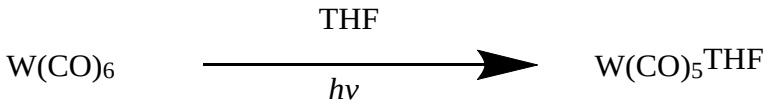

Reaction 5.5 The synthesis of $W(CO)_5THF$.

The synthesis was carried out in the same manner as detailed in section **5.2.5.4** and agrees with reported data.[38,39]

IR υCO: (THF) 2075, 1929 and 1888 cm^{-1}.

5.2.5.6 Synthesis of 1,3,5,7-tetramethyl-8-(3-pyridyl)-4,4'-difluoro-4-bora-3a,4a-diaza-indacene chromium pentacarbonyl (H-BODIPY $Cr(CO)_5$)

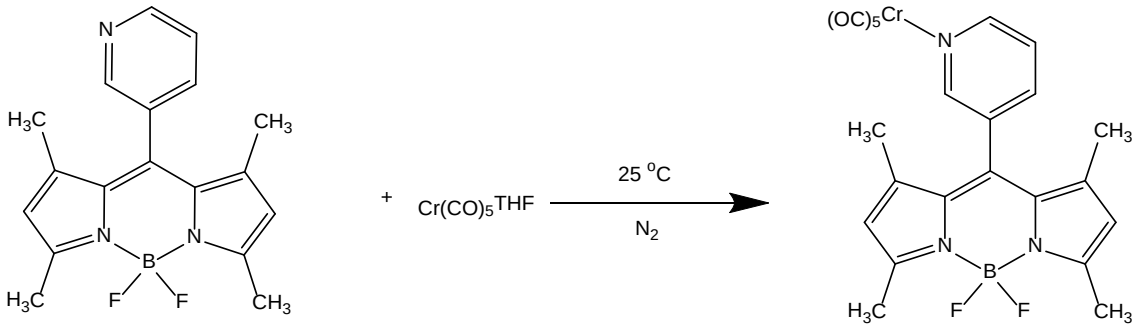

Reaction 5.6 The synthesis of 1,3,5,7-tetramethyl-8-(3-pyridyl)-4,4'-difluoro-4-bora-3a,4a-diaza-indacene chromium pentacarbonyl (H-BODIPY $Cr(CO)_5$).

100 mg (0.31 mmol) of H-BODIPY was added to a clean dry 250 ml round bottomed flask containing an excess (~100 ml) of $Cr(CO)_5THF$ under inert conditions and was allowed to react for 72 hours. The solvent was removed *in vacuo*. Purification was carried out using neutral aluminium oxide and hexane : ethyl acetate (7 : 3).

Appearance: orange / yellow solid.

% Yield: 141 mg, 0.27 mmol, 88 % yield.

^{1}H NMR: (600 MHz, $CDCl_3$) 1.40 (s, 6H, 2 × CH_3), 2.56 (s, 6H, 2 × CH_3), 6.07 (s, 2H), 7.42 (dd, *J* = 8, 5 Hz, 1H), 7.70 (dt, *J* = 8, 2 Hz, 1H), 8.60 (d, *J* = 2 Hz 1H), 8.78 (dd, *J* = 5, 2 Hz, 1H) ppm.

^{13}C NMR: (600 MHz, $CDCl_3$) 14.86, 15.26, 122.55, 125.08, 131.34, 133.01, 134.18, 137.74, 142.33, 154.28, 155.63, 157.64, 214.37, 220.60 ppm.

IR υCO: (CH_3CN) 2071, 1937, and 1895 cm^{-1}.

MS (ESI): $[M-H]^-$ (*m/z*) mass found: 516.0630, mass calculated: 516.0634 for $C_{23}H_{18}BCrF_2N_3O_5$

5.2.5.7 Synthesis of 1,3,5,7-tetramethyl-8-(3-pyridyl)-4,4'-difluoro-4-bora-3a,4a-diaza-indacene tungsten pentacarbonyl (H-BODIPY $W(CO)_5$)

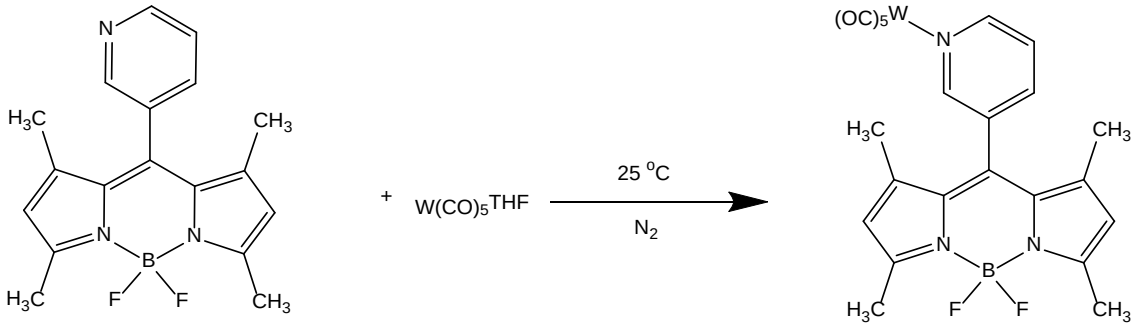

Reaction 5.7 The synthesis of 1,3,5,7-tetramethyl-8-(3-pyridyl)-4,4'-difluoro-4-bora-3a,4a-diaza-indacene tungsten pentacarbonyl (H-BODIPY $W(CO)_5$).

The synthesis and purification were carried out in the same manner as detailed in section **5.2.5.6**. 250 mg (0.77 mmol) of H-BODIPY was reacted with an excess of $W(CO)_5THF$.

Appearance: orange / yellow solid.

% Yield: 328 mg, 0.51 mmol, 66 % yield.

^{1}H NMR: (600 MHz, $CDCl_3$) 1.43 (s, 6H, 2 × CH_3), 2.58 (s, 6H, 2 × CH_3), 6.07 (s, 2H), 7.47 (dd, *J* = 8, 5 Hz, 1H), 7.79 (dt, *J* = 8, 2 Hz, 1H), 8.83 (d, *J* = 2 Hz, 1H), 9.00 (dd, *J* = 5, 2 Hz, 1H) ppm.

^{13}C NMR: (600 MHz, $CDCl_3$) 14.90, 15.45, 122.66, 125.86, 131.31, 133.71, 133.86, 137.88, 142.25, 155.09, 156.29, 157.80, 198.85, 201.99 ppm.

IR υCO: (CH_3CN) 2071, 1937, and 1895 cm^{-1}.

MS (ESI): $[M-H]^-$ (*m/z*) mass found: 648.0729, mass calculated: 648.0739 for $C_{23}H_{18}BF_2N_3O_5W$

5.2.5.8 Synthesis of 2,6-diethyl-1,3,5,7-tetramethyl-8-(3-pyridyl)-4,4'-difluoro-4-bora-3a,4a-diaza-indacene chromium pentacarbonyl (Ethyl-BODIPY $Cr(CO)_5$)

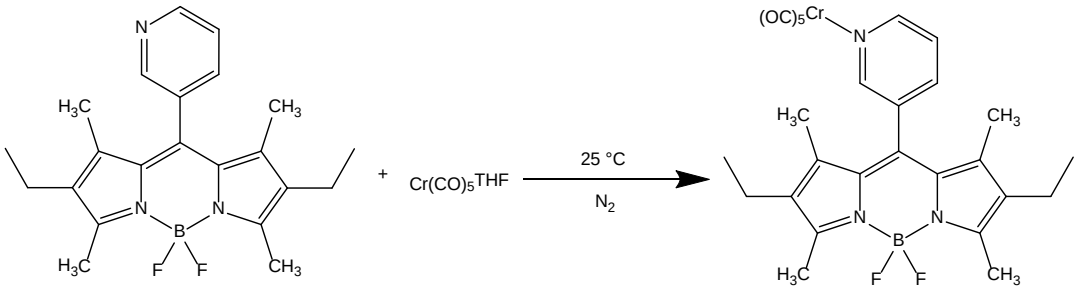

Reaction 5.8 The synthesis of 2,6-diethyl-1,3,5,7-tetramethyl-8-(3-pyridyl)-4,4'-difluoro-4-bora-3a,4a-diaza-indacene chromium pentacarbonyl (Ethyl BODIPY $Cr(CO)_5$).

The synthesis and purification were carried out in the same manner as detailed in section **5.2.5.6.** 100 mg (0.27 mmol) of Ethyl-BODIPY was reacted with an excess of $Cr(CO)_5THF$.

Appearance: red solid.

% Yield: 147 mg, 0.26 mmol, 95 % yield.

^1H NMR: (600 MHz, $CDCl_3$) 1.01 (t, 6H, 2 × CH_3), 1.29 (s, 6H, 2 × CH_3), 2.31 (q, *J* = 8 Hz, 4H, 2 × CH_2), 2.55 (s, 6H, 2 × CH_3), 7.40 (dd, *J* = 8, 5 Hz, 1H), 7.68 (dt, *J* = 8, 2 Hz, 1H), 8.58 (d, *J* = 2 Hz, 1H), 8.75 (dd, *J* = 5, 2 Hz, 1H) ppm.

^{13}C NMR: (600 MHz, $CDCl_3$) 12.57, 12.79, 14.62, 17.22, 124.98, 130.73, 132.63, 133.79, 134.22, 137.43, 137.95, 154.58, 155.39, 155.95, 214.38, 220.62 ppm.

IR υCO: (CH_3CN) 2071, 1938, and 1896 cm^{-1}.

MS (ESI): $[M-H]^-$ (*m/z*) mass found: 572.1263, mass calculated: 572.1260 for $C_{27}H_{26}BCrF_2N_3O_5$

5.2.5.9 Synthesis of 2,6-diethyl-1,3,5,7-tetramethyl-8-(3-pyridyl)-4,4'-difluoro-4-bora-3a,4a-diaza-indacene tungsten pentacarbonyl (Ethyl-BODIPY $W(CO)_5$)

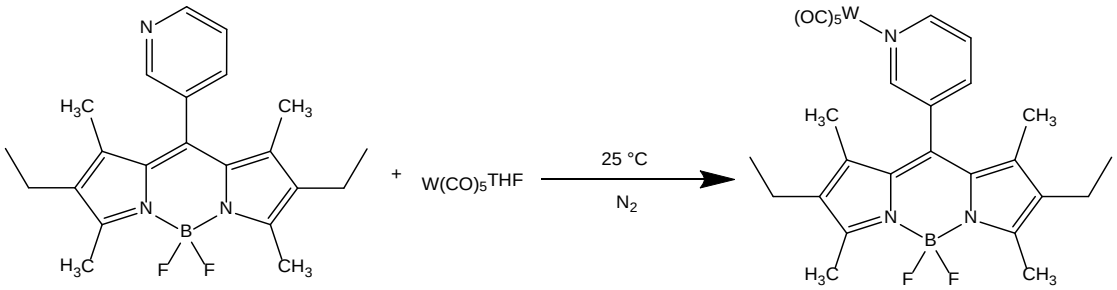

Reaction 5.9 The synthesis of 2,6-diethyl-1,3,5,7-tetramethyl-8-(3-pyridyl)-4,4'-difluoro-4-bora-3a,4a-diaza-indacene tungsten pentacarbonyl (Ethyl-BODIPY $W(CO)_5$).

The synthesis and purification were carried out in the same manner as detailed in section **5.2.5.6.** 250 mg (0.68 mmol) of Ethyl-BODIPY was reacted with an excess of $W(CO)_5THF$.

Appearance: red solid.

% Yield: 310 mg, 0.44 mmol, 65 % yield.

^1H NMR: (600 MHz, $CDCl_3$) 1.00 (t, 6H, J = 8 Hz, 2 × CH_3), 1.33 (s, 6H, 2 × CH_3), 2.33 (q, J = 8 Hz, 4H, 2 × CH_2), 2.55 (s, 6H, 2 × CH_3), 7.45 (dd, J = 8, 5 Hz, 1H), 7.78 (dt, J = 8, 2 Hz, 1H), 8.82 (d, J = 2 Hz, 1H), 8.99 (dd, J = 5, 2 Hz, 1H) ppm.

^{13}C NMR: (600 MHz, $CDCl_3$) 12.75, 12.81, 14.63, 17.23, 125.77, 130.70, 132.17, 134.35, 134.62, 137.34, 138.13, 155.35, 156.06, 156.11, 198.87, 202.05 ppm.

IR υCO: (CH_3CN) 2071, 1937, and 1895 cm^{-1}.

MS (ESI): $[M-H]^-$ (*m/z*) mass found: 704.1368, mass calculated: 704.1365 g for $C_{27}H_{26}BF_2N_3O_5W$

5.2.5.10 Synthesis of 2,6-diiodo-1,3,5,7-tetramethyl-8-(3-pyridyl)-4,4'-difluoro-4-bora-3a,4a-diaza-indacene chromium pentacarbonyl (Iodo-BODIPY $Cr(CO)_5$)

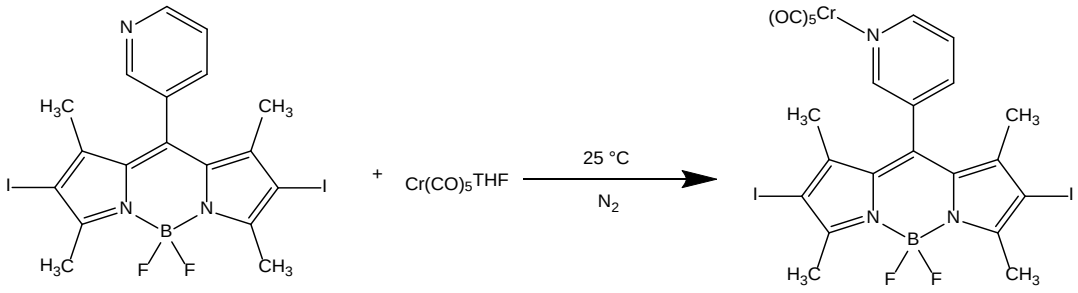

Reaction 5.10 The synthesis of 2,6-diiodo-1,3,5,7-tetramethyl-8-(3-pyridyl)-4,4'-difluoro-4-bora-3a,4a-diaza-indacene chromium pentacarbonyl (Iodo-BODIPY $Cr(CO)_5$).

The synthesis and purification were carried out in the same manner as detailed in section **5.2.5.6**. 100 mg (0.17 mmol) of Iodo-BODIPY was reacted with an excess of $Cr(CO)_5THF$.

Appearance: dark red / purple solid.

% Yield: 105 mg, 0.14 mmol, 81 % yield.

^1H NMR: (600 MHz, $CDCl_3$) 1.41 (s, 6H, 2 × CH_3), 2.67 (s, 6H, 2 × CH_3), 7.45 (dd, *J* = 8, 5 Hz, 1H), 7.66 (dt, *J* = 8, 2 Hz, 1H), 8.58 (d, *J* = 2 Hz, 1H), 8.83 (dd, *J* = 5, 2 Hz, 1H) ppm.

^{13}C NMR: (600 MHz, $CDCl_3$) 16.32, 17.93, 86.51, 125.39, 130.81, 131.71, 132.89, 137.61, 145.15, 153.86, 156.12, 159.01, 214.30, 220.48 ppm.

IR υCO: (CH_3CN) 2071, 1938, and 1895 cm^{-1}.

MS (ESI): $[M-H]^-$ (*m/z*) mass found: 767.8569, mass calculated: 767.8567 for $C_{23}H_{16}BCrF_2I_2N_3O_5$

5.2.5.11 Synthesis of 2,6-diiodo-1,3,5,7-tetramethyl-8-(3-pyridyl)-4,4'-difluoro-4-bora-3a,4a-diaza-indacene tungsten pentacarbonyl (Iodo-BODIPY $W(CO)_5$)

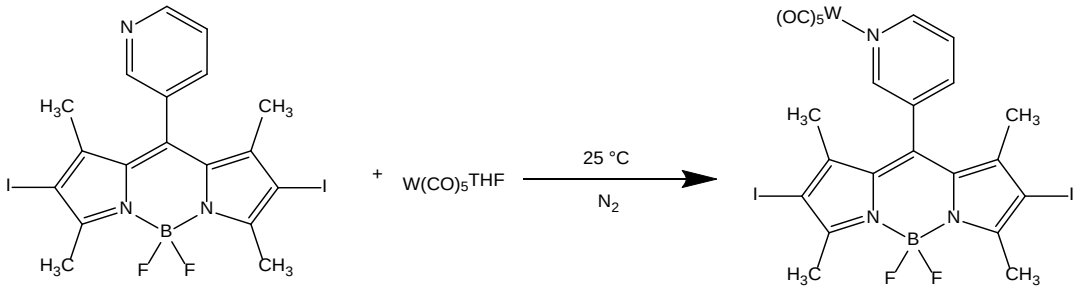

Reaction 5.11 The synthesis of 2,6-diiodo-1,3,5,7-tetramethyl-8-(3-pyridyl)-4,4'-difluoro-4-bora-3a,4a-diaza-indacene tungsten pentacarbonyl (Iodo-BODIPY $W(CO)_5$).

The synthesis and purification were carried out in the same manner as detailed in section **5.2.5.6**. (250 mg (0.43 mmol) of Iodo-BODIPY was reacted with an excess of $W(CO)_5THF$).

Appearance: dark red / purple solid.

% Yield: 203 mg, 0.23 mmol, 53 % yield.

^1H NMR: (600 MHz, $CDCl_3$) 1.44 (s, 6H, 2 × CH_3), 2.67 (s, 6H, 2 × CH_3), 7.51 (dd, *J* = 8, 5 Hz, 1H), 7.76 (dt, *J* = 8, 2 Hz, 1H), 8.81 (d, *J* = 2 Hz, 1H), 9.01 (dd, *J* = 5, 2 Hz, 1H) ppm.

^{13}C NMR: (600 MHz, $CDCl_3$) 16.302, 17.97, 87.21, 126.01, 131.08, 132.96, 133.63, 137.56, 144.32, 154.62, 156.65, 159.06, 198.71, 201.73 ppm.

IR υCO: (CH_3CN) 2071, 1937, and 1895 cm^{-1}.

MS (ESI): $[M-H]^-$ (*m/z*) mass found: 899.8672, mass calculated: 899.8672 for $C_{23}H_{16}BF_2I_2N_3O_5W$

5.2.5.12 Synthesis of 5-(trimethylsilylethynyl)-2-thiophenecarboxaldehyde

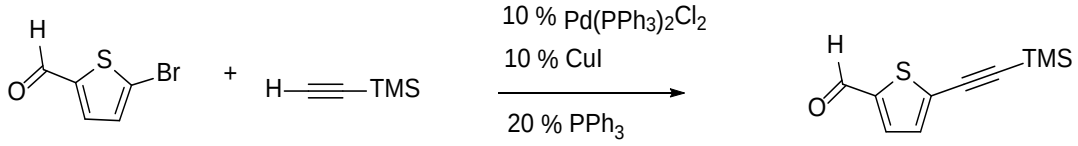

Reaction 5.12 The synthesis of 5-(trimethylsilylethynyl)-2-thiophenecarboxaldehyde.

The synthesis was carried out as previously reported with some modifications.[40] 25 ml of diisopropylamine was added to a clean, dry 50ml round bottomed flask. The solvent was purged for 15 minutes. 0.21 ml (1.77 mmol) of 5-bromo-2-thiophene carboxaldehyde, 0.12 g (0.18 mmol) of $Pd(PPh_3)_2Cl_2$, 0.03 g (0.18 mmol) CuI, 0.09 g (0.35 mmol) of PPh_3 and 0.38 ml (2.66 mmol) were added to the reaction vessel. This was sealed and brought to reflux temperature at 88 °C. The reaction proceeded overnight. The solvent was removed under reduced pressure yielding a brown / yellow oily solid. The crude product was extracted by adding a mixture of dichloromethane and hexane (1 : 5) multiple times. After each addition, the liquid layer was decanted off until the solution was colourless. The organic phase containing the product was dried over $MgSO_4$. The solvent was removed under reduced pressure. Purification was carried out by column chromatography using silica as the stationary phase and hexane : dichloromethane (2 : 3) as the mobile phase. The spectroscopic data are in agreement with reported data.[40]

Appearance: pale yellow oil at room temperature, cream solid upon freezing.

% Yield: 0.33 g (1.58 mmol), 89 % yield.

^1H NMR: (400 MHz, $CDCl_3$) 0.27 ppm (9H, s, 3 × CH_3), 7.25 ppm (1H, d), 7.61 ppm (1H, d), 9.85 (1H, s) ppm.

5.2.5.13 Synthesis of 1,3,5,7-tetramethyl-2,6-diethyl-8-(5-thiophen-2-trimethylsilylethynyl)-4,4-difluoro-4-bora-3a,4a-diaza-indacene (ThioBODIPY-TMS)

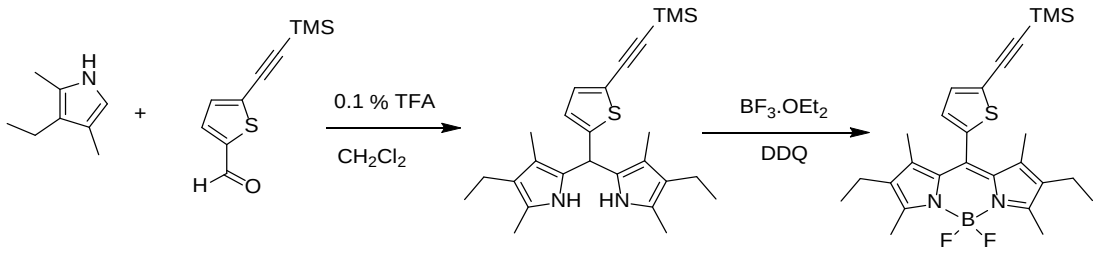

Reaction 5.13 The synthesis of 1,3,5,7-tetramethyl-2,6-diethyl-8-(5-thiophen-2-trimethylsilylethynyl)-4,4-difluoro-4-bora-3a,4a-diaza-indacene (ThioBODIPY-TMS).

20 ml of dichloromethane was added to a clean, dry round bottomed flask. The solvent was purged for 10 minutes. 0.28 g (1.34 mmol) of 5-(trimethylsilylethynyl)-2-thiophenecarboxaldehyde, 0.22 ml (2.68 mmol) of kryptopyrrole (3-ethyl-2,4-dimethylpyrrole) and 20 µL of trifluoroacetic acid (TFA) were added to the reaction vessel. This was sealed and allowed to stir at RT for 24 hours in the absence of light. 0.36 g (1.6 mmol) of DDQ (2,3-dichloro-5,6-dicyano-*p*-benzoquinone) was dissolved in 2 ml of pre-purged CH_2Cl_2 and was added to the reaction vessel. This was allowed to stir for four hours. 1.11 ml (7.91 mmol) of triethylamine was added to the reaction, followed in quick succession by 1.68 ml (13.61 mmol) of $BF_3.OEt_2$. The solution was allowed to stir overnight. The crude reaction mixture was washed with 4 × 10 ml portions of saturated $NaHCO_3$ solution. The organic phase containing the product was dried over $MgSO_4$. The solvent was removed under reduced pressure. Purification was carried out by column chromatography using silica as the stationary phase and hexane : ethyl acetate (8 : 2) as the mobile phase.

Appearance: dark red / purple solid.

% Yield: 128 mg (0.27 mmol), 20 % yield.

^{1}H-NMR: (600 MHz, CD_3CN) 0.25 (s, 9H, 3 × CH_3), 0.99 (t, J = 7.5 6H, 2 × CH_3), 1.57 (s, 6H, 2 × CH_3), 2.35 (q, J = 7.5, 4H, 2 × CH_2), 2.46 (s, 6H, 2 × CH_3), 7.01 (d, J = 3.5, 1H), 7.31 (d, J = 3.7, 1H) ppm.

^{13}C NMR: (600 MHz, CD_3CN) 0.12, 11.91, 13.29, 15.19, 17.98, 97.55, 101.98, 126.34, 130.44, 132.41, 132.66, 132.77, 134.87, 135.14, 138.31, 140.32, 156.28 ppm.

MS MALDI-TOF [M]: (*m/z*) mass found 482.2172, mass calculated: 482.2195 for $C_{26}H_{33}BF_2N_2SSi$

5.2.5.14 Synthesis of 1,3,5,7-tetramethyl-2,6-diethyl-8-(5-thiophene-2-ethynyl)-4,4-difluoro-4-bora-3a,4a-diaza-indacene (ThioBODIPY-H)

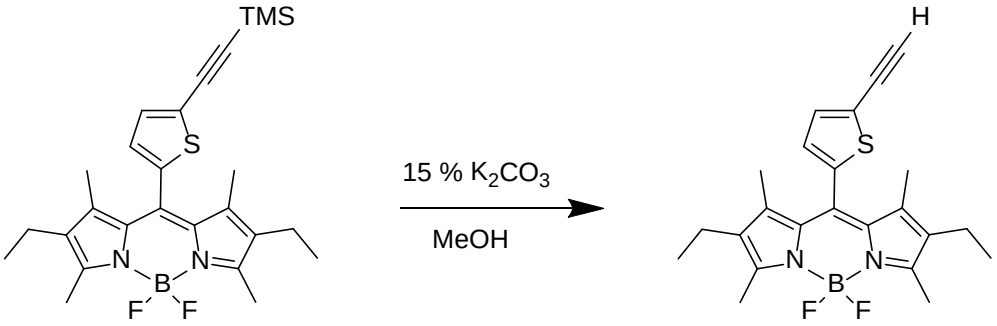

Reaction 5.14 The synthesis of 1,3,5,7-tetramethyl-2,6-diethyl-8-(5-thiophene-2-ethynyl)-4,4-difluoro-4-bora-3a,4a-diaza-indacene (ThioBODIPY-H).

25 ml of freshly distilled methanol was added to a clean, dry round bottomed flask and was purged with nitrogen for 15 minutes. 0.13 g (0.27 mmol) of ThioBODIPY-TMS was added to the reaction flask and the reaction mixture was allowed to purge for a further 10 minutes. 0.005 g (0.04 mmol) of K_2CO_3 was added to the solution and the reaction was allowed to stir overnight under inert conditions. The solvent was removed under reduced pressure. The crude product was dissolved in ~ 10 ml of dichloromethane and was washed with 5 × 25 ml of 5 % (w/v) aqueous $NaHCO_3$. The organic phase was dried over $MgSO_4$. The solvent was removed under reduced pressure. Purification was carried out by column chromatography using silica as the stationary phase and hexane : ethyl acetate (9 : 1) as the mobile phase.

Appearance: bright red solid.

% Yield: 103 mg (0.25 mmol), 93 % yield.

^{1}H NMR: (600 MHz, CD_3CN) 0.99 (t, *J* = 7.5, 6H, 2 × CH_3), 1.57 (s, 6H, 2 × CH_3), 2.35 (q, *J* = 7.5, 4H, 2 × CH_2), 2.46 (s, 6H, 2 × CH_3), 3.82 (s, 1H), 7.02 (d, *J* = 3.8, 1H), 7.38 (d, *J* = 3.7, 1H) ppm.

^{13}C NMR: (600 MHz, CD_3CN) 11.45, 12.86, 14.76, 17.54, 76.41, 84.67, 124.92, 129.62, 129.92, 131.93, 132.34, 134.71, 134.84, 137.98, 139.89, 155.88 ppm.

MS MALDI-TOF [M]: (*m/z*) mass found 410.178, mass calculated: 410.1800 for $C_{23}H_{25}BF_2N_2S$

5.2.5.15 Synthesis of 5-bromo-[2,2´]-bipyridine

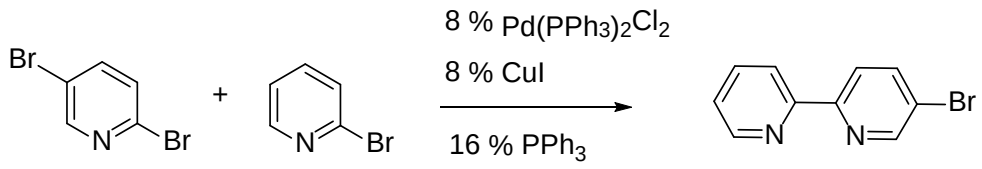

Reaction 5.15 The synthesis of 5-bromo-[2,2´]-bipyridine.

The synthesis was carried out as previously reported with some modifications.[41] 1.18 g (5.0 mmol) of 2,5-dibromopyridine, 0.14 g (0.2 mmol) of $[Pd(PPh_3)_2Cl_2]$, 0.04 g (0.2 mmol) of CuI and 0.11 g (0.4 mmol) of PPh_3 were added to a clean, dry round bottomed flask. 10 ml (5.0 mmol) of 2-pyridylzinc bromide 0.5 M in THF was added and the reaction was allowed to stir overnight under inert conditions. The reaction mixture was very slowly (dropwise with stirring) added to a saturated EDTA / Na_2CO_3 solution. This was washed with 5 × 100 ml of dry dichloromethane. This was repeated until all of the reaction mixture had been added. The organic phase was dried over $MgSO_4$. The organic phase was collected and allowed to evaporate in the fumehood overnight. Purification was carried out by column chromatography using silica as the stationary phase and hexane : ethyl acetate (9 : 1) as the mobile phase. The spectroscopic data are in agreement with reported data.[41]

Appearance: white iridescent solid.

% Yield: 0.76 g (3.23 mmol), 65 % yield.

^{1}H NMR: (400 MHz, $CDCl_3$) 7.32 (td, 1H), 7.81 (td, 1H), 7.93 (dd, 1H), 8.31 (dd, 1H), 8.36 (dt, 1H), 8.67 (m, 1H), 8.72 (d, 1H) ppm.

5.2.5.16 Synthesis of 1,3,5,7-tetramethyl-2,6-diethyl-8-(5-thiophene-2-ethynyl-2,2´-bipyridine)-4,4-difluoro-4-bora-3a,4a-diaza-indacene (ThioBipyBODIPY)

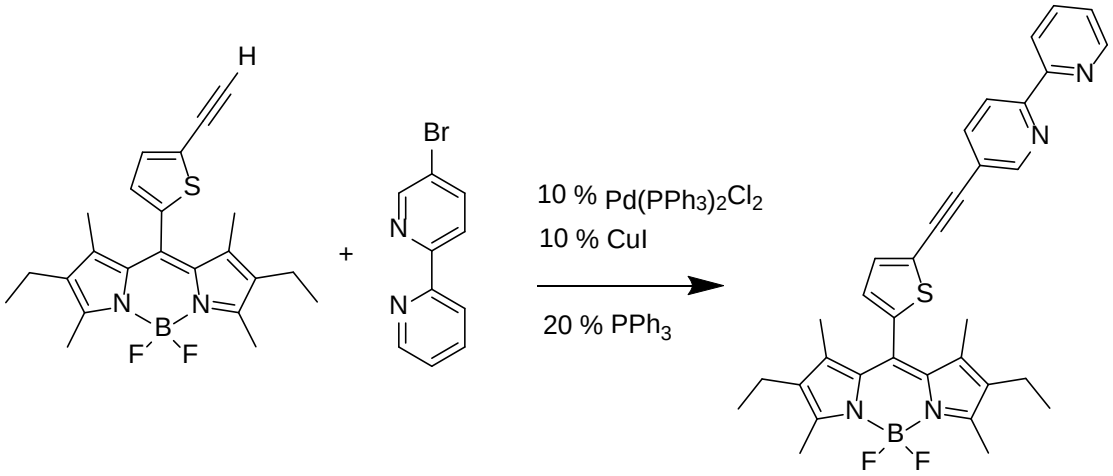

Reaction 5.16 The synthesis of 1,3,5,7-tetramethyl-2,6-diethyl-8-(5-thiophene-2-ethynyl-2,2´-bipyridine)-4,4-difluoro-4-bora-3a,4a-diaza-indacene (ThioBipyBODIPY).

To a clean, dry round bottomed flask, 30 ml of triethylamine was added and purged for 15 minutes with N_2. 107 mg (0.26 mmol) of ThioBODIPY-H was added and the solution was further purged with N_2 for 10 minutes. 74 mg (0.31 mmol) of 5-bromo-2,2´-bipyridine, 18 mg (0.03 mmol) of $Pd(PPh_3)_2Cl_2$, 5 mg of CuI (0.03 mmol) and 14 mg (0.05 mmol) of PPh_3 were added to the reaction vessel under inert conditions. The reaction mixture was allowed to reflux for 18 hours. The reaction mixture was cooled to RT and the solvent was removed under reduced pressure. The excess catalysts were removed by washing the crude product with a mixture of dichloromethane and hexane (1 : 5) as outlined in section **5.2.5.12**. The organic phase was collected and dried over $MgSO_4$. The solvent was removed under reduced pressure. Purification was carried out by column chromatography using silica as the stationary phase and hexane: ethyl acetate (8 : 2) as the mobile phase.

Appearance: bright red solid.

% Yield: 67 mg (0.12 mmol), 46 % yield.

^{1}H-NMR: (400 MHz, $CDCl_3$) 0.98 (t, *J* = 8 Hz, 6H, 2 × CH_3), 1.58 (s, 6H, 2 × CH_3), 2.31 (q, *J* = 8 Hz, 4H, 2 × CH_2), 2.52 (s, 6H, 2 × CH_3), 6.92 (d, *J* = 4 Hz, 1H), 7.38 (s,

2H), 7.87 (t, *J* = 8 Hz, 1H), 7.96 (d, *J* = 8, 1H), 8.40 ppm (s, 2H), 8.71 (d, *J* = 4 Hz, 1H), 8.82 (s, 1H) ppm.

^{13}C-NMR (400 MHz, $CDCl_3$) 11.55, 12.93, 14.89, 17.44, 86.29, 91.97, 120.81, 121.82, 124.44, 124.99, 128.49, 130.82, 131.91, 133.19, 133.76, 137.35, 138.61, 138.83, 139.51, 149.62, 151.66, 155.23 ppm.

MS MALDI [M]: (*m/z*) mass found: 564.2357, mass calculated: 564.2331 for $C_{33}H_{31}BF_2N_4S$

5.2.5.17 Synthesis of 1,3,5,7-tetramethyl-2,6-diethyl-8-(5-thiophene-2-ethynyl-2,2´-bipyridine)-4,4-difluoro-4-bora-3a,4a-diaza-indacene $Cr(CO)_4$ (ThioBipyBODIPY $Cr(CO)_4$)

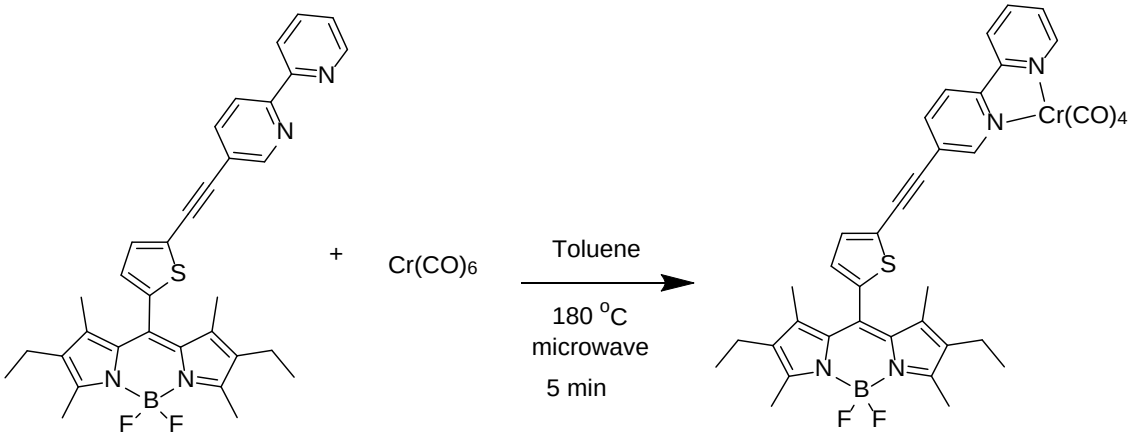

Reaction 5.17 The synthesis of 1,3,5,7-tetramethyl-2,6-diethyl-8-(5-thiophene-2-ethynyl-2,2´-bipyridine)-4,4-difluoro-4-bora-3a,4a-diaza-indacene $Cr(CO)_4$ (ThioBipyBODIPY $Cr(CO)_4$).

15 ml of anhydrous toluene was added to a microwave reactor vessel. 100 mg (0.18 mmol) of ThioBipyBODIPY and 80 mg (0.36 mmol) of $Cr(CO)_6$ were added to the reaction vessel and the vessel was sealed. The reaction was allowed to proceed at 180 °C for 8 minutes. Purification was carried out by column chromatography using silica as the stationary phase and dichloromethane : hexane (9 : 1) as the mobile phase.

Appearance: dark purple solid

% Yield: 105 mg (0.15 mmol), 83 % yield.

^{1}H-NMR: (600 MHz, $CDCl_3$) 1.01 (t, *J* = 7.5 Hz, 6H, 2 × CH_3), 1.60 (s, 6H, 2 × CH_3), 2.35 (q, *J* = 7.4 Hz, 4H, 2 × CH_2), 2.54 (s, 6H, 2 × CH_3), 6.97 (d, *J* = 3.5 Hz, 1H), 7.37 (td, *J* = 1, 6 Hz, 1H), 7.45 (d, *J* = 3.5 Hz, 1H), 7.87-7.95 (m, 2H), 8.00-8.04 (m, 2H), 9.26 (dd, *J* = 1, 6 Hz, 1H), 9.38 ppm (s, 1H) ppm.

^{13}C NMR: (600 MHz, CD_3CN) 11.56, 12.90, 14.79, 17.58, 88.26, 90.71, 122.02, 122.93, 123.92, 124.74, 126.75, 130.47, 131.79, 132.34, 134.79, 135.40, 138.69, 139.47, 139.90, 140.12, 154.15, 155.28, 155.29, 155.49, 155.97, 214.81 ppm.

IR: (CH_3CN) 2306, 2011, 1903, 1884, and 1831 cm^{-1}.

MS ESI^+ [M+H]: (*m/z*) mass found 729.1610, mass calculated: 729.1610 for $C_{37}H_{31}BCrF_2N_4O_4S$

All BODIPY complexes reported in this chapter were stored under inert conditions in the absence of light in the fridge / freezer to help prevent degradation. ^{1}H and ^{13}C NMR spectroscopic data can be found in Appendix B.

5.3 Results and Discussion

5.3.1 NMR Spectroscopy

^{1}H and ^{13}C NMR spectra were recorded in either $CDCl_3$ or CD_3CN. The assignment of the protons present in the ^{1}H spectrum obtained for Ethyl-BODIPY $Cr(CO)_5$ is depicted in Figure 5.19 and the ^{1}H spectrum is displayed in Figure 5.20.

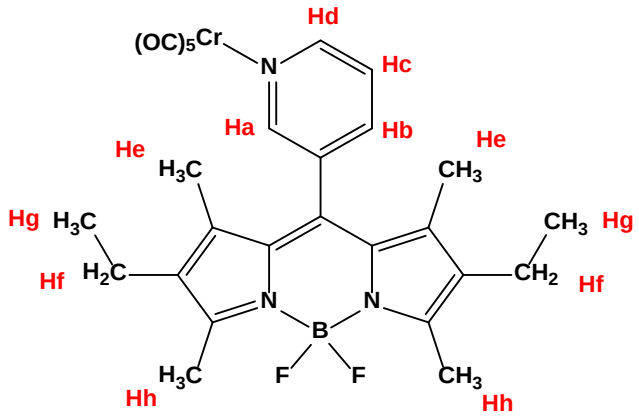

Figure 5.19. Assignment of the protons for a representative BODIPY metal carbonyl complex, Ethyl-BODIPY $Cr(CO)_5$.

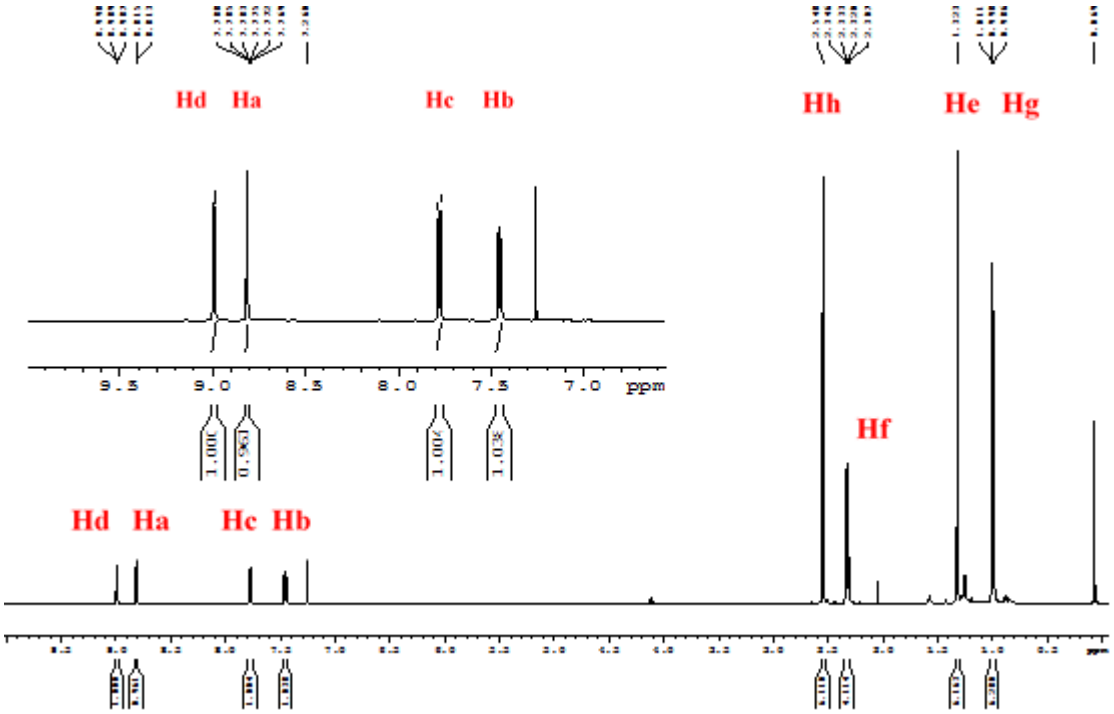

Figure 5.20. ^{1}H spectrum obtained for Ethyl-BODIPY $Cr(CO)_5$ in $CDCl_3$.

Upon inspection of the ^{1}H-NMR spectrum for Ethyl-BODIPY Cr(CO)$_5$, four signals are observed in the aliphatic region. Two signals correspond to the protons of the two sets of unique methyl groups and two signals are assigned to the protons on the ethyl groups of the pyrrolic unit. Four signals are observed for the pyridyl protons in the aromatic region of the spectrum (one signal for each of the four unique pyridyl protons). The proton situated most downfield (**Hd**), exhibits first order coupling with **Hc**, giving rise to a doublet. Long range coupling is also observed with **Hb** which leads to a second doublet. The overall signal that appears for **Hd** is a doublet of doublets. **Ha** undergoes long range coupling with **Hb** forming a doublet. **Hc** exhibits first order coupling from non-equivalent protons, **Hd** and **Hb**, giving rise to a doublet of doublets. **Hb** couples to **Hc** forming a doublet. In addition, long range second order coupling is observed from **Hb** and **Ha** contributing to a doublet of doublets which appear as a doublet of triplets due to spectral overlap. **He** appears as a singlet. Finally, **Hf** couples with **Hg** (first order), giving rise to a quartet for **Hf** and a triplet for **Hg**. The peak at 0.069 ppm is attributed to the TMS reference.

5.3.2 Photophysical Measurements

Table 5.1 outlines the absorbance maxima, extinction coefficients, emission, fluorescent quantum yields and lifetimes of the BODIPY based ligands and organometallic complexes. The Stokes shift was calculated between the most intense absorbance band and most intense emission band.

Table 5.1 Photophysical data of the BODIPY metal carbonyl complexes, recorded in spectrophotometric grade acetonitrile (CH_3CN).

Complex	λ_{max} abs (nm)	ε ($M^{-1}cm^{-1}$)	λ_{em} (nm)	Stokes shift (cm^{-1})	Φ_{fl}	τ (ns)[a]
H-BODIPY	500	69,900	513	507	0.56*	< 3
Ethyl-BODIPY	525	50,622	540	529	0.42*	5.5
Iodo-BODIPY	534	57,000	558	805	0.03*	< 3
H-BODIPY $Cr(CO)_5$	502	42,341	512	389	0.14	< 3
H-BODIPY $W(CO)_5$	504	49,471	513	348	0.11	< 3
Ethyl-BODIPY $Cr(CO)_5$	526	42,558	541	527	0.40	5.2
Ethyl-BODIPY $W(CO)_5$	529	41,858	543	487	0.23	< 3
Iodo-BODIPY $Cr(CO)_5$	537	33,100	561	797	0.02	< 3
Iodo-BODIPY $W(CO)_5$	540	48,400	559	629	0.01	< 3
ThioBipyBODIPY	538	32,564	555	569	0.12	< 3
ThioBipyBODIPY $Cr(CO)_4$	539	19,885	558	632	0.06	< 3

*Reported by Banfi *et al.*[37]

Φ_{fl} represents the quantum efficiency of fluorescence, using Ethyl-BODIPY as a reference in CH_3CN (λ_{exc} = 490 nm).[37]

[a] Lifetimes were recorded following excitation at 360 nm.

5.3.3 UV-vis Absorbance Spectroscopy

The UV-vis absorbance spectra of the 3-pyridyl BODIPY based ligands, ThioBipyBODIPY and corresponding metal carbonyl complexes were recorded in spectrophotometric grade acetonitrile. Figure 5.21 displays the overlaid UV-vis absorbance spectra of the 3-pyridyl BODIPY ligands and the corresponding $W(CO)_5$ complexes. Figure 5.22 shows the UV-vis absorbance spectra of the BODIPY $Cr(CO)_5$ complexes.

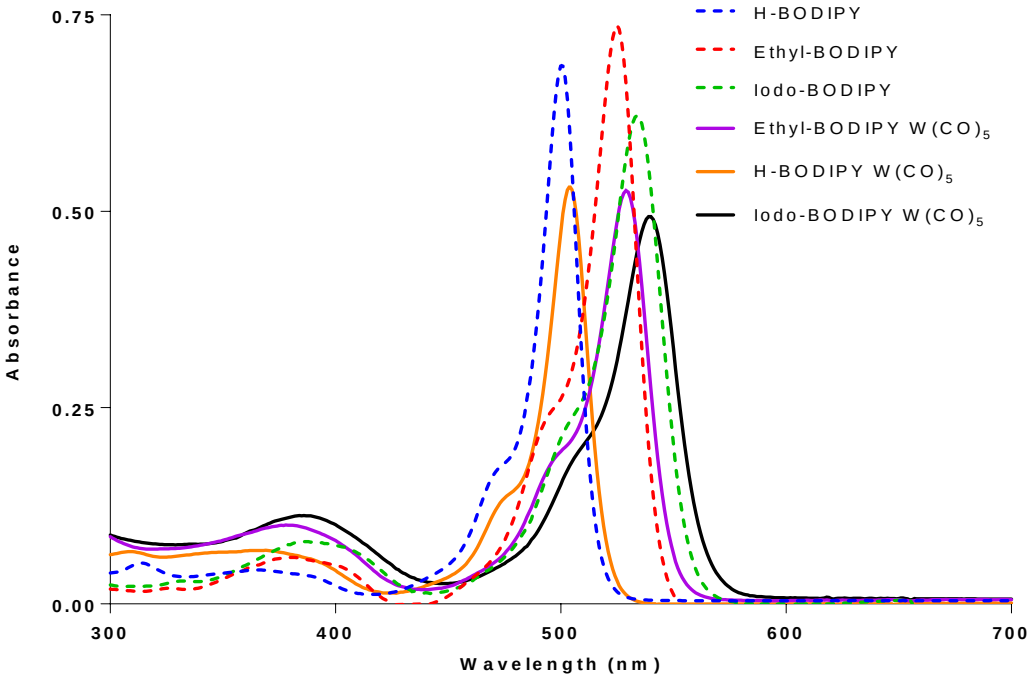

Figure 5.21 Overlaid UV-vis spectra of H-BODIPY (blue dashed), Ethyl-BODIPY (red dashed), Iodo-BODIPY (green dashed), H-BODIPY $W(CO)_5$ (orange), Ethyl-BODIPY $W(CO)_5$ (purple) and Iodo-BODIPY $W(CO)_5$ (black) in spectrophotometric grade acetonitrile at room temperature with concentrations of 10^{-5} mol L^{-1}.

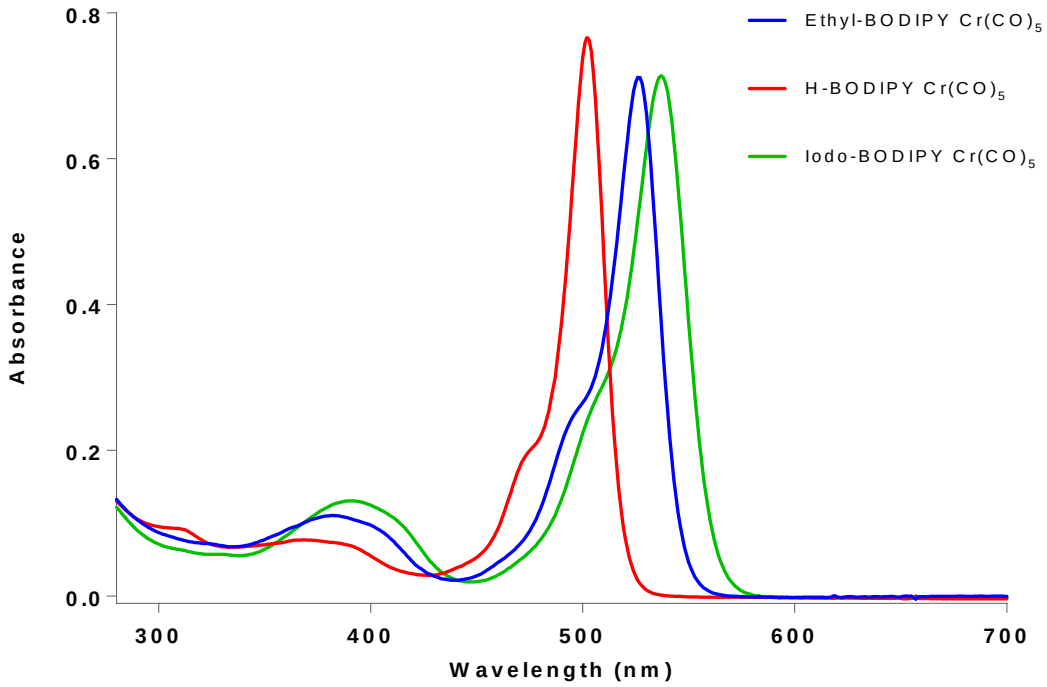

Figure 5.22 Overlaid UV-vis spectra of H-BODIPY $Cr(CO)_5$ (red), Ethyl-BODIPY $Cr(CO)_5$ (blue) and Iodo-BODIPY $Cr(CO)_5$ (green) in spectrophotometric grade acetonitrile at room temperature with concentrations of 10^{-5} mol L^{-1}.

BODIPY based compounds absorb efficiently in the blue-green region of the UV-vis spectrum which gives rise to an intense, sharp absorbance at ~500 - 540 nm. The strong absorbance is attributed to a dipyrromethene based $S_0 \rightarrow S_1$ π-π* transition. A shoulder band is also present on the high energy side of the λ_{max} band due to vibronic coupling of the π-π* transition. In addition, a weaker band evident at approximately 380 nm is due to a $S_0 \rightarrow S_2$ π-π* transition localised within the dipyrromethene region.[30,32,42] Zhao and co-workers reported time dependent density functional theory (TTDFT) calculations on both H-BODIPY and Iodo-BODIPY ligands using a solvation model for acetonitrile to ascertain the transitions involved in the lowest excited states.[43] According to these findings, H-BODIPY possesses a BODIPY (π) based HOMO and a BODIPY (π*) based LUMO. The HOMO-LUMO (π-π*) transition occurs from the first singlet excited state ($S_0 \rightarrow S_1$).[43]

In the case of the 3-pyridyl BODIPYs, differences occur in the absorbance spectra due to the presence of different substituents at the 2, 6 positions of the pyrrole units. As the substituents are changed from hydrogen to ethyl to iodine moieties, a bathochromic shift

occurs respectively. The presence of alkyl groups or iodine groups influences the HOMO-LUMO orbitals and therefore impacts their photophysical properties. The λ_{max} values are dependent on the particular functional groups substituted on the 2, 6 positions of the dipyrromethene unit. Replacement of the hydrogen substituents with ethyl groups results in a bathochromic shift of over 20 nm and with iodine groups causes more than a 30 nm shift with respect to the values obtained for H-BODIPY. This is in agreement with a range of iodo-substituted BODIPY compounds.[32,37,43] Since there is a small difference (~10 nm) between the ethyl *vs.* iodine substituents, it was deduced by Banfi *et al.* that the main parameter affecting λ_{max} values is the bulkiness of the substituent.[37] Upon complexation of the BODIPY chromophore to the metal carbonyl moiety, a minor (< 5 nm) bathochromic shift is observed for each of the BODIPY metal pentacarbonyl complexes, (Figure 5.21). In addition, the band at ~380 nm broadens upon addition of the metal carbonyl unit. This band is attributed to an LF transition. A similar transition has been reported for pyridine $M(CO)_5$ (where M = Cr, W) complexes in alkane solvents.[44,45]

ThioBipyBODIPY $Cr(CO)_4$ was synthesised so as to further extend the UV-vis absorbance spectrum of this family of compounds towards the red region (Figure 5.23).

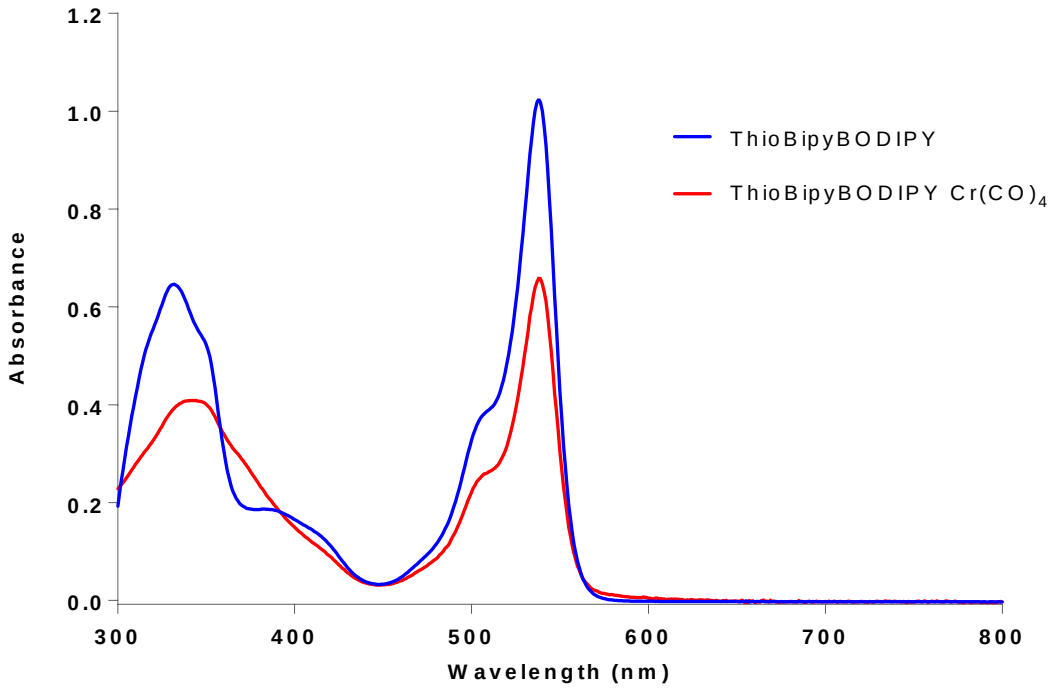

Figure 5.23 UV-vis spectrum of ThioBipyBodipy (blue) and ThioBipyBODIPY $Cr(CO)_4$ (red) in spectrophotometric grade acetonitrile at room temperature with concentrations of 10^{-5} mol L^{-1}.

ThioBipyBODIPY $Cr(CO)_4$ also exhibits the characteristic peak related to the BODIPY functionality with a λ_{max} at 539 nm. The thiophene moiety in this case acts as a linker through an alkynyl spacer group to a polypridyl based unit (2,2´-bipyridine). The main difference between ThioBipyBODIPY and the corresponding metal carbonyl complex, ThioBipyBODIPY $Cr(CO)_4$ is the absorbance peak at approx. 350 nm. The intense transition appearing at 332 nm for ThioBipyBODIPY is due to a bipyridine based transition.[46] Upon complexation of the metal carbonyl fragment, the λ_{max} is red shifted to 342 nm and becomes broader. 2,2´-bipyridine $Cr(CO)_4$, abbreviated to $Cr(CO)_4$(bpy), exhibits absorbance bands at 333, 404 (sh) and 494 nm in methanol at room temperature (reported by Lees and co-worker).[47] The absorbance bands in the range 330 - 420 nm are attributed to a ligand field (LF) or metal to carbonyl charge transfer transitions. The lower energy band at 494 nm is assigned to a metal to ligand charge transfer (MLCT) transition. This MLCT transition is solvent dependent unlike the LF transitions which remain practically unchanged in various solvents. For example, the UV-vis absorbance band present at 494 nm in methanol shifts to 506 nm in dichloromethane, 530 nm in benzene and to 472 nm in acetonitrile.[47,48]

5.3.4 Fluorescence Studies

Fluorescence spectra were recorded at room temperature in spectrophotometric grade acetonitrile for all BODIPY compounds. Excitation in the range 475 - 505 nm, ($S_0 \rightarrow S_1$ transition) of the BODIPY compounds resulted in a sharp emission band in the region 513-558 nm with a small Stoke's shift ranging from 507 - 805 cm^{-1}. This is in agreement with that previously reported for similar BODIPY ligands by Banfi *et al.*[37] Figure 5.24 illustrates the emission profile for a representative set of BODIPY compounds, Iodo-BODIPY and the corresponding metal carbonyl complexes.

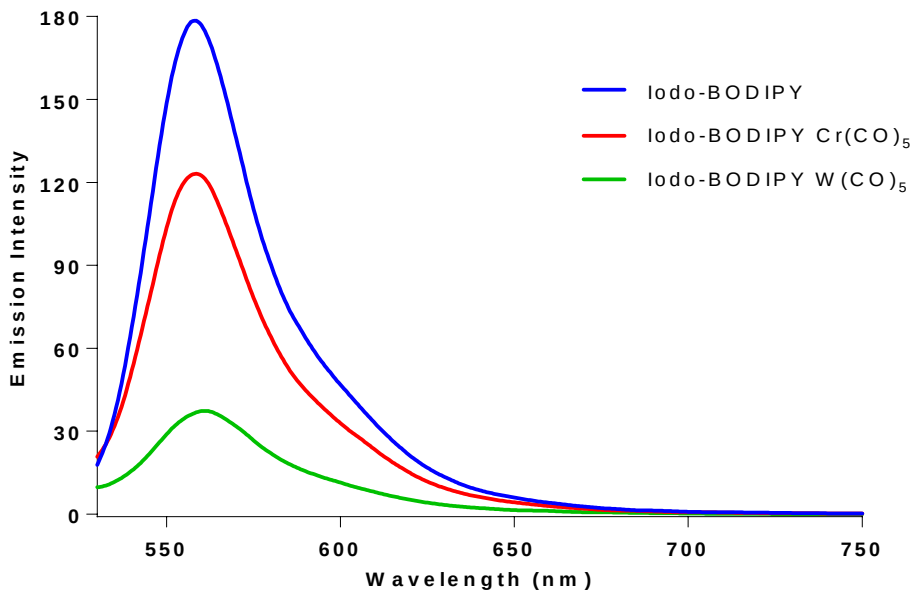

Figure 5.24 Overlaid emission spectra of Iodo-BODIPY, Iodo-BODIPY $Cr(CO)_5$ and Iodo-BODIPY $W(CO)_5$ (λ_{exc} = 500 nm) in acetonitrile at room temperature. All samples were isoabsorptive at the excitation wavelength, O.D. = 0.12.

In the case of the 3-pyridyl BODIPY compounds, upon replacement of the alkyl groups with iodine groups, a significant decrease in the Φ_{fl} is observed. This is in agreement with reported data.[32,37,43] This means that a competing photophysical process is occurring, hence the efficiency by which the emissive state is populated, is reduced. The main impact that occurs upon iodination is the heavy atom effect which leads to intersystem crossing from the lowest singlet state to a triplet state which quenches the emission. Upon addition of the metal carbonyl fragments to the Iodo-BODIPY ligand, the Φ_{fl} is further reduced and the Iodo-BODIPY metal carbonyl complexes are weakly emissive.

Complexation of the metal carbonyl moiety to the various BODIPY ligands, resulted in a small bathochromic shift which suggests that emission is centred on the BODIPY fragment. Figure 5.25 shows the emission profiles for ThioBipyBODIPY and the organometallic analogue, ThioBipyBODIPY $Cr(CO)_4$. Fluorescent quantum yield (Φ_{fl}) values decreased upon addition of metal carbonyl units to the BODIPY ligands. This is in agreement with reported data.[26,49,50]

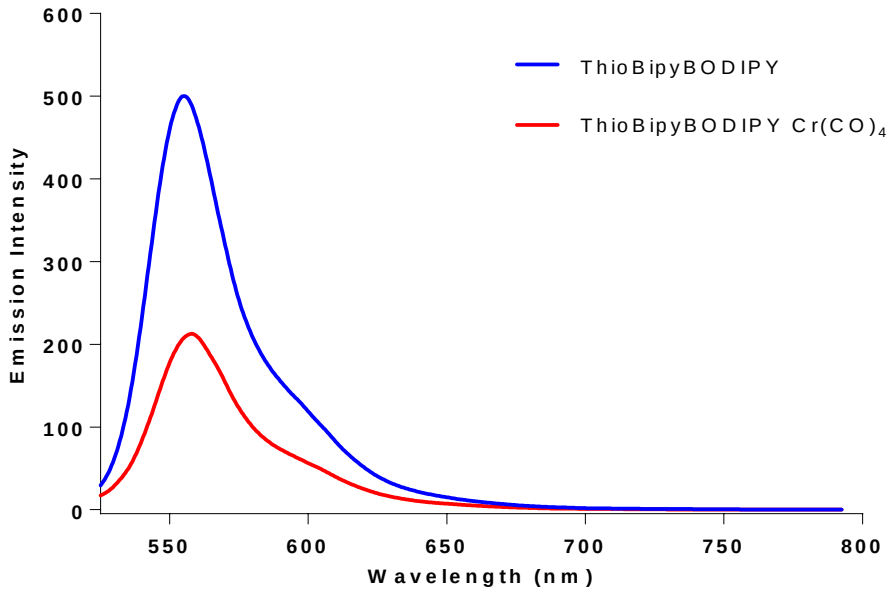

Figure 5.25 Overlaid emission spectra of ThioBipyBODIPY and ThioBipyBODIPY $Cr(CO)_4$ (λ_{exc} = 505 nm) in acetonitrile at room temperature (samples were isoabsorptive at the excitation wavelength, O.D. at λ_{exc} = 0.12).

5.3.5 Lifetime Studies

Singlet lifetimes ($^1\tau$) were recorded at room temperature 20 ± 2 °C and can be found in Table 5.1. Each of the BODIPY ligands and BODIPY metal carbonyl complexes exhibited lifetimes < 3 ns except for Ethyl-BODIPY (5.5 ns) and Ethyl-BODIPY $Cr(CO)_5$ (5.2 ns). This is in agreement with lifetimes reported for similar BODIPY compounds which range from 2.8 - 5.9 ns.[43,51,52] A typical fluorescence decay profile is illustrated in Figure 5.26. The singlet lifetime was monitored with an error of ± 10 %.

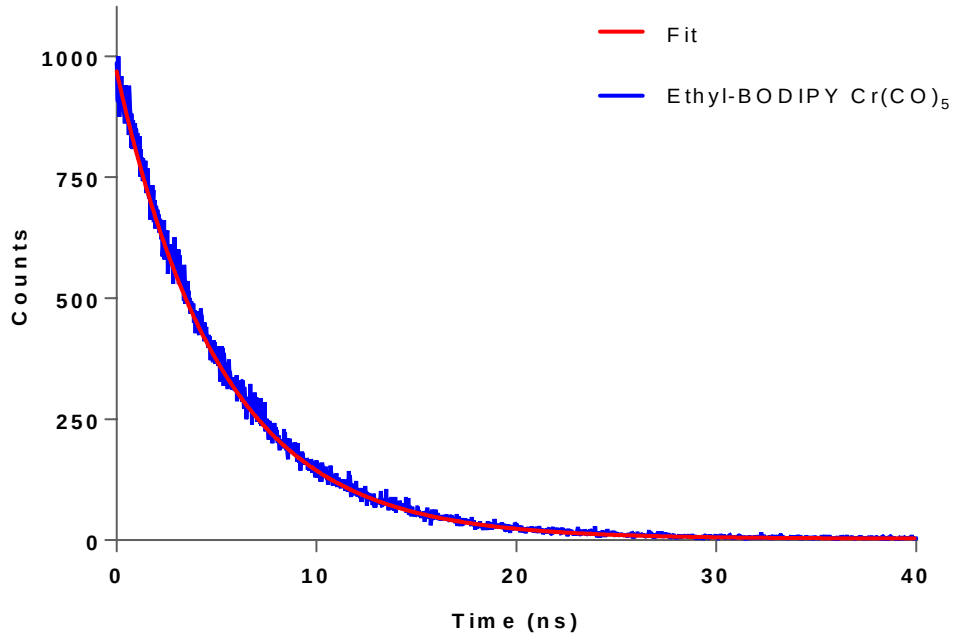

Figure 5.26 Typical room temperature decay observed for Ethyl-BODIPY $Cr(CO)_5$ monitored at 561 nm (λ_{exc} = 360 nm), UV O.D. = 0.2. Singlet lifetime ($^1\tau$ = 5.2 ns) recorded in spectrophotometric grade acetonitrile.

5.3.6 Cyclic Voltammetry

Electrochemical analysis of H-, Ethyl- and Iodo-BODIPY and their corresponding metal carbonyl analogues was carried out in acetonitrile using cyclic voltammetry by a fellow group member, Dr. Diana Hidalgo. Reductive electrochemistry was carried out in the range 0 to -2 V for each of the BODIPY ligands (H-, Ethyl- or Iodo-) and their metal carbonul analogues ($Cr(CO)_5$ or $W(CO)_5$) as shown in Figure 5.27. Each of the BODIPY ligands exhibited a reversible reduction process at the following potentials: H-BODIPY (-1.40 V), Ethyl-BODIPY (-1.47 V) and Iodo-BODOPY (-1.14 V) as reported in Table 5.2, which is the result of a one-electron process and is attributed to the formation of a $[BODIPY]^{\cdot -}$ radical anion.[43,53,54] Ethyl-BODIPY showed the most negative reductive potential due to the electron donating effect of the ethyl group, which can induce a cathodic shift in reductive potentials.[55] The opposite is true for electron withdrawing groups such as iodine. Therefore, due to the electron withdrawing effect of the iodine groups a strong anodic shift to more positive potential was observed for Iodo-BODIPY.[43] As the BODIPY ligands are fully substituted in the meso and β- positions,

formation of a dimer is not expected which is common for non-substituted BODIPY dyes.[53,56,57]

Following coordination of $Cr(CO)_5$ or $W(CO)_5$ to the BODIPY ligands, fully reversible waves are also observed as shown in Figure 5.27. Upon addition of each of the BODIPY ligands with $Cr(CO)_5$ or $W(CO)_5$, an anodic shift in the range 0.06 - 0.09 V occurred. This is in agreement with reported data for BODIPY-cobaloxime complexes. When the metal moiety is attached to the pyridyl functionalised BODIPYs (in this case to H- and Iodo-BODIPYs), the reduction processes occurred at a more positive potential.[26,43] Experiments were performed in triplicate, each of the BODIPY ligands and their corresponding metal carbonyl complexes exhibited electrochemical stability confirming the reversible electron transfer reactions in both directions.

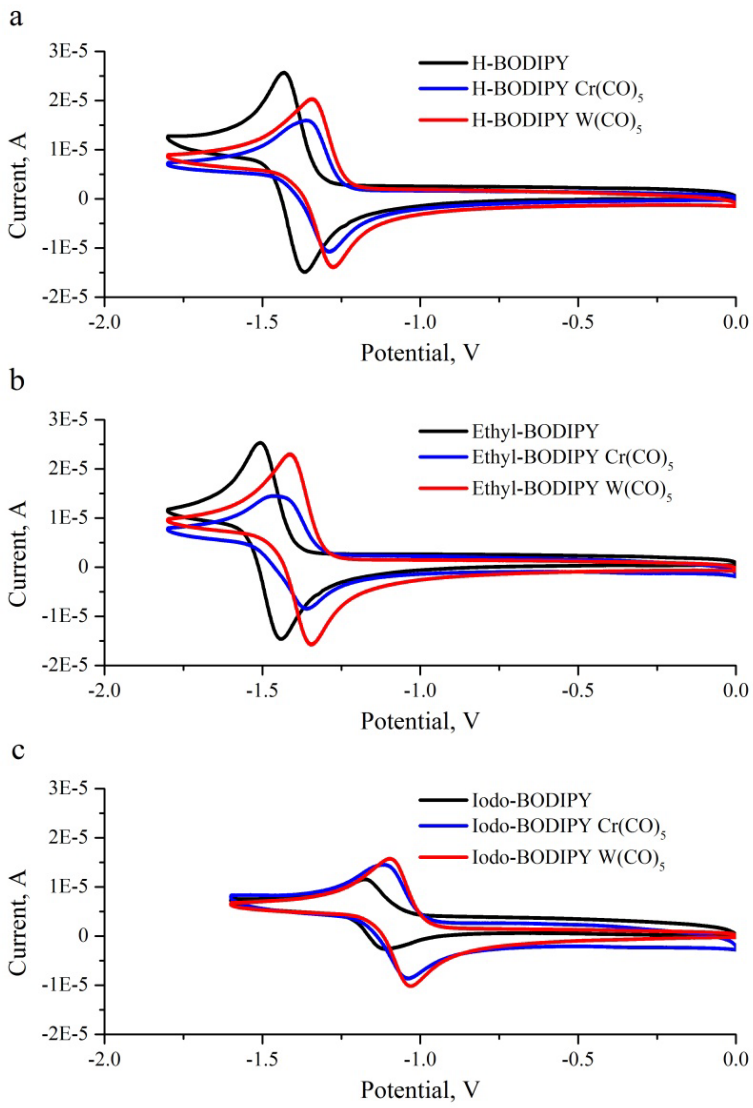

Figure 5.27. Cyclic voltammograms of BODIPY compounds: (a) H-BODIPY (black), H-BODIPY $Cr(CO)_5$ (blue) and H-BODIPY $W(CO)_5$ (red); (b) Ethyl-BODIPY (black), Ethyl-BODIPY $Cr(CO)_5$ (blue) and Ethyl-BODIPY $W(CO)_5$ (red) and (c) Iodo-BODIPY (black), Iodo-BODIPY $Cr(CO)_5$ (blue) and Iodo-BODIPY $W(CO)_5$ (red). Cyclic voltammograms were acquired using the following conditions; working electrode: glassy carbon (0.07 cm^2), counter electrode: Pt wire, reference electrode: Ag/AgCl (1 M $TBAPF_6$ and 0.1 M $AgNO_3$ in CH_2Cl_2), sample concentration: 1 mM, solvent: CH_3CN, supporting electrolyte: 0.1 M $TBAPF_6$ and scan rate: 0.1 V/s.

Table 5.2 Reduction potentials of BODIPY ligands (H-, Ethyl- or Iodo-) and their metallated analogues ($Cr(CO)_5$ or $W(CO)_5$) obtained by cyclic voltammetry.

Sample	**E_{pa*} (V)**	**E_{pc*} (V)**	**$E_{1/2*}$ (V)**
H-BODIPY	-1.43	-1.37	-1.40
H-BODIPY $Cr(CO)_5$	-1.36	-1.29	-1.32
H-BODIPY $W(CO)_5$	-1.34	-1.28	-1.31
Ethyl-BODIPY	-1.51	-1.44	-1.47
Ethyl-BODIPY $Cr(CO)_5$	-1.47	-1.36	-1.41
Ethyl-BODIPY $W(CO)_5$	-1.41	-1.34	-1.38
Iodo-BODIPY	-1.18	-1.11	-1.14
Iodo-BODIPY $Cr(CO)_5$	-1.12	-1.04	-1.08
Iodo-BODIPY $W(CO)_5$	-1.10	-1.03	-1.06

*The subscript letters indicate: potential of the anodic peak ($_{pa}$), potential of the cathodic peak ($_{pc}$) and half-height potential of the cathodic and anodic peaks ($_{1/2}$). Reduction potentials were acquired using working electrode: glassy carbon (0.07 cm^2), counter electrode: Pt wire, reference electrode: Ag/AgCl (1 M $TBAPF_6$ and 0.1 M $AgNO_3$ in CH_2Cl_2), sample concentration: 1 mM, solvent: CH_3CN, supporting electrolyte: 0.1 M $TBAPF_6$ and scan rate: 0.1 V/s.

The introduction of electron donating and withdrawing substituents can greatly affect the redox potentials of BODIPY dyes. The substituent at the 2,6 position resulted in the occurrence of reduction processes at less negative potentials in the following order, Iodo > H > Ethyl. A further shift towards more positive potential was obtained by the incorporation of $Cr(CO)_5$ or $W(CO)_5$ to the BODIPY ligands. Each of the BODIPY ligands and their organometallic complexes were stable under the conditions of the electrochemical experiments. Electrochemical oxidation profiles were not well defined and it was not possible to assign their redox properties. This is in agreement with that reported for a similar BODIPY rhenium carbonyl based complex.[50] This suggests that the BODIPY metal carbonyl complexes are stable only under electrochemically reductive conditions.

5.3.7 IR Spectroscopy

IR spectra were recorded in spectrophotometric grade acetonitrile. The stretching frequencies are compared in Table 5.3. The BODIPY $M(CO)_5$ complexes, where M = Cr or W exhibit three IR υCO stretching vibrations in the M-CO infrared region (2100 - 1750 cm^{-1}). This is in agreement with the bands reported for pyridine $Cr(CO)_5$ and $W(CO)_5$.[39,44,45] Figure 5.28 illustrates the overlaid IR spectra of the BODIPY pentacarbonyl complexes.

Table 5.3 Comparison of the M-CO stretching frequencies recorded for pyridine BODIPY $Cr(CO)_5$, pyridine BODIPY $W(CO)_5$ and ThioBipyBODIPY $Cr(CO)_4$ complexes in spectrophotometric grade acetonitrile.

BODIPY Complexes	**CO Stretching Frequencies (cm^{-1})**
H-BODIPY $Cr(CO)_5$	2071, 1937, 1895
H-BODIPY $W(CO)_5$	2071, 1937, 1895
Ethyl-BODIPY $Cr(CO)_5$	2071, 1938, 1896
Ethyl-BODIPY $W(CO)_5$	2071, 1937, 1895
Iodo-BODIPY $Cr(CO)_5$	2071, 1938, 1895
Iodo-BODIPY $W(CO)_5$	2071, 1937, 1895
ThioBipyBODIPY $Cr(CO)_4$	2011, 1903, 1884, 1831

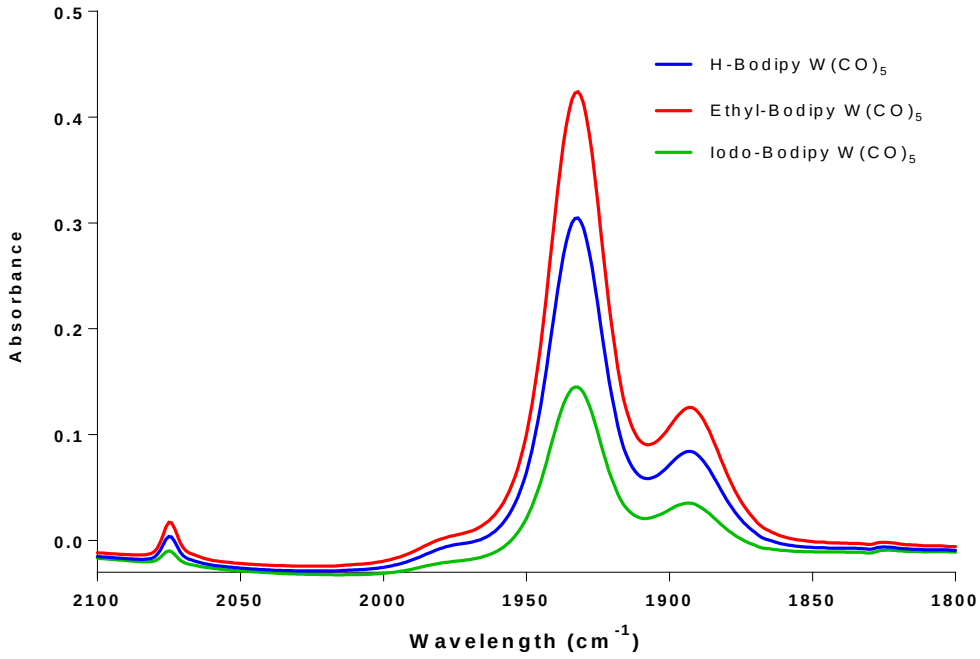

Figure 5.28. Overlaid IR spectra of H-, Ethyl- and Iodo-BODIPY $W(CO)_5$ in acetonitrile.

ThioBipyBODIPY $Cr(CO)_4$ displays four bands characteristic of a chromium tetracarbonyl complex. These bands are in agreement with those reported for 2,2´-bipyridine $Cr(CO)_4$, $Cr(CO)_4$(bpy) which are depicted in Figure 5.29.[58]

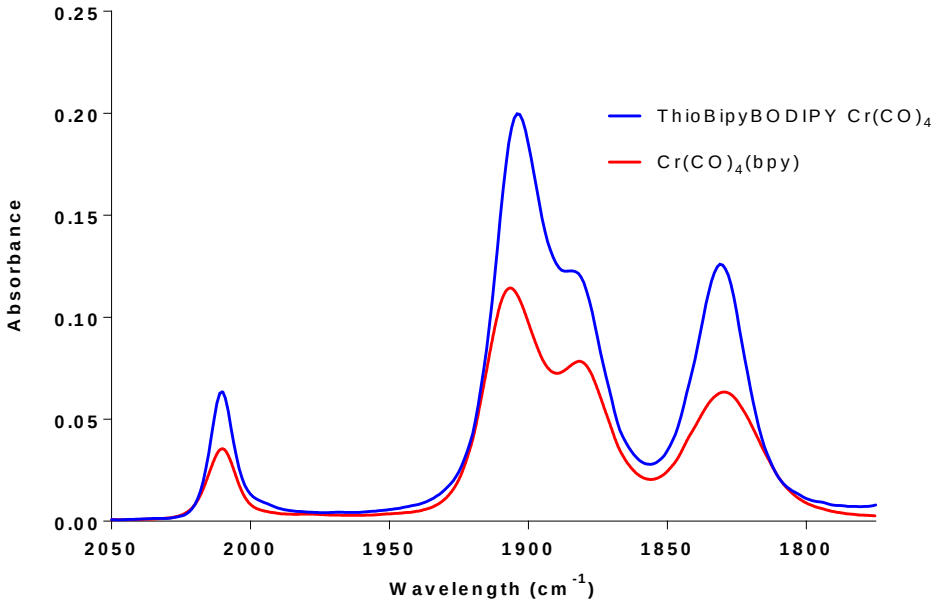

Figure 5.29 Overlaid IR spectra of ThioBipyBODIPY $Cr(CO)_4$ and $Cr(CO)_4$(bpy) in spectrophotometric grade acetonitrile.

5.3.8 Steady State Photolysis

Steady state photolysis measurements were carried out for each of the 3-pyridyl BODIPY complexes. The BODIPY metal carbonyl complex under investigation was dissolved in dichloromethane in the presence of a trapping ligand (PPh_3, in 1.1 molar equivalent excess). The points of irradiation (528, 470 and 355 nm) are shown in Figure 5.30 (indicated by the arrows). Table 5.4 displays the formation of new bands for each of the complexes upon excitation at 528, 470 and 355 nm.

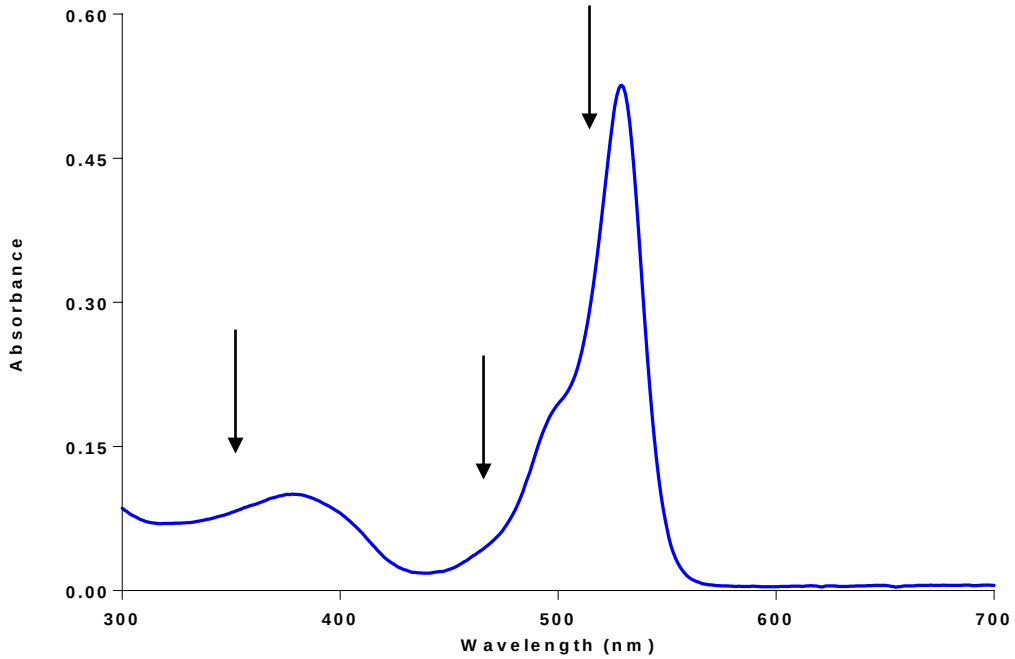

Figure 5.30 A representative UV-vis absorbance spectrum of Ethyl-BODIPY $W(CO)_5$ illustrating the points of irradiation used in IR photolysis experiments (528, 470 and 355 nm) represented by the downward arrows in CH_2Cl_2.

The following IR spectra show the results from the representative example, Ethyl-BODIPY $W(CO)_5$ upon irradiation at each of the wavelengths (528, 470 and 355 nm). The arrows indicate the formation of new peaks over time.

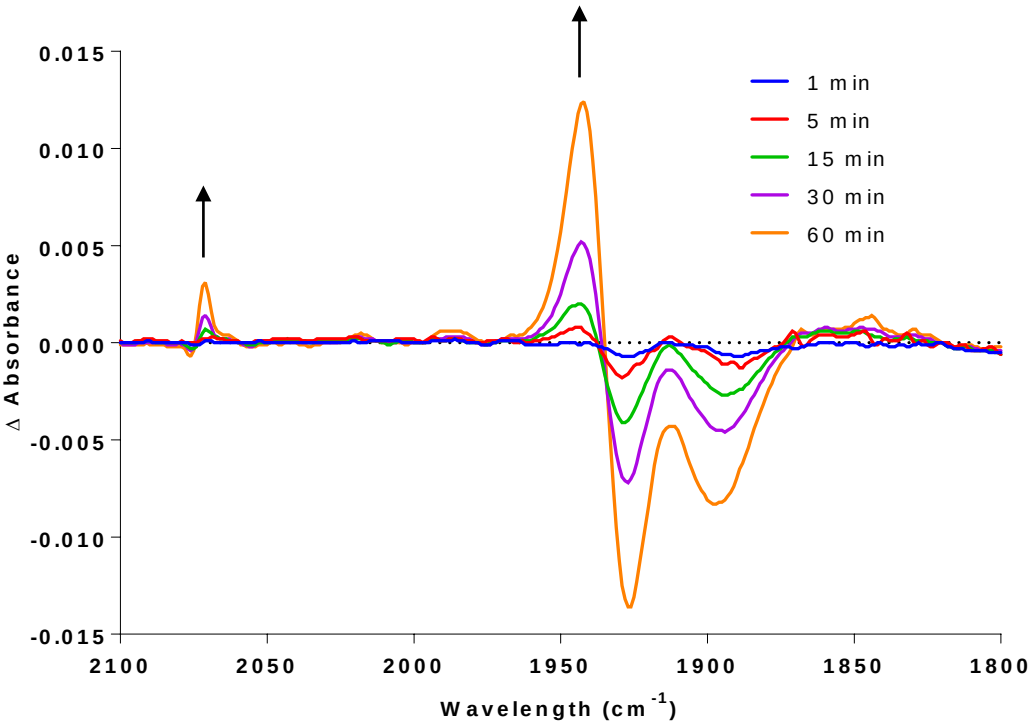

Figure 5.31 IR difference spectra following 528 nm photolysis of Ethyl-BODIPY $W(CO)_5$ in dichloromethane using PPh_3 as a trapping ligand at selected time intervals.

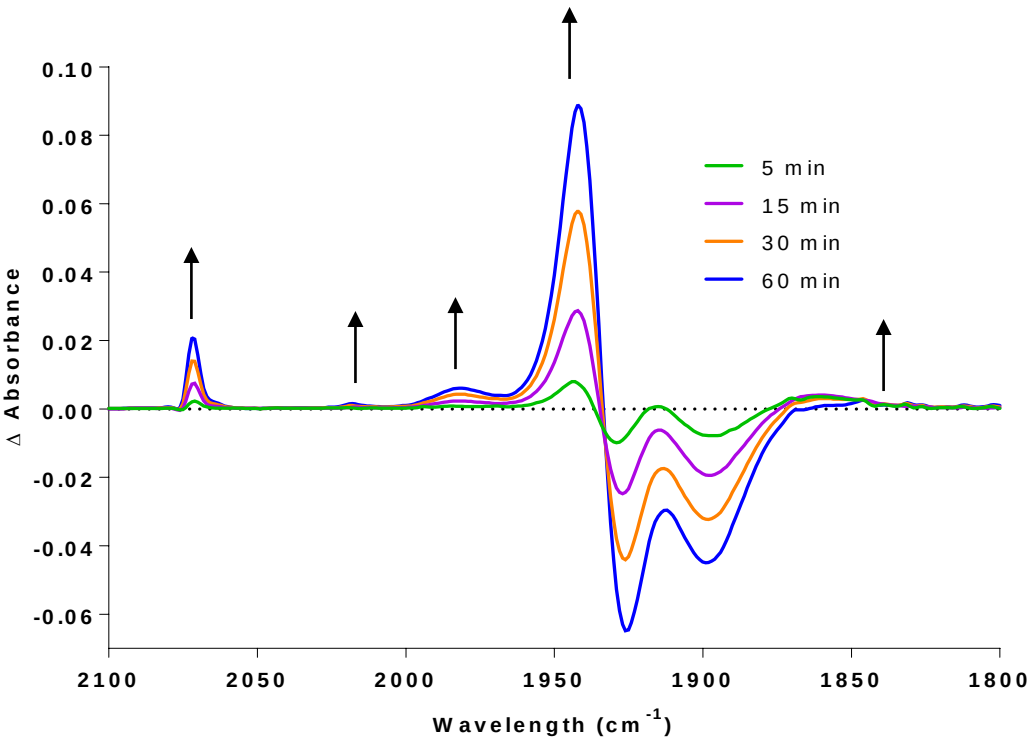

Figure 5.32 IR difference spectra following 470 nm photolysis of Ethyl-BODIPY $W(CO)_5$ in dichloromethane using PPh_3 as a trapping ligand at selected time intervals.

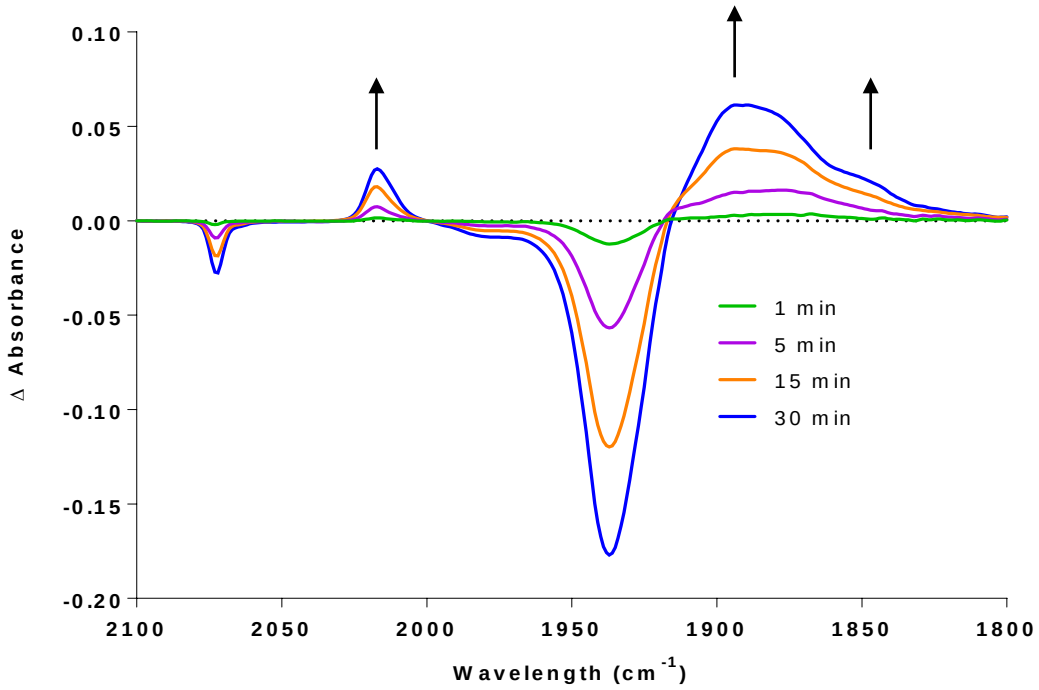

Figure 5.33 IR difference spectra following 355 nm photolysis of Ethyl-BODIPY $W(CO)_5$ in dichloromethane using PPh_3 as a trapping ligand at selected time intervals.

Table 5.4 IR bands for each of the BODIPY complexes following photolysis in CH_2Cl_2 in the presence of PPh_3.

Complex	New bands at 528 nm (cm^{-1})	New bands at 470 nm (cm^{-1})	New bands at 355 nm (cm^{-1})
H-BODIPY $Cr(CO)_5$	2064, 1942, 1884	2064, 1942, 1886	2009, 1887
Ethyl-BODIPY $Cr(CO)_5$	2063,1946, 1884	2063,1953, 1902	2015, 1893,1885
Iodo-BODIPY $Cr(CO)_5$	2063, 1944,1882	2065, 1941, 1888	2000, 1886
H-BODIPY $W(CO)_5$	2071, 1943	2072, 1942	2017, 1891, 1850
Ethyl-BODIPY $W(CO)_5$	2070, 1942	2072, 2018, 1981, 1942, 1847	2017, 1891, 1847
Iodo-BODIPY $W(CO)_5$	2072, 1943	2072, 1941	2017, 1888

As a representative example, Ethyl-BODIPY $W(CO)_5$ is discussed. The IR spectrum of the parent complex exhibits metal carbonyl stretching bands at 2071, 1937, and 1895 cm^{-1}. Figures 5.31, 5.32 and 5.33, display the IR spectral changes over time upon photolysis at 528, 470 and 355 nm, respectively. The spectrum obtained 15 minutes following irradiation at 528 nm, illustrated in Figure 5.31, shows depletion of the parent bands as the negative features in the difference spectrum with new bands at 2070 and ~1942 cm^{-1}. These new bands are assigned to the formation of $W(CO)_5(PPh_3)$ which indicates that the N-W bond has been cleaved. The chromium analogue, $Cr(CO)_5(PPh_3)$ has been reported in the literature to have bands at 2066 and 1945 cm^{-1}.[59] Similar spectral changes were observed following irradiation at 470 nm in addition to further very weak bands at 2018, 1981 and 1847 cm^{-1} (Figure 5.32). These peaks suggest that the CO loss product, Ethyl-BODIPY $W(CO)_4(PPh_3)$, is also formed at this wavelength (albeit, the additional formation of tetracarbonyl bands for H- and Iodo-BODIPY, $W(CO)_5$

analogues are not observed). The bands reported compare closely with those reported in the literature.[38,39] For the pyridine complex, [$W(CO)_5$(pyridine)] (as well as a range of substituted pyridine ligands), excitation at 436 nm, lead to photosubstitution of the pyridine compound as shown in Scheme 5.1 (**a**) with a quantum efficiency of 0.62 ($\pm$ 10 %) in isooctane / 1-pentene at 298 K.[39] CO loss was also detected as depicted in Scheme 5.1 (**b**), forming, $W(CO)_4$(pyridine)(1-pentene) + CO. However, this was a very inefficient process with quantum yield values of $\leq$ 1 % at λ_{exc} = 436 nm.

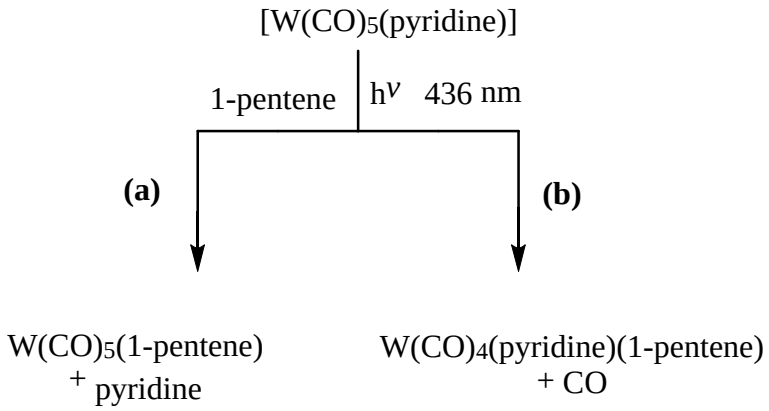

Scheme 5.1 Two plausible schemes for [$W(CO)_5$(pyridine)], upon excitation at 436 nm in the presence of isooctane / 1-pentene at 298 K.[39]

In contrast, upon irradiation at 355 nm, as observed in Figure 5.33, bands characteristic of a tetracarbonyl species are formed (2017, 1888, 1847 cm^{-1}) with the depletion of parent bands illustrated as negative features in the difference spectra. The bands obtained are in agreement with those reported for the isolated compound $W(CO)_4(PPh_3)(NC_5H_5)$ which displays bands at 2011, 1898, 1878 and 1837 cm^{-1} in chloroform solution.[38] One of the four tetracarbonyl bands of the Ethyl-BODIPY $W(CO)_4(PPh_3)(NC_5H_5)$ complex may be obscured under the parent bands or the broad band at 1888 cm^{-1}. This indicates that at higher energy, CO loss is the predominant photo-process. Since, these spectral features are not observed at 528 nm, it can be deduced that the BODIPY-metal carbonyl complexes exhibit wavelength dependent photochemistry in organic solvents. The BODIPY chromium carbonyl complexes exhibit similar behaviour to the BODIPY $W(CO)_5$ complexes at 528 nm and at 355 nm. When irradiated at 470 nm, a mixture of products are observed, $Cr(CO)_5(PPh_3)$ and BODIPY $Cr(CO)_4(PPh_3)$. Previously,

Darensburg and co-workers have indicated that $Cr(CO)_4(PPh_3)(NC_5H_5)$ is extremely reactive and may interact with CO from neighbouring molecules or may react with free PPh_3 in solution forming $Cr(CO)_5(PPh_3)$ or $Cr(CO)_4(PPh_3)_2$, respectively.[38]

Trapping studies were attempted with the BODIPY metal carbonyl complexes in the DMSO / RPMI media used to determine photoinduced CO release (see section **5.3.9**). However, it was not possible to determine any spectral changes using FTIR due to solubility issues.

5.3.9 Photochemical CO Release

At present, gas chromatography is believed to be the most accurate form of CO detection.[60,61,62] It is advantageous as CO release studies can be explored in many different solvents under different conditions, for example, pH.

The photochemical CO releasing ability of each of the seven BODIPY carbonyl complexes was assessed using headspace analysis monitored *via* gas chromatography. The aim of this investigation was to assess which of the BODIPY carbonyl complexes were the most efficient photoCORMs for progression to cellular studies. Therefore, time points 0, 30, 60, 120 and 180 minutes were selected for direct comparison of the compounds. To mimic biological conditions, CORMs were studied in a mix of $\leq$ 0.5 % DMSO / 5 % fetal bovine serum (FBS) in indicator free RPMI media (to eliminate any further source of absorbance in the UV-vis region under examination). The UV-vis spectra of FBS / RPMI prior to and post irradiation can be found in Appendix D. FBS and RPMI contain a range of proteins, hormones, salts, amino acids and growth factors and are very commonly used in cell culture studies.[11] Different concentrations of the CORMs were analysed at λ_{exc} = 525 nm and 355 nm based on the absorbance spectra of the complexes. In general, the absorbance at 525 nm is approximately double that at 355 nm. Therefore 25 µM of the CORM which equates to 0.25 % DMSO / (FBS/RPMI) media and 50 µM of CORM which equates to 0.5 % DMSO / (FBS/RPMI) media were used at 525 nm and 355 nm, respectively, to ensure isoabsorbance. The UV-vis absorbance spectra (Figure 5.34) and emission spectra (Figure 5.35) were monitored prior to and post irradiation for each experiment. Figure 5.34 depicts the UV-vis absorbance spectra for a representative compound Iodo-BODIPY $Cr(CO)_5$ in 0.25 %

DMSO / (FBS/RPMI) media. The absorbance of the BODIPY compounds undergoes a bathochromic shift in aqueous media. In addition, band broadening was observed. This may be due to the possible formation of aggregates within the solution which is in agreement with reported data on other BODIPY systems.[63]

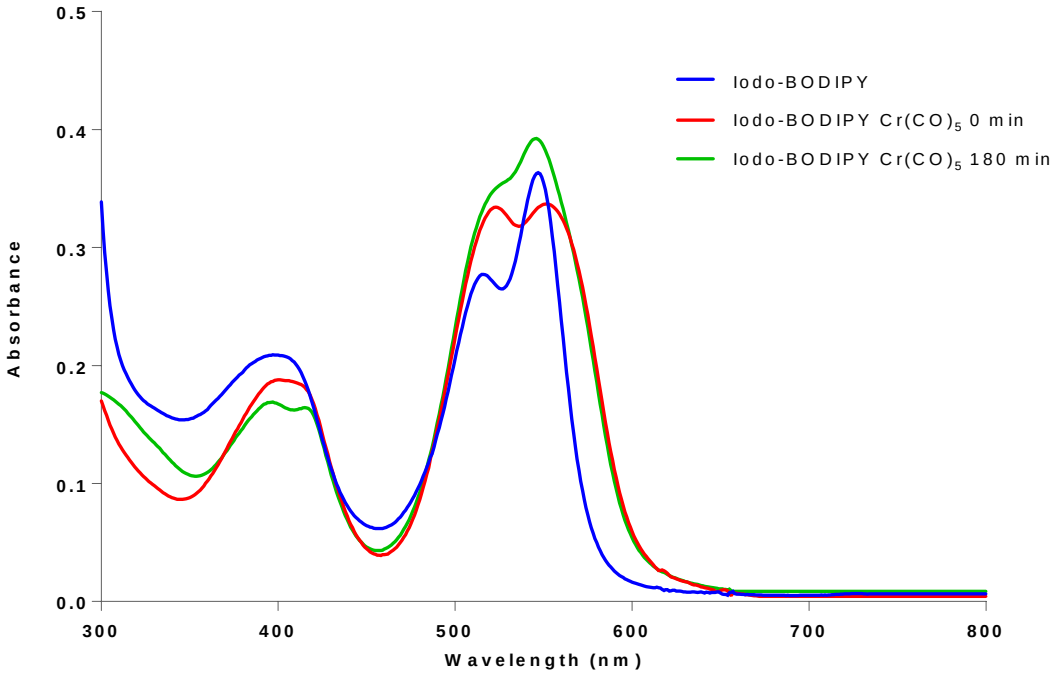

Figure 5.34 UV-vis absorbance spectrum of Iodo-BODIPY $Cr(CO)_5$ (25 µM in 0.25 % DMSO / (FBS/RPMI) media prior to (0 min) and post (180 min) irradiation at 525 nm and the corresponding metal free analogue, Iodo-BODIPY in 0.25 % DMSO / (FBS/RPMI) media .

The emission spectra were recorded prior to and following irradiation in the DMSO / (FBS/RPMI) media. In all cases, the emission increased. For example, shown in Figure 5.35 is the emission profiles prior to (0 min) and following irradiation (180 min) of Ethyl-BODIPY $W(CO)_5$. For Ethyl-BODIPY $W(CO)_5$, it is clear that there is over a two-fold increase in emission, suggesting cleavage of the N-$W(CO)_5$ bond.

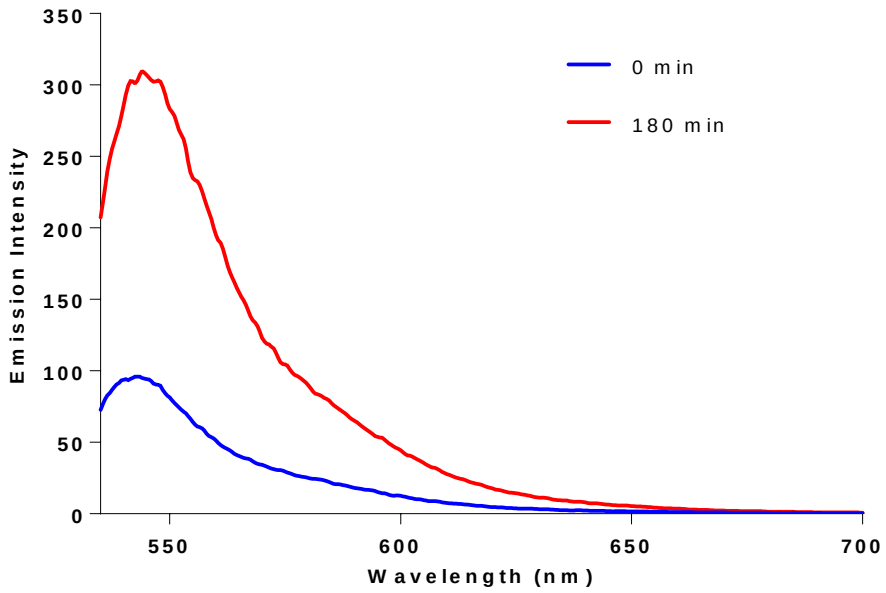

Figure 5.35 Emission profile of Ethyl-BODIPY $W(CO)_5$ (λ_{exc} = 525 nm) at 0 min and 180 min in 0.25 % DMSO / (FBS/RPMI) media.

ThioBipyBODIPY $Cr(CO)_4$ was also synthesised to extend the UV-vis absorbance by increasing the π conjugation so that lower energy light sources closer to the therapeutic window could be used to stimulate CO release. The ThioBipyBODIPY $Cr(CO)_4$ complex exhibited an absorbance tailing to the visible region in aqueous media (Figure 5.36). Therefore, the CO releasing potential was measured at 620 nm. The emission spectra was also recorded prior to and following irradiation in the DMSO / (FBS/RPMI) media. An increase in emission was observed following irradiation at 180 min. For example, shown in Figure 5.37 is the emission profile for ThioBipyBODIPY $Cr(CO)_4$ prior to (0 min) and following irradiation (180 min) at 525 nm. The BODIPY compounds presented in this chapter remain emissive in aqueous solution which will allow such reactions to be monitored in cells.

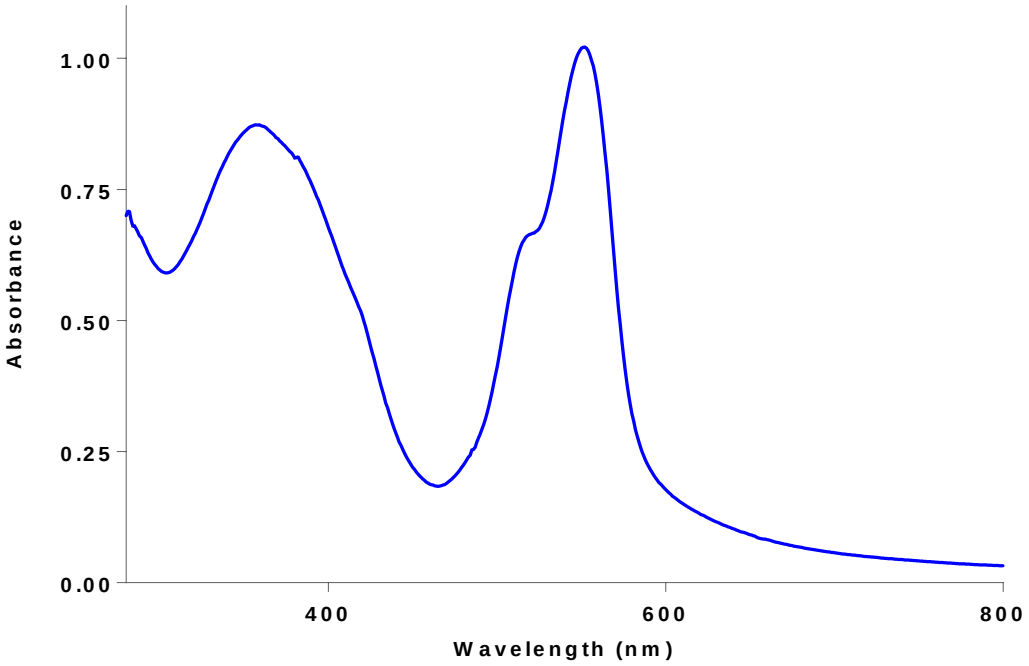

Figure 5.36 UV-vis absorbance spectrum of ThioBipyBODIPY $Cr(CO)_4$ (50 µM in 0.5 % DMSO / (FBS/RPMI) media.

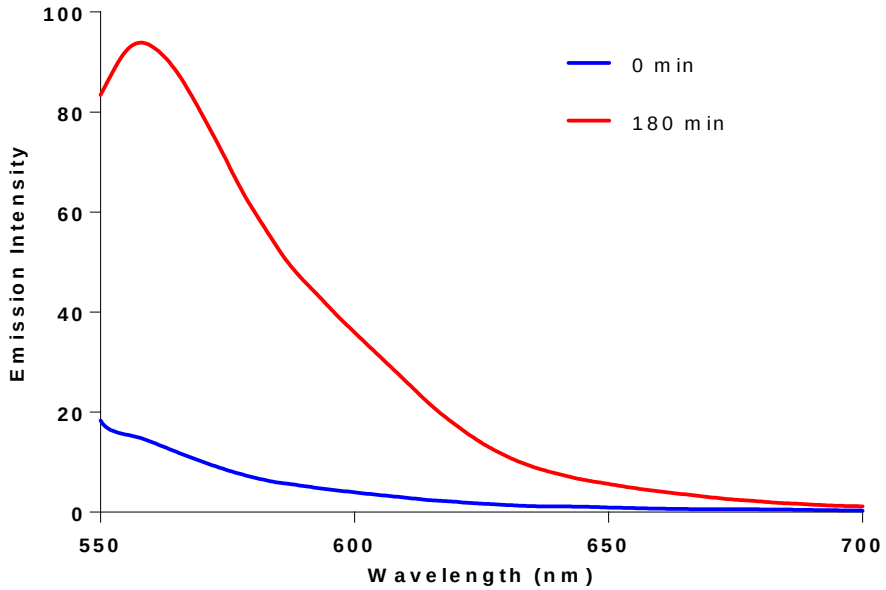

Figure 5.37 Emission profile of ThioBipyBODIPY $Cr(CO)_4$ (λ_{exc} = 525 nm) at 0 min and 180 min in 0.25 % DMSO / (FBS/RPMI) media.

Due to the low absorbance of the complex in this region, it was necessary to increase the concentration to 100 µM of CORM (0.5 % DMSO / (FBS / RPMI) media). These concentrations have been previously reported in CORM cellular assays and therefore

mimic physiological conditions.[11,12,36] The results of the trends of CO release at 525 and 355 nm for the 3-pyridyl BODIPY metal carbonyl complexes are displayed in Figure 5.38 and 5.39, respectively.

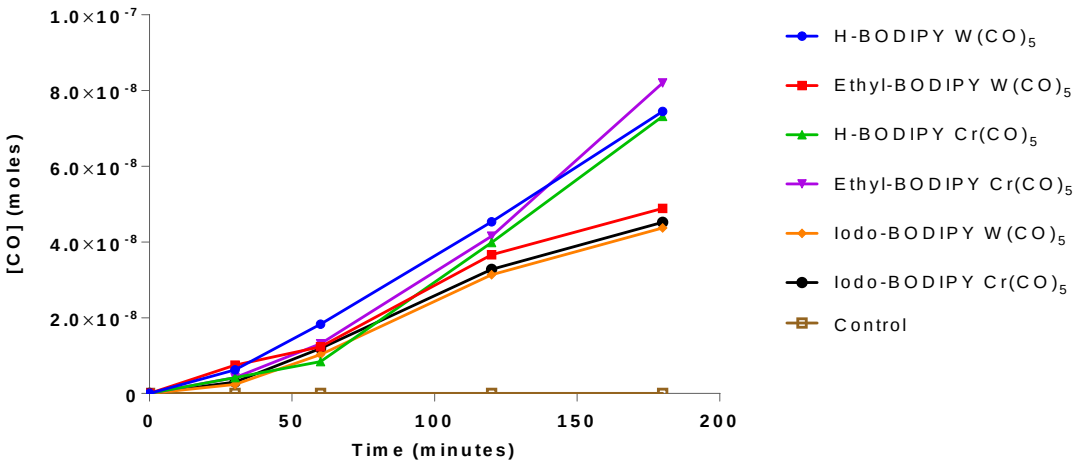

Figure 5.38 CO release profiles for 3-pyridyl BODIPY $M(CO)_5$ where M = Cr, W at 525 nm (n = 2). Final concentration (25 μM of CORM (0.25 % DMSO / (FBS/RPMI) media). Standard deviation was within ± 15 %.

Under uniform conditions at 525 nm, it was evident that Ethyl-BODIPY $Cr(CO)_5$, H-BODIPY $Cr(CO)_5$ and H-BODIPY $W(CO)_5$ released very similar quantities of CO over the timeframe of the experiments. Ethyl-BODIPY $Cr(CO)_5$ released the greatest amount of CO over 180 minutes. This was followed by H-BODIPY $Cr(CO)_5$ and H-BODIPY $W(CO)_5$ which released almost equivalent amounts of CO over the timeframe of the experiments. Ethyl-BODIPY $W(CO)_5$ followed in succession with respect to the amount of CO released. Finally, Iodo-BODIPY $M(CO)_5$ where M= Cr, W released the least amounts of CO. The control experiments carried out in the absence of light over the time frame of the experiments, resulted in no CO release or very negligible quantities.

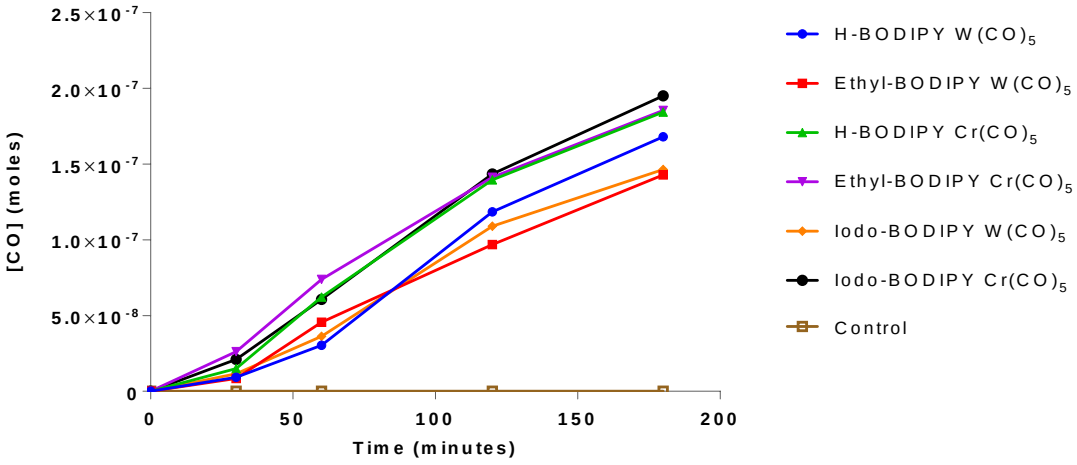

Figure 5.39 CO release profiles for 3-pyridyl BODIPY $M(CO)_5$ where M = Cr, W at 355 nm (n = 2). Final concentration (50 µM of CORM (0.5 % DMSO / (FBS/RPMI) media). Standard deviation was within ± 15 %.

Under uniform conditions at 355 nm, it was evident that the BODIPY chromium carbonyl complexes released a greater amount of CO at 355 nm over 180 minutes. Similar amounts of CO release were observed for the three chromium complexes, A similar trend was also observed for the tungsten based CORMs, Ethyl-BODIPY $W(CO)_5$, H-BODIPY $W(CO)_5$ and Iodo-BODIPY $W(CO)_5$ released very similar amounts of CO over the timeframe of the experiments. Control experiments carried out in the absence of light over the time frame of the experiments, resulted in no CO release or very negligible quantities.

The CO releasing ability of ThioBipyBODIPY $Cr(CO)_4$ was also assessed at λ_{exc} = 620, 525 and 355 nm. The CO release profile is displayed in Figure 5.40.

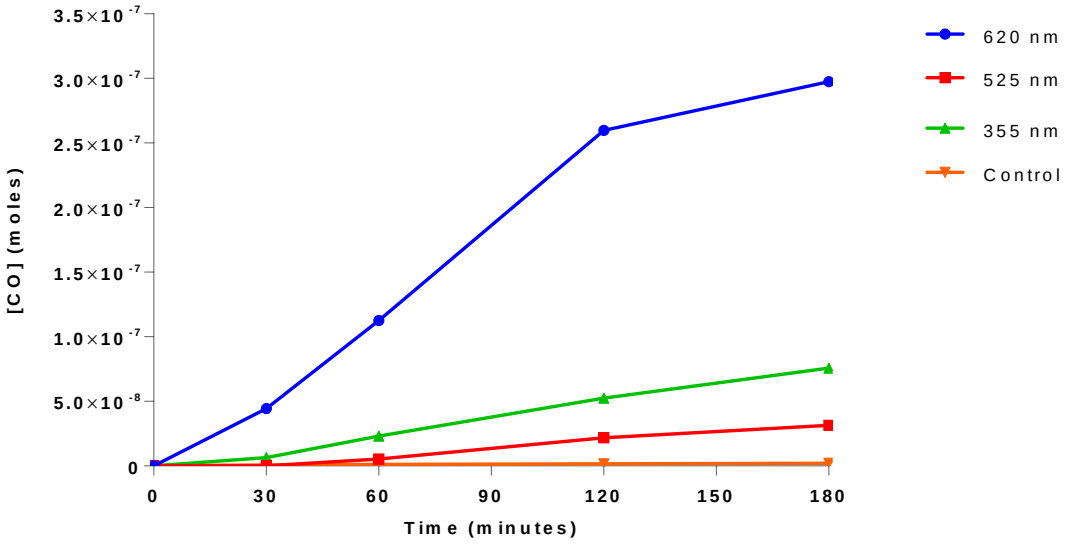

Figure 5.40 CO release profiles for ThioBipyBODIPY $Cr(CO)_4$ at 620 nm (blue), 525 nm (red) and 355 nm (green), (n = 2). Final concentration was 100, 50 and 25 µM (≤0.5 % DMSO / (FBS/RPMI) media) respectively. Standard deviation was within ± 15 %.

CO release was observed at all three wavelengths (λ_{exc} = 620, 525 and 355 nm). The amounts of CO released at each wavelength cannot be directly compared as they were measured at different concentrations. Control experiments carried out in the absence of light resulted in the release of negligible quantities of CO. CO release was very efficient at low energy, 620 nm. This wavelength is close to the therapeutic window (650 - 800 nm), and phototherapy applied at this wavelength would be less harmful to cells in comparison to UV irradiation. This is the lowest energy wavelength reported to date, to the best of our knowledge, to induce CO release from a CORM in biologically compatible media.

It was not possible to assess the CO release from $Cr(CO)_4$(bpy) due to solubility issues in the media used for the GC experiments (DMSO / (FBS/RPMI) mix). Photoinduced CO loss from $Cr(CO)_4$(bpy) is widely reported in the literature in organic solvents. CO loss is observed upon irradiation into the MLCT (532 nm) or LF (355 nm) absorption bands.[64] The quantum efficiency for CO loss is reduced at longer wavelengths and is ~ 10 times greater at 355 nm in comparison to 532 nm.[64,65] This is in agreement with the quantum yield values for CO loss reported for $Cr(CO)_4$(bpy) by Vichova *et al.* in

dichloromethane in the presence of triphenylphosphine, at λ_{exc} = 362 nm, Φ_{co} = 0.19 and at λ_{exc} = 549 nm, Φ_{co} = 0.03.[65]

The BODIPY complexes each release CO upon irradiation in biologically compatible media. It may be possible that the photoproducts produced can coordinate to the proteins present in the biological media. However, further studies are required to elucidate the intermediates / photoproducts produced.

In addition, due to the luminescent properties of the BODIPY dye, they should be able to serve as tracking and reporting devices to indicate the localisation of the CORMs in the cell by using fluorescence microscopy. Finally, since the intensity of emission increases as CO is released, this can act as an indicator for CO release.

5.4 Conclusion

The synthesis, characterisation and CO releasing potential of a range of novel BODIPY metal carbonyl complexes is reported. In the case of the ThioBipyBODIPY $Cr(CO)_4$, the UV-vis absorbance spectra has been extended into the therapeutic window and CO release was observed following excitation at 620 nm. This is the first photoCORM of its kind to release CO using such low energy excitation in biologically compatible media. The pyridine based BODIPY $M(CO)_5$ complexes, exhibit wavelength dependent photochemistry in organic solvents with CO loss observed following irradiation at 355 nm whereas on moving towards longer irradiation wavelength for example, 525 nm, cleavage of the N-$M(CO)_5$ bond occurs. In summary, CO release is observed for each of the seven BODIPY carbonyl complexes at 355 nm and 525 nm in biologically compatible media. These complexes may serve as multifunctional CORMs as they release CO and have the ability to serve as future imageable reporters by exploiting their luminescent properties.

5.5 References

1. Rimmer, R. D.; Richter, H.; Ford, P. C. A Photochemical Precursor for Carbon Monoxide Release in Aerated Aqueous Media. *Inorg. Chem.* **2010**, *49*, 1180-1185.

2. Garcia-Gallego, S.; Bernardes, G. J. L. Carbon-Monoxide-Releasing Molecules for the Delivery of Therapeutic CO In Vivo. *Angew. Chem. -Int. Edit.* **2014**, *53*, 9712-9721.

3. Chakraborty, I.; Carrington, S. J.; Mascharak, P. K. Design Strategies To Improve the Sensitivity of Photoactive Metal Carbonyl Complexes (photoCORMs) to Visible Light and Their Potential as CO-Donors to Biological Targets. *Acc. Chem. Res.* **2014**, *47*, 2603-2611.

4. Rimmer, R. D.; Pierri, A. E.; Ford, P. C. Photochemically activated carbon monoxide release for biological targets. Toward developing air-stable photoCORMs labilized by visible light. *Coord. Chem. Rev.* **2012**, *256*, 1509-1519.

5. Schatzschneider, U. PhotoCORMs: Light-triggered release of carbon monoxide from the coordination sphere of transition metal complexes for biological applications. *Inorg. Chim. Acta* **2011**, *374*, 19-23.

6. Niesel, J.; Pinto, A.; N'Dongo, H. W. P.; Merz, K.; Ott, I.; Gust, R.; Schatzschneider, U. Photoinduced CO release, cellular uptake and cytotoxicity of a tris(pyrazolyl) methane (tpm) manganese tricarbonyl complex. *Chem. Commun.* **2008**, *15*, 1798-1800.

7. Meister, K.; Niesel, J.; Schatzschneider, U.; Metzler-Nolte, N.; Schmidt, D. A.; Havenith, M. Label-Free Imaging of Metal-Carbonyl Complexes in Live Cells by Raman Microspectroscopy. *Angew. Chem. -Int. Edit.* **2010**, *49*, 3310-3312.

8. Doerdelmann, G.; Pfeiffer, H.; Birkner, A.; Schatzschneider, U. Silicium Dioxide Nanoparticles As Carriers for Photoactivatable CO-Releasing Molecules (PhotoCORMs). *Inorg. Chem.* **2011**, *50*, 4362-4367.

9. Doerdelmann, G.; Meinhardt, T.; Sowik, T.; Krueger, A.; Schatzschneider, U. CuAAC click functionalization of azide-modified nanodiamond with a photoactivatable CO-releasing molecule (PhotoCORM) based on $[Mn(CO)_3(tpm)]^+$. *Chem. Commun.* **2012**, *48*, 11528-11530.

10. Kianfar, E.; Schaefer, C.; Lornejad-Schaefer, M. R.; Portenkirchner, E.; Knoer, G. New photo-CORMs: Deeply-coloured biocompatible rhenium complexes for the controlled release of carbon monoxide. *Inorg. Chim. Acta* **2015**, *435*, 174-177.

11. Pierri, A. E.; Pallaoro, A.; Wu, G.; Ford, P. C. A Luminescent and Biocompatible PhotoCORM. *J. Am. Chem. Soc.* **2012**, *134*, 18197-18200.

12. Arrowsmith, R. L.; Atkin, A. J.; Botchway, S. W.; Fairlamb, I. J. S.; Lynam, J. M.; Moir, J. W. B.; Pascu, S. I.; Ward, J. S.; Zhang, W. Confocal and fluorescence lifetime imaging sheds light on the fate of a pyrene-tagged carbon monoxide-releasing Fischer carbene chromium complex. *Dalton Trans.* **2015**, *44*, 4957-4962.

13. Carrington, S. J.; Chakraborty, I.; Bernard, J. M. L.; Mascharak, P. K. Synthesis and Characterization of a "Turn-On" photoCORM for Trackable CO Delivery to Biological Targets. *ACS Med. Chem. Lett.* **2014**, *5*, 1324-1328.

14. Ward, J. S.; Lynam, J. M.; Moir, J.; Fairlamb, I. J. S. Visible-Light-Induced CO Release from a Therapeutically Viable Tryptophan-Derived Manganese(I) Carbonyl (TryptoCORM) Exhibiting Potent Inhibition against E. coli. *Chem. -Eur. J.* **2014**, *20*, 15061-15068.

15. Antony, L. A. P.; Slanina, T.; Sebej, P.; Solomek, T.; Klan, P. Fluorescein Analogue Xanthene-9-Carboxylic Acid: A Transition-Metal-Free CO Releasing Molecule Activated by Green Light. *Org. Lett.* **2013**, *15*, 4552-4555.

16. Peng, P.; Wang, C.; Shi, Z.; Johns, V. K.; Ma, L.; Oyer, J.; Copik, A.; Igarashi, R.; Liao, Y. Visible-light activatable organic CO-releasing molecules (PhotoCORMs) that simultaneously generate fluorophores. *Org. Biomol. Chem.* **2013**, *11*, 6671-6674.

17. Jiang, X.; Chen, L.; Wang, X.; Long, L.; Xiao, Z.; Liu, X. Photoinduced Carbon Monoxide Release from Half-Sandwich Iron(II) Carbonyl Complexes by Visible Irradiation: Kinetic Analysis and Mechanistic Investigation. *Chem. -Eur. J.* **2015**, *21*, 13065-13072.

18. Chakraborty, I.; Carrington, S. J.; Mascharak, P. K. Photodelivery of CO by Designed PhotoCORMs: Correlation between Absorption in the Visible Region and

Metal-CO Bond Labilization in Carbonyl Complexes. *ChemMedChem* **2014**, *9*, 1266-1274.

19. Carrington, S. J.; Chakraborty, I.; Mascharak, P. K. Exceptionally rapid CO release from a manganese(I) tricarbonyl complex derived from bis(4-chloro-phenylimino)acenaphthene upon exposure to visible light. *Dalton Trans.* **2015**, *44*, 13828-13834.

20. Gonzalez, M. A.; Carrington, S. J.; Fry, N. L.; Martinez, J. L.; Mascharak, P. K. Syntheses, Structures, and Properties of New Manganese Carbonyls as Photoactive CO-Releasing Molecules: Design Strategies That Lead to CO Photolability in the Visible Region. *Inorg. Chem.* **2012**, *51*, 11930-11940.

21. Carrington, S. J.; Chakraborty, I.; Mascharak, P. K. Rapid CO release from a Mn(I) carbonyl complex derived from azopyridine upon exposure to visible light and its phototoxicity toward malignant cells. *Chem. Commun.* **2013**, *49*, 11254-11256.

22. Pierri, A. E.; Huang, P.; Garcia, J. V.; Stanfill, J. G.; Chui, M.; Wu, G.; Zheng, N.; Ford, P. C. A photoCORM nanocarrier for CO release using NIR light. *Chem. Commun.* **2015**, *51*, 2072-2075.

23. Treibs, A.; Kreuzer, F. Di- and Tri-Pyrrylmethene Complexes with Di-Fluoro Boron. *Justus Liebigs Ann. Chem.* **1968**, *718*, 208.

24. Gorman, A.; Killoran, J.; O'Shea, C.; Kenna, T.; Gallagher, W.; O'Shea, D. In vitro demonstration of the heavy-atom effect for photodynamic therapy. *J. Am. Chem. Soc.* **2004**, *126*, 10619-10631.

25. Xu, J.; Zhu, L.; Wang, Q.; Zeng, L.; Hu, X.; Fu, B.; Sun, Z. meso-C_6F_5 substituted BODIPYs with distinctive spectroscopic properties and their application for bioimaging in living cells. *Tetrahedron* **2014**, *70*, 5800-5805.

26. Manton, J. C.; Long, C.; Vos, J. G.; Pryce, M. T. A photo- and electrochemical investigation of BODIPY-cobaloxime complexes for hydrogen production, coupled with quantum chemical calculations. *Phys. Chem. Chem. Phys.* **2014**, *16*, 5229-5236.

27. Michel, B. W.; Lippert, A. R.; Chang, C. J. A Reaction-Based Fluorescent Probe for Selective Imaging of Carbon Monoxide in Living Cells Using a Palladium-Mediated Carbonylation. *J. Am. Chem. Soc.* **2012**, *134*, 15668-15671.

28. Ni, Y.; Wu, J. Far-red and near infrared BODIPY dyes: synthesis and applications for fluorescent pH probes and bio-imaging. *Org. Biomol. Chem.* **2014**, *12*, 3774-3791.

29. Ulrich, G.; Ziessel, R. Convenient and efficient synthesis of functionalized oligopyridine ligands bearing accessory pyrromethene-BF_2 fluorophores. *J. Org. Chem.* **2004**, *69*, 2070-2083.

30. Kesavan, P. E.; Das, S.; Lone, M. Y.; Jha, P. C.; Mori, S.; Gupta, I. Bridged bis-BODIPYs: their synthesis, structures and properties. *Dalton Trans.* **2015**, *44*, 17209-17221.

31. Kim, K.; Jo, C.; Easwaramoorthi, S.; Sung, J.; Kim, D. H.; Churchill, D. G. Crystallographic, Photophysical, NMR Spectroscopic and Reactivity Manifestations of the "8-Heteroaryl Effect" in 4,4-Difluoro-8-(C_4H_3X)-4-bora-3a,4a-diaza-s-indacene (X=O, S, Se) (BODIPY) Systems. *Inorg. Chem.* **2010**, *49*, 4881-4894.

32. Chen, Y.; Zhao, J.; Xie, L.; Guo, H.; Li, Q. Thienyl-substituted BODIPYs with strong visible light-absorption and long-lived triplet excited states as organic triplet sensitizers for triplet-triplet annihilation upconversion. *RSC Adv.* **2012**, *2*, 3942-3953.

33. Wang, J.; Karpus, J.; Zhao, B. S.; Luo, Z.; Chen, P. R.; He, C. A Selective Fluorescent Probe for Carbon Monoxide Imaging in Living Cells. *Angew. Chem. -Int. Edit.* **2012**, *51*, 9652-9656.

34. Schatzschneider, U. Novel lead structures and activation mechanisms for CO-releasing molecules (CORMs). *Br. J. Pharmacol.* **2015**, *172*, 1638-1650.

35. Seixas, J. D.; Chaves-Ferreira, M.; Montes-Grajales, D.; Goncalves, A. M. L.; Marques, A. R.; Saraiva, L. M.; Olivero-Verbel, J.; Romao, C. C.; Bernardes, G. J. L. An N-Acetyl Cysteine Ruthenium Tricarbonyl Conjugate Enables Simultaneous Release of CO and Ablation of Reactive Oxygen Species. *Chem. -Eur. J.* **2015**, *21*, 14708-14712.

36. Pai, S.; Hafftlang, M.; Atongo, G.; Nagel, C.; Niesel, J.; Botov, S.; Schmalz, H.; Yard, B.; Schatzschneider, U. New modular manganese(I) tricarbonyl complexes as PhotoCORMs: in vitro detection of photoinduced carbon monoxide release using COP-1 as a fluorogenic switch-on probe. *Dalton Trans.* **2014**, *43*, 8664-8678.

37. Banfi, S.; Nasini, G.; Zaza, S.; Caruso, E. Synthesis and photo-physical properties of a series of BODIPY dyes. *Tetrahedron* **2013**, *69*, 4845-4856.

38. Schwenze, G.; Darensbourg, D.; Darensbourg, M. Photochemical Substitution Reactions of Substituted Group VI Metal-Carbonyls. *Inorg. Chem.* **1972**, *11*, 1967-1970.

39. Wrighton, M.; Abrahamson, H.; Morse, D. Photosubstitution Reactivity of a Series of Pentacarbonylpyridinotungsten(0) Complexes having Ligand-Field Or Charge-Transfer Lowest Excited-States. *J. Am. Chem. Soc.* **1976**, *98*, 4105-4109.

40. Fillaut, J. L.; Perruchon, J.; Blanchard, P.; Roncali, J.; Golhen, S.; Allain, M.; Migalska-Zalas, A.; Kityk, I. V.; Sahraoui, B. Design and synthesis of ruthenium oligothienylacetylide complexes. New materials for acoustically induced nonlinear optics. *Organometallics* **2005**, *24*, 687-695.

41. Fang, Y.; Hanan, G. Rapid and efficient synthesis of functionalized bipyridines. *Synlett* **2003**, *6*, 852-854.

42. Ziessel, R.; Goze, C.; Ulrich, G.; Cesario, M.; Retailleau, P.; Harriman, A.; Rostron, J. Intramolecular energy transfer in pyrene-bodipy molecular dyads and triads. *Chem. - Eur. J.* **2005**, *11*, 7366-7378.

43. Luo, G.; Fang, K.; Wu, J.; Dai, J.; Zhao, Q. Noble-metal-free BODIPY-cobaloxime photocatalysts for visible-light-driven hydrogen production. *Phys. Chem. Chem. Phys.* **2014**, *16*, 23884-23894.

44. Moralejo, C.; Langford, C.; Sharma, D. Wavelength-Dependent Photochemical Ligand Substitution in $W(CO)_5L$ (L = Pyridine, Piperidine). *Inorg. Chem.* **1989**, *28*, 2205-2209.

45. Kolodziej, R.; Lees, A. Photophysics and Photochemistry of a Series of $M(CO)_5L$ Complexes Where M = Cr Or Mo and L = Pyridine Or a Substituted Pyridine. *Organometallics* **1986**, *5*, 450-455.

46. Rosenthal, J.; Nepomnyashchii, A. B.; Kozhukh, J.; Bard, A. J.; Lippard, S. J. Synthesis, Photophysics, Electrochemistry, and Electrogenerated Chemiluminescence of a Homologous Set of BODIPY-Appended Bipyridine Derivatives. *J Phys Chem C* **2011**, *115*, 17993-18001.

47. Manuta, D. M.; Lees, A. J. Photophysics of Metal-Carbonyl-Complexes - Multiple Emissions from Diimine-Tetracarbonyl Complexes of Group-6b Metals in Room-Temperature Solution. *Inorg. Chem.* **1983**, *22*, 572-573.

48. Guillaumont, D.; Daniel, C.; Vlcek, A. Electronic structure of the lowest excited states of $Cr(CO)_4$(2,2'-bipyridine): A CASSCF/CASPT2 analysis. *Inorg. Chem.* **1997**, *36*, 1684-1688.

49. Manton, J. C.; Long, C.; Vos, J. G.; Pryce, M. T. Porphyrin-cobaloxime complexes for hydrogen production, a photo- and electrochemical study, coupled with quantum chemical calculations. *Dalton Trans.* **2014**, *43*, 3576-3583.

50. Lakshmi, V.; Lee, W.; Ravikanth, M. Synthesis, structure and spectral and electrochemical properties of 3-pyrrolyl BODIPY-metal dipyrrin complexes. *Dalton Trans.* **2014**, *43*, 16006-16014.

51. Khan, T. K.; Shaikh, M. S.; Ravikanth, M. Synthesis and photophysical properties of covalently linked boron dipyrromethene dyads. *Dyes Pigments* **2012**, *94*, 66-73.

52. Donuru, V. R.; Vegesna, G. K.; Velayudham, S.; Green, S.; Liu, H. Synthesis and Optical Properties of Red and Deep-Red Emissive Polymeric and Copolymeric BODIPY Dyes. *Chem. Mat.* **2009**, *21*, 2130-2138.

53. Manton, J. PhD Thesis, Dublin City University. **2013**.

54. Poirel, A.; De Nicola, A.; Retailleau, P.; Ziessel, R. Oxidative Coupling of 1,7,8-Unsubstituted BODIPYs: Synthesis and Electrochemical and Spectroscopic Properties. *J. Org. Chem.* **2012**, *77*, 7512-7525.

55. Krumova, K.; Cosa, G. Bodipy Dyes with Tunable Redox Potentials and Functional Groups for Further Tethering: Preparation, Electrochemical, and Spectroscopic Characterization. *J. Am. Chem. Soc.* **2010**, *132*, 17560-17569.

56. Nepomnyashchii, A. B.; Cho, S.; Rossky, P. J.; Bard, A. J. Dependence of Electrochemical and Electrogenerated Chemiluminescence Properties on the Structure of BODIPY Dyes. Unusually Large Separation between Sequential Electron Transfers. *J. Am. Chem. Soc.* **2010**, *132*, 17550-17559.

57. Li, F.; Yang, S.; Ciringh, Y.; Seth, J.; Martin, C.; Singh, D.; Kim, D.; Birge, R.; Bocian, D.; Holten, D.; Lindsey, J. Design, synthesis, and photodynamics of light-harvesting arrays comprised of a porphyrin and one, two, or eight boron-dipyrrin accessory pigments. *J. Am. Chem. Soc.* **1998**, *120*, 10001-10017.

58. Stiddard, M. 2,2'-Bipyridyl Derivatives of Group V1 Carbonyls. *J. Chem. Soc* **1962**, *910*, 4712-4715.

59. Cotton, F.; Darensbourg, D.; Ilsley, W. Pi Acidity of Tris(2-Cyanoethyl)phosphine - X-Ray Structural Studies of $M(CO)_5P(CH_2CH_2CN)_3$(M=Cr,Mo) and $Mo(CO)_5P(C_6H_5)_3$. *Inorg. Chem.* **1981**, *20*, 578-583.

60. Pitchumony, T. S.; Spingler, B.; Motterlini, R.; Alberto, R. Syntheses, structural characterization and CO releasing properties of boranocarbonate $[H_3BCO_2H]^-$ derivatives. *Org. Biomol. Chem.* **2010**, *8*, 4849-4854.

61. Crook, S. H.; Mann, B. E.; Meijer, A. J. H. M.; Adams, H.; Sawle, P.; Scapens, D.; Motterlini, R. $[Mn(CO)_4\{S_2CNMe(CH_2CO_2H)\}]$, a new water-soluble CO-releasing molecule. *Dalton Trans.* **2011**, *40*, 4230-4235.

62. McLean, S.; Mann, B. E.; Poole, R. K. Sulfite species enhance carbon monoxide release from CO-releasing molecules: Implications for the deoxymyoglobin assay of activity. *Anal. Biochem.* **2012**, *427*, 36-40.

63. Allampally, N. K.; Florian, A.; Mayoral, M. J.; Rest, C.; Stepanenko, V.; Fernandez, G. H-Aggregates of Oligophenyleneethynylene (OPE)-BODIPY Systems in Water: Guest Size-Dependent Encapsulation Mechanism and Co-aggregate Morphology. *Chem. -Eur. J.* **2014**, *20*, 10669-10678.

64. Virrels, I.; George, M.; Turner, J.; Peters, J.; Vlcek, A. Photochemistry of $Cr(CO)_4$(bpy) (bpy=2,2'-bipyridine) studied by time-resolved infrared spectroscopy. *Organometallics* **1996**, *15*, 4089-4092.

65. Vichova, J.; Hartl, F.; Vlcek, A. Wavelength-Dependent Photosubstitution and Excited-State Dynamics of [$Cr(CO)_4$(2,2'-Bipyridine)] - a Quantum Yield and Picosecond Absorption Study. *J. Am. Chem. Soc.* **1992**, *114*, 10903-10910.

6 Chapter 6 Conclusions and Future Work

Chapter 1 introduces the topic of CO as a therapeutic agent and highlights the work previously reported based on transition metal carbonyl complexes as CO releasing molecules. Thermal, photochemical and electrochemical stimulated CO release is presented with an emphasis on photochemically induced CO release. To understand the process of CO release from metal carbonyl complexes, it is necessary to study their photochemical mechanisms. Consequently, Chapter 2 describes the photochemical and photophysical properties of methoxy Fischer carbene complexes. Various techniques such as matrix isolation and psTRIR spectroscopy with the aid of quantum chemical calculations were used to identify the excited state species formed following excitation and hence elucidate the photochemical mechanisms. Originally, Hegedus investigated the photochemistry of these compounds and proposed that a metallacyclopropanone or metallaketene intermediate may be produced during the synthesis of β-lactams.[1,2] The results presented in this chapter provide evidence that both of these intermediates are formed photochemically. In addition, a novel method of stimulating CO release by electrochemical means is presented.

In Chapter 3, the photochemistry of pyrrolidine based Fischer carbene complexes were investigated also by psTRIR spectroscopy. In contrast to the findings in Chapter 2, a metallacyclopropanone or metallaketene intermediate was not observed spectroscopically which further supports the previous work carried out by Hafner *et al.* which showed that amino based Fischer carbene complexes did not readily form β-lactams.[3]

Chapter 4 focused on the photochemistry of ferrocenyl and styryl based Fischer carbene complexes. These compounds were synthesised with the aim of extending the UV-vis absorption spectra towards the photodynamic therapeutic window to investigate if low energy excitation could induce CO release to ensure minimal damage to tissues and ensure sufficient light penetration. However, although the UV-vis absorbance spectra were shifted to lower energy, photoinduced CO release was not efficient following excitation at 470, 400 and 320 nm. A range of excited states were produced upon irradiation which lead to a deactivation pathway, regenerating the ground state parent complexes, particularly so for the ferrocenyl compounds and to a lesser extent for the styryl analogues. Subtle differences were observed between both sets of compounds

with wavelength dependent photochemistry and spectral features consistent with the formation of a ketene intermediate species occurring for both the chromium and tungsten based methoxy styryl compounds, $[(CO)_5M(OMe)C_2H_2Ph]$ (M = Cr, W). These features were not observed for the ferrocenyl carbene complexes which is in agreement with that reported by Sierra and co-workers which deduced that ferrocene carbenes did not undergo β-lactam synthesis and were 'photo-inert'.[4-6]

Chapter 5 highlights the development of more biocompatible BODIPY based metal carbonyl complexes. BODIPY compounds are relatively stable to physiological conditions, absorb strongly in the UV-vis region with a high molar absorptivity, are easily tuned, and are particularly emissive with high quantum yields.[7-9] In addition, they are widely used in biological studies, for example in photodynamic therapy, labelling and in cellular imaging.[10,11] A range of novel BODIPY metal carbonyl complexes were synthesised and characterised and their CO releasing potential was assessed in a biocompatible media to mimic biological environments. CO release was observed at 355, 525 and 620 nm with up to 2 molecules of CO released per mole of complex over the timeframe of the experiments (180 min). Not only are these compounds efficient CORMs, they also demonstrate that as CO is released the emission intensity increases. This dual functionality is interesting as their unique emissive profiles can serve as an indicator for CO release and allows for cellular tracking.

Future work on these particular compounds should include the identification of the reaction pathways to CO release in biological media. In addition, the toxicity and cellular imaging properties of the CORMs and any side products produced during degradation should be investigated.

Next, the development of more biocompatible BODIPY based CORMs should be studied by incorporating bioavailable metals and solubilising groups to aid cellular uptake. When further studies are carried out on the bioactivity of these compounds, it may be possible to direct the CORMs to target areas by introducing peptide conjugates or cell surface receptors. Finally, photochemical CO release should be induced using low energy photons within the photodynamic therapeutic window (> 600 nm), thus minimising damage to healthy tissues and allowing for sufficient penetration at the site of interest.

6.1 References

1. Hegedus, L.; McGuire, M.; Schultze, L.; Yijun, C.; Anderson, O. Reaction of Chromium Carbene Complexes with Imines - Synthesis of Beta-Lactams. *J. Am. Chem. Soc.* **1984**, *106*, 2680-2687.

2. Hegedus, L.; DeWeck, G.; Dandrea, S. Evidence for the Intermediacy of Chromium Ketene Complexes in the Synthesis of Beta-Lactams by the Photolytic Reaction of Chromium Carbene Complexes with Imines - use in Amino-Acid Synthesis. *J. Am. Chem. Soc.* **1988**, *110*, 2122-2126.

3. Hafner, A.; Hegedus, L.; DeWeck, G.; Hawkins, B.; Dotz, K. Chromium-53 Nuclear Magnetic-Resonance Studies of Pentacarbonylchromium Carbene Complexes. *J. Am. Chem. Soc.* **1988**, *110*, 8413-8421.

4. Lage, M. L.; Fernandez, I.; Mancheno, M. J.; Gomez-Gallego, M.; Sierra, M. A. Metal-Tuned Photochemistry of Metallocene-Substituted Chromium(0)-Carbene Complexes. *Chem. -Eur. J.* **2009**, *15*, 593-596.

5. Lage, M. L.; Fernandez, I.; Mancheno, M. J.; Gomez-Gallego, M.; Sierra, M. A. The Electronic Structure and Photochemistry of Group 6 Bimetallic (Fischer) Carbene Complexes: Beyond the Photocarbonylation Reaction. *Chem. -Eur. J.* **2010**, *16*, 6616-6624.

6. Sierra, M.; Mancheno, M.; Vicente, R.; Gomez-Gallego, M. Synthesis of ferrocene-substituted 2-azetidinones. *J. Org. Chem.* **2001**, *66*, 8920-8925.

7. Treibs, A.; Kreuzer, F. Di- and Tri-Pyrrylmethene Complexes with Di-Fluoro Boron. *Justus Liebigs Ann. Chem.* **1968**, *718*, 208.

8. Manton, J. C.; Long, C.; Vos, J. G.; Pryce, M. T. A photo- and electrochemical investigation of BODIPY-cobaloxime complexes for hydrogen production, coupled with quantum chemical calculations. *Phys. Chem. Chem. Phys.* **2014**, *16*, 5229-5236.

9. Banfi, S.; Nasini, G.; Zaza, S.; Caruso, E. Synthesis and photo-physical properties of a series of BODIPY dyes. *Tetrahedron* **2013**, *69*, 4845-4856.

10. Gorman, A.; Killoran, J.; O'Shea, C.; Kenna, T.; Gallagher, W.; O'Shea, D. In vitro demonstration of the heavy-atom effect for photodynamic therapy. *J. Am. Chem. Soc.* **2004**, *126*, 10619-10631.

11. Michel, B. W.; Lippert, A. R.; Chang, C. J. A Reaction-Based Fluorescent Probe for Selective Imaging of Carbon Monoxide in Living Cells Using a Palladium-Mediated Carbonylation. *J. Am. Chem. Soc.* **2012**, *134*, 15668-15671.

Appendix A Myoglobin Assay Calculation

The quantity of [Mb-CO] is carried out using the standard assay data treatment procedure reported by Fairlamb and co-workers with some modifications.[1]

There is an absorbance maximum peak at ~ 560 nm for deoxy-Mb. When CO is bubbled through this solution, two new peaks are formed; 540 and 578 nm and are assigned to saturated Mb-CO. The maximal absorption peak of Mb-CO at 540 nm corresponds to the exact concentration of myoglobin in the stock solution. The following equation was used to find $t_{½}$.

Equation 1

This calculates the total concentration of myoglobin in a saturated solution of Mb-CO. ε represents the extinction co-efficient of Mb-CO which is, 15.4 mM^{-1} cm^{-1}.

OD_{540} = Absorbance of Mb-CO solution at 540 nm.

$\text{Mb-CO}_{max} = \left(\frac{OD_{540}}{\varepsilon}\right) \times 1000$

e.g. From the graph of the Mb-CO standard, $OD_{540} = 0.739$

Therefore, $\text{Mb-CO}_{max} = \left(\frac{0.739}{15.4}\right) \times 1000$

= 47.99 µM.

Intermediate concentrations of Mb-CO may be calculated from OD_{540} at different timepoints.

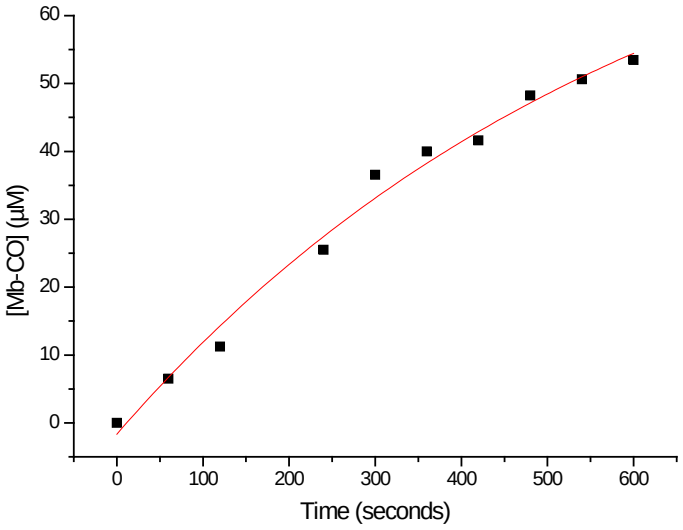

Figure A1 The formation of Mb-CO over time from the CORM, $[(CO)_5Cr(NC_4H_8)Me]$.

From this plot, it is possible to find, $t_{½}$ which is the time taken for the concentration of Mb-CO produced to be equal to half of the initial concentration of the CORM i.e. the time taken for a solution of CORM with a concentration of 60 μM to produce a solution of Mb-CO with a concentration of 30 μM by subbing in the data to Origin 8.0 which incorporates the equation of a line y = *m*x + c. The slope is calculated as follows $m = \frac{y2-y1}{x2-x1}$.

Reference

1. Atkin, A. J.; Lynam, J. M.; Moulton, B. E.; Sawle, P.; Motterlini, R.; Boyle, N. M.; Pryce, M. T.; Fairlamb, I. J. S. Modification of the deoxy-myoglobin/carbonmonoxy-myoglobin UV-vis assay for reliable determination of CO-release rates from organometallic carbonyl complexes. *Dalton Trans.* **2011**, *40*, 5755-5761.

Appendix B NMR Spectroscopic Data

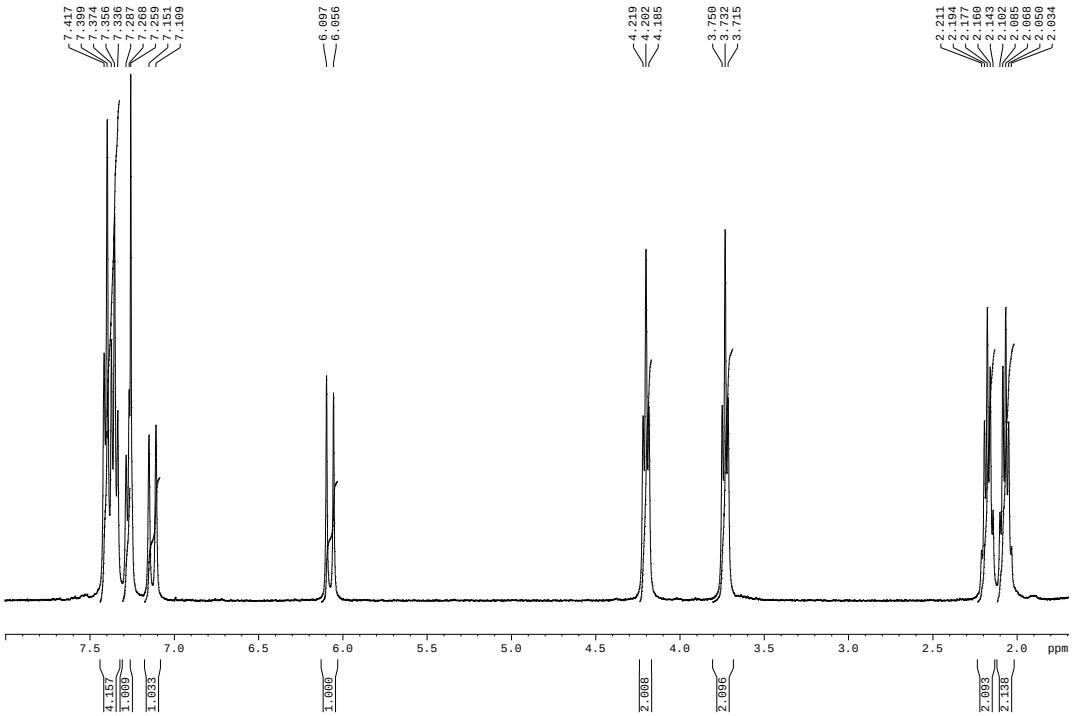

Figure B1 ^{1}H NMR of $[(CO)_5Cr(NC_4H_8)C_2H_2Ph]$ in $CDCl_3$.

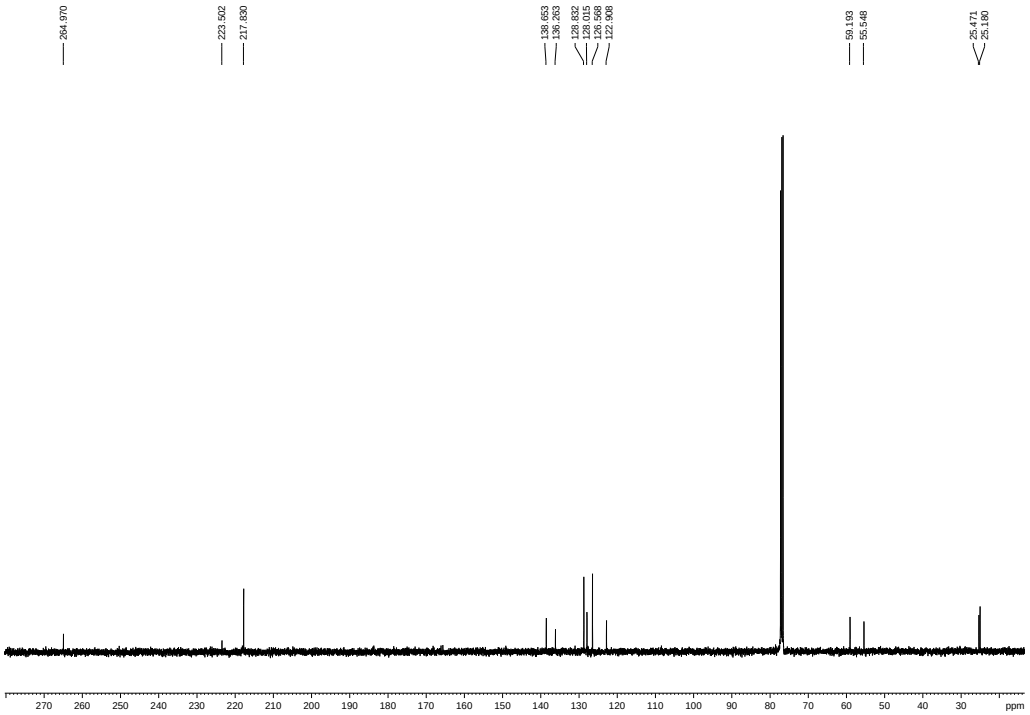

Figure B2 ^{13}C NMR of $[(CO)_5Cr(NC_4H_8)C_2H_2Ph]$ in $CDCl_3$.

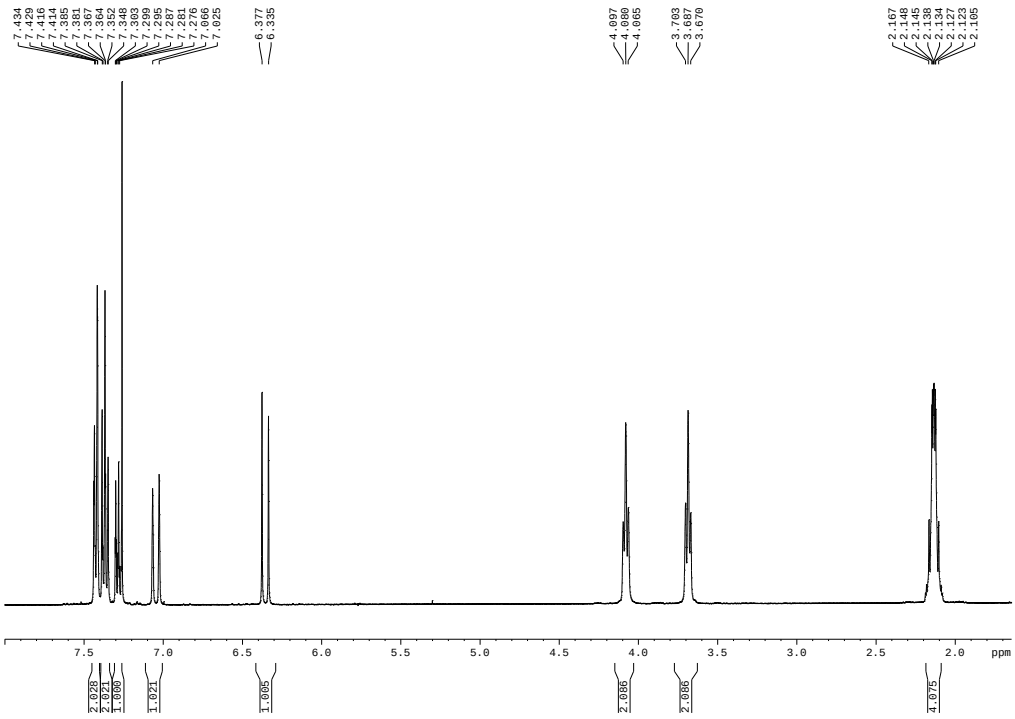

Figure B3 ^{1}H NMR of $[(CO)_5W(NC_4H_8)C_2H_2Ph]$ in $CDCl_3$.

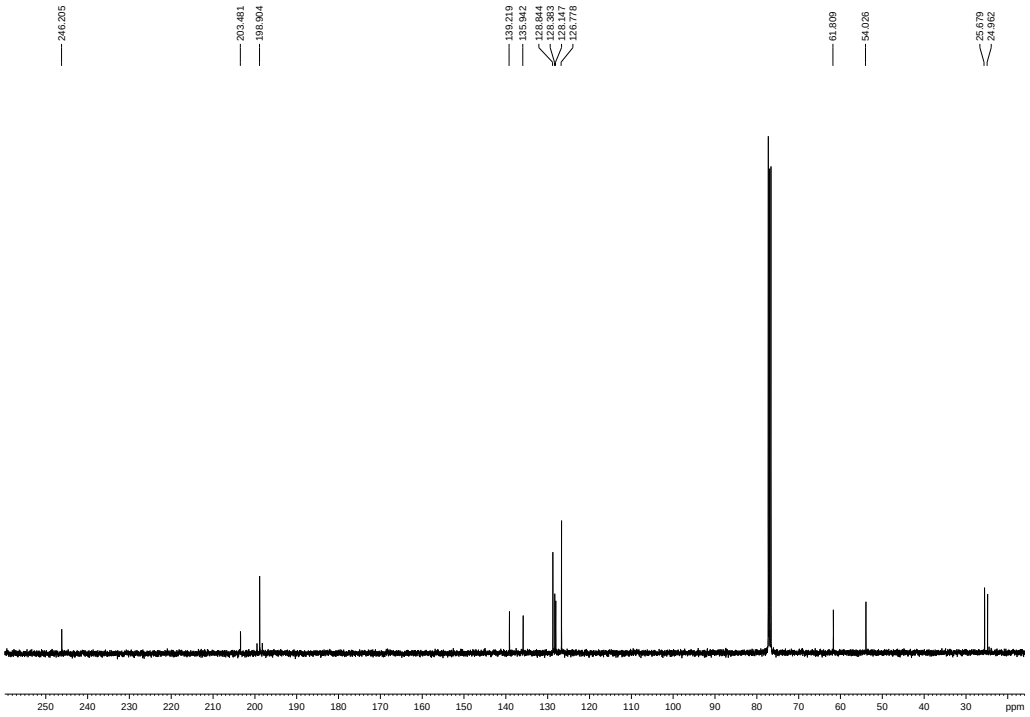

Figure B4 ^{13}C NMR of $[(CO)_5W(NC_4H_8)C_2H_2Ph]$ in $CDCl_3$.

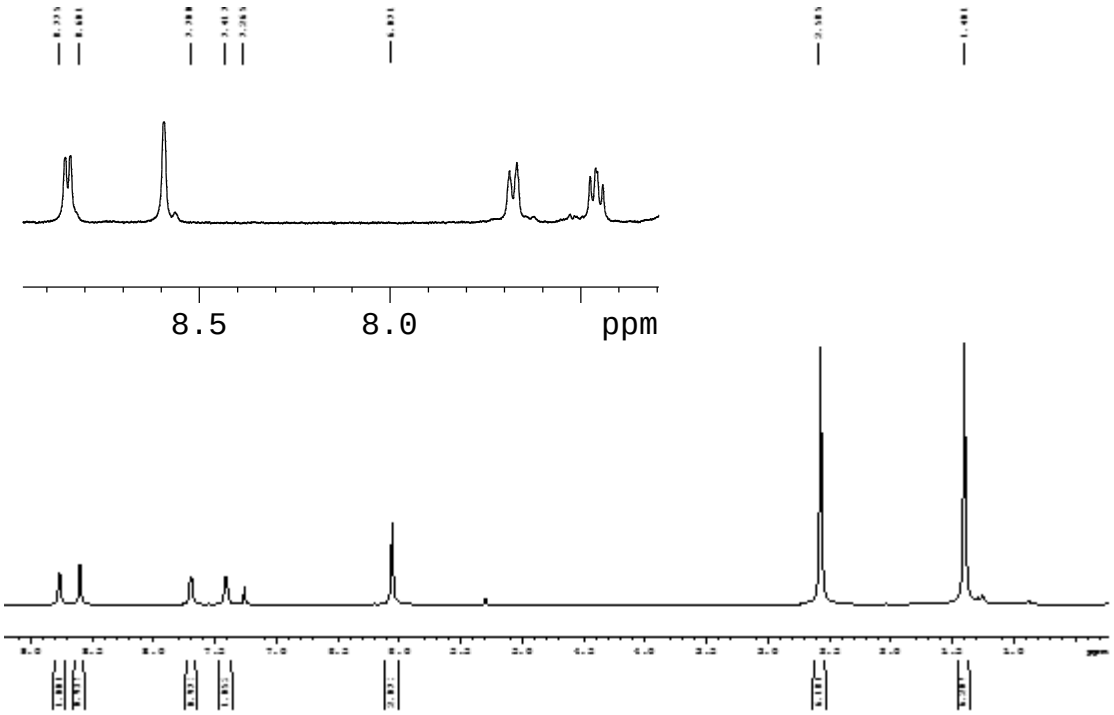

Figure B5 ^{1}H-NMR spectrum of H-BODIPY $Cr(CO)_5$ in $CDCl_3$.

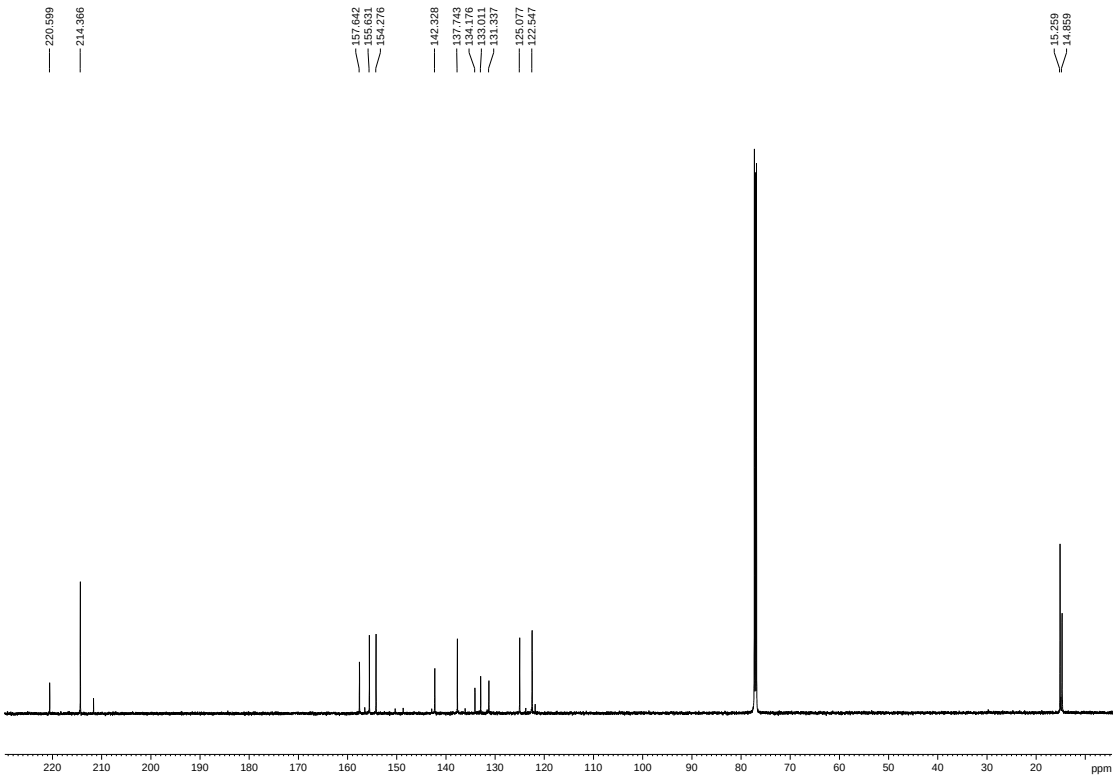

Figure B6 ^{13}C-NMR spectrum of H-BODIPY $Cr(CO)_5$ in $CDCl_3$.

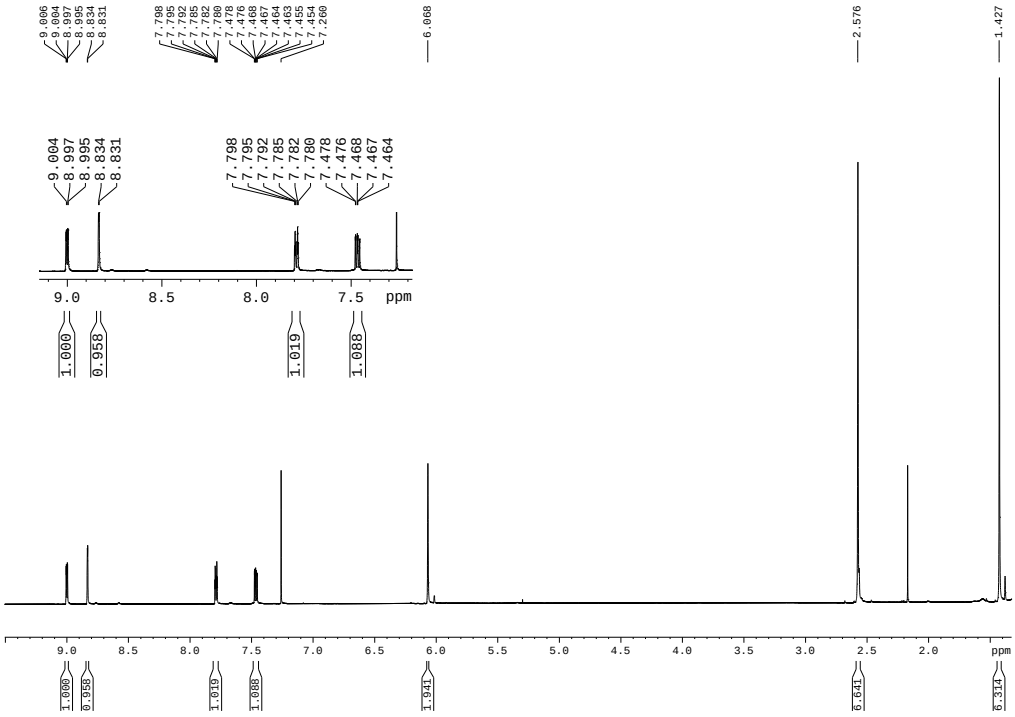

Figure B7 ^{1}H-NMR spectrum of H-BODIPY W(CO)$_5$ in CDCl$_3$.

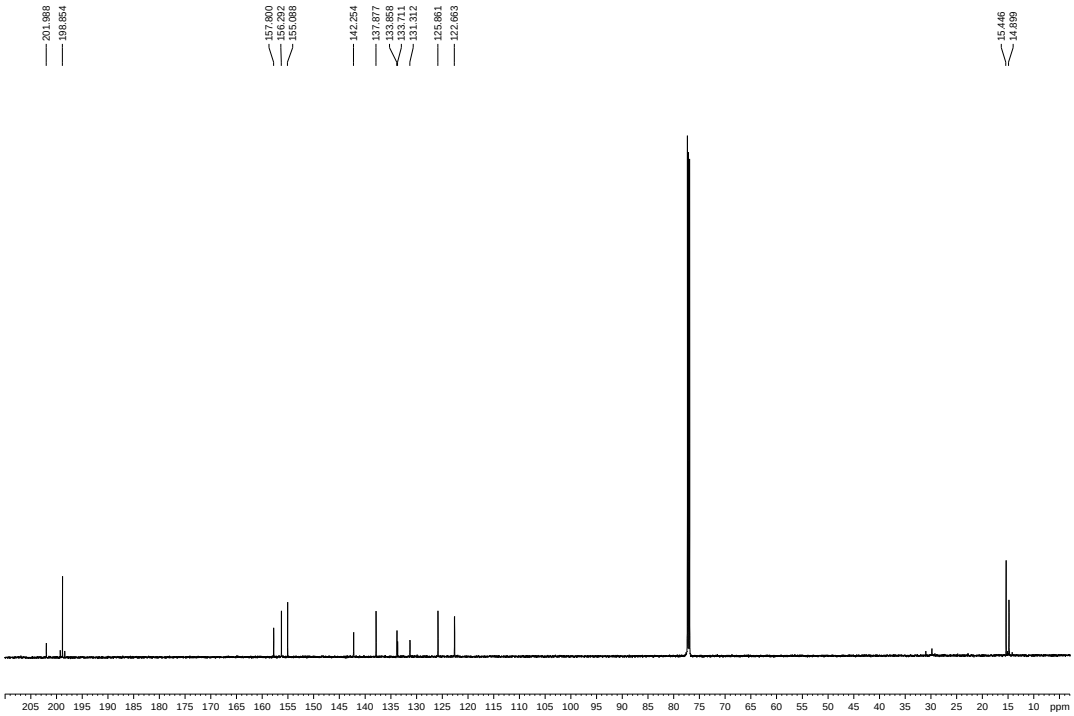

Figure B8 ^{13}C-NMR spectrum of H-BODIPY W(CO)$_5$ in CDCl$_3$.

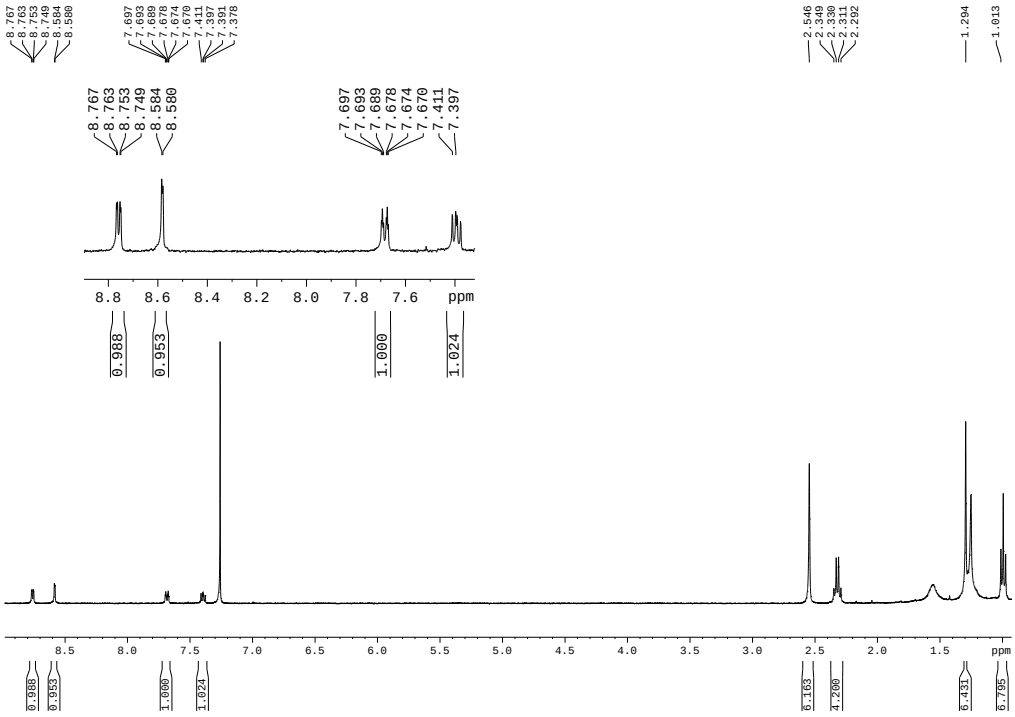

Figure B9 ^{1}H-NMR spectrum of Ethyl-BODIPY $Cr(CO)_5$ in $CDCl_3$.

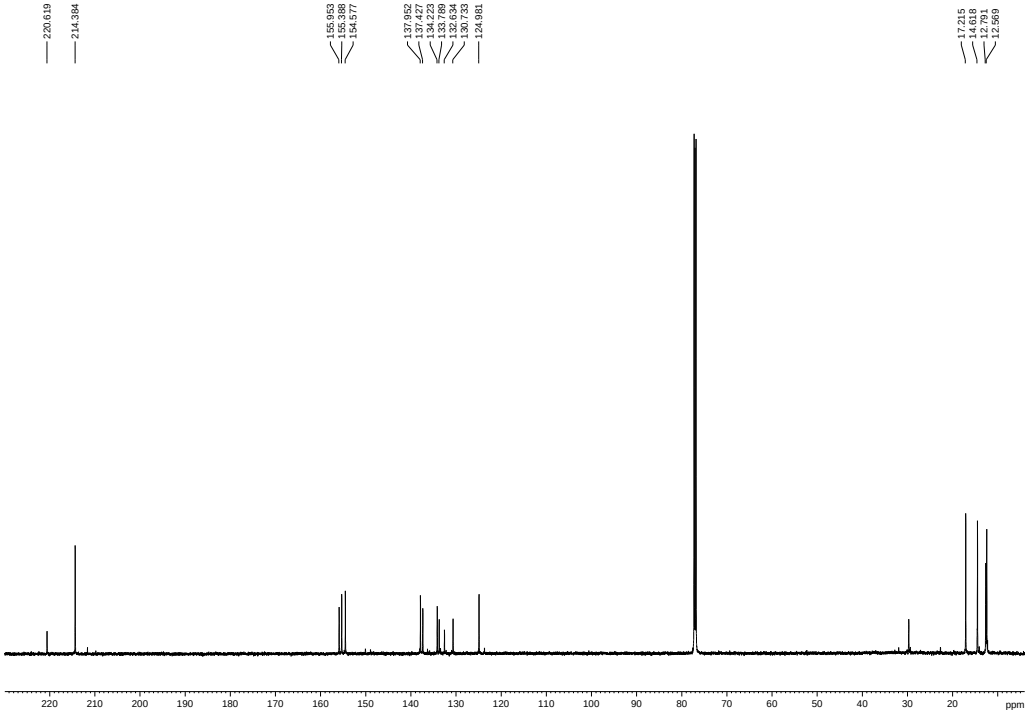

Figure B10 ^{13}C-NMR spectrum of Ethyl-BODIPY $Cr(CO)_5$ in $CDCl_3$.

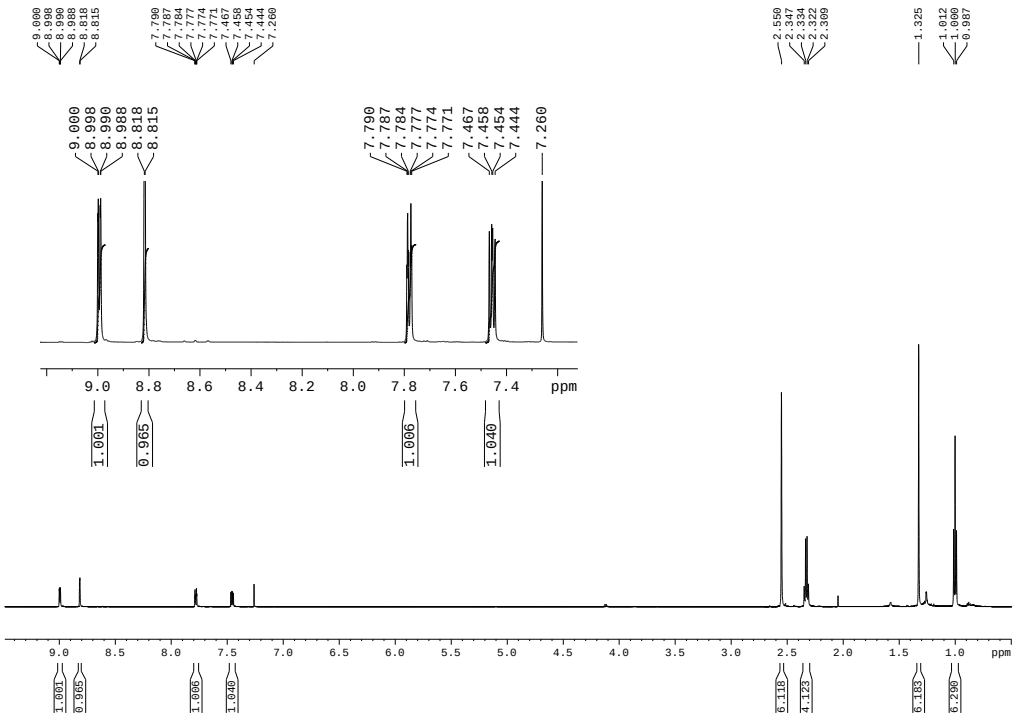

Figure B11 ^{1}H-NMR spectrum of Ethyl-BODIPY W(CO)$_5$ in CDCl$_3$.

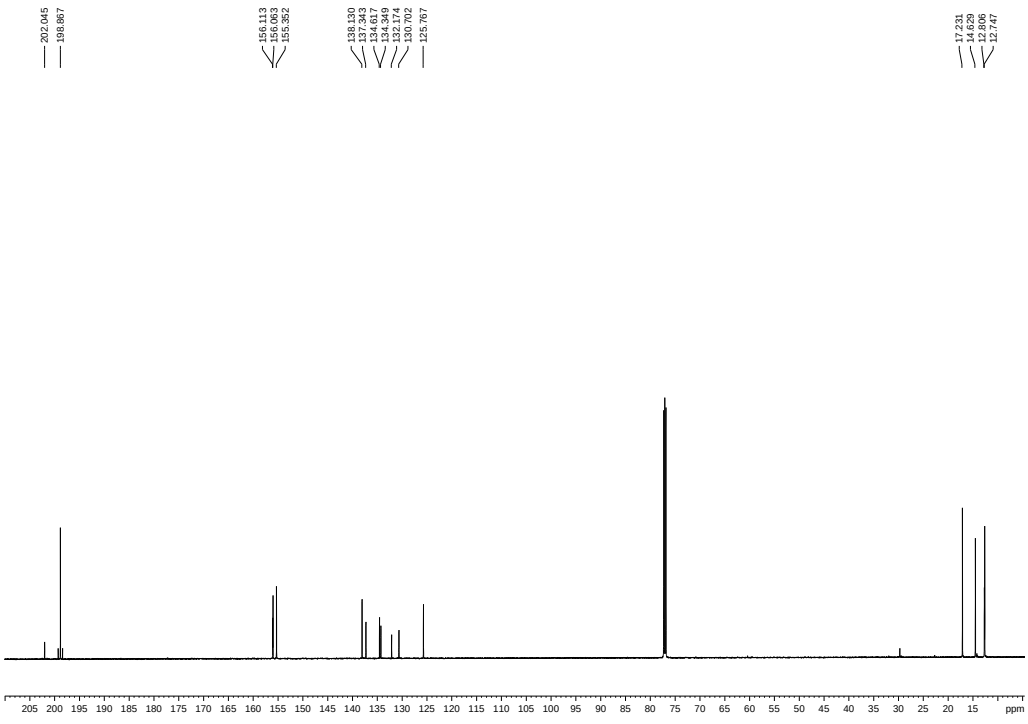

Figure B12 ^{13}C-NMR spectrum of Ethyl-BODIPY W(CO)$_5$ in CDCl$_3$.

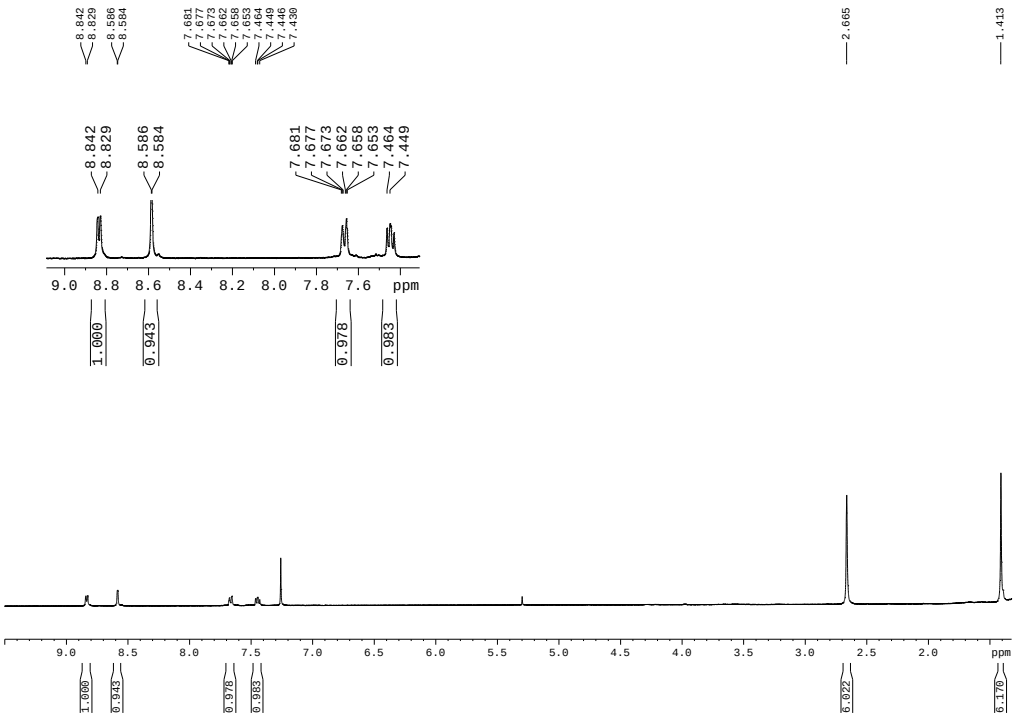

Figure B13 ^{1}H-NMR spectrum of Iodo-BODIPY $Cr(CO)_5$ in $CDCl_3$.

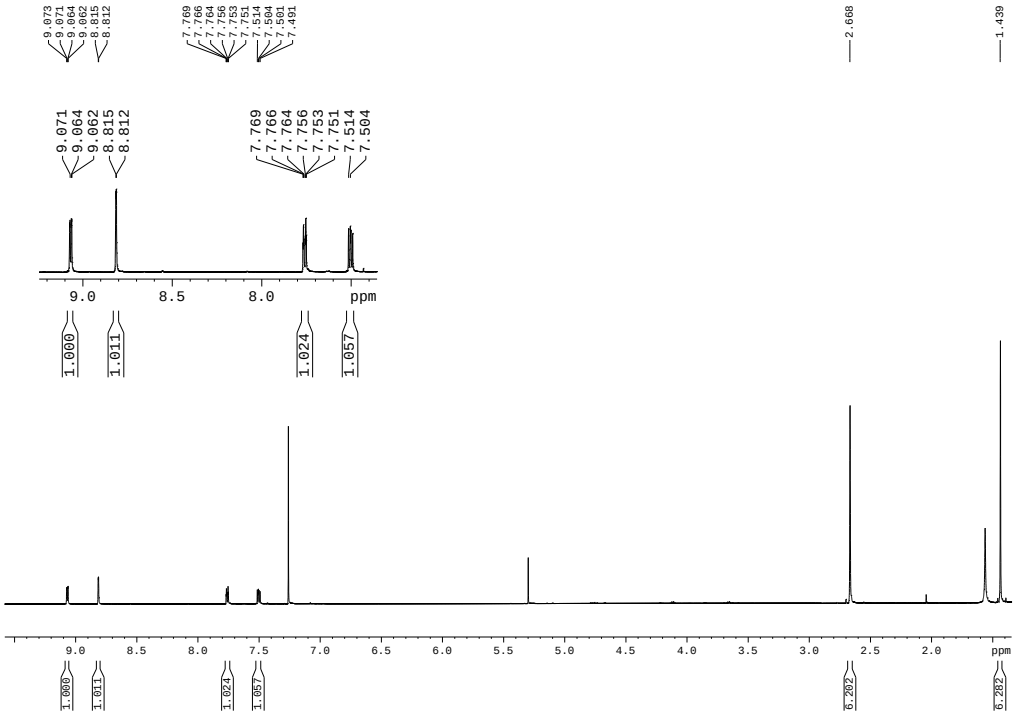

Figure B14 ^{1}H-NMR spectrum of Iodo-BODIPY $W(CO)_5$ in $CDCl_3$.

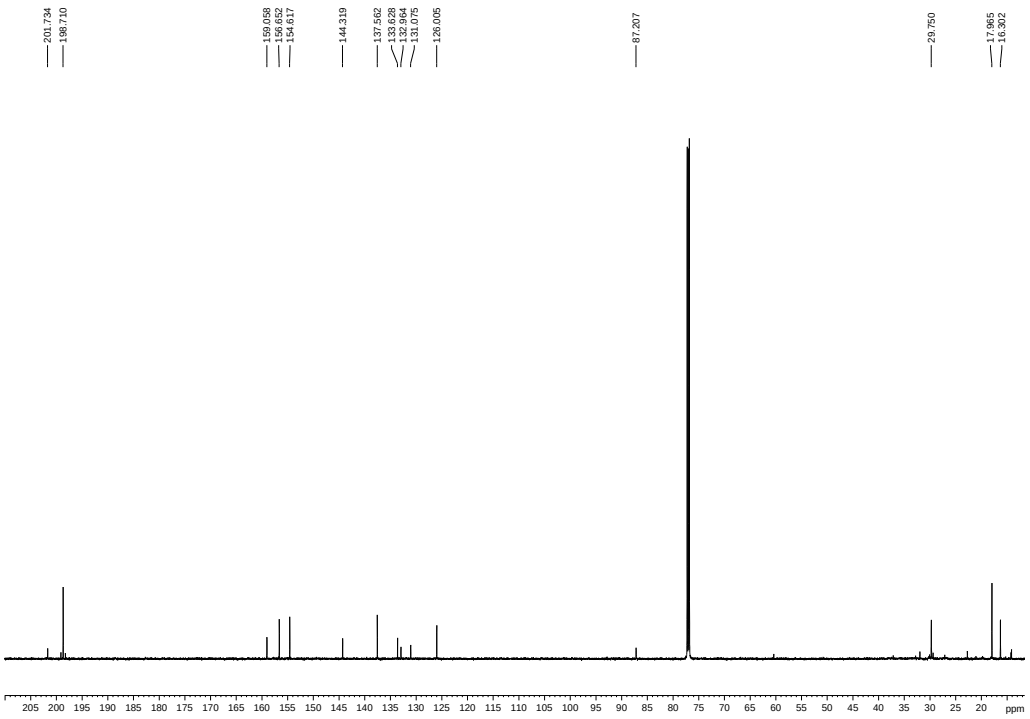

Figure B15 ^{13}C-NMR spectrum of Iodo-BODIPY W(CO)$_5$ in CDCl$_3$.

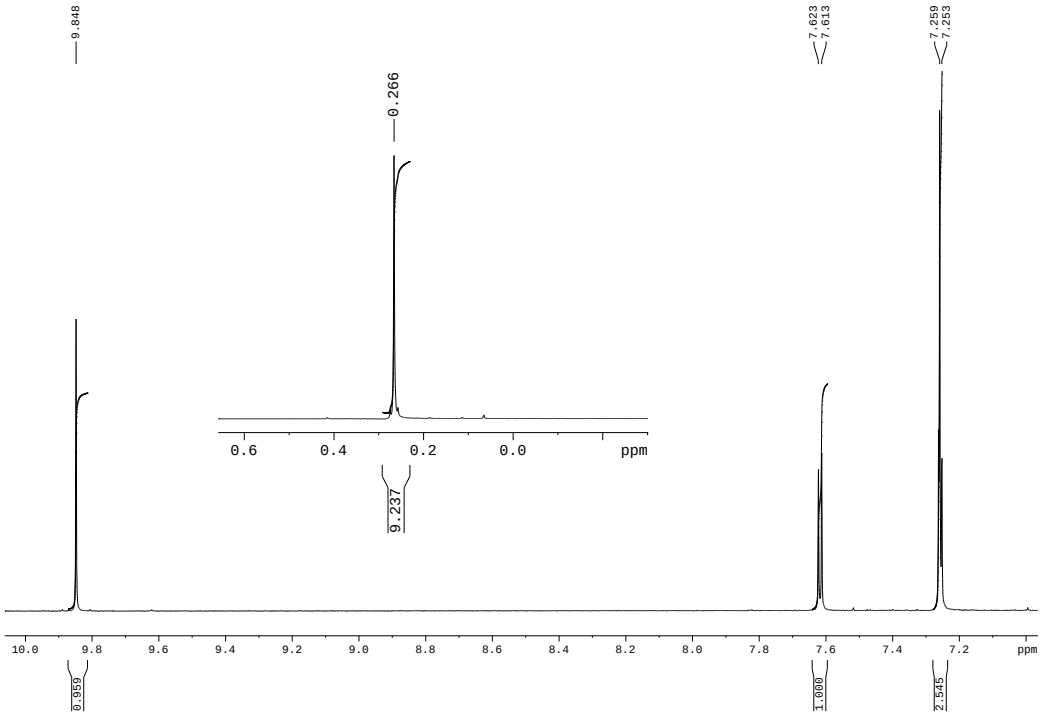

Figure B16 ^{1}H-NMR spectrum of 5-(trimethylsilylethynyl)-2-thiophenecarboxaldehyde in CDCl$_3$.

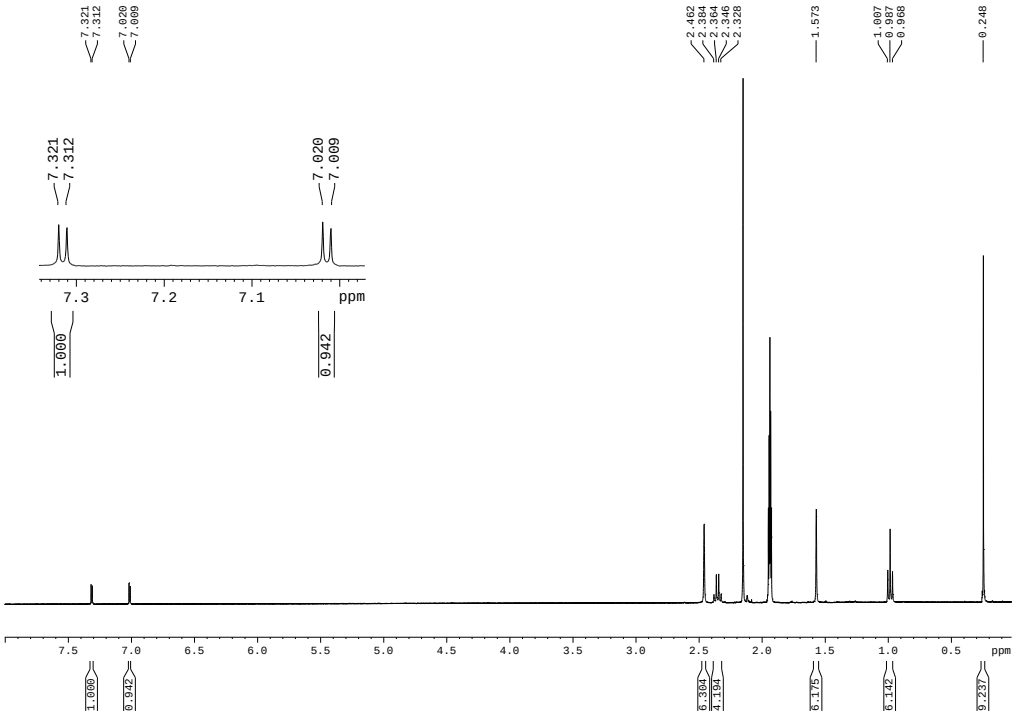

Figure B17 ^{1}H-NMR spectrum of ThioBODIPY-TMS in CD_3CN.

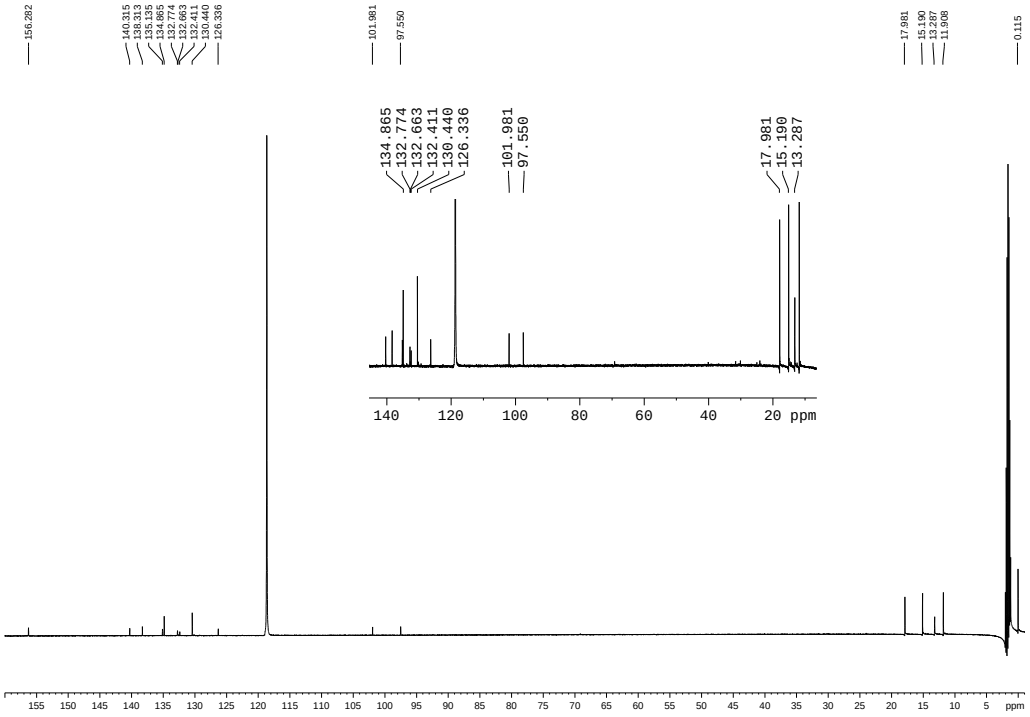

Figure B18 ^{13}C-NMR spectrum of ThioBODIPY-TMS in CD_3CN.

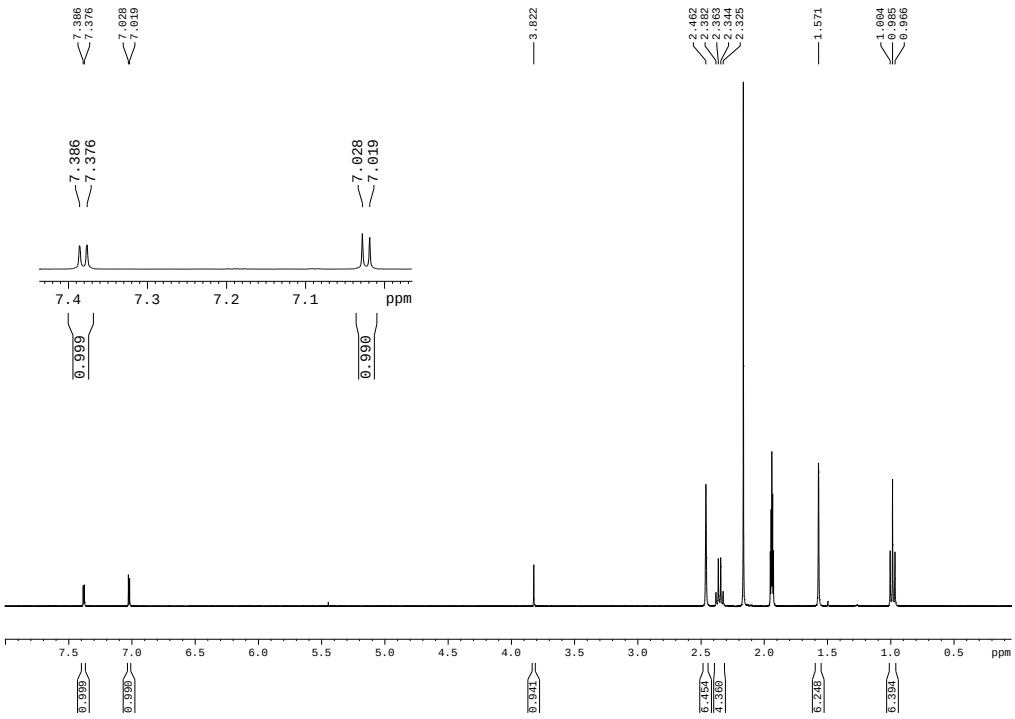

Figure B19 ^{1}H-NMR spectrum of ThioBODIPY-H in CD_3CN.

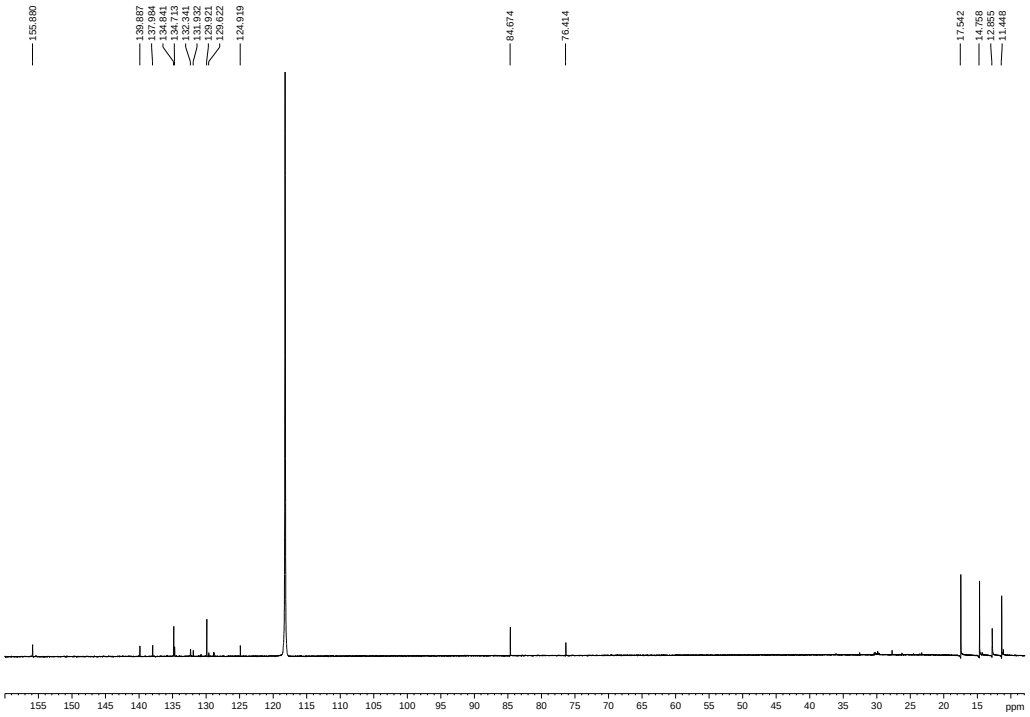

Figure B20 ^{13}C-NMR spectrum of ThioBODIPY-H in CD_3CN.

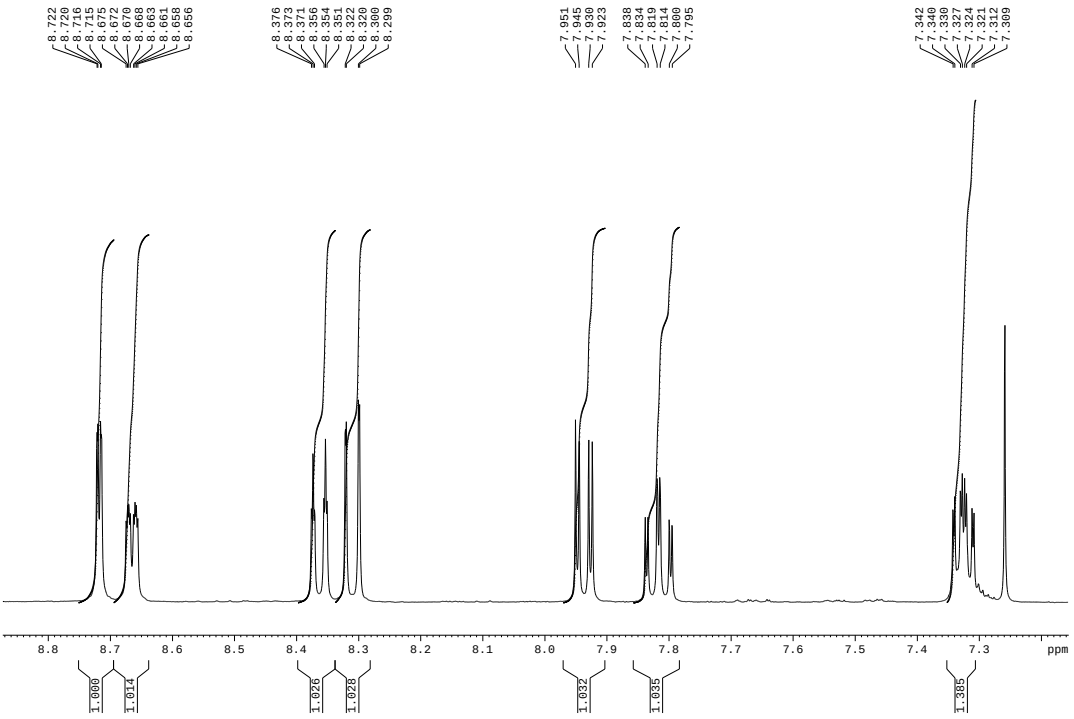

Figure B21 ^{1}H-NMR spectrum of 5-bromo-[2,2´]-bipyridine in $CDCl_3$.

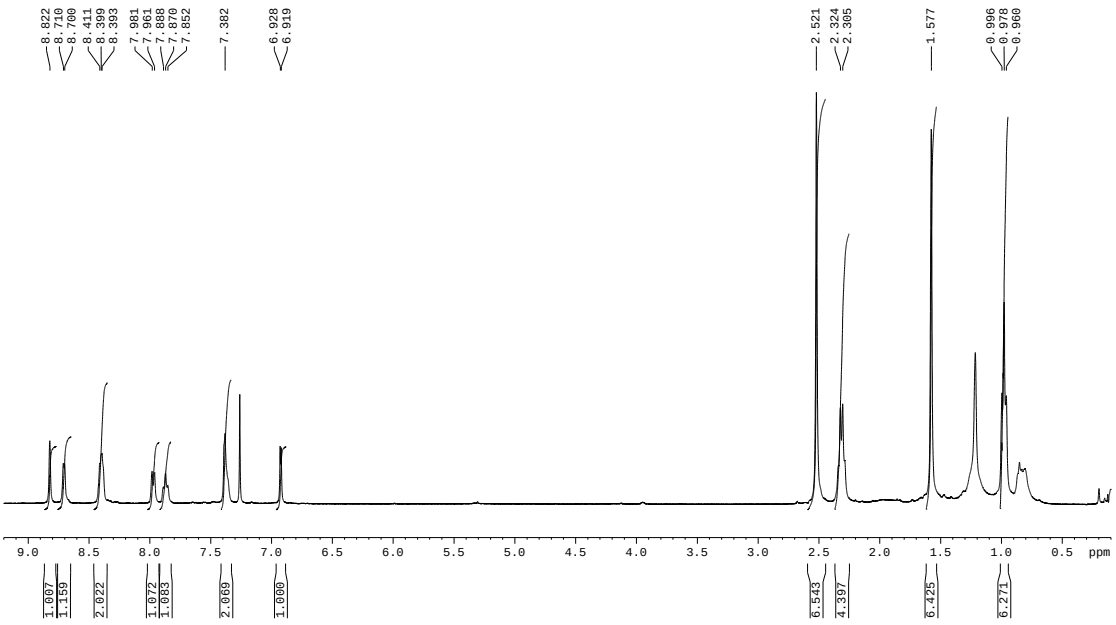

Figure B22 ^{1}H-NMR spectrum of ThioBipyBODIPY in $CDCl_3$.

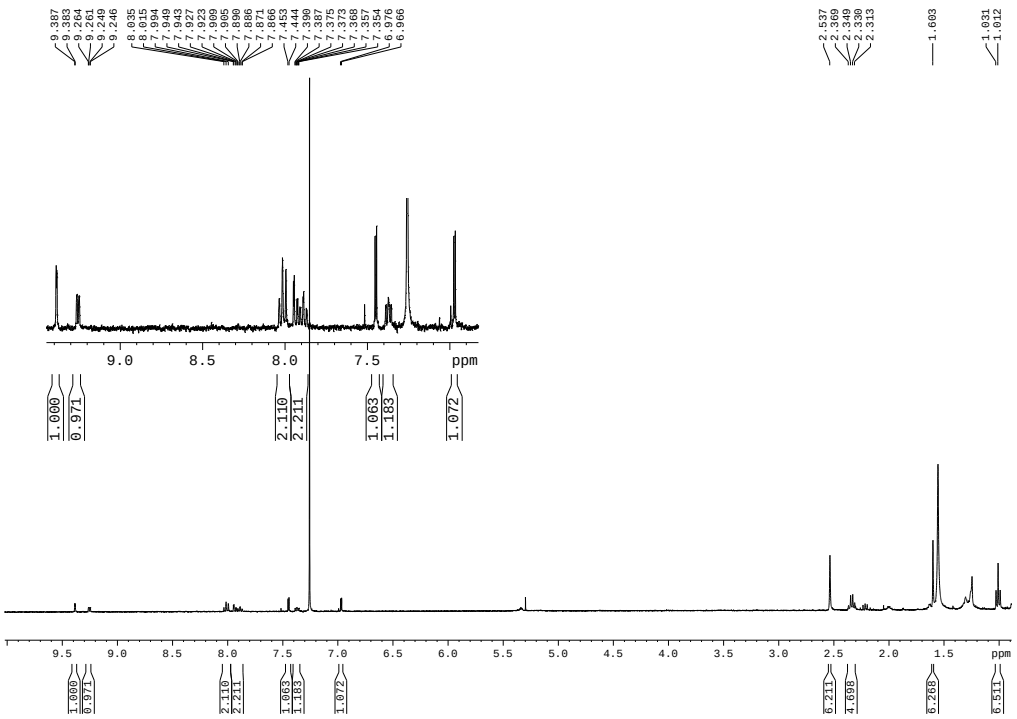

Figure B23 ^{1}H-NMR spectrum of ThioBipyBODIPY $Cr(CO)_4$ in $CDCl_3$.

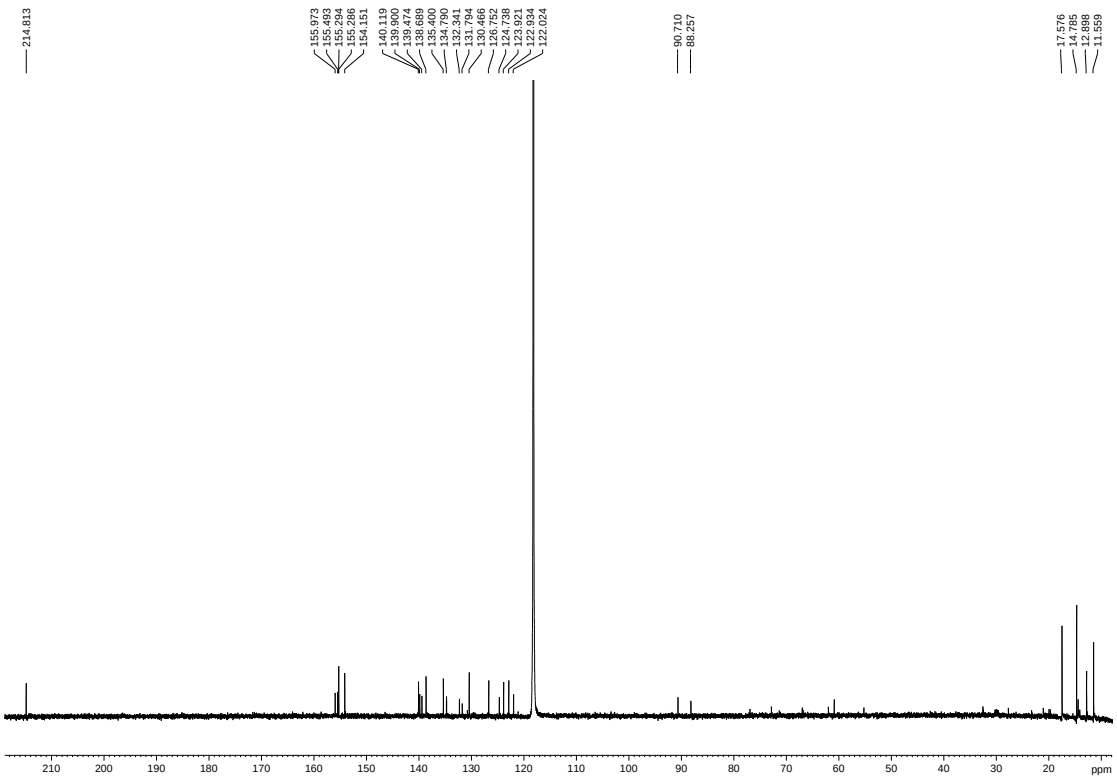

Figure B24 ^{13}C-NMR spectrum of ThioBipyBODIPY $Cr(CO)_4$ in CD_3CN.

Appendix C IR Spectroscopic Data

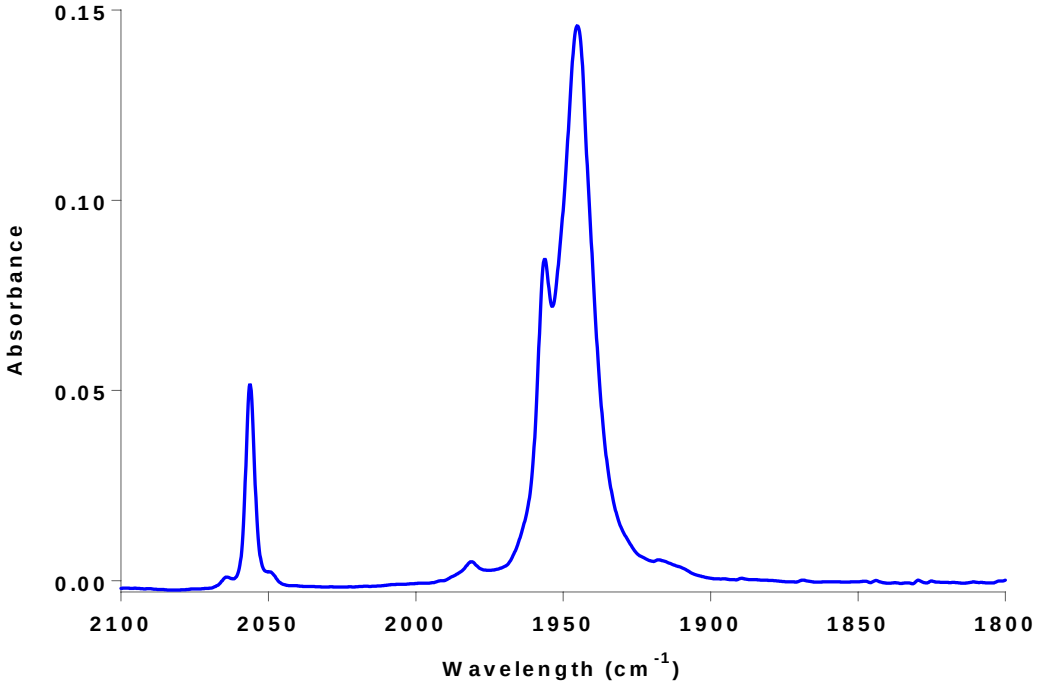

Figure C1 FT-IR spectrum of $(CO)_5Cr=C(OMe)C_2H_2Fc$ in *n*-heptane.

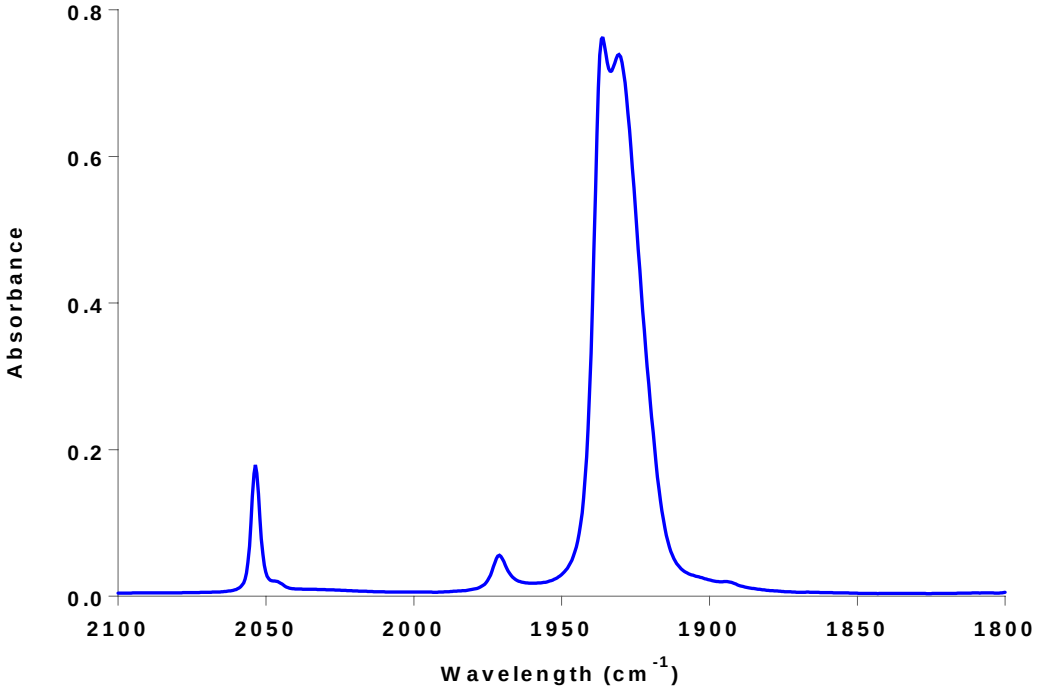

Figure C2 FT-IR spectrum of $(CO)_5Cr=C(C_4H_8N)C_2H_2Fc$ in *n*-heptane.

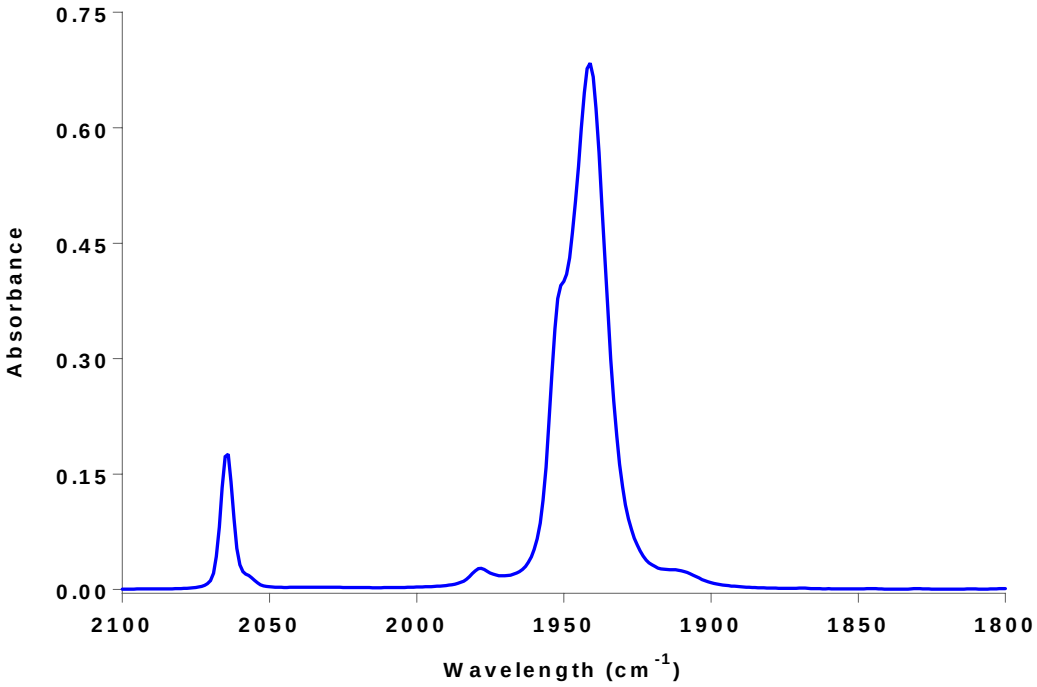

Figure C3 FT-IR spectrum of $(CO)_5W{=}C(OMe)C_2H_2Fc$ in *n*-heptane.

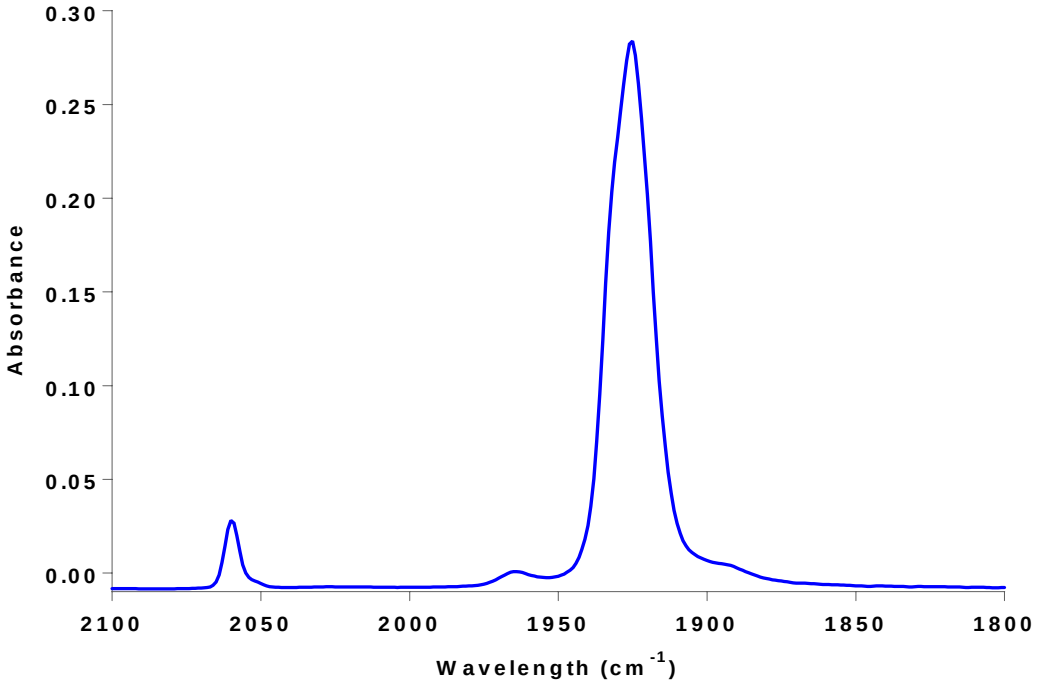

Figure C4 FT-IR spectrum of $(CO)_5W{=}C(C_4H_8N)C_2H_2Fc$ in *n*-heptane.

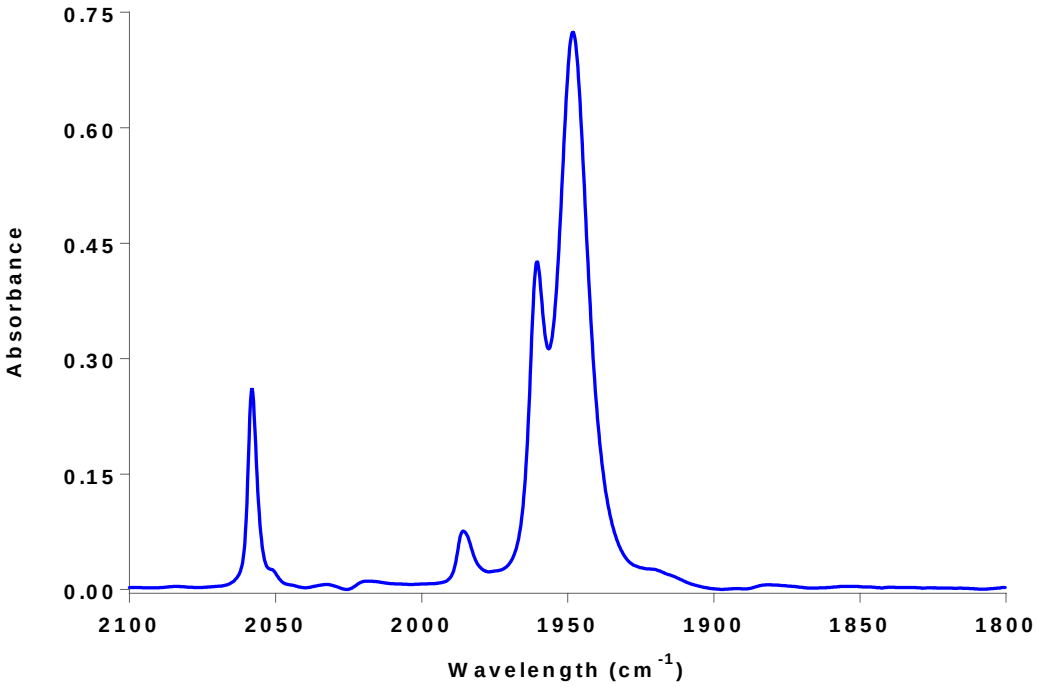

Figure C5 FT-IR spectrum of $(CO)_5Cr=C(OMe)C_2H_2Ph$ in *n*-heptane.

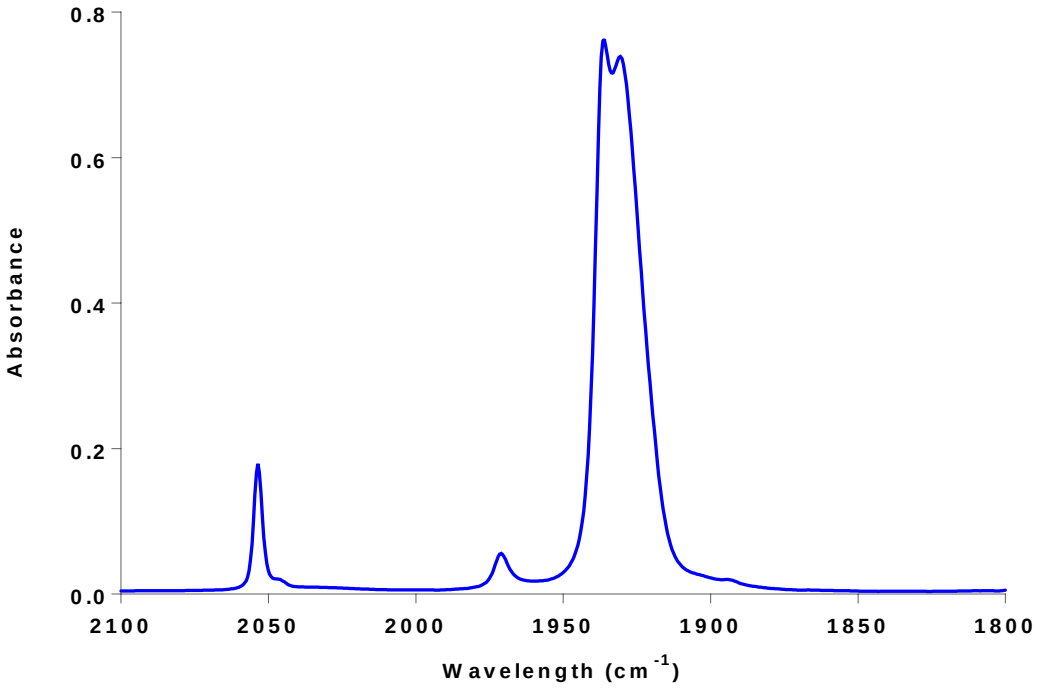

Figure C6 FT-IR spectrum of $(CO)_5Cr=C(C_4H_8N)C_2H_2Ph$ in *n*-heptane.

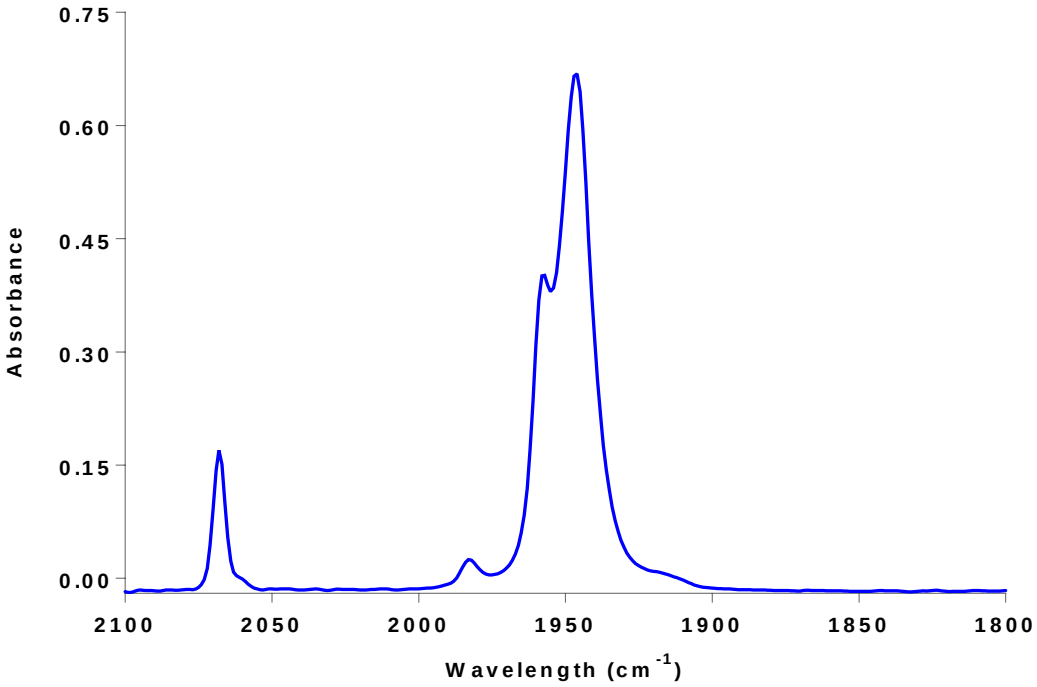

Figure C7 FT-IR spectrum of $(CO)_5W{=}C(OMe)C_2H_2Ph$ in *n*-heptane.

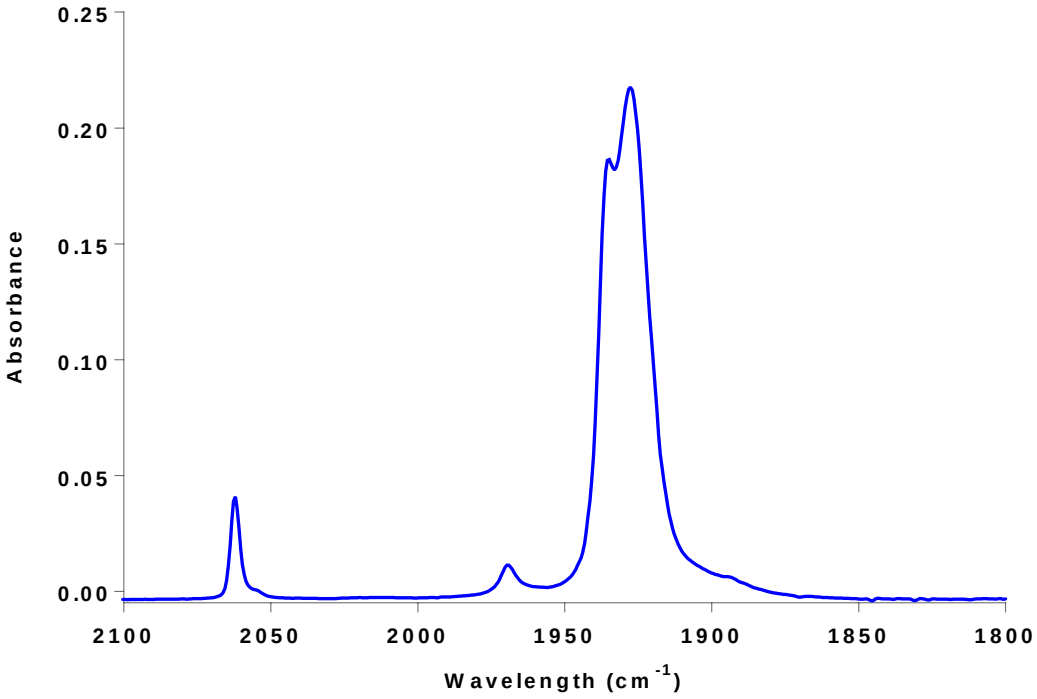

Figure C8 FT-IR spectrum of $(CO)_5W{=}C(C_4H_8N)C_2H_2Ph$ in *n*-heptane.

Appendix D UV-vis Data

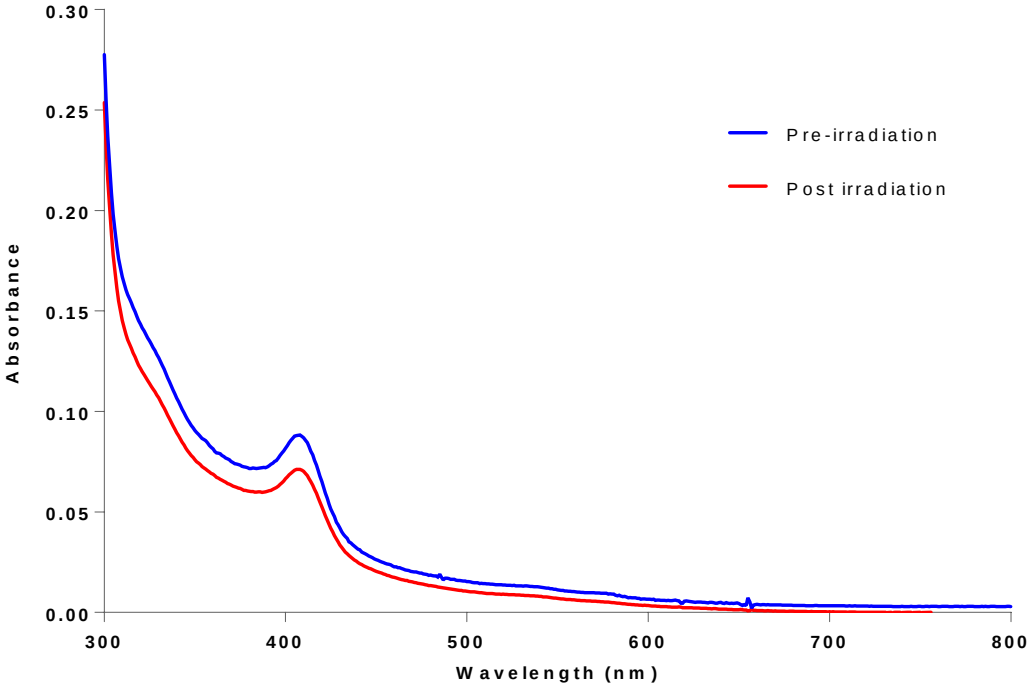

Figure D1 UV-vis absorbance spectrum of 5 % FBS in RPMI media prior to irradiation and post irradiation at 355 nm.

Appendix E Publications

1. Jennifer C. Manton, Saeed Amirjalayer, Anthony C. Coleman, Suzanne McMahon, Emma C. Harvey, Gregory M. Greetham, Ian P. Clark, Wybren Jan Buma, Sander Woutersen, Mary T. Pryce, and Conor Long. 'Excited state evolution towards ligand loss and ligand chelation at group 6 metal carbonyl centres' *Dalton Trans.* **2014**, *43*, 17797-17805

2. Suzanne Mc Mahon, Jonathan Rochford, Yvonne Halpin, Jennifer C. Manton, Emma C. Harvey, Gregory M. Greetham, Ian P. Clark, A. Denise Rooney, Conor Long and Mary T. Pryce. 'Controlled CO release using photochemical, thermal and electrochemical approaches from the Amino Carbene complex $[(CO)_5CrC(NC_4H_8)CH_3]$' *Phys. Chem. Chem. Phys.* **2014**, *16*, 21230-21233.

3. Suzanne Mc Mahon, Saeed Amirjalayer, Wybren J. Buma, Yvonne Halpin, Conor Long, A. Denise Rooney, Sander Woutersen, and Mary T. Pryce. 'An Investigation into the Photochemistry of, and the Electrochemically Induced CO-loss from, $[(CO)_5MC(OMe)Me]$(M = Cr or W) Using Low-temperature Matrix Isolation, Picosecond Infrared Spectroscopy, Cyclic Voltammetry, and Time-dependent Density Functional Theory' *Dalton Trans.* **2015**, *44*, 15424-15434.

Appendix F Posters and Oral Presentations

1. Suzanne Mc Mahon, Jonathan Rochford, Conor Long, Jennifer C. Manton, Emma C. Harvey, Gregory M. Greetham, Ian P. Clark, Mary T. Pryce. 'The Assessment of the Amino Carbene, [$(CO)_5CrC(NC_4H_8)Me$], as a Potential CO Releasing Molecule by Thermal and Photochemical Means.' Presented at Dalton 2014, 'Joint Interest Group Meeting' at the University of Warwick, Coventry CV4 7AL, United Kingdom, 15-17th April 2014.

2. Suzanne Mc Mahon, and Mary T. Pryce. 'Fluorescent BODIPY Metal Carbonyls'. Presented at 'Metal ions in Medical Imaging: Optical, Radiopharmaceutical and MRI contrast.' (Dalton Discussion) at the University of York, Heslington, York YO10 5DD, United Kingdom, 8-10th September 2014.

3. Suzanne Mc Mahon, Saeed Amirjalayer, Wybren J. Buma, Sander Woutersen, A. Denise Rooney, Conor Long, and Mary T. Pryce. 'The Photochemistry of the Methoxy Carbene Complex, [$(CO)_5CrC(OMe)Me$]; A Time Resolved Infrared and Matrix Isolation Study.' Presented at 'Inorganic Ireland Symposium 2014' at the Royal College of Surgeons in Ireland, 11th December 2014.

4. Suzanne Mc Mahon, Saeed Amirjalayer, Wybren J. Buma, Sander Woutersen, A. Denise Rooney, Conor Long, and Mary T. Pryce. 'An investigation into the Photochemistry of, [$(CO)_5CrC(OMe)Me$] (M = Cr, W); using low temperature matrix isolation and picosecond time resolved infrared spectroscopy.' Presented at the First Inaugural Chemistry Research Day' at Dublin City University, Dublin Ireland, 19th June 2015.

5. Suzanne Mc Mahon, Aoife Kinahan, Diana Hidalgo and Mary T. Pryce. 'The use of Fluorescent BODIPY Metal Carbonyls to function as CO Releasing Molecules.' Presented at 'The 67th Irish Universities Chemistry Colloquium' at Maynooth University, Maynooth, Co. Kildare, Ireland, 25-26th June 2015.

6. Suzanne Mc Mahon, Aoife Kinahan, and Mary T. Pryce. 'Novel Fluorescent BODIPY Metal Carbonyls; Wavelength dependent photochemistry.' Presented at 'The 21st International Symposium on the Photochemistry and Photophysics of Co-ordination Compounds' at Krakow, Poland, 5-9th July 2015.

Oral Presentation

1. Suzanne Mc Mahon, Aoife Kinahan, Diana Hidalgo and Mary T. Pryce. 'The use of Fluorescent BODIPY Metal Carbonyls to function as CO Releasing Molecules.' (The 67th Irish Universities Chemistry Colloquium) at Maynooth University, Maynooth, Co. Kildare, Ireland, 25-26th June 2015.